

Geo.Alp



Volume 7

2010



Geo.Alp

A yearly journal devoted to Alpine geology

Jahreszeitschrift zur Alpengeologie

La rivista per la Geologia delle Alpi

Geo.Alp

Redaktionskomitee: Rainer Brandner, Innsbruck; Karl Krainer, Innsbruck; Peter Tropper, Innsbruck; Volkmar Mair, Bozen;
Benno Baumgarten, Naturmuseum Südtirol, Bozen; Lorenz Keim, Bozen

Technische Redaktion/Layout: Sarah Krainer, Wien

Herausgeber, Eigentümer und Verleger:
Institut für Geologie und Paläontologie, Universität Innsbruck; Naturmuseum Bozen

Chefredakteur: Karl Krainer

Erscheinungsweise und Bezug:

Geo.Alp erscheint einmal jährlich und kann bei beiden herausgebenden Institutionen im Abonnement oder einzeln bezogen werden:
Institut für Geologie und Paläontologie, Innrain 52, A-6020 Innsbruck, Austria
Naturmuseum Südtirol/Museo Scienze Naturali Alto Adige, Bindergasse/via Bottai 1, I-39100 Bozen/Bolzano, Italy

© Institut für Geologie und Paläontologie, Universität Innsbruck; Naturmuseum Südtirol/Museo Scienze Naturali Alto Adige

Genehmigung des Landesgerichtes Bozen Nr. 12/2004 vom 5/11/2004
Verantwortlicher Direktor: Dr. Vito Zingerle

ISSN 1824-7741

Umschlagbild: Zunge des aktiven Blockgletschers im Gletscherkar, Hohe Gaisl, östliche Dolomiten, Südtirol (Foto: K. Krainer).

Druck: Karo Druck KG

INSTRUCTIONS TO AUTHORS

Articles may be submitted in English, German or Italian. In case of a German or Italian text, the captions and figures, plates and tables must be also in English, and an English abridged version (1000 – 1500 words) and abstract is to be delivered.

Articles shall be submitted in three copies to:

Karl Krainer, Institute of Geology and Palaeontology, University of Innsbruck, Innrain 52, A-6020 Innsbruck, Austria.
E-mail: Karl.Krainer@uibk.ac.at

or to:

Benno Baumgarten, Naturmuseum Südtirol/Museo Scienze Naturali Alto Adige, Bindergasse 1/Via Bottai 1, I-39100 Bozen/Bolzano, Italy: E-mail: benno.baumgarten@naturmuseum.it

Articles must be typed double-space. The quality of line-drawings must be ready for print. In line-drawings and figures of any sort, all labellings, numbers and letters should be readable upon 50% reduction in size.

Publication titles and authors name (citations) not in capital letters and not in small capitals!

Photographs and line drawings can be submitted in original hardcopy, or in an electronic format. All photographs must be clearly labelled on the backside.

For photographic tables (plate header – e.g. "Plate 1" – included) and for text-figures: please note that the page setup of Geo.Alp is 23,47 x 16,70 cm (8 cm column width)

The final text (Word file) must be submitted on CD. The name of the author, the name and version of the word processing program(s) and type of computer on which the text was prepared must be indicated. To avoid obsolete passages in the manuscript please note that Word files should be saved after using the option "Accepted Changes" in the Tools Menu.

Word tables must be on single pages for transformation into pdf format or already in pdf format.

The text should be submitted in single column format, and should be formatted as simple as possible (e.g. no bulleets and no automatic numbering). Electronic versions of figures and/or photographs must be submitted as separate files; file format: tif without LZW compression (high-resolution jpg files are also possible), photographs with a resolution of 300 dpi (due to print size), line drawings at least 600 dpi; colour images all in CMYK mode.

Referencing (Authors names not in capital letters and not in small capitals):

Articles:

Author 1, X.Y., Author 2, Z.A. (2002): Title of article. – International journal abbreviation (e.g. Sediment. Geol.), vol.: pp-pp.

Articles in books:

Author 1, X.Y., Author 2, Z.A. (2002): Title of article. – In: Person A., Person B. (eds): Title of book, pp-pp, publisher, place of publication.

Books:

Author 1, X.Y., Author 2, Z.A. (2002): Title of book. – no. of pages, publisher, place of publication.

Inhalt

Natalia Zavialova, Evelyn Kustatscher & Johanna H.A. van Konijnenburg-van Cittert: Spore ultrastructure of Selaginellites leonardii and diversity of Selaginellalean spores	1-17
Christian Pott & Michael Krings: Gymnosperm foliage from the Upper Triassic of Lunz, Lower Austria: an annotated checklist and identification key	19-38
Verena Rofner, Peter Tropper & Volkmar Mair: Petrologie, Geochemie und Geologie des Amphibolit/Metagabbro Komplexes von Gufidaun (Südtirol, Italien).....	39-53
Pietro Frizzo, Luca Peruzzo, & Elio Dellantonio: The copper-wolfram deposit of Bedovina (Trento, Italy)	55-70
Andreas Piber und Peter Tropper: Tectonometamorphic evolution of the Austroalpine nappes in the northern Zillertal area (Tyrol, Eastern Alps)	71-92
Permafrost Workshop Obergurgl, Kurzfassungen der Beiträge (Vorläufe und Poster)	93-108
Buchbesprechung.....	109-110

SPORE ULTRASTRUCTURE OF *SELAGINELLITES LEONARDII* AND DIVERSITY OF SELAGINELLALEAN SPORES

Natalia Zavialova¹, Evelyn Kustatscher² & Johanna H.A. van Konijnenburg-van Cittert³

With 2 tables and 3 plates

¹ Borissiak Palaeontological Institute, Russian Academy of Sciences, Profsoyusnaya st., 123, Moscow, 117647, Russia,
e-mail zavial@paleo.ru.

² Naturmuseum Südtirol, Bindergasse 1, 39100 Bolzano/Bozen, Italy, e-mail Evelyn.Kustatscher@naturmuseum.it.

³ Johanna H.A. van Konijnenburg-van Cittert, Laboratory of Palaeobotany and Palynology, Budapestlaan 4, 3584 CD Utrecht,
e-mail j.h.a.vankonijnenburg@uu.nl and National Centre for Biodiversity Naturalis, PO Box 9517, 2300 RA Leiden, The Netherlands,
e-mail: Han.Konijnenburg@ncbnaturalis.nl.

Abstract

The morphology and ultrastructure of spores of *Selaginellites leonardii* Kustatscher et al. 2010 from the Anisian (Middle Triassic) of the Dolomites is studied. The microspores are assignable to *Uvaesporites* Döring, 1965. Distally and equatorially they are covered with verrucae fused into rugae; proximally they are smooth or finely granulate. The sporoderm includes two layers, which appear homogeneous; the outer layer greatly varies in thickness at the expense of the sculptural elements, is much thicker and slightly less electron dense than the inner layer. The microspores were probably originally acavate, with an homogeneous sporoderm. Although a multi-layered sporoderm forming a cavum is the most common type occurring in selaginellalean microspores, acavate sporoderms are also known with a very high ratio between sporopollenin units and the spaces between them. The megaspores are rounded to rounded-triangular, with a very dense two-layered sporoderm, with the outer layer many times as thick as the inner layer. We suppose that originally the megaspore sporoderm was granular, formed by fused spheroid units, and could belong to the irregularly granular type or to the laterally fused type of selaginellalean sporoderms. The occurrence of various spore types in the Selaginellales is known from the Carboniferous until the present day. Available data on the sporoderm ultrastructure in the Selaginellales and Isoetales, similarities and dissimilarities between the two groups are discussed in light of the newly obtained information.

Keywords. *Selaginellites*, *in situ* spores, sporoderm ultrastructure, *Uvaesporites*, Middle Triassic, Dolomites.

1. Introduction

The genus *Selaginellites* was defined by Zeiller (1906) for fossil herbaceous lycophytes resembling the living genus *Selaginella* Palisot de Beauvois, 1804. *Selaginellites* is restricted to heterosporous species, whereas *Lycopodites* Lindley et Hutton, 1833 (fossil representatives of the extant *Lycopodium* Linnaeus, 1753) includes isosporous taxa, but also taxa of which it is unknown if they are hetero- or isosporous (Zeiller, 1906; Halle, 1907; Seward, 1910; Andrews, 1961).

The oldest *Selaginellites* fossils have been found in Carboniferous sediments; they are often based on sterile fragments only (Thomas, 1992), because fertile remains are rare (but known already from the Carboniferous, e.g., *Selaginellites fraipontii* (Leclercq) Schlanker et Leisman, 1969). Leaves are organized generally in four ranks with two ranks being smaller in size, like in living *Selaginella*. Some authors (e.g., Schimper, 1869; Lee, 1951; Pal, 1984; Schweitzer et al., 1997) consider these dimorphic (anisophyllous)

leaves typical of *Selaginellites* even if no spores have been found. Others, however, do not consider the presence of anisophyllous leaves enough evidence to distinguish between *Selaginellites* and *Lycopodites* (Halle, 1907; Thomas, 1992).

There is some debate as to whether fossil species should be assigned to the extant genus *Selaginella* or kept apart in the fossil genus *Selaginellites* (e.g. Thomas, 1992; Schweitzer et al., 1997). One of the main differences between *Selaginella* and *Selaginellites* is the higher amount of megaspores per sporangium in the fossil material (16–24 against 4 in extant *Selaginella*; Zeiller, 1906; Halle, 1907), although there are some living species with more than four megaspores per sporangium (Thomas, 1992, and references therein).

From the Triassic only few lycophytes were attributed to the genera *Selaginella* or *Selaginellites*: *Selaginella anasazia* Ash, 1972 from the Upper Triassic of Arizona, *Selaginellites polaris* Lundblad, 1948 from the Triassic of East Greenland, *Selaginellites hallei* Lundblad, 1950 from the Rhaetian of Sweden and *Selaginellites yunnanensis* Hsü, 1950 from the Rhaetian of China. Megaspores and microspores are known only in two of them: *Selaginellites hallei* and *Selaginellites polaris*.

The Triassic was an important moment during the evolution of this particular genus, and also a time of high abundance and diversity of lycophytes. With the disappearance of the arborescent Lepidodendrales during the Permian, various "pseudoherbaceous" or herbaceous forms radiated in the Early–Middle Triassic (Taylor et al., 2009). These genera are, however, not closely related but belong to various groups, such as Lycopodiales (e.g. *Lycopodites*), Selaginellales (e.g. *Selaginellites* Zeiller, 1906), Pleuromeiales (e.g., *Pleuromeia* Corda ex Giebel, 1853, *Chinlea* Daugherty, 1941, *Takhtajanodoxa* Snigirevskaya, 1980, and *Cyclomeia* White, 1981) and Isoetales (e.g. *Isoetes* Linnaeus, 1753 / *Isoetites* Münster, 1842, *Lepacyclotes* Emmons, 1856, and *Tomiosstrobus* Neuburg, 1936 sensu Retallack, 1997).

Recently, a new species was described (*Selaginellites leonardii* Kustatscher et al., 2010) from an Anisian (Middle Triassic) fossil locality in the NW-Dolomites (Kühwiesenkopf). The present paper supplements this description with additional information on the spore morphology and provides new data on the sporoderm ultrastructure. We believe these data will help to understand better the genus in general and its evolution into the extant *Selaginella*.

2. Selaginellalean spore morphology

Microspores

The morphology of selaginellalean spores underwent many changes through geological times and they were represented by more than one type of microspores and megaspores in each epoch. Modern spores are also quite diverse in terms of morphology.

The most ancient, Carboniferous, members are known to have produced trilete, zonate, labrate, and distally hilate (or with a few distal foveolae, depending on morphological interpretation) microspores ascribed to *Cirratiradites* Wilson et Coe, 1940 and trilete, cingulate or cinguli-zonate spores attributed to *Densosporites* (Berry) Butterworth et al., 1964. Spore dimensions range from 36 to 80 µm. *Cirratiradites* spores were extracted from *Selaginella guttieri* (Göeppert) Thomas, 1997 and S. cf. *leptostachys* (Bek et al., 2001). Taylor & Taylor (1990), who studied with SEM and TEM *Cirratiradites* type of microspores extracted from *S. frapontii*, suggested similarities between these fossil microspores and those from modern *Isoetes* and *Selaginella*, such as the presence of a paraexospore (a layer external to and largely free from the exospore, but with a similar ontogeny and staining characteristics, as defined by Tryon & Lugardon, 1991) and proximal multilamellate zones. Although multilamellate zones are usually considered an isoetalean feature, they are also known in the Selaginellaceae. Taylor & Taylor (1990) considered their microspores to be closer to *Selaginella*, namely, *S. selaginoides* (Linnaeus) Link, 1841. The sporoderm of the dispersed spore *Densosporites meyeriae* Telnova, 2004 probably consists of one homogeneous layer only (though the author mentioned lamellae in the sporoderm, they are not visible in the published section). No traces of a cavum are seen, thus questioning the paracavate nature of this spore type, hypothesized on LM basis (Telnova, 2004). Spores of *Cirratiradites* were found *in situ* only in selaginellalean strobili, spores of *Densosporites* were also found in the Chaloneriaceae (Balme, 1995).

The Permian *Selaginella harrisiana* Townrow, 1968 yields circular, paracavate (zonate, cingulate?), trilete, endopapillate, distally spinose microspores, of 43–58 µm diameter attributed to the genus *Indotriradites* Tiwari emend. Foster, 1979 (Townrow, 1968). Such microspores are also known from the Permian lycopsid of uncertain affinity *Azaniodendron fer-*

tile Rayner, 1986 (Balme, 1995). No information is available about its sporoderm ultrastructure.

Triassic *in situ* microspores are represented by two types. The first one is subcircular, cavate, endo-tri-papillate, scabrate, 40 µm in diameter and assigned to the genus *Densoisporites* (Weyland et Krieger) Dettmann, 1963. These spores are known *in situ* from the Pleuromeiaceae, and also as *sporae dispersae* in pre- and post-Triassic deposits (e.g., Guy-Olsson, 1979; Retallack et al., 2006). Triassic *Densoisporites* extracted from *Pleuromeia rossica* Neuburg, 1936 (= *Lycomeia rossica* (Neuburg) Dobruskina, 1985) shows a lamellate sporoderm with multilamellate zones around the proximal pole (Lugardon et al., 1999). A similar structure was revealed in Permian *Densoisporites* associated with another pleuromeiaceous plant, *Viatcheslavia vorcutensis* Zalessky 1936 (Naugolnykh & Zavialova, 2004). The ultrastructure of the dispersed microspores *D. psilatus* (de Jersey) Raine & de Jersey, 1988 and *D. microrugulatus* Brenner, 1963 (now synonymized with *D. velatus* Weyland et Krieger, 1953) was documented from the Triassic by Raine et al. (1988) and interpreted as a lycopsid sporoderm ultrastructure. Consequently, though some information on the *Densoisporites* ultrastructure is available, we still do not know if and how selaginellalean *Densoisporites* differ from pleuromeiaceous *Densoisporites* in its sporoderm ultrastructure.

Uvaesporites Döring, 1965 includes subcircular, cingulate, distally rugulo-verrucate spores, 29–50 µm in size. So far, *Uvaesporites* spores were never found *in situ*, only associated with selaginellalean macroremains. Ultrastructural information about this spore type was related to end-Permian dispersed spores (Looy et al., 2005). The sporoderm is complex, consisting of several sublayers, interpreted as a faint solid inner exospore, wavy and more electron dense outer exospore and three layers of paraexospore: the outer thicker solid layer forms sculptural elements, the middle thinner layer is composed of thin interwoven filaments, and the inner layer is composed of elements similar to those of the outer layer, but smaller in size. Additionally, Collinson (1991) reported *Lundbladispora* Balme, 1963 emend. Playford, 1965 as selaginellalean microspores, while Balme (1995) attributed the same *in situ* spores to the genus *Densoisporites*. The ultrastructure of dispersed end-Permian *Lundbladispora* resembles closely those of *Densoisporites*, although the presence or absence of multilamellate zones is not proved (Looy et al., 2005).

Microspores of *Foveosporites* Balme, 1957 (convexotriangular, trilete, distally foveolate and proximally smooth, 38–52 µm in diameter) are known from Cretaceous deposits. So far, *in situ* such a spore type is only known from selaginellalean macroremains.

Microspores of modern *Selaginella* are 18–60 µm in diameter, tetrahedral-globose, or slightly flattened, often with an equatorial flange and a trilete aperture with the arms varying in length between 1/2 and almost 7/8 of the spore radius. The surface is variable: often finely to coarsely echinate, sometimes rugulate, cristate, baculate, striate, papillate, or with large spherules. The exospore is plain, verrucate, or spinulose, usually overlain by either perispore or paraexospore; sometimes one of them or both may be lacking (Tryon & Lugardon, 1991).

Modern analogues can be found for most microspore types known from fossil Selaginellaceae. Moreover, the microspore diversity of modern *Selaginella* is much higher (e.g., their sculpture) than that so far known of *in situ* microspores of fossil Selaginellaceae. On the other hand, dispersed assemblages from various geological periods, starting from the Carboniferous or even Late Devonian, contain plenty of spores which are comparable with microspores of modern *Selaginella* in their ornamentation and could, thus, have a selaginellalean origin, but so far have not been found *in situ*. In addition, some types of microspores are recorded *in situ* in both selaginellalean and isoetalean remains, as well as from lycopsid macroremains of unclear position (Table 1).

Megaspores

Three types of megaspores were extracted from Carboniferous selaginellalean macroremains. The most commonly occurring type, *Triangulatisporites* (Potonié et Kremp) Karkiewska, 1976, includes subtriangular trilete, labrate megaspores, although the main spore body of permineralised specimens may appear spherical. These spores are paracavate and zonate: they are characterized by an equatorial flange which usually appears as a flattened wing. Both hemispheres are covered with a more or less developed reticulum (Cottnam et al., 2000; Bek et al., 2001). Taylor (1994) described the sporoderm of *Triangulatisporites* from *Selaginellites fraipontii* as a complex of interconnected units forming a fine 3D reticulum sharing common features with modern members of

Geological age	microspore/megaspore	Isoetalean	Lycopod taxon of unclear affinity
Carboniferous	<i>Cirratriradites/</i> <i>Triangulatisporites</i>	-/-	-/-
Carboniferous	?/ <i>Bentzisporites</i>	-/-	-/-
Carboniferous	<i>Densosporites/</i> <i>Setosisporites</i>	Chaloneriaceae/-	-/ <i>Bothrodendrostrobus</i> , ?/ <i>Barostrobus</i>
Permian	<i>Indotriradites/</i> <i>Bacutriletes</i>	-/-	<i>Azaniodendron/</i> <i>Synlycostrobus tyrmensis</i> (from Jurassic/Cretaceous)
Triassic	<i>Densoisporites/</i> <i>Banksisporites</i>	Pleuromeiaceae/ Pleuromeiaceae	<i>Bisporangiostrobus/-</i>
Triassic and Triassic/Jurassic	<i>Uvaesporites/</i> <i>Banksisporites</i>	- /Pleuromeiaceae	-/-
Cretaceous	<i>Foveosporites/</i> <i>Minerisporites (?)</i>	-/Isoetaceae	-/ <i>Limnoniobe</i>

Table 1. Occurrence of micro- and megaspores known from selaginellalean remains *in situ* in non-selaginellalean taxa (compiled from Balme, 1995 and including our data)

the Selaginellaceae and Isoetaceae. Nevertheless, *in situ* *Triangulatisporites* finds are so far restricted to selaginellalean macroremains. Cottman et al. (2000) studied dispersed *Triangulatisporites* from several Carboniferous localities and *in situ* megaspores of the same type extracted from *Selaginellites guttieri* and showed the diversity of the sporoderm ultrastructure: they described some sporoderms as particulate and others as more laminate.

The second Carboniferous type is *Setosisporites* (Ibrahim) Potonié et Kremp, 1954 emend. Dybova-Jachowicz et al., 1979 (circular, labrate, trilete, distally with bifurcating spines, proximally smooth, 300–400 µm in diameter). The sporoderms of dispersed Carboniferous *S. hirsutus* (Loose) Ibrahim, 1933 and *S. brevispinosus* (Zerndt) Brzozowska, 1969 are two-layered; the outer layer is much thicker than the inner, very dense, indistinctly stratified toward the inner hollow (Kempf, 1973). The third type is *Bentzisporites* Potonié et Kremp, 1954, which is 315–400 µm in dia-

meter, convexotriangular, cingulate, curvaturate, labrate, trilete, subverrucate and endopapillate. *Triangulatisporites* and *Bentzisporites* were found *in situ* only in selaginellalean strobili, while *Setosisporites* was also found in lycopsid macroremains of unclear systematic position (Balme, 1995).

Megaspores of the Permian *Selaginella harrisiae* belong to the *Bacutriletes* (van der Hammen) Potonié, 1956 type, which is described as circular, cavate, trilete, endopapillate, baculate, and 180–320 µm in diameter (Townrow, 1968). Such megaspores were also recorded in *Synlycostrobus tyrmensis* Krassilov, 1978, a lycopsid of uncertain affinity (Krassilov, 1978). Electron microscopical data are available on dispersed *Bacutriletes*: *B. ferulus* Koppelhus et Batten, 1989 and *B. majorinus* Koppelhus et Batten, 1989 were studied with SEM (Koppelhus & Batten, 1989), TEM studies were made on Lower Cretaceous *B. triangulatus* Taylor et Taylor, 1988 and *Bacutriletes* spp. (Taylor & Taylor, 1988), *B. guttula* Archangelsky

et Villar de Seoane, 1991 (Archangelsky & Villar de Seoane, 1991).

Megaspores of *Banksisporites* Dettmann, 1961 emend. Banerji et al., 1978, described as circular, trilete, cavate, labrate, scabrate, 392–421 µm in diameter, are found *in situ* in selaginellalean strobili in sediments of Triassic–Jurassic age. *Selaginellites hallei* from the Rhaetian of Sweden (Lundblad, 1950) yields putatively immature, spheroidal, trilete, smooth-granulate, cavate megaspores of 330–425 µm diameter, attributed to *Triletes pinguis* Harris, 1935 (now *Banksisporites pinguis* (Harris) Dettmann, 1961). Unfortunately, no information was given on its ultrastructure. TEM data are available from dispersed *B. jerseyi* Scott et Playford, 1985, *B. viriosus* Scott et Playford, 1985 (Hemsley & Scott, 1989) and Upper Keuper *B. pinguis* (Harris) Dettmann, 1961 (Kempf, 1971).

Cretaceous *Selaginella dawsonii* (Seward) Watson, 1969 yields megaspores supposedly assignable to *Minerisporites* Potonié, 1956 (Watson, 1969). The megaspores are convexo-triangular, paracavate, labrate, distally coarsely vermiculate, with verrucate contact faces, 284–305 µm in diameter. Such a spore type is also known in *Limnoniobe* Krassilov, 1982. However, much more often, this type was reported from the Isoetaceae. A considerable bulk of information is obtained with application of electron microscopes, albeit on dispersed specimens. SEM data were obtained on Cretaceous *M. labiosus* Baldoni et Taylor, 1985 (Baldoni & Taylor, 1985), *M. dissimilis* Tschudy, 1976 and *M. marginatus* (Dijkstra) Potonié, 1956 (Kovach & Dilcher, 1988) and *M. aequatus* Villar de Seoane et Archangelsky, 2008 (Villar de Seoane & Archangelsky, 2008). SEM and TEM data were obtained on Lower Cretaceous *M. elegans* Archangelsky et Villar de Seoane, 1989, *M. patagonicus* Archangelsky et Villar de Seoane, 1989 (*M. laceratus* Archangelsky et Villar de Seoane, 1990) (Archangelsky & Villar de Seoane, 1990), Maastrichtian *M. succrassulus* Tschudy, 1976 (Bergad, 1978), and Upper Paleocene and Paleocene/Eocene of *M. glossoferus* (Dijkstra) Tschudy, 1976, *M. mirabilis* (Miner) Potonié, 1956, and *M. mirabilissimus* (Dijkstra) Potonié, 1966 (Batten & Collinson, 2001). Sporoderms of all studied megaspores are rather similar and show a multilamellate ultrastructure common in Isoetales, with considerable spaces between lamellae. In addition, monolete spores (comparable with the typically isoetalean microspore *Aratrisporites* Leeschik, 1955) were reported associated with dispersed

megaspores, e.g., those found in hollows of the surface of *M. mirabilis* (Miner) Potonié, 1956 (Batten & Collinson, 2001). Keeping in mind that most indices point to an isoetalean affinity of *Minerisporites*, ultrastructural study of the megaspores of *S. dawsonii* would be very pertinent to find out if any differences between such megaspores of selaginellalean and isoetalean affinities exist at ultrastructural level.

Several genera of dispersed megaspores (or some of their species) have not been so far reported *in situ* but are considered as supposedly selaginellalean in affinity because of their ultrastructure: *Thylakosporites retarius* (Hughes) Potonié, 1956, *Triletes persimilis* Erdtman, 1947 ex Potonié, 1956, *Hughesporites patagonicus* Archangelsky, 1963, *Erlansporites* Potonié, 1956 (see e.g. Takahashi et al., 2001), *Horstisporites* Potonié, 1956, *Rugotriletes* van der Hammer, 1955 ex Potonié, 1956, *Ricinospora* Bergad, 1978, and *Cabochonicus* Batten et Ferguson, 1987 (Kovach, 1994).

Megaspores of modern species of *Selaginella* are 200–1033 µm in diameter, tetrahedral-globose, often with an equatorial flange, trilete, with the arms reaching 2/3 of the radius or equal to it. The surface is often reticulate, sometimes rugate, baculate, verrucate, scabrate, or granulate. The exospore consists of two layers, the outer usually with distinctive zones. A perispore is lacking (Tryon & Lugardon, 1991).

Selaginellalean megaspores are very diverse and represented by more than one morphological type in each geological period. The number of dispersed megaspore genera showing presumably selaginellalean features is much greater than the number of selaginellalean megaspores so far found *in situ*. With new *in situ* finds, our concept of selaginellalean megaspores will be corrected. Several types of megaspores are known from both selaginellalean and isoetalean macroremains (Table 1), posing two problems: unclear affiliation of dispersed megaspores of spore types known in both groups (such as *Setosisporites*, *Banksisporites*, and *Minerisporites*), and a possibility that spores so far known only in one of the groups can be later found in macroremains of the other. In this relation, accumulation of data on *in situ* megaspores is important as ultrastructural information may differentiate between selaginellalean and isoetalean megaspores.

Both selaginellalean microspores and megaspores are very diverse, and there are enough grounds to believe that a considerable portion of this diversity has

been still undiscovered. More studies on *in situ* material with application of SEM and TEM will help us to understand better the morphological diversity of one of the oldest groups of higher plants (Table 2). The comparison between selaginellalean and isoetalean spores from various epochs is important in order to reveal characters allowing to differentiate between the two groups on the basis of spore morphology and ultrastructure as well as to estimate their similarities. The diagnostics of dispersed spores as members of one of the two groups also should be mentioned.

The present study deals with *in situ* spores of Triassic *Selaginellites leonardii*. Data on their morphology and ultrastructure contribute to these aims.

3. Material and Methods

The strobili of *Selaginellites leonardii* belong to the rich flora from Kühwiesenkopf / Monte Prà della Vacca section in the Dolomites (for more information see Broglio Loriga et al., 2002; Kustatscher, 2004; Kustatscher et al., 2006, 2010), stored nowadays at the Museum of Nature South Tyrol (BZ, Italy). The well-known section (Bechstädt & Brandner, 1970; De Zanche et al., 1993; Senowbari-Daryan et al., 1993) has been dated by brachiopods (Bechstädt & Brandner, 1970), foraminifers (Fugagnoli & Posenato, 2004), ammonoids and palynomorphs (Kustatscher et al., 2006; Kustatscher & Roghi, 2006) to the middle-late Pelsonian (upper Anisian, Middle Triassic).

The strobili have been studied with a dissecting microscope and *in situ* spore preparations were made (for more details see also Batten, 1999). For this purpose, small sporophyll fragments were macerated in Schulze's reagent (KClO₃ and 30% HNO₃) and neutralized with 5% ammonia. The sporangia were separated with the aid of needles, and monads or groups of spores (depending on their maturity) were extracted, mounted in glycerine jelly and sealed with paraplast.

In transmitted light, the spores were studied with a ZEISS AXIOPLAN-2 and a Leica DFC-420 digital camera, under 100x oil immersion objective at the Paleontological Institute of the Russian Academy of Sciences, Moscow. In addition, some microspores were studied with help of a Leica DM6000 fluorescent microscope using a Leica DC300F camera, HBO 103 W/2 Mercury Lamp reflected light source and A filtercube (BP340-380, LP 425) at the Institute of Molecular Genetics (Moscow). Slides were observed under 63x

oil objective. Image-Pro AMS has been used as acquisition software. To calculate an EDF (extended depth of field) composite image, a stack of 30 slices was produced using motorized Z-drive function of the microscope, and the composite image calculated in Image-Pro (Pl. 1, fig. 6).

Several groups and individual microspores were mounted on scanning electron microscopy (SEM) stubs and coated with platinum/palladium and viewed on a CAMSCAN SEM at Lomonosov Moscow State University, at 20 kV accelerating voltage.

For transmission electron microscopy (TEM), megaspores and microspores were removed from temporary light-microscopical slides and embedded following the method of Meyer-Melikian & Zavialova (1996). Ultrathin sections of 50 nm thick were made with an LKB ultra-microtome, the sections were viewed unstained on Jeol 100 B and Jeol 400 TEM and photographed. The accelerating voltage was 80 kV.

Although the terminology developed by Tryon & Lugardon (1991) is most desirable to describe strata in sporoderms, the definitions imply sufficient data on the position, ultrastructure, electron density, and ontogenesis of particular strata of the sporoderm. No ontogenetic information can be deduced for the fossil sporoderms at hand, and the preservation is far from ideal: at least some ultrastructural information is probably lost. Therefore, we refrain from designating the sublayers revealed as exospore or paraexospore and use instead such neutral terms as outer and inner layers of the sporoderm.

4. The strobilus

So far only two strobilus fragments (up to 17 mm long and 3 mm wide) of *Selaginellites leonardii* Kustatscher et al., 2010 have been found. They are not in organic connection but preserved on slightly different horizons on the same rock sample (collection number PAL536). The sporophylls are helically to decussately arranged in four irregular vertical rows of microsporophylls and megasporophylls (Kustatscher et al., 2010, pl. 1, figs. 1-3). The sporophylls are ovate (1.5-2 x 1-1.2 mm) and entire margined, with a long, acuminate apex (about 2 mm long).

Maceration of the sporophylls resulted in small cuticle fragments with isodiametric cells and slightly immature micro- and megasporangia. Additionally, megaspores were found dispersed in the sediment at the apex of one strobilus.

Geological age	Spore type	Data on sporoderm ultrastructure, if available, with the interpretation of sporoderm layers, which can be preserved in fossil state	Parent plant, references
Microspores			
Carboniferous	<i>Cirratiradites</i>	Thin exospore and paraexospore of three sublayers. Multilamellate zones are present	<i>S. crassicinctus</i> = <i>S. fraipontii</i> , Taylor & Taylor 1990
Triassic	<i>Uvaesporites</i>	Supposed exospore of two homogeneous layers. Multilamellate zones are not found.	<i>S. leonardii</i> , present paper
Modern	Spores are trilete, tetrahedral-globose, often with an equatorial flange; the surface is often echinate, sometimes rugulate, cristate, baculate, striate, papillate, or with large spherules.	The exospore consists of inner lamellate and outer amorphous layers. It can either include multilamellate zones or be pierced with numerous radial canals. In some species, paraexospore and/or perispore may be present enveloping the exospore.	General characteristic of the modern genus <i>Selaginella</i> , Tryon &Lugardon, 1990
Megaspores			
Carboniferous	<i>Triangulatisporites</i>	Exospore of highly interconnected network of wall units, which are thickest and least compressed in the center.	<i>S. crassicinctus</i> = <i>S. fraipontii</i> , Taylor 1994
Triassic	?	Supposed exospore of two layers: thin inner layer and thicker outer layer of granular elements.	<i>S. leonardii</i> , present paper
Modern	Spores are trilete, tetrahedral-globose, often with an equatorial flange; the surface is often reticulate, sometimes rugate, baculate, verrucate, scabrate, or granulate.	The exospore of two layers: an inner compact layer and a much larger, outer labyrinth or gridlike layer, often heavily infiltrated with silica. The perispore is absent.	General characteristic of the modern genus <i>Selaginella</i> , Tryon & Lugardon, 1990

Table 2. Available ultrastructural data on *in situ* selaginellalean spores compared with modern *Selaginella*

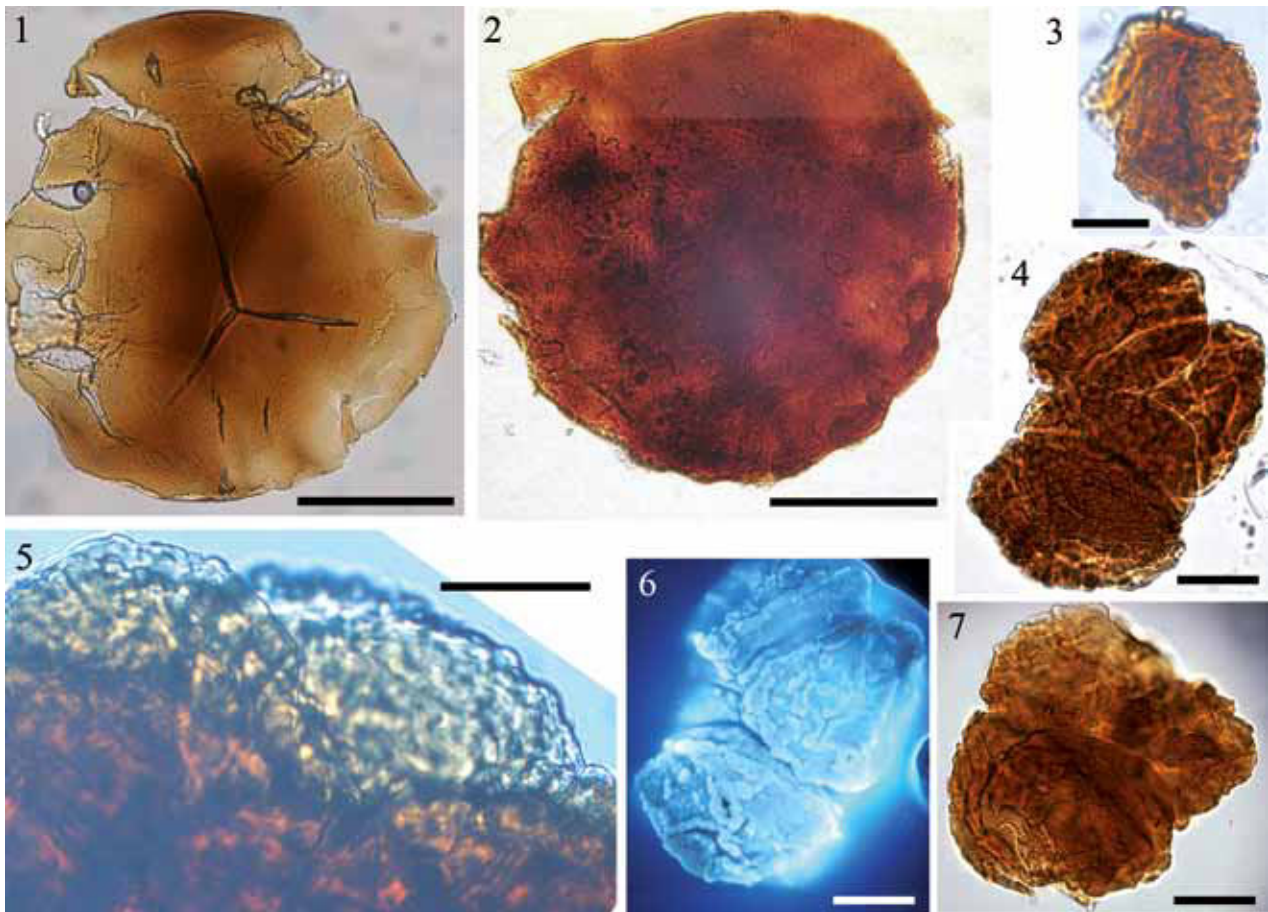


Plate 1 (LM)

1. Megaspore with a trilete scar. 2. Megaspore, no proximal scar is visible. 3. Microspore, equatorial view. 4. Group of microspores, distal sculpturing is distinct. 5. Group of microspores under higher magnification, note uneven contours of microspores. 6. Microspore tetrad, fluorescence microscopy. 7. The same tetrad as in fig. 4. Scale bar (1, 2) 100 µm, (3-7) 20 µm.

5. Microspore morphology and ultrastructure

Microspores are in clusters as well as in damaged tetrads and monads, significantly varying in sizes (Pl. 1, figs. 3, 4-7; Pl. 2, figs. 1, 3). The spores are rounded-triangular and most probably trilete (no monad preserved in polar position was found). The distal and equatorial surfaces of the microspores are rugulate: covered with verrucae mostly fused into ridges elevated at a various height over the surface of the spores (Pl. 1, figs. 4, 6, 7; Pl. 2, figs. 1, 2, 4). The specimens greatly vary in the development of the sculptural elements. The proximal sporoderm is smooth or covered

with small granules (Pl. 2, fig. 2). In general morphology and sculpturing, the microspores are assignable to the dispersed genus *Uvaesporites*. The sporoderm is two-layered, both layers look homogeneous, the outer layer is slightly less electron dense than the inner layer (Pl. 3, figs. 3, 4, 6). The outer layer greatly varies in thickness at the expense of the sculptural elements: equatorial areas are thickest, and proximal areas are thinnest (Pl. 3, fig. 4). The sculptural elements more often appear in sections as elongate appendages, stretched along the rest of the sporoderm (Pl. 3, fig. 6). No cavum between the outer and inner layers or within the outer layer was found, but some

gaps were detected between sculptural elements and the rest of the sporoderm. The inner layer is more or less constant in thickness, about 0.22–0.26 µm.

In the microspores of modern *Selaginella* the sporoderm layer enveloping the exospores varies: it may form a perispore, an paraexospore, or may be missing (Tryon & Lugardon, 1991), and the perispore is rarely preserved in fossil state. Thus, the two layers of the sporoderm most probably can be either two sublayers of the exospore or correspond to exospore and paraexospore. We consider the former theory more probable, since the paraexospore is usually largely detached from the exospore, and that is not the case of the outer layer of the sporoderm under study.

6. Megaspore morphology and ultrastructure

Megaspores are irregularly rounded or rounded-triangular, 265–303 x 306–336 µm in size (about 283 x 320 µm on average). Most specimens do not show a tetrad scar (Pl. 1, fig. 2); the only specimen that retains it shows an open trilete scar, occupying more than a half of the radius (Pl. 1, fig. 1). The megaspores are deep brown (Pl. 1, fig. 2) or uneven in colour (Pl. 1, fig. 1), with numerous traces of corrosion and mechanical damage.

No inner hollow of the spore is visible in optical sections. No unequivocal cavum is visible, but a torn specimen (Pl. 1, fig. 1) shows a space between the layers of the sporoderm that, however, can be of mechanical origin. Since we are not sure that all general morphological characteristics are preserved, we refrain from assigning the megaspores to a particular genus of *sporae dispersae*. The sporoderm is very dense, two-layered. The outer layer varies in thickness from 4.9 µm to 11.3 µm, pierced with numerous minute alveolae, 0.01–0.05 µm in diameter (Pl. 3, figs. 1, 2, 5, 7–9). In some places, globular units of about 0.4 µm also pierced with alveolae are vaguely recognizable (Pl. 3, figs. 1, 5, 7). The inner layer is of constant thickness, 0.17–0.23 µm, appearing homogeneous (Pl. 3, fig. 2). No definite cavum was revealed. In places, gaps in the outer layer were observed (Pl. 3, fig. 5). The inner hollow looks like a narrow slit (Pl. 3, fig. 2).

The uneven coloring of the megaspores, traces of corrosion and the fact that the inner hollow which once contained the gametophyte now is indistinguishable in transmitted light allow us to suspect that the megaspores are too much secondarily changed

to reveal the original sporoderm ultrastructure in ultrathin sections. Our TEM observations confirmed this suspicion. In our opinion, the minute alveolae numerous in the outer layer of the sporoderm are secondary changes not reflecting its original ultrastructure. This is supported by the fact that they are also present at the contact between the inner sporoderm layer and the megaspore hollow (Pl. 3, fig. 2). Besides, one of the authors (N.Z.) observed very similar minute alveolae in places in the sporoderm of *Biharisporites capillatus* Fuglewicz et Prejbisz, 1981, a megaspore from much older deposits and supposedly produced by an unrelated plant group (Turnau et al., 2009, pl. IV, fig. 5); in case of *Biharisporites*, it was also concluded that such alveolae did not reflect the typical ultrastructure of the sporoderm (Turnau et al., 2009). On the other hand, the areas of the sporoderm where globular units are distinguishable, are altered in a less degree than the majority of the sporoderm, in our opinion. The outer layer of the sporoderm might have been composed of such globular units fusing with each other and more or less elongated around the inner layer of the sporoderm. A few gaps observed in the sporoderm are most probably traces of mechanical damage: one of them is situated in the outer layer, cuts the inner layer, and reaches the inner hollow of the spore (Pl. 3, fig. 5). Dealing with such degree of preservation, we cannot decide about the presence or absence of a cavum. However, if our guess about globular units constituting the outer layer of the sporoderm is correct, such an ultrastructural type quite easily allows sporoderm splitting.

In modern *Selaginella* megaspores, the exospore consists of two layers: a thin and usually lamellate inner exospore and a much thicker outer exospore containing the aperture (Tryon & Lugardon, 1991). The inner layer under study appears homogeneous, and the ultrastructure of the aperture has remained unknown; however, the relative development of the two layers (thin inner layer and much thicker outer layer) implies that they may represent inner exospore and outer exospore.

7. Discussion

New finds of *in situ* spores have contributed to the knowledge on selaginellalean spores characterizing this group of plants during various periods of its geological history. Keeping in mind the diversity of

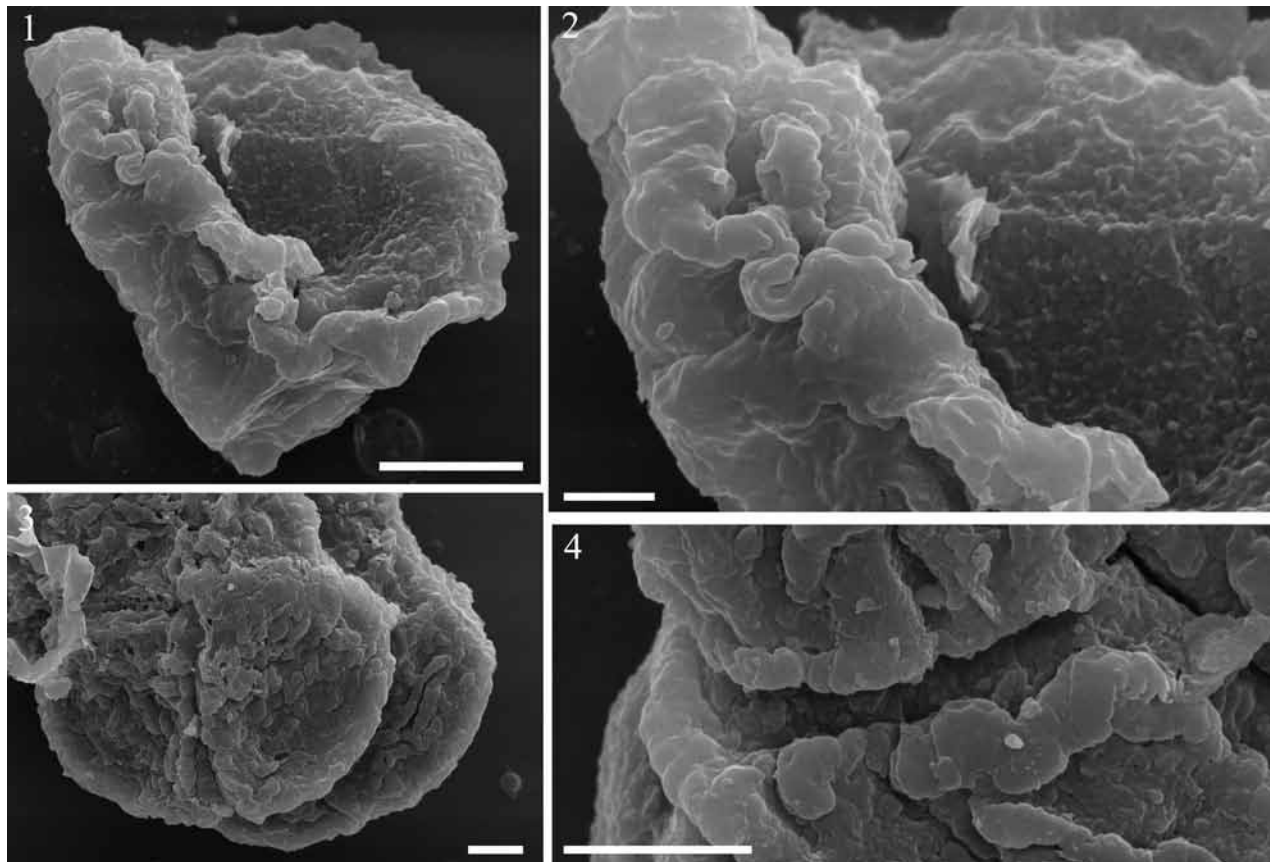
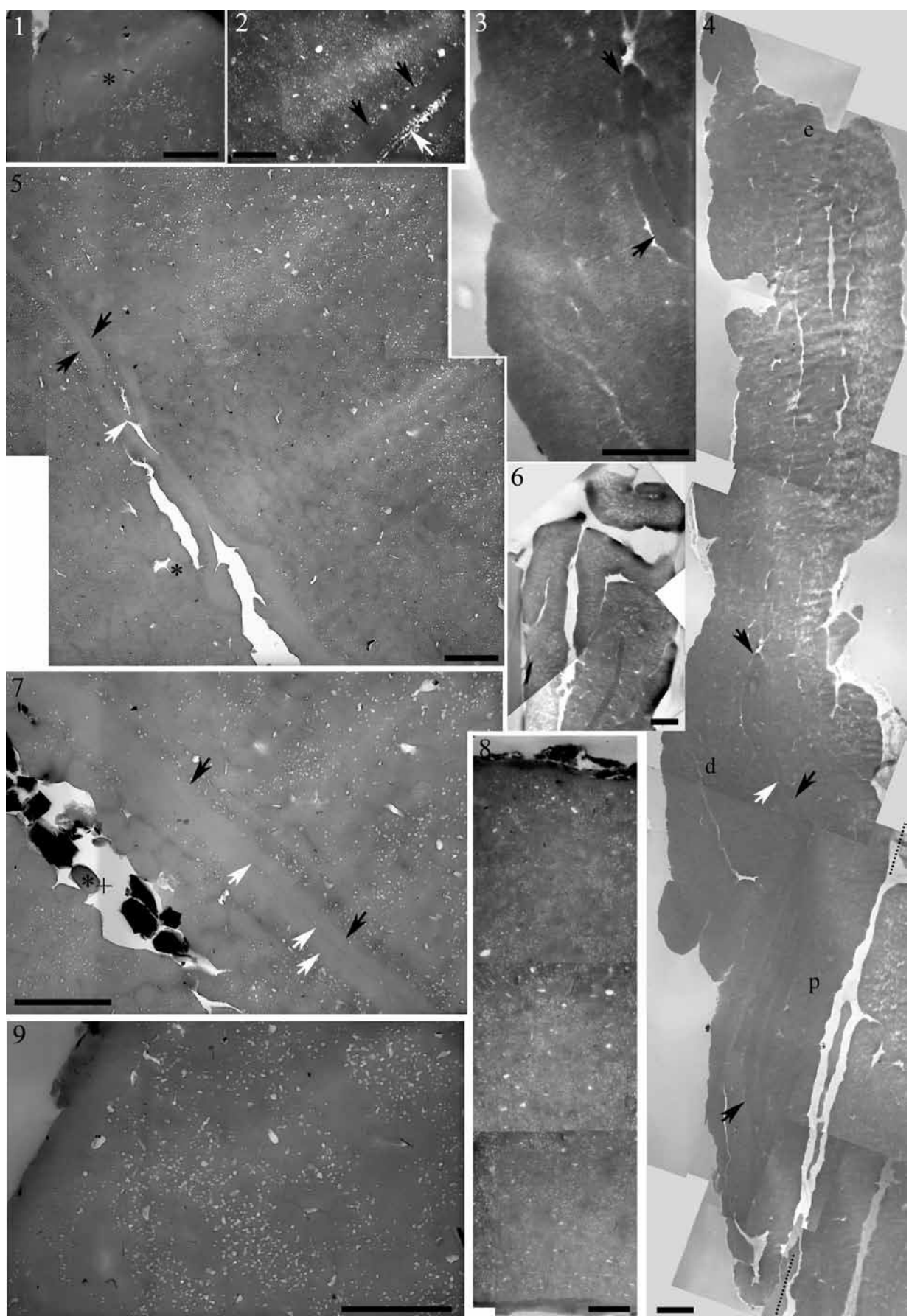


Plate 2 (SEM)

1. Individual microspore in lateral position. 2. Blowing-up of fig. 1 showing rugulate sculpturing of the equatorial to distal area and finely granulate sculpturing of the proximal area. 3. Cluster of several microspores showing rugulate distal sculpturing. 4. Enlargement of distal and equatorial sculpturing. Scale bar (1, 3, 4) 10 µm, (2) 3 µm.

Plate 3 (TEM)

1, 2, 5, 7-9. Ultrathin sections of megaspore sporoderm. 3, 4, 6. Ultrathin sections of microspore sporoderm. 1. Area of the section (closer to the surface of the megaspore), supposedly showing a region of the outer sporoderm with less alternated ultrastructure; nonetheless, minute alveolae are present. 2. Area of the section showing outer (to the left) and inner (to the right) layers of the sporoderm, the inner hollow of the megaspore is visible between the proximal and distal portions of the inner layer; minute alveolae are present in the outer layer and at the contact between the inner layer and the inner hollow. 3. Blowing up of fig. 4 showing outer and inner layer of microspore sporoderm. 4. Composite image of ultrathin section of microspore sporoderm. 5. An area of the section showing gaps in the sporoderm. Note outer and inner layers of the sporoderm. 6. Area of section of microspore sporoderm, elongated sculptural elements are cut. 7. Area of the section showing inner layer of the sporoderm and the outer layer of the megaspore sporoderm that in part pertains its supposed original globular ultrastructure. Note the globular units between the gap filled with black mineral stuff and the inner layer of the sporoderm. The inner hollow of the megaspore is traceable only as a darker contour between proximal and distal portions of the inner layer. 8. Area of section of megaspore sporoderm in the equatorial region, the most common appearance of megaspore sporoderm. 9. Minute alveolae piecing the megaspore sporoderm, an area of the outer layer shown situated close to the surface. Legend: black arrows – inner layer of sporoderm; white arrows – inner hollow of spore; asterisks – supposed globular units in megaspore sporoderm; p – proximal area of sporoderm; d – distal area of sporoderm; e – equatorial area of sporoderm; dotted line – boundary between two members of microspore tetrad. Scale bar (1-9) 1 µm.



spores in hundreds of modern species of *Selaginella* and the diversity of supposed selaginellalean spores from dispersed palynological assemblages that have never been reported from strobili, our concept about selaginellalean spores will become much more ramified with accumulation of additional data on *in situ* spores.

Spores of *Uvaesporites*, a dispersed genus suitable for microspores of *S. leonardii*, were already reported *in situ* from *Selaginellites hallei*, the macromorphologically most similar Triassic *Selaginellites* species to *S. leonardii* (Lundblad, 1950). Microspores of *S. hallei* are slightly smaller than those of *S. leonardii* (29–50 µm against 45–62.5 µm), but fall partly within its variability range. Although Lundblad (1950) interpreted the sculpturing of *S. hallei* as damaged (because of taphonomy or maceration), microspores of both species show a similar rugulate sculpturing. Unfortunately, no data about the ultrastructure of microspores of *S. hallei* are available. End-Permian dispersed *Uvaesporites* spores have a complex sporoderm that differs strongly in ultrastructure from microspores of *S. leonardii*: the sporoderm of the Permian spores was interpreted as consisting of an exospore and a complex paraexospore, whereas the two layers of the sporoderm of the Triassic microspores more probably both represent exosporal layers. To date, *Uvaesporites* was only reported from Selaginellales, but the ultrastructure of the Permian *Uvaesporites* does not exclude an isoetalean affinity. No *Uvaesporites* is so far known *in situ* from Permian strobili (either selaginellalean or isoetalean). Indeed, all these indices imply that the Permian *Uvaesporites* may be of isoetalean rather than selaginellalean origin. Similar spores are found *in situ* in both groups (Table 1). Future studies of the sporoderm ultrastructure will show if any differences exist between selaginellalean and isoetalean spores similar in gross morphology.

Although a sporoderm that includes several layers and easily allows splitting under forming a cavum is the most common type in selaginellalean microspores, acavate and much denser sporoderms are also known, where the ratio between sporopollenin units and spaces between them is very high. For example, dispersed Carboniferous *Densosporites* probably has a homogeneous sporoderm (Telnova, 2004). Taylor & Taylor (1989) studying dispersed the Lower Cretaceous megaspore *Erlansonisporites sparassis* (Murray) Potonié, 1956 of supposed selaginellalean affinity, found in their surface reticulum small trilete spores, which could have been produced by the same parent plant. The proximally smooth and distally verrucate

spores are two-layered; both layers appear homogeneous. Although the preservation of our material forces us to be cautious in our conclusions, we consider the microspores acavate and with a homogeneous sporoderm. Of interest is that though *Uvaesporites* type was not reported *in situ* from younger than Jurassic strobili, it seems to exist in some modern species. Thus, modern *Selaginella gracillima* (Kunze) Spring ex Salomon, 1883 has microspores that, as one can judge by illustrations, fit the genus *Uvaesporites*, if found as fossil *sporae dispersae* (Tryon & Lugardon, 1991, fig. 231.3).

Non-selaginellalean lycophytes are also abundant in Lower-lower Middle Triassic sediments, but strobili are only known for a few of them, and even less have preserved *in situ* spores. Thus, only *Aratrisporites*, *Lundbladispora*, and *Densoisporites* are known *in situ*. The microspores of *S. leonardii* differ from these types in general morphology and from *Densoisporites* (on which ultrastructural information is available) also in sporoderm ultrastructure. The intriguing question if Triassic *Densoisporites* of selaginellalean affinity differs in its ultrastructure from contemporaneous *Densoisporites* of isoetalean affinity is pending till *in situ* spores of the former will be studied by TEM.

There are classifications of extant selaginellalean megaspore sporoderms, proposed by Morbelli (1977), Minaki (1984) and Taylor (1989). The first two authors distinguished granular and spongy types; Minaki subdivided the granular type into irregular and ordered types, and the spongy type into two types. Taylor (1989) distinguished an ordered granular type and two spongy types: laterally and laminar fused. The laterally fused type is composed of anastomosing rod-like or spherical elements (so, in part it corresponds to an irregular granular type), and the laminar type is composed of wider sheet-like elements, often forming closed vesicles. These types can be used to reveal selaginellalean ultrastructure in fossil sporoderms. We incline that, when unaltered, the sporoderm of megaspores *S. leonardii* was granular, formed by fused spheroid units. In terms of the above classifications, it belongs to irregular granular type or to laterally fused type. Most dispersed megaspores of presumed selaginellalean affinity can be incorporated into this group, e.g., *Banksisporites* and *Bacutriletes* (other Triassic *in situ* finds of megaspores).

In dimensions, megaspores of *S. leonardii* are slightly smaller than those of *S. hallei* (270–340 x 300–410 µm against 330–425 µm) but fall partly within its variability range (Lundblad, 1950). The megaspore surfaces of both species lack distinct

sculptural elements, but megaspores of *S. hallei* are distinctly labrate, and their sporoderm is thicker than that in *S. leonardii* (about 15 µm against about 5.1–11.5 µm). The megaspores of *S. hallei* were assigned by Lundblad (1950) to *Triletes pinguis* Harris, 1935, which is now *Banksisporites pinguis* (Harris) Dettmann, 1961. Ultrastructural data on dispersed megaspores of this species from the Upper Keuper of Denmark were obtained by Kempf (1971). The sporoderm is two-layered. The outer layer is 15–20 µm thick, composed of numerous, irregularly distributed, more or less spherical particles (0.3–0.5 µm in diameter against about 0.4 µm of *S. leonardii*), partly fused and interconnected, with considerable spaces between them; the porosity of this layer does not seem to vary over the distance from the sporoderm surface. Such a sporoderm can be incorporated in the irregular granular type, the same type we have chosen for *S. leonardii*. However, the sporoderm of *S. leonardii* is so much denser and some of the units we managed to distinguish seem to be aligned along the inner layer. The inner layer in *B. pinguis* seems nearly homogeneous and reaching about 1–2 µm proximally (comparable with *S. leonardii*), but transforms into a loose lamellate net more than 10 µm in thickness distally (nothing comparable was observed in *S. leonardii*). Unlike *S. leonardii*, a cavum is clearly seen in *B. pinguis* (Kempf, 1971). Dettmann (1961, pl. 1, fig. 5) published a microtome section viewed in transmitted light of *B. pinguis* from the Triassic of Tasmania showing a cavate nature of the spore.

Kovach (1994) pointed out that the differences in sporoderm ultrastructure between two living groups of heterosporous lycopsids are less obvious than in their gross morphology. The sporoderms are composed of anastomosing sporopollenin elements, which range from rod-like to granular and form a porous network. Rod-like elements of living *Isoetes* tend to orient parallel to the surface of the spore and the sporoderm has a high porosity; sporopollenin elements of *Selaginella* are oriented more randomly and the sporoderm has lower porosity than in *Isoetes*: the sporopollenin elements tend to have less open space between them. Using these criteria, Kovach (1989) succeeded at differentiating between Cretaceous megaspores of the Selaginellales and Isoetales. However, Taylor (1994) dealing with older megaspores failed: isoetalean coats were very dense and fell into selaginellalean group. Although the general criterium (by higher/lower porosity) for differentiation between Isoetales and Selaginellales does not work for pre-Cretaceous specimens, some fossil sporoderms can

be considered selaginellalean with much confidence because of their similarity to certain ultrastructural types of modern species. Thus, very characteristically looking labyrinthine structure (e.g. *Selaginella erythropus* (Mart.) Spring, 1840, Tryon & Lugardon, 1991, fig. 231.83) and highly ordered grid-like structure (e.g. *S. marginata* (von Humboldt & Bonpland ex von Willdenow) Spring, 1838, Morbelli and Rowley, 1996, fig. 14; *S. sulcata* (Desvaux ex Poir.) Spring ex Mart., 1837, Morbelli et al., 2001, fig. 36D) were repeatedly observed in dispersed fossil megaspores: e.g. *Horstisporites harrisii* (Murray) R. Potonié illustrates the former type (Bergad, 1978, pl. 3, fig. 6) and *Erlansonisporites sparassis* (Taylor & Taylor, 1988, pl. 2, fig. 7), and *Richinospora cryptoreticulata* Bergad, 1978 (Bergad, 1978, pl. 5, figs. 1, 3) show the latter structure.

However, other types are not as easy to differentiate from the isoetalean ultrastructure, and this problem is still pending. Further ultrastructural studies will contribute to differentiation between these two groups or, alternatively, might show clearly overlapping characteristics. The current rarity of TEM studies on *in situ* selaginellalean spores by comparison to those accomplished on dispersed material should be underlined (Table 2), as well as the greater importance of the former for differentiation between the Selaginellales and Isoetales on the basis of sporoderm ultrastructure.

Outlining non-selaginellalean Triassic lycophytes, a greater number of *in situ* finds of megaspores can be mentioned compared to microspores. These *in situ* megaspores can be ascribed to *Dijkstraisporites* Potonié, 1956, *Minerisporites*, and *Tenellisporites* Potonié, 1956, *Horstisporites*, and *Maiturisporites* Maheshwari et Banerji, 1975. Megaspores of two species of *Banksisporites* were extracted from *Cylostrobus strobili* (one of them, *B. pinguis*, is the same species as was extracted from *Selaginellites hallei*). Some of the above-mentioned spore types are known in the Selaginellaceae as well; some (e.g. *Minerisporites* and *Horstisporites*) being found as *sporae dispersae* although in younger deposits, were considered by different authors as megaspores of selaginellalean (Archangelsky & Villar de Seoane, 1989) or isoetalean (Batten & Collinson, 2001) affinity.

Although the ultrastructural characteristics ascribed to the Selaginellales and Isoetales are often merging and certain types of megaspores are known from both groups, megaspores of the species under study show an ultrastructure that is quite dissimilar from typical isoetalean ultrastructure and corre-

sponds quite well to one of the known types of selaginellalean ultrastructure.

8. Conclusions

This study further elucidates the diversity in spore morphology and ultrastructure in one of the most long-living groups of higher plants and documents for the first time the ultrastructure of its *in situ* spores dated to the Middle Triassic. The microspores are supposedly acavate and have a two-layered homogeneous sporoderm; similar sporoderms are rare but not a unique case among selaginellalean microspores. Further ultrastructural studies on the Triassic material seem very promising, in particular, to estimate how typical selaginellalean the ultrastructure revealed in the microspores of *Selaginellites leonardii* is. *In situ* finds of Permian *Uvaesporites* might resolve the significance of the ultrastructural differences revealed between Permian *Uvaesporites* and *in situ* microspores of *S. leonardii*. The sporoderm ultrastructure of the megaspores is interpreted as belonging to the irregular granular or laterally fused types, which are common among megaspores of presumed selaginellalean affinity, including Triassic megaspores.

Acknowledgments. We are thankful to Dr. Sergei Lavrov (Institute of Molecular Genetics, Moscow, Russia) for his assistance with the fluorescence microscopy, Dr. Maria Tekleva (Paleontological Institute, Moscow, Russia) for making SEM micrographs, Dr. Guido Roghi (University of Padova, Padova, Italy) and Dr. Olga Yaroshenko (Geological Institute, Moscow, Russia) for valuable discussion. The manuscript benefited greatly from the remarks and comments of Maria Tekleva and Cindy V. Looy. The study was in part supported by the Russian Foundation for Basic Research, no. 09-04-01241.

References

- Andrews, H. N. (1961): Studies in Palaeobotany. - 487 pp., Wiley and Sons Ed., New York and London.
- Archangelsky, S., Villar de Seoane, L. V. (1989): Ultraestructura de dos nuevas megasporas cretacicas de Santa Cruz, Argentina. - Boletín Asociación Latinoamericana Paleobotánica y Palinología, 12: 13-25.
- Archangelsky, S., Villar de Seoane, L. V. (1990): Morfología y estructura de megasporas cretacicas de Patagonia. República Argentina. - Revista Española de Micropaleontología, 22 (3): 419-450.
- Archangelsky, S., Villar de Seoane, L. V. (1991): Notas sobre la flora fosil de la Zona de Tico, provincia de Santa Cruz: XI. Morfología y estructura de tres megasporas. Ameghiniana (Rev. Asoc. Paleontol. Argent.) 28(3-4): 353-364.
- Baldoni, A. M., Taylor, T. N. (1985): Megasporas Cretacicas de la formacion Springhill et El Subsuelo de Argentina y Chile austral. - Ameghiniana, 21(2-4): 151-167.
- Balme, B.E., 1995. Fossil *in situ* spores and pollen grains: An annotated catalogue. - Rev. Palaeobot. Palynol., 87: 1-323.
- Batten, D. J. (1999): Small palynomorphs. - In: Jones, T. P., Rowe, N. P. (eds.): Fossil plants and spores. - Modern Techniques, 15-19, The Geological Society, London.
- Batten, D. J., Collinson, M. E. (2001): Revision of species of *Minerisporites*, *Azolla* and associated plant microfossils from deposits of the Upper Palaeocene and Palaeocene/Eocene transition in the Netherlands, Belgium and the USA. - Rev. Palaeobot. Palynol., 115: 1-32.
- Bechstädt, T., Brandner, R. (1970): Das Anis zwischen St. Vigil und dem Höhlensteintal (Pragser-und Olinger Dolomiten, Südtirol). - In: Mostler, H. (ed): Beiträge zur Mikrofazies und Stratigraphie von Tirol und Vorarlberg, 9-103, Festband des Geologischen Institutes, 300-Jahr-Feier Universität Innsbruck, Wagner, Innsbruck.
- Bek, J., Oplustil, S., Drabkova, J. (2001): The species of *Selaginella* cones and their spores from the Bohemian Carboniferous continental basins of the Czech Republic. - Rev. Palaeobot. Palynol., 114: 57-81.
- Bergad, R. D. (1978): Ultrastructural studies of selected North American Cretaceous megaspores of *Minerisporites*, *Erlansonisporites*, *Horstisporites* and *Richinospora*, n. gen. - Palynology, 2: 39-51.

- Bernard, S., Benzerara, K., Beyssac, O., Brown, G. E. Jr., Grauvogel-Stamm, L., Düringer, P. (2009): Ultrastructural and chemical study of modern and fossil sporoderms by Scanning Transmission X-ray Microscopy (STXM). – Rev. Palaeobot. Palynol., 156: 248–261.
- Broglio Loriga, C., Fugagnoli, A., van Konijnenburg-van Cittert, J. H. A., Kustatscher, E., Posenato, R., Wachtler, M. (2002): The Anisian macroflora from the Northern Dolomites (Monte Prà della Vacca/Kühwiesenkopf, Braies): a first report. – Riv. Ital. Paleont. Stratigr., 108: 381–390.
- Collinson, M. E. (1991): Diversification of modern heterosporous pteridophytes. – In Blackmore, S., Barner, S. H. (eds.): Pollen and Spores. Systematic Association Special Volume, 44: 119–150, Clarence Press, Oxford.
- Cottman, C. F., Hemsley A. R., Rössler R., Collinson M. E., Brain, A. P. R. (2000): Diversity of exine structure in Upper Carboniferous (Westphalian) selaginellaceous megaspores. – Rev. Palaeobot. Palynol., 109: 33–44.
- Dettmann, M. E. (1961): Lower Mesozoic megaspores from Tasmania and South Australia. – Micropaleontology, 7 (1), 71–86.
- De Zanche, V., Gianolla, P., Mietto, P., Siorpaes, C., Vail, P. R. (1993): Triassic sequence stratigraphy in the Dolomites (Italy). – Mem. Sci. Geol., 45: 1 – 27.
- Fugagnoli, A., Posenato, R. (2004): Middle Triassic (Anisian) benthic Foraminifera from the Monte Prà della Vacca/Kühwiesenkopf section (Dont Fm, Braies Dolomites, Northern Italy). – Boll. Soc. Paleontol. Ital., 43 (3): 347–360.
- Guy-Olsson, D. (1979): A new species of *Densoisporites* (Weyland & Krieger) Dettman in the Jurassic of southern Sweden. – Grana, 18(2): 129–131.
- Halle, T. G. (1907): Einige krautartige Lycopodiaceen paläozoischen und mesozoischen Alters. – Kungl. Svensk. Vetenskapsakad. Handl., 7 (5): 1–17.
- Hemsley A. R., Scott, A. (1989): The ultrastructure of four Australian Triassic megaspores. – Pollen et Spores, 31: 133–154.
- Kempf, E. K. (1971): Electron microscopy of Mesozoic megaspores from Denmark. – Grana, 11: 151–163.
- Kempf, E. K. (1973): Transmission electron microscopy of fossil spores. – Paleontology, 16: 787–797.
- Koppelhus, E.B., Batten, D.J. (1989): Late Cretaceous megaspores from southern Sweden: morphology and paleoenvironmental significance. – Palynology, 13: 91–120.
- Kovach, W. L., (1989): Quantitative method for the study of lycopod megasporule ultrastructure. – Rev. Paleobot. Palynol., 57: 233–246.
- Kovach, W. L. (1994): A review of Mesozoic megasporule ultrastructure. – In: Kurmann, M. H., Doyle, J. A. (eds.): Ultrastructure of fossil spores and pollen, p. 23–38.
- Kovach, W. L., Dilcher, D. L. (1988): Megaspores and other dispersed plant remains from the Dakota Formation (Cenomanian) of Kansas, U.S.A. – Palynology, 12: 89–119.
- Krassilov, V. A. (1978): Mesozoic lycopods and ferns from the Bureja basin. – Palaeontographica, Abt. B., 166 (1–3): 16–29.
- Kustatscher, E. (2004): Macroflore terrestri del Triassico Medio delle Dolomiti e loro inquadramento bio-cronostratigrafico e paleoclimatico mediante palinomorfi. – 220 pp., unpublished PhD Thesis. University of Ferrara, Ferrara.
- Kustatscher, E., Manfrin, S., Mietto, P., Posenato, R., Roghi, G. (2006): New biostratigraphic data on Anisian (Middle Triassic) palynomorphs from the Dolomites (Italy). – Rev. Paleobot. Palynol., 140: 79–90.
- Kustatscher, E., Roghi, G. (2006): Anisian palynomorphs from the Dont Formation of Kühwiesenkopf / Monte Prà della Vacca section (Braies Dolomites, Italy). – Micropalaeontology, 52 (3): 223–244.
- Kustatscher E., Wachtler, M., van Konijnenburg-van Cittert J.H.A. (2010): Lycophytes from the Middle Triassic (Anisian) locality Kühwiesenkopf (Monte Prà della Vacca) in the Dolomites (Northern Italy). – Palaeontology, 53(3): in press.
- Lee, H. H., (1951): On some *Selaginellites* remains from the Tatung Coal series. – Science Record, 4 (2): 193–196.
- Looy, C. V., Collinson, M. E., Van Konijnenburg-Van Cittert, J. H. A., Visscher, H., Brain, A. P. R. (2005): The ultrastructure and botanical affinity of end-Permian spore tetrads. – Int. J. Plant Sci., 166(5): 875–887.
- Lugardon, B., Grauvogel-Stamm, L., Dobruskina, I. (1999): The microspores of *Pleuromeia rossica* Neuburg (Lycopida, Triassic): comparative ultrastructure and phylogenetic implications. – Compt. Rend. Acad. Scienc., ser. II, fasc. A, Scienc. Terr. Plan., 329 (6): 435–442.
- Lugardon, B., Grauvogel-Stamm, L., Dobruskina, I. (2000): Comparative ultrastructure of the megaspores of the Triassic lycopid *Pleuromeia rossica* Neuburg. – Compt. Rend. Acad. Scienc., ser. II, fasc. A, Scienc. Terr. Plan., 330 (7), 501–508.

- Lundblad, B. (1950): On a fossil *Selaginella* from the Rhaetic Hyllinge, Scania. - Svenska Botanisk Tidskrift, 44 (3), 475-487.
- Meyer-Melikian, N.R., Zavialova, N.E. (1996): Disperse distal-sulcate pollen grains from the Lower Jurassic of Western Siberia. - Botanich Zhurn., 81(6): 10-22 [In Russian].
- Minaki, M., (1984): Macrospore morphology and taxonomy of *Selaginella*. - Pollen et Spores, 26: 421-480.
- Morbelli, M. A. (1977): Esporas de las especies argentinas de *Selaginella* (Selaginellaceae-Pteridophyta). - Obra Cent. Mus. La Plata, 3: 121-150.
- Morbelli, M. A., Rowley, J. R., 1996. Application of confocal microscopy to exospore ultrastructure of megaspores of *Selaginella convoluta* and *S. marginata*. - J. Plant Res., 109: 33-44.
- Morbelli, M. A., Rowley, J. R., Claugher, D. (2001): Spore wall structure in *Selaginella* (Lycopodiophyta) species growing in Argentina. - Bol. Soc. Argent. Bot., 36(3-4): 315-368.
- Naugolnykh, S. V., Zavialova, N. E. (2004): *Densoisporites polaznensis* sp. nov.: with comments on its relation to *Viatcheslavia vorcutensis* Zalessky. - The Paleobotanist, 53: 21-33.
- Pal, P.K. (1984): Morphotaxonomy of heterophyllous Lycopod shoot from the Rajmahl Hills, India. - The Palaeobotanist, 32 (3): 321-325.
- Raine, J.I., N.J. De Jersey, and K.G.Ryan (1988): Ultrastructure and lycopod affinity of *Densoisporites pilatus* (de Jersey) comb. nov. from the Triassic of New Zealand and Queensland. - Mem. Ass. Australas. Palaeontols, 5: 79-88.
- Retallack, G.J., 1997. Earliest Triassic origin of *Isoetes* and Quillwort evolutionary radiation. - Jour. Palaeont., 71(3): 500-521.
- Retallack, G. J., Metzger, C. A., Graver, T., Jahren, A. H., Smith, R. M. H., Sheldon, N. D. (2006): Middle-Late Permian mass extinction on land. - Geol. Soc. Amer. Bull., 118: 1398-1411.
- Schimpfer, W. P. (1869): Traité de Paléontologie végétale ou la flore du monde primitif dans ses rapports avec les formations géologiques et la flore du monde actuel. - 738 pp., I. J. B. Baillière et Fils éd., Paris.
- Schweitzer, H.-J., van Konijnenburg-Van Cittert, J. H. A., van de Burgh, J. (1997): The Rhaeto-Jurassic flora of Iran and Afghanistan. 10. Bryophyta, Lycopodiophyta, Sphenophyta, Pterophyta-Eusporangiatae and -Protolептоспорангиятаe. - Palaeontographica, Abt. B, 243: 103-192.
- Senowbari-Daryan, B., Zühlke, R., Bechstädt, T., Flügel, E. (1993): Anisian (Middle Triassic) Buildups of the Northern Dolomites (Italy): The Recovery of Reef Communities after the Perm/Triassic Crisis. - Facies, 28: 181-256.
- Seward, A. C. (1910): Fossil Plants II – A Textbook for students of Botany and Geology. - 624 pp., Cambridge University Press, Cambridge.
- Skog, J. E., Hill, C. R. (1992): The Mesozoic herbaceous lycopsids. - Annals of the Missouri Botanical Garden, 79 (3): 648-675.
- Srivastava, G. K., Srivastava, P. C., Shukla, P. K. (1993): Antiquity and diversification of *Isoetes* through the ages. - In: Srivastava, P. C. (ed.): Vistas in Palaeobotany and Plant Morphology: Evolution and Environmental Perspectives, Prof. D.D. Pant Memorial Volume, U.P. Offset, Lucknow, India.
- Takahashi, M., Crane P.R., Ando, H. (2001): Fossil Megaspores of Marsileales and Selaginellales from the Upper Coniacian to Lower Santonian (Upper Cretaceous) of the Tamagawa Formation (Kuji Group) in Northeastern Japan. - Int. Journ. Plant Scienc., 162 (2): 431-439.
- Taylor, T. N., Taylor, E. J., Krings, M. (2009): The Biology and Evolution of plants. - 1230 pp., Elsevier, Amsterdam.
- Taylor, W. A. (1989): Megaspore wall organization in *Selaginella*. - Pollen et Spores, 31: 251-288.
- Taylor, W. A. (1994): Tests and application of a method of quantitative analysis of fossil and extant lycopod megaspore walls. - In: Kurmann, M. H., Doyle, J. A. (eds.): Ultrastructure of Fossil spores and Pollen. pp. 39-52, Royal Botanical Garden, Kew.
- Taylor, W. A., Taylor, T. N. 1988. Ultrastructural analysis of selected Cretaceous megaspores from Argentina. - J. Micropaleontol. 7: 73-87.
- Taylor, W. A., Taylor, T. N. (1990): Persistent ultrastructural features in microspores of heterosporous lycopophytes. - Grana, 29: 219-228.
- Telnova, O. P. (2004): New species of spores from the Devonian deposits of southern Timan Region. - Bull. Moscow Society of Naturalists, Biol., 109(1): 63-70 [in Russian].
- Thomas, B. A. (1992): Paleozoic herbaceous lycopsids and the beginnings of extant *Lycopodium* sens. lat. and *Selaginella* sens. lat. - Ann. Miss. Bot. Garden, 79: 624-631.
- Townrow, J.A. (1968): A fossil *Selaginella* from the Permian of New South Wales. - J. Linn. Soc. London Bot., 61: 13-23.

- Tryon, A. F., Lugardon, B. (1991): Spores of Pteridophyta: surface, wall structure and diversity based on electron microscope studies. - Springer. New York.
- Turnau, E., Zavialova, N., Prejbisz, A. (2009): Wall ultrastructure in some dispersed megaspores and seed-megaspores from the Middle Devonian of northern Poland. - Rev. Palaeobot. Palynol., 156: 14-33.
- Villar de Seoane, V., Archangelsky, S. (2008): Taxonomy and biostratigraphy of Cretaceous megaspores from Patagonia, Argentina. - Cretac. Res., 29: 354-372.
- Watson, J. (1969): A revision of the English Wealden flora. I. Charales - Ginkgoales. - Bull. Mus. Nat. Hist. Geol., 17: 207-254.
- Zeiller, R. (1906): Bassin houiller et Permien de Blanzy et du Creusot. II. Flore fossile. Études Gîtes Minéraux de la France. - 265 pp., Ministère des Travaux Publics, Paris.

Manuscript submitted: 25.1.2010

Revised manuscript accepted: 20.5.2010



FASZINATION ENGINEERING

ILF Beratende Ingenieure ZT GmbH
Feldkreuzstraße 3
6063 Rum bei Innsbruck
Österreich
Tel. (+43) 512 24 12-0
Fax (+43) 512 24 12-5900
Email info@ibk.ilf.com



SCHWERPUNKT GEOLOGIE, HYDROLOGIE UND GEOTECHNIK

Herausragende Projekte:

- A12 Inntalautobahn, Roppener Tunnel 2. Röhre
- Neubaustrecke Kundl/Radfeld - Baumkirchen
- Brenner Basistunnel - Abschnitt Franzensfeste und Erkundungsstollen Innsbruck / Ahrental
- Brennerkorridor von Kundl-Radfeld bis Aicha-Mauls, Wasserwirtschaftliche Beweissicherung
- Niagara Tunnel Project, Hydropower Plant
- Devil's Slide Tunnel and Caldecott Tunnel 4
- S10 Mühlviertler Schnellstraße
- Neubaustrecke Nürnberg - Ingolstadt
- Ausbau der Straßenverbindung Eschenlohe bis Garmisch-Partenkirchen
- Baku-Tbilisi-Ceyhan (BTC) Rohölpipeline
- Winter und Sommer Tourismus und Erholungskomplex „Shahdag“

GYMNOSPERM FOLIAGE FROM THE UPPER TRIASSIC OF LUNZ, LOWER AUSTRIA: AN ANNOTATED CHECK LIST AND IDENTIFICATION KEY

Christian Pott¹ & Michael Krings²

With 7 figures and 1 table

¹ Naturhistoriska riksmuseet, Sektionen för paleobotanik, Box 50007, SE-104 05 Stockholm, Sweden; christian.pott@nrm.se

² Department für Geo- und Umweltwissenschaften, Paläontologie und Geobiologie, Ludwig-Maximilians-Universität, and Bayerische Staatssammlung für Paläontologie und Geologie, Richard-Wagner-Straße 10, 80333 München, Germany; m.krings@lrz.uni-muenchen.de

Abstract

The famous Lunz flora from Lower Austria is one of the richest and most diverse Late Triassic floras of the Northern Hemisphere. The historical outcrops (mainly coal mines) are no longer accessible, but showy fossils can still be collected from natural exposures around the town of Lunz-am-See and from several of the old spoil tips. This paper presents an annotated check list with characterisations of all currently recognised gymnosperm foliage taxa in the Lunz flora. The descriptions are exemplified by illustrations of typical specimens and diagnostic features of the leaf morphology and epidermal anatomy. Moreover, a simple identification key for the taxa based on macromorphological features is provided that facilitates identification of newly collected specimens.

1. Introduction

The Carnian (Late Triassic) flora from Lunz in Lower Austria is one of only a few well-preserved floras from the Alpine Triassic (Cleal, 1993; Dobruskina, 1998). The flora includes sphenophytes, ferns, cycadaleans, bennettitaleans, conifers, and putative ginkgophytes (Dobruskina, 1989, 1998), and is currently comprised of more than 4,000 specimens (compressions) kept in various museum, geological survey, and university collections in Austria and beyond. The Lunz flora represents one of the richest and most diverse Late Triassic floras of the Northern Hemisphere. Although the classic outcrops (mainly coal mines) are long since closed, Lunz fossils can still be collected from several natural exposures around the town of Lunz-am-See (Figure 1), as well as from some of the old spoil tips in the vicinity of the coal mines. Apart from the unusually high proportion of fertile ele-

ments (i.e. reproductive structures) among the fossils (see e.g., Krasser, 1917, 1919; Kräusel, 1948, 1949, 1953; Pott et al., 2010), the most striking feature of the Lunz flora is the superabundance of exquisitely preserved gymnosperm foliage.

It has been suggested that the Lunz flora represents a standard for Carnian floras that can be used for the identification, correlation, and comparison of coeval and slightly younger Mesozoic floras elsewhere (Dobruskina, 1989, 1998). In order to fully serve this purpose, however, a detailed documentation of the composition of the Lunz flora, together with user-friendly identification keys for, and descriptions of, the individual taxa are instrumental. Such tools have not been available to date since the various elements of the Lunz flora have been (formally) described in series of separate papers by different authors (e.g.,

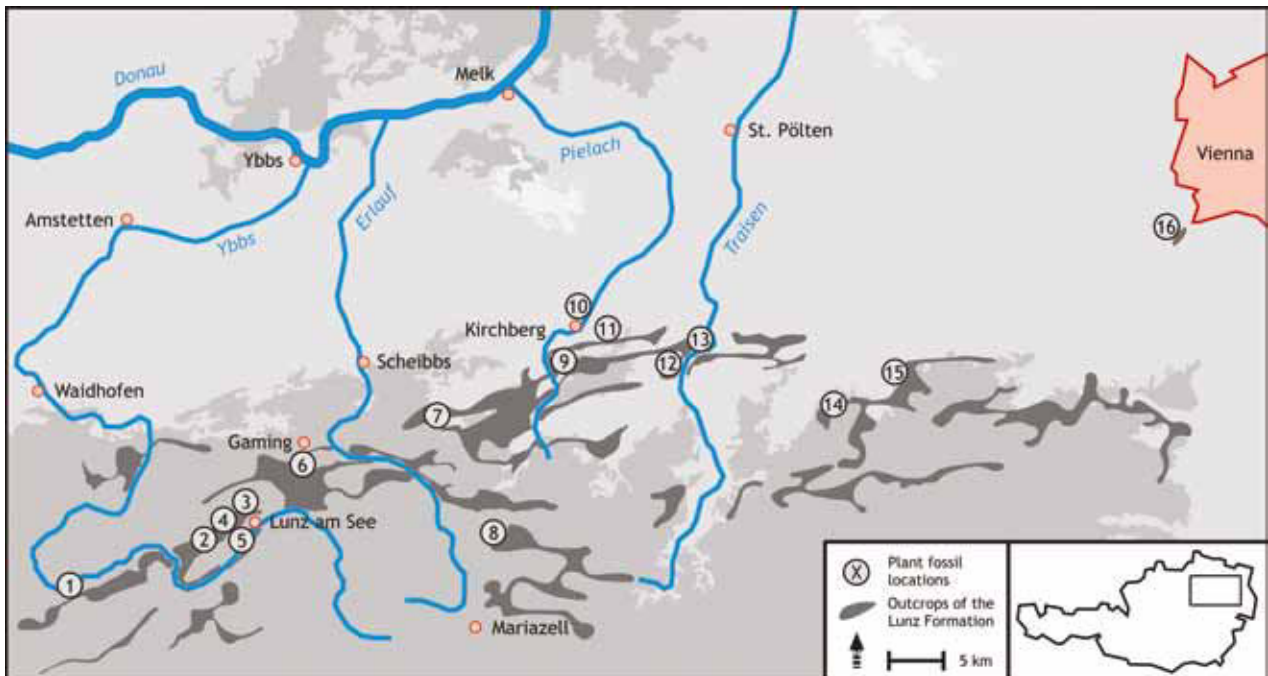


Figure 1

Map of the area of Lunz-am-See in Lower Austria showing the historical fossil localities. 1-Hollenstein/Ybbs, 2-Ahornberg, 3-Holzapfel, 4-Pramelreith, 5-Lunz am See, 6-Gaming, 7-Sankt Anton/Jeßnitz, 8-Wienerbrück, 9-Loich, 10-Kirchberg/Pielach, 11-Tradigist, 12-Schrambach, 13-Lilienfeld, 14-Kleinzell, 15-Ramsau, 16-Kaltenleutgeben.

Stur, 1871, 1885, 1888; Krasser, 1909a–b; Kräusel, 1921, 1943, 1949; Kräusel & Schaarschmidt, 1966, and subsequent synopses did not include detailed descriptions of individual taxa (e.g., Dobruskina, 1998). Moreover, some of the historical binominals that were established based on Lunz fossils are invalid, and only a few forms are sufficiently illustrated.

During the last six years, a research project focusing on the entirety of gymnosperm foliage fossils from Lunz has been conducted that resulted in a revision and detailed photographic documentation of most of the taxa based on both macromorphology and epidermal anatomy (Pott et al., 2007a–e). Based on the results from this project, we have compiled an annotated check list with brief descriptions for all currently recognised gymnosperm foliage taxa in the Lunz flora that is presented in this paper. The descriptions are accompanied by illustrations of typical specimens and of characteristic features of the morphology and epidermal anatomy. Moreover, an identification key for the taxa is given. A synopsis at the end of the paper lists the various names historically assigned to the gymnosperm foliage fossils from Lunz against the current binominals that are based on our revision (Table 1).

Brief overview of the genera and species

Thirteen gymnosperm foliage taxa, in the rank of species, are currently recognised in the Lunz flora, including five bennettitalean and five cycadalean foliage types, two putative ginkgophytes, and one conifer. In the following sections, brief characterisations of the macromorphology of these foliage types are given. Information on the epidermal anatomy is provided for those taxa that have yielded cuticles and where species definition and discrimination from morphologically similar forms heavily rely on epidermal features such as the architecture of the stomatal apparatus.

BENNETTITALES

Genus *Pterophyllum* Brongniart, 1825

Pterophyllum is a morphogenus used for bennettitalean foliage characterised by segmented leaves with laterally or almost laterally inserted, almost parallel-sided leaf segments or leaflets (Figure 2), a striate rachis and cuticles displaying brachyparacytic (syndetocheilic) stomata (Pott et al., 2007e; Pott



Figure 2
Midrib portion of leaves of *Pterophyllum* (above) and *Nilssonia* (below), illustrating the two different types of leaflet insertion (above: lateral insertion; below: adaxial insertion).

& McLoughlin, 2009; syndetochilelic in the sense of Thomas, 1930; Florin, 1933; Harris, 1969a; Van Konijnenburg-van Cittert, et al., 2001). Two species assignable to *Pterophyllum*, *P. filicoides* and *P. brevipenne*, occur in the Lunz flora. They represent by far the most common sterile gymnosperm foliage taxa, and are present on nearly every slab.

***Pterophyllum filicoides* (Schlotheim, 1822)**
Zeiller, 1906

Estimated total leaf size: up to 60 cm long (probably more) and 20 cm wide
Characters: segmented, leaflets insert laterally to rachis, terminal leaflet similar in shape and size to lateral ones, leaflet length/width ratio always >7:1.
Figures: 3G, H; 4H, K, L

Pterophyllum filicoides leaves are petiolate impari-segmented and oblong to broadly oval. The largest specimens (all incomplete) from Lunz are ~47 cm long and 20 cm wide. The lamina is subdivided into numerous long and narrow, parallel-sided to spatoolate leaflets, which are oppositely arranged, >100

mm long and 2–9 mm wide. Leaflets insert laterally to the prominent and longitudinally striate rachis and are basally more or less constricted. Constriction is usually prominent in leaflets positioned in the proximal portion of the leaf, but rather indistinct or absent in distally positioned leaflets. Leaflet apices are obtuse to acutely rounded. The length/width-ratio of the leaflets is always >7:1; in some specimens, it reaches up to 22:1. The distal five leaf segments form the apex. The terminal leaflet does not differ in shape from the laterally positioned subterminal leaflets. Numerous parallel veins enter each leaflet and usually fork once near the base. Occasionally additional bifurcations occur in the proximal portions of the leaflets.

Cuticles of *Pterophyllum filicoides* are well-known. The leaves are amphistomatic but with only a few stomata present on the adaxial side, and produce robust cuticles; costal and intercostal fields are distinguishable on both sides of the leaf. Occurrence of stomata is limited to the intercostal fields. Epidermal cells are narrow, rectangular, and elongate to isodiametric (square) in outline. Anticlinal cell walls are generally straight, but cells on the abaxial side may occasionally display faint and irregular undulations. Cells often bear a long and hollow papilla. The diacytic stomatal complexes are brachyparacytic; stomatal pores are oriented perpendicularly to the veins, stomata are slightly sunken (see Pott et al., 2007e).

***Pterophyllum brevipenne* Kurr ex Schenk, 1864
emend. Pott et al., 2007**

Estimated total leaf size: up to 25 cm long (probably not longer) and 6 cm wide

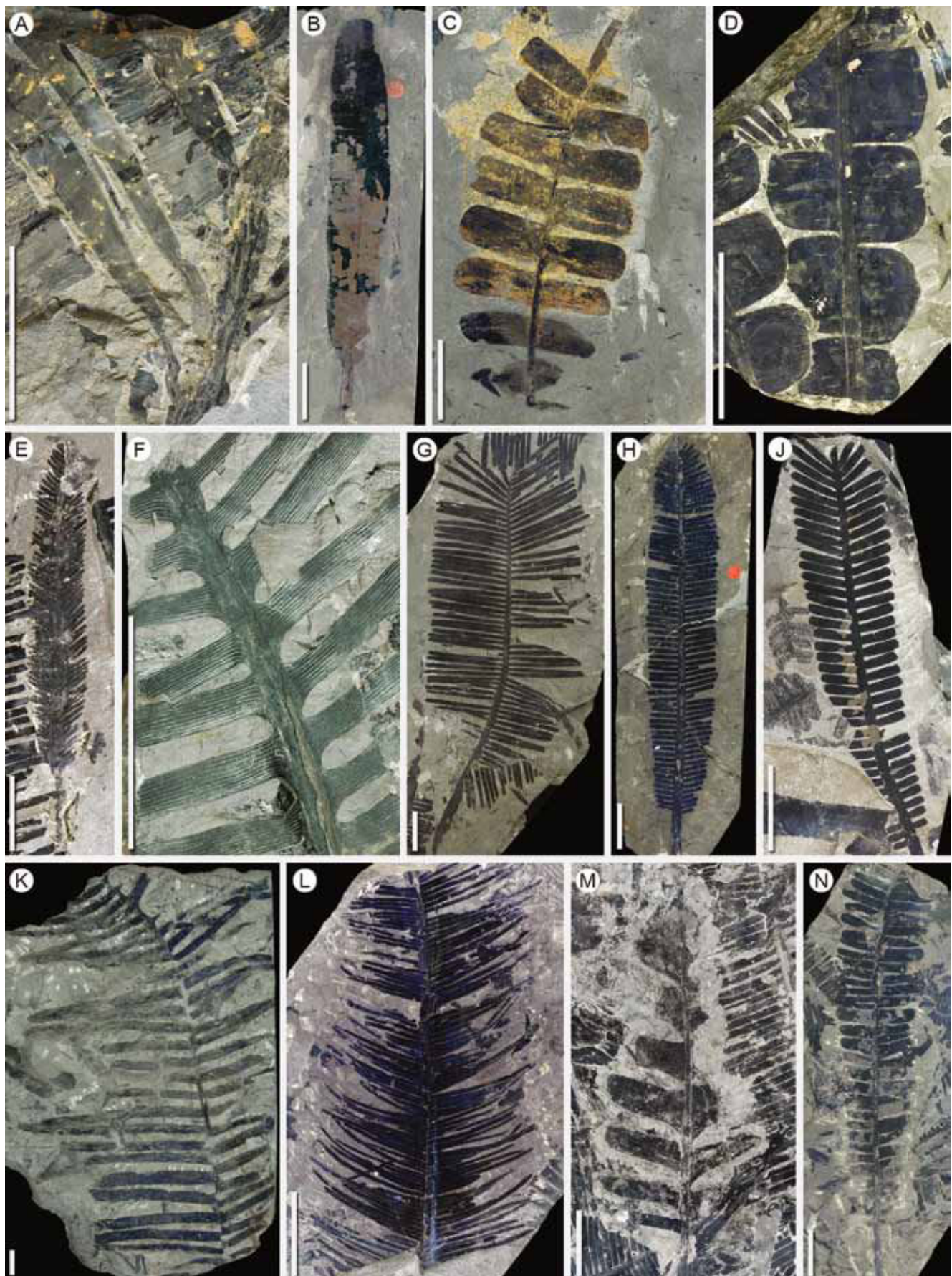
Characters: segmented, leaflets insert laterally to rachis, terminal leaflet differs from lateral ones, leaflet length/width ratio always <7:1.

Figures: 3J; 4J, M

Pterophyllum brevipenne, leaves are petiolate and impari-segmented. They differ from *P. filicoides* in that they are oblong and more lanceolate or spatulate to inverted-conical in outline. The largest leaf portions are up to 22.7 cm long and 6 cm wide. The lamina is subdivided into numerous narrow and short, spatoolate leaflets, which are oppositely arranged and closely spaced. Leaflets are up to 27 mm long and 2.5–5 mm wide. Proximal leaflets are short, but increase in length toward the distal third of the leaf.

Figure 3

Gymnosperm foliage fossils from Lunz. A-*Arberophyllum florinii* (NHMW 1889/VI/0008), B-*Nilssoniopteris angustior* (GBAW 1909/002/0187), C-*Nilssoniopteris lunzensis* (NHMW 1888/I/0018), D-*Nilssoniopteris haidingeri* (NHMW 2006B0008/0042), E-*Stachytaxis (Elatocladus) lipoldii* (NRM S148587), F-*Pseudoctenis cornelii* (NHMW 1887/I/0037), G, H-*Pterophyllum filicoides* (NRM S148314, GBAW 1909/003/0403), J-*Pterophyllum brevipenne* (NHMW 1884/D/1209), K-*Nilssonia neuberi* (GBAW 2006/004/0014), L-*Nilssonia riegeri* (GBAW 1909/003/0589), M-*Nilssonia lunzensis* (NRM S148602), N-*Nilssonia sturii* (GBAW 1909/003/0396). Scale bars 2 cm.



The proximal one or two leaflets often lack counterparts on the opposite side of the rachis. The leaflets are usually broadly attached to the rachis, but may occasionally display a distinct basal constriction. They are bluntly rounded apically. The length/width-ratio of the leaflets ranges from 4:1 to 6:1 but is always <7:1. The segments insert laterally to the prominent and longitudinally striate rachis. The apical portion of the leaf usually consists of three, sometimes up to five, leaflets; the terminal leaflet usually differs in morphology from the laterally positioned ones in that it is more rounded in outline and distinctly wider distally. Numerous parallel veins enter each of the leaflets. Veins usually fork once near the base. Additional vein bifurcations may sporadically occur; however, the occurrence of additional bifurcations is not limited to the proximal portion of the leaflet as it is in the very similar *P. filicoides*.

Leaves are amphistomatic but with only a few stomata present on the adaxial surface, and produce robust cuticles; costal and intercostal fields are distinguishable on both sides of the leaf. Occurrence of stomata is limited to the intercostal fields. Adaxial stomatal density in *Pterophyllum brevipenne* is distinctly higher than that of *P. filicoides*. Epidermal cells are rectangular, and elongate to isodiametric (square) in outline. Anticlinal cell walls are straight. In contrast to *P. filicoides*, anticlinal cell walls in *P. brevipenne* are never sinuous or faintly undulating. Cells often bear a long and hollow papilla. The diacytic stomatal complexes are brachyparacytic; stomatal pores are oriented perpendicularly to the veins, stomata are slightly sunken (see Pott et al., 2007e).

Genus *Nilssoniopteris* Nathorst, 1909 emend. Pott et al., 2007

Nathorst (1909) introduced the genus *Nilssoniopteris* for entire-margined cycadophyte leaves from the Jurassic of Europe. With regard to macromorphology, some *Nilssoniopteris* fossils may resemble *Anomozamites* Schimper, 1870 emend. Harris, 1969a (see Pott & McLoughlin, 2009). Typical representatives of *Nilssoniopteris* are characterised by an entire-margined leaf lamina. However, some specimens from Lunz show a lamina that is partially lobed or dissected up to the rachis. Fully segmented leaves are traditionally assigned to *Anomozamites*. However, several authors, e.g., Harris (1969a) and Boyd (2000), have illustrated intermediate types. Unfortunately,

the information available on the epidermal anatomy of *Anomozamites* is incomplete (Harris 1969a; Pott & McLoughlin, 2009) and does not provide features useful in the discrimination of *Anomozamites* from *Nilssoniopteris*. Boyd (2000) emended the diagnosis of *Nilssoniopteris* to include the lobed leaves that are intermediate between *Nilssoniopteris* and *Anomozamites* and display bennettitalean epidermal anatomy. In order to include also leaves dissected down to the rachis, Pott et al. (2007c) further expanded Boyd's (2000) diagnosis of *Nilssoniopteris*.

Three morphospecies of *Nilssoniopteris*, i.e. *N. haidingeri*, *N. angustior* and *N. lunzensis*, have recently been described from Lunz (Pott et al., 2007c) based on specimens that were originally interpreted as marattialean ferns of the genus *Macrotaeniopteris* Schimper, 1869 by Krasser (1909a). Epidermal anatomy, especially stomatal morphology, demonstrates that they in fact belong to the Bennettiales.

Nilssoniopteris haidingeri (Krasser, 1909) Pott et al., 2007

Estimated total leaf size: up to 70 cm long and 15 cm wide

Characters: usually entire-margined, but may also be partly segmented; lanceolate, lamina/leaflets insert laterally to rachis

Figures: 3D; 4E, G

Nilssoniopteris haidingeri leaves are quite large, (up to nearly 70 cm long and 15 cm), petiolate entire-margined or partially segmented, almost regular, broadly oval or oblong to lanceolate in outline, and have an obtuse-rounded apex. The rachis is markedly striate. The lamina is usually coarsely divided into several squarish segments that are oppositely to suboppositely arranged and insert laterally to the rachis. Segmentation is typically more profound in the proximal portion of the lamina. Segments are 2–4 cm long and 3–13 cm wide, and generally increase in length toward the leaf apex; some may taper distally and become slightly wider proximally. The width of the individual segments varies considerably; some are more than twice as wide as others. Numerous parallel veins enter each segment and run straight to the margin. Veins usually fork twice in the basal part of the segment.

The cuticles provide evidence that the leaves are amphistomatic; stomatal density is considerably high-

her on the abaxial side of the leaf. The leaves have robust cuticles. Costal and intercostal fields are distinct on the abaxial, but indistinct on the adaxial side of the leaf. The epidermal cells are rectangular and elongate to isodiametric in outline. Anticlinal walls are smooth. Epidermal cells on the abaxial side often bear a small, solid papilla. Stomata are slightly sunken and only occur close to the rachis on the adaxial side of the leaf, while they are regularly distributed within the intercostal fields on the abaxial side. Stomata are brachyparacytic; stomatal pores are orientated perpendicular to the veins. Subsidiary cells are often slightly more heavily cutinised than the normal epidermal cells. The arrangement of epidermal cells in distinct rows gradually disappears towards the rachis. Epidermal cells positioned close to the lamina margin are much smaller than cells located in the middle portion of the lamina (see Pott et al., 2007c).

Remark: The material was originally assigned to *Taeniopteris haidingeri* Goeppert mnsc. nec Ett. by Stur (1885), which is a nomen nudum and not conspecific with *T. haidingeri* Ettingshausen, 1851 (a marattialean fern), as clearly stated by Stur (1885: 'nec'). Krasser (1909a) transferred the material to a different genus (i.e. *Macrotaeniopteris*) and *M. haidingeri* is a valid name; it has a good diagnosis, illustrations were not necessary before 1912. Pott et al. (2007c) assigned all species of *Macrotaeniopteris* from Lunz to *Nilssoniopteris* based on the bennettitalean nature of their cuticles but erroneously named this species *Nilssoniopteris haidingeri* (Stur ex Krasser); the correct indication of authorities is *Nilssoniopteris haidingeri* (Krasser) Pott et al., 2007.

Nilssoniopteris angustior (Stur ex Krasser, 1909) Pott et al., 2007

Estimated total leaf size: up to 35 cm long and 6 cm wide

Characters: segmented, leaflets insert laterally to rachis
Figures: 3B; 4C, D

Nilssoniopteris angustior leaves appear to have been relatively large (the largest fragments are up to 29 cm long and 5.2 cm wide). They are petiolate, narrow, oblong to lanceolate in outline, and have an acute apex. The lamina is not subdivided into segments, but occasionally growth aberrations of the leaf margin occur that resemble faint lobations. The

lamina is inserted laterally to the striate rachis. It is very narrow close to the petiole, but then rapidly increases in width. Numerous parallel veins enter perpendicular to the lamina and run straight to the margin. Veins usually fork twice close to the rachis.

Cuticles reveal that the leaves are amphistomatic, and stomatal density is considerably higher on the abaxial side of the leaf. The leaves have relatively thin cuticles. Costal and intercostal fields are not clearly differentiated. Epidermal cells are isodiametric, usually rectangular. Virtually every epidermal cell possesses a distinct central cuticular thickening on the outer periclinal wall. This feature becomes more distinct towards the margin of the lamina. Anticlinal cell walls are smooth and well cutinised, partly with triangular cuticular thickenings in the cell corners. Stomata are brachyparacytic, slightly sunken, and occur sporadically in areas close to the rachis on the adaxial side, while stomata and subsidiary cells on the abaxial side are arranged in long rows that are orientated perpendicularly to the rachis; stomatiferous rows alternate with non-stomatiferous bands of cells (see Pott et al., 2007c).

Nilssoniopteris lunzensis (Stur ex Krasser, 1909) Pott et al., 2007

Estimated total leaf size: up to 25 cm long and 7 cm wide

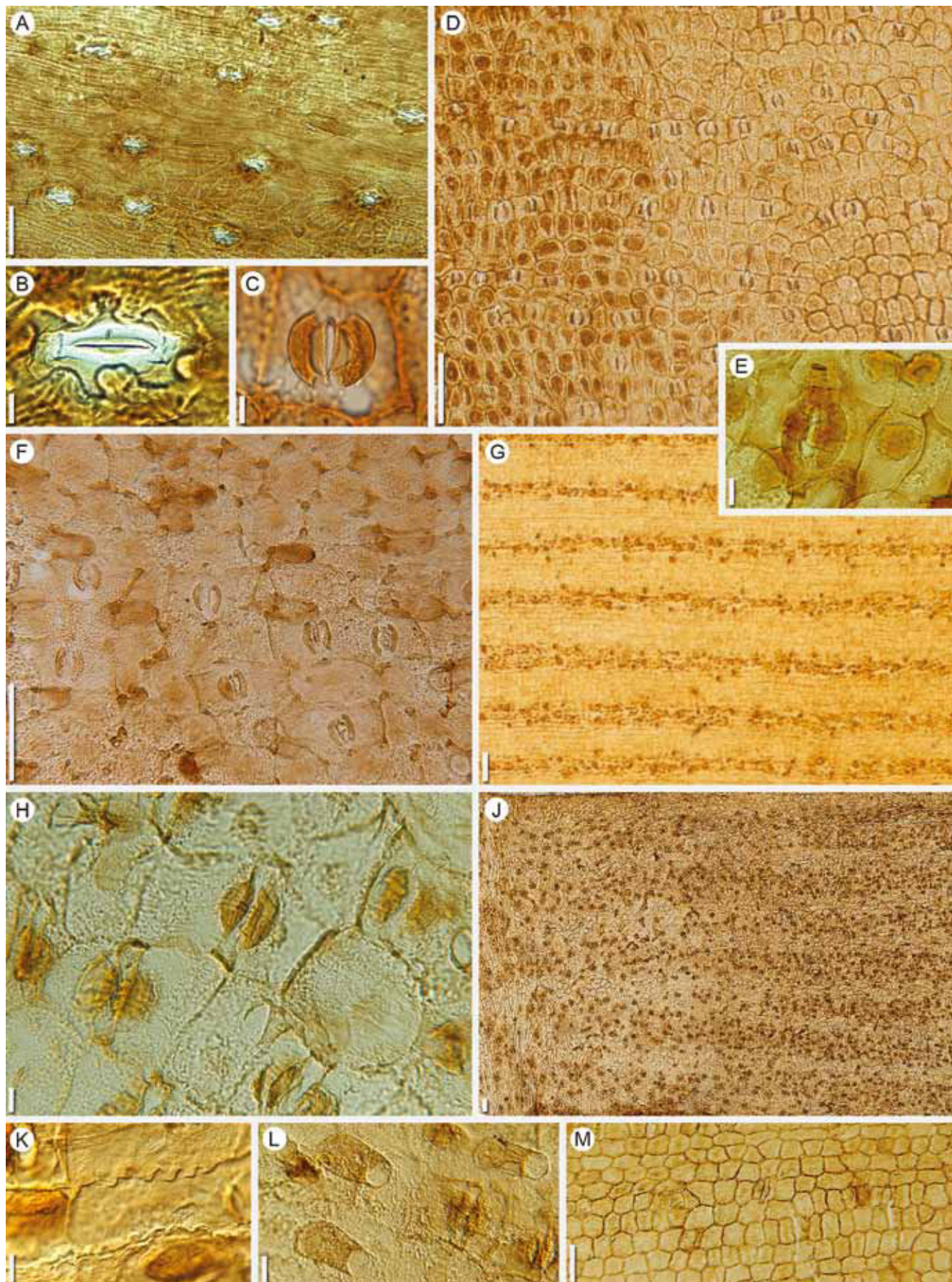
Characters: segmented, leaflets insert laterally to rachis, terminal leaflet differ from lateral ones

Figures: 3C; 4F

Nilssoniopteris lunzensis is characterised by relatively small petiolate leaves (up to 17.2 cm long and 6.2 cm wide). They are imparipinnate, lanceolate to oval in overall outline and possess a longitudinally striate rachis. The lamina is subdivided into individual segments, which insert laterally to the rachis. Leaf segments are broadly attached, slightly decurrent, irregularly to regularly opposite in position and up to 32.0 mm long and between 4.4 mm and 17.5 mm wide. The apex is formed by the uppermost three leaf segments. Individual leaf segments are more or less rectangular in outline and obtusely rounded apically. The apical leaf segment differs from the lateral segments in being much narrower; however, it is rarely preserved. Numerous parallel veins enter each leaf segment. Veins usually fork once or twice immediately after entering the segment. This species may

Figure 4

Gymnosperm foliage cuticles (ginkgophytes and bennettitaleans). A, B—*Arberophyllum florinii* (abaxial cuticle and stoma, NHMW 1886/I/0022/0001), C, D—*Nilssoniopteris angustior* (stoma, NHMW 1884/0015/0012; and abaxial cuticle, NHMW 1884/0015/0010), E—*Nilssoniopteris haidingeri* (stoma, NHMW 1885/D/3983/0003), F—*Nilssoniopteris lunzensis* (abaxial cuticle, NHMW 1885/D/4021/0001), G—*Nilssoniopteris haidingeri* (abaxial cuticle, GBAW 1909/002/0247/0008), H—*Pterophyllum filicoides* (abaxial cuticle, NHMW 1884/0021/0007), J—*Pterophyllum brevipenne* (abaxial cuticle, GBAW 2006/004/0003/0001), K, L—*Pterophyllum filicoides* (sinuous cell walls, GBAW 1909/003/0518/0005; and papillae, GBAW 1909/003/0518/0005), M—*Pterophyllum brevipenne* (adaxial cuticle, NHMW 1885/D/4087/0003). Scale bars 100 µm (A, D, F, G, J, M), 10 µm (B, C, E, H, K, L).



be confused with *Pterophyllum*; however, leaflets are much wider in *N. lunzensis* than in both *Pterophyllum* species known from Lunz (see above).

Cuticles are well-known. The leaves are amphistomatic; however, stomatal density is considerably higher on the abaxial side of the leaf. Cuticles are robust; costal and intercostal fields are not clearly differentiated. Epidermal cells are isodiametric, typically rectangular or squarish, not or only slightly elongated. Anticinal cell walls are smooth and sometimes have triangular cuticular thickenings in the corners. A central idiocuticular thickening may occur on the outer periclinal cell wall. Stomata sporadically occur on the adaxial side, while they are arranged in long rows orientated perpendicular to the rachis on the abaxial side. The stomatiferous rows alternate with non-stomatiferous bands of cells. Stomata are brachyparacytic, sunken, and the pores are orientated perpendicular to the cell rows. Long and hollow papillae may occur on the epidermal cells of both leaf sides (see Pott et al., 2007c).

CYCADALES

Genus *Nilssonia* Brongniart, 1825

Brongniart (1825) introduced the genus *Nilsonia* for once-pinnate leaves from the Lower Jurassic of Scania (Sweden) that are characterised by a prominent venation. The spelling *Nilsonia*, which is sometimes seen in the older literature, is a typographical error, and the spelling *Nilssonia* is today widely accepted in literature. The most important character used to distinguish *Nilssonia* leaves from *Pterophyllum* is the insertion of the leaf segments to the rachis. Segments are inserted to the upper side of the rachis in *Nilssonia*, while they are laterally inserted in *Pterophyllum* (Figure 2). Additional characters of *Nilssonia* leaves include conical to tongue-shaped leaf segments and veins that do not fork. Cuticles show in most cases actinocytic (or more rarely cyclocytic) stomata (haplocheilic in the sense of Florin, 1933) and often papillate surfaces.

Four species are currently recognised in the Lunz flora, including *Nilssonia sturii*, *N. riegeri*, *N. lunensis* and *N. neuberi*. *Nilssonia sturii* is the most common representative of the genus in the Lunz flora.

Nilssonia sturii Krasser, 1909 emend.

Pott et al., 2007

Estimated total leaf size: up to 80 cm long and 26 cm wide

Characters: segmented, leaflets inserted to the upper side of rachis, terminal leaflet unknown, veins unforked

Figures: 3N; 5B, E, F

Nilssonia sturii leaves are petiolate, pinnate (segmented), of almost regular, oblong, more or less lanceolate shape; the apex remains unknown. The lamina is subdivided into numerous, irregularly oppositely positioned segments whose length continuously decreases towards the leaf tip. Segments are crescent- to sword-shaped, all of the same general shape, distally tapering and slightly widened at the base. The width of the individual segments may vary considerably, some segments being twice as wide as others. Segments are attached to the upper side of the rachis. Numerous parallel, unforked veins enter each segment and run straight to the segment tip. In adaxial surface view, the prominent rachis is nearly completely covered by the bases of the leaf segments. The largest incomplete leaf portions from Lunz are up to 54.5 cm long and 26.2 cm wide. Leaf segments are up to 13.2 cm long and ranging from 6.7 mm up to 18.8 mm in width at their base.

Cuticles are delicate, but well-known for this species. Leaves are hypostomatic. Costal and intercostals fields are distinguishable on the abaxial but not on the adaxial side. Epidermal cells are polygonal or rectangular in outline, elongate with acute or pointed ends. Anticinal cell walls are smooth. Stomata are absent from the adaxial side, which does not show any other special features. The epidermis of the abaxial side shows a clear differentiation into costal and intercostal fields. Every second or third cell bears a short, thick-walled, hollow papilla positioned at one end of the cell. Stomata are irregularly orientated within the intercostal fields. Actinocytic stomatal apparatus are mono- to diacyclic, with 6–8 trapezoid to rectangular subsidiary cells (see Pott et al., 2007a).

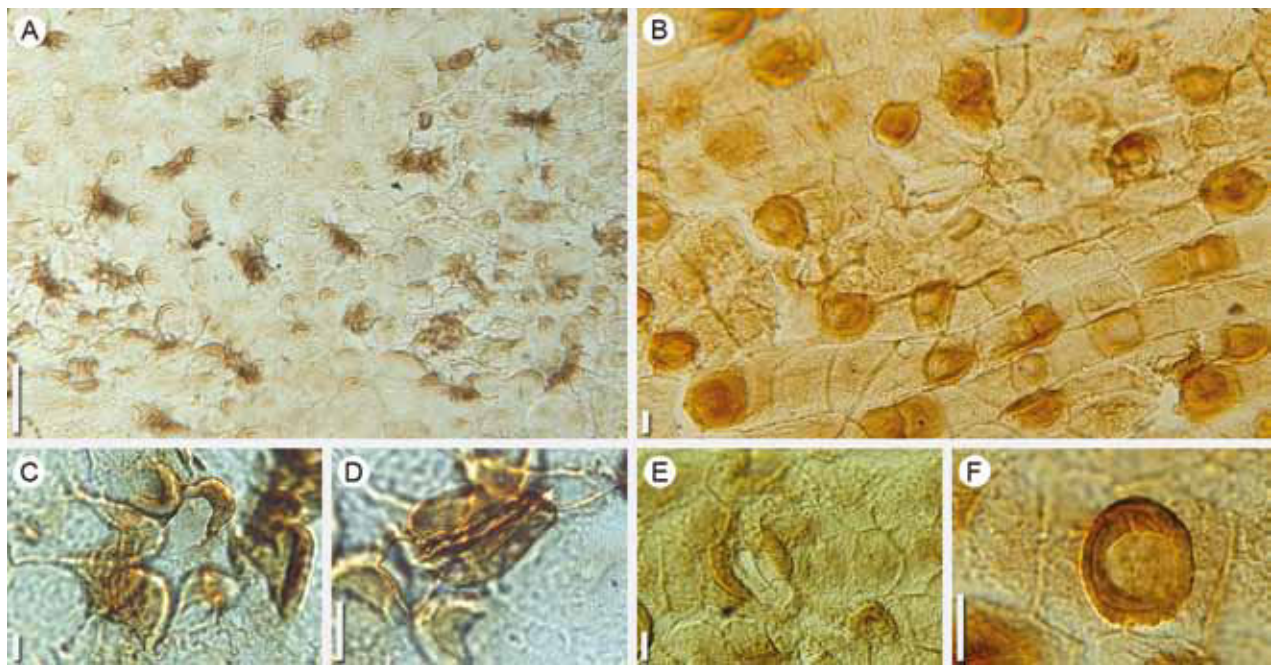


Figure 5
Gymnosperm foliage cuticles (cycadaleans). A–*Pseudoctenis cornelii* (abaxial cuticle, NHMW 2007B0002/0005), B–*Nilssonia sturii* (abaxial cuticle, GBAW 1909/002/0518/0007), C, D–*Pseudoctenis cornelii* (stomata, NHMW 2007B0002/0005), E, F, *Nilssonia sturii* (stoma and papilla, GBAW 1909/002/0518/0006). Scale bars 100 µm (A), 10 µm (B–F).

Nilssonia riegeri (Stur ex Krasser, 1909)

Pott et al., 2007

Estimated total leaf size: up to 35 cm long and 9 cm wide

Characters: segmented, leaflets inserted to the upper side of rachis, terminal leaflet unknown, veins unforcked

Figure: 3L

Nilssonia riegeri leaves are oblong to lanceolate in outline, pinnate, and the narrow leaf segments are densely spaced. The lamina is subdivided into numerous, irregularly faced, narrow and lanceolate segments. Segments are attached to the upper side of the rachis in a way that they cover most of the rachis. Individual segments taper towards the tip, which results in an irregular outline of the leaf. Leaf segments are narrow, basally slightly expanded, the tip is rounded. All segments are almost equal in width, bent slightly towards the leaf apex, more than five times as long as wide. Five to eight parallel, unforked veins enter the segments. Incomplete leaves are up to 16.0 cm long and 8.9 cm wide. Leaf segments are up to 5.2 cm long; their width ranges between 1.7 mm and 3.3 mm.

Leaves are amphistomatic and possess delicate cuticles. Costal and intercostals fields are distinguishable on the abaxial, but not on the adaxial side. Epidermal cells are polygonal or rectangular, elongate with acute or pointed ends. The adaxial and abaxial cuticles of *Nilssonia riegeri* are quite similar to those of *N. sturii*, morphologically as well as with regard to cell sizes, but *N. riegeri* differs from *N. sturii* in having stomata on the adaxial side. The monocyclic stomata of *N. riegeri* are oriented irregularly. Stomata are surrounded by an actinocytic ring of 6–8 trapezoid to rectangular subsidiary cells (see Pott et al., 2007a).

Nilssonia lunzensis Stur ex Pott et al., 2007

Estimated total leaf size: up to 50 cm long and 15 cm wide

Characters: segmented, leaflets inserted to the upper side of rachis, terminal leaflet rhomboidal

Figure: 3M

Nilssonia lunzensis leaves are characterised by impari-pinnate, individual segments, which are attached to the upper side of the rachis, strongly decurrent basiscopically and tapering towards their tips, resulting in a rather open appearance of the leaf.



Figure 6
Ginkgoites lunzensis (GBAW 1942/001/0002). Scale bar 1 cm.

The differences in width of the individual segments, some being twice as wide as the adjacent, create an irregular appearance. The overall outline of the leaf is oblong to pointed-oval. Segment length gradually decreases towards the leaf apex. The apex consists of a large terminal segment that is rhomboidal in outline. Leaf segments are bent towards the leaf apex. Numerous parallel veins enter each segment at angles of c. 80°, and run straight towards the segment tip without forking; each vein consists of two narrow vascular strands. Incomplete leaves from Lunz are up to 24.6 cm long and 13.9 cm wide. Individual leaf segments are up to 85.0 mm long and 16.8 to 42.1 mm wide.

Studying the cuticles of this form is difficult since they are very delicate. Leaves are amphistomatic. A differentiation into costal and intercostal fields is recognisable on both the adaxial and abaxial epidermis. Cells are elongate, rectangular to polygonal or isodiametric in outline, occasionally ending acutely. Anticlinal cell walls are smooth and heavily cutinised. Stomata are confined to the intercostal fields, irregularly oriented and slightly sunken; they are monocyclic with a ring of 6–7 polygonal subsidiary cells (see Pott et al., 2007a).

Nilssonia neuberi Stur ex Pott et al., 2007

Estimated total leaf size: up to 150 cm long and 40 cm wide

Characters: segmented, leaflets inserted to the upper side of rachis, terminal leaflet unknown, veins unforked

Figure: 3K

Nilssonia neuberi leaves clearly differ from all other *Nilssonia* species in the Lunz flora by their large size. Leaves are robust, regularly pinnate with leaf segments widely spaced. Individual leaf segments are slightly decurrent, attached to the upper side of the rachis, long and narrow in outline, and hardly tapering towards their tips. The striate rachis is remarkably thin. Leaf petiole and apex remain unknown. Venation is dense, and consisting of a large number of parallel, unforked veins that enter the leaf segments at 90° angles. The largest incomplete leaf portions are 52.5 cm long and 39.3 cm wide, with segments of each up to 23.3 cm long and 12.3–26.4 mm wide.

Cuticles are delicate and rather poorly preserved. Leaves are hypostomatic; costal and intercostals fields are distinguishable only on the abaxial side. Epidermal cells are rectangular, elongate, and narrow to isodiametric in outline. Anticlinal cell walls are straight, periclinal walls smooth, some bearing a thick-walled hollow papilla. Haplocheilic stomata are randomly oriented, monocyclic, and sunken (see Pott et al., 2007a).

Genus *Pseudoctenis* Seward, 1911

The genus *Pseudoctenis* was introduced by Seward (1911) for *Zamites*-type leaves from the Jurassic of Sutherland, Great Britain. However, Seward did not provide a generic diagnosis, but only a comparison to *Ctenis* Lindley et Hutton, 1834 (cycadalean foliage). Although *Ctenis* and *Pseudoctenis* are similar in macromorphology, Seward (1911) noted that they are easily distinguishable based on the occurrence of anastomoses in the venation of *Ctenis*. Harris (1950) concurs with Seward (1911) in that the *Ctenis/Pseudoctenis* series consists of two distinct groups.

The epidermal anatomy of the type species *Pseudoctenis eathiensis* Seward, 1911, and of two addi-

Identification key

- 1 Lamina entire-margined 2
 - Lamina partially or completely segmented 3
- 2 Leaves lack petioles and rachis, tongue-shaped,
narrow, up to 1.5 cm wide and 20 cm long *Arberophyllum florinii* (A)
 - Leaves with distinct robust rachis,
up to 6 cm wide *Nilssoniopteris angustior* (B)
- 3 Segments inserted laterally to rachis 4
 - Segments inserted to upper side of rachis 9 (*Nilssonia*)
- 4 Segments broad, laminar,
less than 3 times longer than wide 5
 - Segments narrow, more than 3 times longer
than wide 6
- 5 Leaves completely segmented, segments narrow,
leaf length <20 cm *Nilssoniopteris lunzensis* (C)
 - Leaves only partially segmented, entire-margined
at base and/or tip, large segments, leaves large,
up to 60 cm long *Nilssoniopteris haidingeri* (D)
- 6 Segments actually represent individual leaves,
each with a single central vascular strand (vein);
leaves densely arranged, arcuated towards tip,
leafy twigs small *Elatocladus (Stachyotaxus) lipoldii* (E)
 - Segments with more than 5 parallel veins 7
- 7 Segments long, conical towards tip, segment
base decurrent, typically loosely spaced,
venation robust *Pseudocetenis cornelii* (F)
 - Segments parallel-sided or conical towards base,
segment bases not decurrent, consistently
densely spaced, venation dense, veins delicate 8 (*Pterophyllum*)
- 8 Segments parallel-sided, long, always >7 times
longer than wide, apical segment identical to
lateral ones, leaves parallel-sided, >50 cm long *Pterophyllum filicoides* (G)
 - Segments parallel-sided or conical at base,
consistently appearing rounded, always <7 times
longer than wide, apical segment distinctly different,
leaf conical in shape, up to 25 cm long *Pterophyllum brevipenne* (H)
- 9 Leaves very large and robust, segments up to
25 cm long, parallel-sided *Nilssonia neuberi* (J)
 - Segments distinctly shorter, conical 10
- 10 Segments acute, pointed, leaves delicate *Nilssonia riegeri*
 - Segments wide, conical, apically
obtuse-rounded 11
- 11 Segment bases distinctly decurrent, segment
spacing typically wide *Nilssonia lunzensis* (K)
 - Segments not decurrent, segment spacing
typically rather dense *Nilssonia sturii* (L)



tional species, i.e. *P. spectabilis* Harris, 1932 and *P. depressa* Harris, 1932 establishes the cycadalean affinities of *Pseudocatenis* based on the presence of haplocheilic stomata (Harris, 1932; Van Konijnenburg-van Cittert & Van der Burgh, 1989), which are especially valuable in distinguishing *Pseudocatenis* leaves from those bennettitalean foliage types that are similar in macromorphology, e.g., certain types of *Pterophyllum* and *Zamites* Brongniart, 1828. One leaf type assignable to the genus *Pseudocatenis* has been described from Lunz (Pott et al. 2007b) that represents one of the earliest occurrences for the genus.

Pseudocatenis cornelii Pott et al., 2007

Estimated total leaf size: up to 70 cm long and 15 cm wide

Characters: loosely segmented, leaflets insert laterally to rachis, terminal leaflet unknown, venation prominent

Figures: 3F; 5A, C, D

Pseudocatenis cornelii leaf fragments are up to 14.5 cm long; based on the material at hand adult leaves of *P. cornelii* are estimated to have grown up to 70 cm long. The blade has a somewhat lax appearance because the leaf segments are relatively loosely spaced. Tongue-shaped leaf segments extend from the rachis at angles between 80° and 90°. They are oppositely to sub-oppositely positioned, polymorphous (size and shape strongly depend on the position in the leaf), generally oblong in outline, tapering, and with rounded tips. The largest leaf segments may be >70 mm long and up to 6.5 mm wide. The segments are wholly adherent to the rachis and basiscopically decurrent. The venation is conspicuous. Seven to twelve parallel veins, forking once shortly after entering, enter each leaf segment from the rachis

Cuticles are well-preserved. The leaves are hypostomatic. Both the adaxial and abaxial epidermis are differentiated into costal and intercostals fields. Epidermal cells are rectangular or elongate to isodiametric in outline; anticlinal walls are slightly undulated to sinuous. The intercostal fields of the abaxial cuticle are broad, between 350 and 450 µm wide, and composed of polygonal to broadly rectangular, isodiametric cells. Stomata are confined to the intercostal fields, haplocheilic, regularly scattered across the intercostal fields, randomly oriented, and surrounded by 4–6 subsidiary cells. Each subsidiary cell

bears a small hollow papilla that overarches the pit mouth and covers the sunken guard cells (see Pott et al., 2007b).

GINKGOALES

Genus *Arberophyllum* Doweld, 2000

Arberophyllum forms an isolated taxon that differs in various morphological traits from other members of the Mesozoic ginkgophytes (Tralau, 1968; Dobruskina, 1998). The most characteristic features of *Arberophyllum* are strap-shaped leaves that lack petioles. The genus name *Arberophyllum* is a substitute for the original genus name *Glossophyllum* Kräusel, 1943, used i.a. by Kräusel (1943), since *Glossophyllum* (Müller Hal., 1851) Hampe, 1879 is preoccupied by a genus of mosses and the name of the fossil genus thus is a younger synonym and had to be replaced (for details, see Doweld 2000).

Arberophyllum florinii (Kräusel, 1943)

Doweld, 2000

Estimated total leaf size: up to 20 cm long and 2 cm wide

Characters: tongue-shaped leaves without petioles, lamina entire-margined

Figures: 3A; 4A, B

Arberophyllum florinii leaves are common in the Lunz flora and usually yield excellently preserved cuticles. Kräusel (1943) assigned the species to the gymnosperm order Ginkgoales based on epidermal anatomy. The most characteristic features of *A. florinii* are tongue-shaped leaves, up to 20 cm long and 1.5 cm wide, that lack petioles and a central rachis. Leaves of *A. florinii* in the Lunz flora are very distinctive, also due to their thick, leathery cuticles that easily chip off from the rock.

Cuticles reveal that the leaves are amphistomatic. Stomatiferous costal and non-stomatiferous intercostal fields are well-defined. Epidermal cells are polygonal to rectangular elongate or isodiametric. The anticlinal cell walls are straight and the outer periclinal walls smooth, producing only faint idiocuticular striae. Stomata are regularly distributed in the costal fields; stomatal pores are randomly oriented. The adaxial cuticle is thicker than the lower cuticle.

Stur (1871) classification (p. 290)	Stur (1885) classification (p. 5-7)	Krasser (1909a-b) classification	Pott et al. (2007a-e) classification	specimen assignment and other comments
	<i>Pterophyllum irregulare</i> Stur	<i>Nitsonia sturni</i> Krasser n. sp.	<i>Nitsonia sturni</i> Krasser 1909 emend. Pott et al. 2007	one specimen assigned to <i>Pterophyllum brevipenne</i> and one to <i>P. jaegeri</i>
<i>Pterophyllum riegeri</i> n. sp.	<i>Pterophyllum riegeri</i> Stur	<i>Pterophyllum riegeri</i> Stur	<i>Nitsonia riegeri</i> (Stur ex Krasser 1909) Pott et al. 2007	several specimens assigned to <i>Nitsonia sturni</i> , <i>N. lunzensis</i> and <i>Pseudocnitis cornelli</i>
	<i>Ctenis lunzensis</i>	<i>Ctenis lunzensis</i>	<i>Nitsonia lunzensis</i> Stur ex Pott et al. 2007	several specimens assigned to <i>Nitsonia sturni</i>
	<i>Ctenis angustior</i>			specimens assigned to <i>Nitsonia lunzensis</i>
	<i>Pterophyllum neuberi</i> Stur	<i>Pterophyllum grandifolium</i> (Font.) Krasser	<i>Nitsonia neuberi</i> Stur ex Pott et al. 2007	several specimens assigned to <i>N. sturni</i> and one to <i>Pterophyllum jaegeri</i>
<i>Pterophyllum pichleri</i> n. sp.	<i>Pterophyllum pichleri</i> Stur	<i>Pterophyllum pichleri</i>		specimens assigned to <i>Nitsonia neuberi</i> and <i>N. lunzensis</i>
<i>Pterophyllum guembeli</i> Stur	<i>Pterophyllum guembeli</i> Stur	<i>Pterophyllum guembeli</i> Stur et Krasser		specimens assigned to <i>Nitsonia neuberi</i> , <i>N. sturni</i> and <i>N. lunzensis</i>
<i>Pterophyllum haueri</i> n. sp.	<i>Pterophyllum haueri</i> Stur	<i>Pterophyllum haueri</i>		specimens assigned to <i>Nitsonia neuberi</i> , <i>N. sturni</i> , <i>N. lunzensis</i> , <i>Pterophyllum brevipenne</i> (one specimen) and <i>P. jaegeri</i> (one specimen)
			<i>Pseudocnitis cornelli</i> Pott et al. 2007	incl. specimens originally labelled as <i>Ctenophyllum lunzense</i>
<i>Pterophyllum jaegeri</i> Brongn.		<i>Pterophyllum jaegeri</i> Brongn.	<i>Pterophyllum filicoides</i> (Schiltzheim 1822) Zeller 1906	a few specimens now assigned to <i>Pterophyllum brevipenne</i>
	<i>Pterophyllum longifolium</i> Jaeg.	<i>Pterophyllum longifolium</i> Brongn.		specimens assigned to <i>Pterophyllum jaegeri</i> , <i>P. brevipenne</i> and <i>Pseudocnitis cornelli</i> (one specimen)
	<i>Pterophyllum approximatum</i> Stur	<i>Pterophyllum approximatum</i> Stur		specimens assigned to <i>Pterophyllum jaegeri</i>
	<i>Pterophyllum macrophyllum</i> Kur.	<i>Pterophyllum macrophyllum</i> Kur.		specimens assigned to <i>Pterophyllum jaegeri</i> and <i>P. brevipenne</i>
<i>Pterophyllum brevipenne</i> Kurr	<i>Pterophyllum brevipenne</i> Kurr	<i>Pterophyllum brevipenne</i> Kurr ex Schenk 1864 emend. Pott et al. 2007	<i>Pterophyllum brevipenne</i> Kurr ex Schenk 1864 emend. Pott et al. 2007	a few specimens now assigned to <i>Pterophyllum jaegeri</i>
	<i>Pterophyllum rectum</i> Stur	<i>Pterophyllum rectum</i> Stur		specimens assigned to <i>Pterophyllum brevipenne</i>
<i>Pterophyllum merianii</i> Heer	<i>P. cf. pulchellum</i> Heer	<i>Pterophyllum pulchellum</i> Heer		specimens assigned to <i>Pterophyllum brevipenne</i> and <i>P. jaegeri</i>
	<i>Pterophyllum haberfeleri</i> Stur	<i>Pterophyllum haberfeleri</i> Stur		specimens assigned to <i>Pterophyllum brevipenne</i> and <i>P. jaegeri</i> (one specimen)
<i>Pterophyllum haidingeri</i> Goepp.	<i>Taeniopteris haidingeri</i> Goepp. mnsc. nec Ett.	<i>Macrotaeniopteris haidingeri</i> Krasser	<i>Nitsoniopteris haidingeri</i> (Krasser 1909) Pott et al. 2007	<i>Pterophyllum haidingeri</i> Goepp. (Stur, 1871) is to identify with <i>Taeniopteris haidingeri</i> Goepp. mnsc. nec Ett. (Stur, 1885) and consequently belongs to <i>Macrotaeniopteris haidingeri</i> (Krasser, 1909a, b)
	<i>Taeniopteris latior</i> Stur	<i>Macrotaeniopteris latior</i> Krasser		most specimens assigned to <i>Nitsoniopteris haidingeri</i> ; a few specimens assigned to <i>Nitsoniopteris angustior</i>
	<i>Taeniopteris simplex</i> Stur	<i>Macrotaeniopteris simplex</i> Krasser		most specimens assigned to <i>Nitsoniopteris angustior</i> ; a few specimens labelled as <i>Danaceopsis simplex</i> assigned to <i>Nitsoniopteris haidingeri</i>
	<i>Taeniopteris parvula</i> Stur			specimens assigned to <i>Nitsoniopteris angustior</i>
	<i>Taeniopteris angustior</i> Stur	<i>Macrotaeniopteris angustior</i> Krasser	<i>Nitsoniopteris angustior</i> (Stur ex Krasser 1909) Pott et al. 2007	
	<i>Taeniopteris lunzensis</i> Stur	<i>Macrotaeniopteris lunzensis</i> Krasser	<i>Nitsoniopteris lunzensis</i> (Stur ex Krasser 1909) Pott et al. 2007	several specimens assigned to <i>Nitsonia sturni</i> and <i>N. lunzensis</i>
<i>Pterophyllum lunzense</i> n. sp.	<i>Pterophyllum lunzense</i> Stur	<i>Pterophyllum lunzense</i>		specimens identical to those of <i>Macrotaeniopteris lunzensis</i> and thus assigned to <i>Nitsoniopteris lunzensis</i> ; few assigned to <i>Nitsonia sturni</i>
	<i>Pterophyllum cteniforme</i> Stur	<i>Pterophyllum taxinum</i> (L. et H.) Goepp.		only one specimen labelled as <i>P. cteniforme</i> was found in the collections that clearly belongs to <i>Dicroidiaceae</i> (NRM, S148565). This specimen was correctly identified by Krause (1953) as <i>D. keuperianum</i>
	<i>Pterophyllum pectiniforme</i> Stur			Specimens of this taxon were neither retrieved by Krasser (1909b), nor did we find any specimen in the collections labelled <i>P. pectiniforme</i> . This species is to be classified as lost, since it was never diagnosed or illustrated validly
<i>Pterophyllum lipoldii</i> n. sp.	<i>Pterophyllum? lipoldii</i> Stur	<i>Palissya lipoldii</i>		later referred to as <i>Stachyotaxus lipoldii</i> by Krause (1949); we favour to include the species in <i>Elatocladus lipoldii</i> (Krause 1949); several of the specimens assigned to <i>Nitsonia nigeri</i>
		<i>Noeggerathiopsis</i> sp.	<i>Glossophyllum florini</i> Krause 1943	Doweld (2000) introduced <i>Arberophyllum</i> as a new and valid genus name for <i>Glossophyllum</i> Krause, 1943. Consequently, this species has to be treated as <i>Arberophyllum florini</i> (Krause 1943) Doweld 2000
	<i>Clathrophyllum lunzense</i> Stur	<i>Clathrophyllum lunzense</i> Stur		<i>Ginkgoites lunzensis</i> (Stur 1885) Florin 1936
<i>Zamites lunzensis</i> n. sp.				no specimen labelled as <i>Zamites lunzensis</i> was found, perhaps synonymous with <i>Ctenis lunzensis</i>

CYCADALES

BENNETTITALES

PIN

GINKGO

?

Table 1.
Comparison of the historical and modern taxa names (green) of gymnosperm foliage from Lunz.

Stomata are separated from one another by one to several ordinary epidermal cells. However, they are usually interconnected by idiocuticular striae. Guard cells are sunken and possess prominent circum-poral thickenings. The guard cells are surrounded by 5–7 subsidiary cells, which are more heavily cutinised than the normal epidermal cell. A distinct and solid papilla extends from each subsidiary cell and overarches the pit mouth (see Pott et al., 2007d).

Genus *Ginkgoites* Seward, 1919

Based on works by himself, Seward (1919) introduced the genus *Ginkgoites* to accommodate fossil leaves that are similar in morphology to leaves of the extant *Ginkgo biloba* Linnaeus, 1771, but that cannot be positively assigned to the extant genus *Ginkgo* Linnaeus, 1771 with certainty.

Ginkgoites lunzensis (Stur, 1885) Florin, 1936

Estimated total size: up to 15 cm long and 10 cm wide

Characters: fan-shaped, dissected, leaflets band-like

Figure: 6

Kräusel (1943) described several specimens from Lunz under the name *Ginkgoites lunzensis* and provided illustrations of well preserved cuticles. Although the specimens based on morphology alone could also be interpreted as fern aphlebiae, the cuticles provide evidence for seed plant affinities. Kräusel (1921) first assigned the leaves to the genus *Baiera* Braun, 1843 but later changed his opinion and reassigned them to *Ginkgoites* based on earlier studies by Florin (1936). Leaves of *G. lunzensis* resemble very large leaves of the extant *Ginkgo biloba*. They are fan-shaped with an actinomorphically dissected lamina. The dissection may reach down to the leaf base. Leaf segments are band-like with almost parallel margins and several delicate parallel veins producing a palmate venation due to regular bifurcation. Preserved leaf fragments are up to 10 cm long; Kräusel (1921) suggested a total leaf length of up to 15 cm. Due to the fragmentary preservation of the less-than-ten specimens that have been discovered from Lunz to date, this species was not included in the identification key included in this paper (see below). Details of the epidermal anatomy of the leaves are given in Kräusel (1943).

PINALES

Genus *Elatocladus* Halle, 1913 emend. Harris, 1979

The systematic position of this Mesozoic conifer-like leaf type remains uncertain. Although affiliation with the Coniferales has been invoked, this issue is by no means settled (Florin, 1958; Harris, 1969b, 1979; Arndt, 2002). The general difficulties in assigning sterile leafy conifer or conifer-like twigs to clearly demarcated morphogenera were discussed in detail by Harris (1979). This author used criteria such as leaf proportions, leaf base and tip shapes, leaf divergence and manner of leaf insertion as discriminative features of genera. He favoured the assignment of sterile conifer shoots bearing divergent, elongate, dorsiventrally flattened, univeined leaves to *Elatocladus* in agreement with an earlier proposal by Berry (1924). Rees and Cleal (2004) adopted a similar strategy and, in accordance with their study, we here follow Harris' (1979) diagnosis of *Elatocladus*. However, we note that very similar or conspecific leafy axes have been inferentially linked, although never convincingly found attached, to *Palissya* Endlicher, 1847 cones by several workers (Nathorst, 1908; Florin, 1958; Parris et al., 1995; Schweitzer & Kirchner, 1996). Although *Elatocladus* has generally been used for younger (Jurassic–Cretaceous) shoots and leaves than those described below (Late Triassic), temporal separation is not a strong basis for differentiation of morphotaxa, and we note that Harris (1935) also recognised several species of this genus from Rhaetian deposits of Greenland. *Stachytaxis* Nathorst, 1886 in contrast includes both cones and shoots and is known only from Rhaetian strata. Shoots are dimorphic with a proximal part covered with small scale-like leaves and a distal part bearing longer ensiform leaves that are confined (distichously) in one level (Nathorst 1886, 1908; Harris, 1935). The cones consist of loose, spirally arranged bract-scale complexes each bearing a single seed inserted within a cup-like structure on the adaxial surface (cf. Pott & McLoughlin, in press).

Elatocladus (Stachytaxis) lipoldii Kräusel, 1949

Estimated total size: up to 20 cm long and 4 cm wide

Characters: leafy twigs, leaves with prominent

mid-vein

Figure: 3E

The leafy coniferalean twigs from Lunz were assigned to *Stachyotaxus lipoldii* by Kräusel (1949), who also studied cuticles of the leaves. Originally, they were erroneously included in *Pterophyllum* by Stur (1885), but the leaves show only a single prominent midvein, which separates it from *Pterophyllum* that possesses several parallel veins per leaflet. Following the definitions and studies by Harris (1979), as well as those by several other workers, we feel that it would be more reasonable to transfer the leafy twigs from Lunz to *Elatocladus*. The twigs are stalked, up to 20 cm long, and bear several acute leaves (not leaflets in the sense of Kräusel, 1949), which are bent slightly forward towards the apex of the twigs. Leaf apices are somewhat acute, but mainly bluntly rounded. Leaves are up to 20 mm long and 3 mm wide. Kräusel (1949) described cuticles with haplocheilic stomata. *Elatocladus lipoldii* is the only conifer species known from the Lunz flora to date; it is a less common element than, e.g., *Pterophyllum* and *Nilssonia* leaves, but adds another typically Rhaetian genus to the inventory of the Lunz flora (cf. Pott et al., 2007e, 2008; Pott & McLoughlin, in press).

Comments on the key:

Drawings included in the key are simplified or generalised, and slightly oversubscribed to underline the main characteristics of the species. A typical specimen of each species, along with typical features of the cuticles, is illustrated in Figures 3–6.

The identification key largely relies on macromorphological features because it was our intention to keep it as simple as possible and make it usable for a broad audience. Characteristics of the epidermal anatomy are not included since cuticular analysis requires some effort and may not be available to everyone interested in the fossils from Lunz. The key was tested and works well for most hand specimens. It has to be taken into account, however, that some small and/or ill-preserved specimens may not be safely identified down to species level based exclusively on macromorphology. The macromorphological differences between the species are sufficiently well recognisable in fossils that show a larger portion of the leaf. Fossils of entire but particularly small leaves pose

another problem with regard to identification since they may represent immature foliage or mature foliage of juvenile plants or seedlings that does not display all the features characteristic of mature leaves from full-grown individuals of the same taxon (cf. Pott et al., 2007e; Pott & McLoughlin, 2009). In all of these instances, only the preparation of cuticles provides a data set of sufficient clarity for species identification. For detailed information on the epidermal anatomy of the species, the reader is referred to the publications that are indicated along with the species descriptions.

Acknowledgements

Hans Kerp, Institut für Geologie und Paläontologie, Westfälische Wilhelms-Universität Münster, Germany, is thanked for all his help and support through the course of the whole project and for the co-supervision of CP's PhD. We wish to thank the following people who provided access to the several collections under their care: David Cantrill, now Royal Botanic Gardens, Melbourne, Australia; Thomas Denk, Else Marie Friis, Steve McLoughlin and Ove Johansson, Naturhistoriska riksmuseet, Stockholm, Sweden; Irene Zorn, Geologische Bundesanstalt, Vienna, Austria; Barbara Meller, Universität Wien, Vienna, Austria; Andreas Kroh and Matthias Harzhauser, Naturhistorisches Museum, Vienna, Austria; Johanna van Konijnenburg-van Cittert, Netherlands Centre for Biodiversity Naturalis, Leiden University, The Netherlands; Johan van der Burgh, Institute of Environmental Biology, Utrecht University, The Netherlands; Martin Groß, Universalmuseum Joanneum, Graz, Austria; Lutz Kunzmann, Senckenberg Naturhistorische Sammlungen Dresden, Germany; Stephan Schultka, Museum für Naturkunde, Berlin, Germany; Volker Wilde, Senckenberg Forschungsinstitut und Naturmuseum, Frankfurt am Main, Germany; Harald Steininger, Niederösterreichisches Landesmuseum, St. Pölten, Austria; Birgitt Aschauer, Waidhofen, Austria. Financial support was provided by the Deutsche Forschungsgemeinschaft (DFG), Bonn, Germany (grants KR 2125/3-1 and KR 2125/3-2). We thank Johanna H. A. van Konijnenburg-van Cittert, Leiden, The Netherlands, and Mihai E. Popa, Bucharest, Romania, for reviewing the manuscript.

References

- Arndt, S. (2002): Morphologie und Systematik ausgewählter mesozoischer Koniferen. – *Palaeontographica Abt. B*, 262: 1–23.
- Berry, E. W. (1924): Mesozoic plants from Patagonia. – *American Journal of Science*, Series 5, 7: 473–482.
- Boyd, A. (2000): Bennettitales from Early Cretaceous floras of West Greenland: *Pterophyllum* and *Nilssoniopoteris*. – *Palaeontographica Abt. B*, 255: 47–77.
- Braun, C. F. W. (1843): Beiträge zur Urgeschichte der Pflanzen. – *Beiträge zur Petrefacten-Kunde*, 1–46.
- Brongniart, A. (1825): Observations sur les végétaux fossiles renfermés dans les grès de Hoer en Scanie. – *Annales des Sciences Naturelles*, 4: 200–224.
- Brongniart, A. (1828): Prodrome d'une histoire des végétaux fossiles. – VIII+223 p., Levrault, Paris.
- Cleal, C. J. (1993): Gymnospermophyta. – In: Benton, M. (ed.): *The fossil record II*, 795–808, Chapman & Hall, London.
- Dobruskina, I. A. (1989): The alpine Lunz-Flora – a standard flora for the Carnian stage of the Triassic. – *International Geological Review*, 31: 1209–1215.
- Dobruskina, I. A. (1998): Lunz flora in the Austrian Alps – a standard for Carnian floras. – *Palaeogeography, Palaeoclimatology, Palaeoecology*, 143: 307–345.
- Doweld, A. B. (2000): *Arberophyllum* – a new generic name for *Glossophyllum* Kräusel, 1943 (Ginkgoiphyta). – *Paleontological Journal*, 34: 674–675.
- Endlicher, S. (1847): *Synopsis Coniferarum*. – IV+368 p., Scheitlin & Zöllikofer, St. Gallen.
- Ettingshausen, C. von (1851): Beiträge zur Flora der Vorwelt. – *Haidinger's Naturwissenschaftliche Abhandlungen*, 4: 65–99.
- Florin, R. (1933): Zur Kenntnis der Spaltöffnungsapparate der Bennettitales. – *Kungliga Svenska Vetenskapsakademiens Handlingar, Tredje Serien*, 12: 11–31.
- Florin, R. (1936): Die fossilen Gingkophyten aus Franz-Joseph-Land nebst Erörterungen über vermeintliche Cordaitales mesozoischen Alters. I. Spezieller Teil. – *Palaeontographica Abt. B*, 81: 71–173.
- Florin, R. (1958): On Jurassic taxads and conifers from north-western Europe and Eastern Greenland. – *Acta Horti Bergiani*, 17: 257–402.
- Halle, T. G. (1913): The Mesozoic flora of Graham Land. Wissenschaftliche Ergebnisse der schwedischen Südpolar-Expedition 1901–1903 unter Mitwirkung zahlreicher Fachgenossen. – 123 p., Generalstabens litografiska anstalt, Stockholm.
- Hampe, E. (1879): *Enumeratio muscorum frondosorum Brasiliæ centralis, præcipue provinciarum Rio de Janeiro et Sao Paulo, adhuc cognitorum*. – *Videnskabelige Meddelelser fra Dansk Naturhistoriske Forening i Kjøbenhavn*, 26: 73–163.
- Harris, T. M. (1932): The fossil flora of Scoresby Sound East Greenland. Part 2: Description of seed plants incertae sedis together with a discussion of certain cycadophyte cuticles. – *Meddelelser om Grønland*, 85: 1–112.
- Harris, T. M. (1935): The fossil flora of Scoresby Sound, East Greenland. Part 4: Ginkgoales, Coniferales, Lycopodiales and isolated fructifications. – *Meddelelser om Grønland*, 112: 1–176.
- Harris, T. M. (1950): Notes on the Jurassic flora of Yorkshire, 46–48. – *Annals and Magazine of Natural History*, Series 7, 3: 1001–1030.
- Harris, T. M. (1969a): The Yorkshire Jurassic Flora. III. Bennettitales. – VI+186 p., Trustees of the British Museum (Natural History), London.
- Harris, T. M. (1969b): Naming a fossil conifer. In: Santarau, H. (ed.): *J. Sen Memorial Volume*, 243–252, Botanical Society of Bengal, Calcutta.
- Harris, T. M. (1979): The Yorkshire Jurassic Flora. V. Coniferales. – II+166 p., Trustees of the British Museum (Natural History), London.
- Krasser, F. (1909a): Die Diagnosen der von Dionysius Stur in der obertriadischen Flora der Lunzer Schichten als Marattiaceenarten unterschiedenen Farne. – *Sitzungsberichte der Kaiserlichen Akademie der Wissenschaften Wien*, Abt. 1, 118: 13–43.
- Krasser, F. (1909b): Zur Kenntnis der fossilen Flora der Lunzer Schichten. – *Jahrbuch der Kaiserlich-Königlichen geologischen Reichsanstalt*, 59: 1–26.
- Krasser, F. (1917): Studien über die fertile Region der Cycadophyten aus den Lunzer-Schichten: Mikrosporophylle und männliche Zapfen. *Denkschriften der Kaiserlichen Akademie der Wissenschaften (Wien)*, Mathematisch-Naturwissenschaftliche Klasse, 94: 489–553.
- Krasser, F. (1919): Studien über die fertile Region der Cycadophyten aus den Lunzer-Schichten: Makrosporophylle. – *Denkschriften der Kaiserlichen Akademie der Wissenschaften (Wien)*, Mathematisch-Naturwissenschaftliche Klasse, 97: 1–32.
- Kräusel, R. (1921): Über einige Pflanzen aus dem Keuper von Lunz (Nieder-Österr.). – *Jahrbuch der Preußischen Geologischen Landesanstalt*, 41: 192–209.
- Kräusel, R. (1943): Die Gingkophyten der Trias von Lunz in Niederösterreich und von Neue Welt bei Basel. – *Palaeontographica Abt. B*, 87: 59–93.

- Kräusel, R. (1948): *Sturiella langeri* nov. gen., nov. sp., eine Bennettitee aus der Trias von Lunz (Nieder-Österreich). – Senckenbergiana, 29: 141–149.
- Kräusel, R. (1949): Koniferen und andere Gymnospermen aus der Trias von Lunz, Nieder-Österreich. – Palaeontographica Abt. B, 89: 35–82.
- Kräusel, R. (1953): Ein neues *Dioonitocarpidium* aus der Trias von Lunz. – Senckenbergiana, 34: 105–108.
- Kräusel, R., Schaarschmidt, F. (1966): Die Keuperflora von Neuewelt bei Basel. IV. Pterophylen und Tae-niopteriden. – Schweizer Paläontologische Abhandlungen, 84: 3–44.
- Lindley, J., Hutton, W. (1831–1836): The fossil flora of Great Britain, or figures and descriptions of the vegetable remains found in a fossil state in the country. – LIX+223 & XXVIII+208 p., James Ridgway, London.
- Linnæus, C. (1771) *Mantissa plantarum altera gene-rum editionis VI. Et specierum editionis II.* – 588 p., Laurentii salvii, Stockholm.
- Müller, C. (1851): *Synopsis muscorum frondosorum omnium hucusque cognitorum. Pars secunda.* – 772 p., A. Foerstner, Berlin.
- Nathorst, A. G. (1878–1886): Om florān i Skånes kol-förande bildningar. – Sveriges Geologiska Undersökning Serie C, 27, 33, 85: 1–126.
- Nathorst, A. G. (1908): Paläobotanische Mitteilungen 7. Über *Palissya*, *Stachytaxis* und *Palaeotaxus*. – Kungliga Svenska Vetenskapsakademiens Handlin-gar, 43: 3–20.
- Nathorst, A. G. (1909): Über die Gattung *Nilssonia* Brongn. mit besonderer Berücksichtigung schwe-discher Arten. – Kungliga Svenska Vetenskapsaka-demiens Handlingar, 43: 3–37.
- Parris, K. M., Drinnan, A. N., Cantrill, D. J. (1995): *Palis-sya* cones from the Mesozoic of Australia and New Zealand. – Alcheringa, 19: 87–111.
- Pott, C., Kerp, H., Krings, M. (2007a): Morphology and epidermal anatomy of *Nilssonia* (cycadalean folia-ge) from the Upper Triassic of Lunz (Lower Austria). – Review of Palaeobotany and Palynology, 143: 197–217.
- Pott, C., Kerp, H., Krings, M. (2007b): *Pseudooctenis cor-nelii* nov. spec. (cycadalean foliage) from the Carnian (Upper Triassic) of Lunz, Lower Austria. – An-nalen des Naturhistorischen Museums Wien, 109A: 1–17.
- Pott, C., Krings, M., Kerp, H. (2007c): The first record of *Nilssoniopterus* (Gymnospermophyta, Bennettitales) from the Carnian (Upper Triassic) of Lunz, Lower Austria. – Palaeontology, 50: 1299–1318.
- Pott, C., Krings, M., Kerp, H. (2007d): A surface micro-relief on the leaves of *Glossophyllum florinii* (?Ginkgoales) from the Upper Triassic of Lunz, Austria. – Botanical Journal of the Linnean Society, 153: 87–95.
- Pott, C., Krings, M., Kerp, H. (2008): The Carnian (Late Triassic) flora from Lunz in Lower Austria: palaeo-ecological considerations. – Palaeoworld, 17: 172–182.
- Pott, C., Krings, M., Kerp, H., Friis, E. M. (2010): Re-construction of a bennettitalean flower from the Carnian (Upper Triassic) of Lunz, Lower Austria. – Review of Palaeobotany and Palynology, 159: 94–111.
- Pott, C., McLoughlin, S. (2009): Bennettitalean foliage in the Rhaetian-Bajocian (latest Triassic-Middle Ju-rassic) floras of Scania, southern Sweden. – Review of Palaeobotany and Palynology, 158: 117–166.
- Pott, C., McLoughlin, S. (in press): The Rhaeto-Liassic flora from Rögla, northern Scania, Sweden – Pa-laeontology.
- Pott, C., Van Konijnenburg-van Cittert, J. H. A., Kerp, H., Krings, M. (2007e): Revision of the *Pterophyllum* species (Cycadophytina: Bennettitales) in the Carnian (Late Triassic) flora from Lunz, Lower Austria. – Review of Palaeobotany and Palynology, 147: 3–27.
- Rees, P. M., Cleal, C. J. (2004): Lower Jurassic floras from Hope Bay and Botany Bay, Antarctica. – Spe-cial Papers in Palaeontology, 72: 1–90.
- Schenk, A. (1864): Beiträge zur Flora des Keupers und der rhätischen Formation. – Berichte der naturfor-schenden Gesellschaft zu Bamberg, 7: 1–91.
- Schimper, W. P. (1869): Traité de paléontologie végétale ou la flore du monde primitif dans ses rap-ports avec les formations géologiques et la flore du monde actuel. – IV+738 p. Baillièrre et fil), Paris.
- Schimper, W. P. (1870–1872): Traité de paléontologie végétale ou la flore du monde primitif dans ses rap-ports avec les formations géologiques et la flore du monde actuel. – 996 p. Baillièrre et fils, Paris.
- Schlotheim, E. F. von (1822): Nachträge zur Petre-factenkunde. 100 & 114 p., Becker'sche Verlags-buchhandlung, Gotha.
- Schweitzer, H.-J., Kirchner, M. (1996): Die rhäto-juras-sischen Floren des Iran und Afghanistan: 9. Conife-rophyta. – Palaeontographica Abt. B, 238, 77–139.
- Seward, A. C. (1911): The Jurassic flora of Sutherland. – Transactions of the Royal Society of Edinburgh, 47: 643–709.

- Seward, A. C. (1919): Fossil Plants – A Textbook for Students of Botany and Geology. Volume IV. – XVI+543 p., Cambridge University Press, Cambridge.
- Stur, D. (1871): Geologie der Steiermark. – XXXI+654p., Verlag des geognostisch-montanen Vereines für Steiermark, Graz.
- Stur, D. (1885): Die obertriadische Flora der Lunzer Schichten und des bituminösen Schiefers von Raibl. – Denkschriften der Kaiserlichen Akademie der Wissenschaften (Wien), 3: 93–103.
- Stur, D. (1888): Die Lunzer (Lettenkohle-)Flora in den „older mesozoic beds of the coalfield of eastern Virginia“. – Verhandlungen der Kaiserlich-Königlich Geologischen Reichsanstalt, 10: 203–217.
- Thomas, H. H. (1930): Further observations on the cuticle structure of Mesozoic cycadean fronds. – The Journal of the Linnean Society of London/Botany, 48: 389–415.
- Tralau, H. (1968): Evolutionary trends in the genus *Ginkgo*. – Lethaia, 1: 63–101.
- Van Konijnenburg-van Cittert, J. H. A., Mikuz, V., Pavsic, J. (2001): *Pterophyllum* (Cycadopsida) from Carnian beds in Poljane valley (Slovenia). – Geologija, 44: 317–323.
- Van Konijnenburg-van Cittert, J. H. A., Van der Burg, J. (1989): The flora from the Kim-meridgian (Upper Jurassic) of Culgower, Sutherland, Scotland. – Review of Palaeo-botany and Palynology, 61: 1–51.
- Zeiller, R. 1906. Bassin Houiller et Permien de Blanzy et du Creusot. Fascicule II. Flore fossile. – 265 p., Ministère des travaux publics, Paris.

Manuscript submitted: 12.4.2010

Revised Manuscript accepted: 5.7.2010

PETROLOGIE, GEOCHEMIE UND GEOLOGIE DES AMPHIBOLIT/METAGABBRO KOMPLEXES VON GUFIDAUN (SÜDTIROL, ITALIEN)

Verena Rofner¹, Peter Tropper¹, Volkmar Mair²

Mit 25 Abbildungen

¹ Institut für Mineralogie und Petrographie, Fakultät für Geo- und Atmosphärenwissenschaften,
Universität Innsbruck, Innrain 52f, A-6020 Innsbruck, Österreich

² Amt für Geologie und Baustoffprüfung, Eggentalerstrasse 48, I-39053 Kardaun (BZ), Italien

E-mail: Peter.Tropper@uibk.ac.at

Zusammenfassung

Das Kartierungsgebiet befindet sich bei Gufidaun/Gudon (Südtirol, Italien), nordöstlich von Klausen (BZ, I). Geologisch gesehen liegt das Arbeitsgebiet im nördlichsten Südalpin und umfasst den Amphibolit/Metagabbro Komplex sowie Quarzphyllit, Klausenit (Diorit), Hornfels, Orthogneis und Grünschiefer. Das Ziel der Arbeit war einerseits die petrologische Untersuchung der Metamorphoseentwicklung des Amphibolit/Metagabbro Komplexes von Gufidaun mittels thermobarometrischer Auswertung sowie eine geologische Kartierung im Maßstab 1:5000. Mineralchemisch wurden in beiden Gesteinsarten ähnliche Beobachtungen gemacht. Die Metagabbros enthalten folgende Mineralparagenese: Amphibol + Plagioklas + Klinozoisit + Chlorit + Titanit ± Ilmenit ± Quarz ± Kalzit. Die Amphibole der Metagabbros und Amphibolite zeigen teilweise starke chemische Zonierungen. In den Amphiboliten konnten texturell zwei Amphibolgenerationen (Amp I, Amp II) unterschieden werden. Chemisch sind sie aber sehr ähnlich in ihrer Zusammensetzung. Amp I könnte möglicherweise einen reliktischen, spätmagmatischen Amphibol darstellen. Amp II weist eine prograde, metamorphe Zonierung, wie in den Metagabbros, auf. Die Amphibole der Metagabbros weisen eine prograde Zonierung mit einem variszisch metamorphen, aktinolithischen Kern, und Mg-Hornblende und Pargasit bzw. Edennit in den Rändern, auf. Bei den nicht zonierte Amphibolen handelt es sich um Mg-Hornblenden. Es kann daher ein Temperaturanstieg während des Amphibolwachstums (vom Kern zum Rand hin) angenommen werden. Gegen Ende oder möglicherweise auch nach der Abkühlung der Intrusion setzte eine Dekompression ein. Die Granate der Hornfelse (kontaktmetamorpher Quarzphyllit) besitzen einen variszischen Kern und einen jüngeren Anwachsssaum, wobei dieser z.B. die Folge der permischen Kontaktmetamorphose darstellt. Thermobarometrische Berechnungen mit den Programmen THERMOCALC v.3.21 und PET 5.01 sowie semiquantitative Methoden ergaben für die Metagabbros und Amphibolite variszische Metamorphosebedingungen von 488–588°C und 3–5 kbar. Die Ergebnisse aus den untersuchten Metagabbros und Amphiboliten stimmen mit den P-T Daten von ca. 450–550°C und 5–6.5 GPa von Ring & Richter (1994) gut überein. Die P-T Bedingungen von 520–550°C und 5.3 GPa aus den Quarzphylliten bei Brixen (Wyhlidal, 2008), stimmen ebenfalls mit den errechneten Daten des Amphibolit/Metagabbro Komplexes überein. Auffällig ist das primäre, magmatische Gefüge der Metagabbros, die mit den randlichen Amphiboliten zusammen einen alkalischen Intrusivkörper bilden. Fraglich ist allerdings, wann die Platznahme des Komplexes erfolgt ist. Anhand der mineralchemischen Untersuchungen und der thermobarometrischen Ergebnissen lässt sich schließen, dass dieser Komplex bereits vor der variszischen Orogenese in das kristalline Basement des Südalpins intrudierte.

Abstract

This study area is located in the northernmost Southalpine basement. Geographically it is located in the Eisack Valley near Klausen (BZ, I). The area around the village Gufidaun was the focus of the mapping project in the course of this study. The aim of this study was the investigation of the petrology of the metagabbros and amphibolites and mapping on a scale of 1:5000. Within this rather uniform quartzphyllite basement a large metagabbro/amphibolite complex occurs near the village Gufidaun. Since this basement has only been overprinted by the Variscan amphibolite-facies metamorphic event, it was the aim of this study to obtain Variscan P-T conditions from these metabasic rocks. The amphibolites and metagabbros contain the mineral assemblage amphibole + plagioclase + clinozoisite + chlorite + titanite \pm ilmenite \pm quartz \pm calcite. Chemical zoning in idiomorphic amphiboles shows evidence for a prograde growth history. The cores of the chemical zoned amphiboles show actinolite composition and the rims can be chemically classified as Mg-hornblende, edenite, Mg-hastingsite and pargasite. The chemical zoning shows increasing edenite- and tschermakite substitutions towards the rims which indicates increasing T conditions during amphibole growth. On the other hand, matrix plagioclase is almost pure albite (Ab₉₅An₅). Garnet in the hornfelses shows Variscan cores and Permian rims. Application of multi-equilibrium thermobarometry (THERMOCALC v.3.21, PET) to the matrix assemblages of the metagabbros and amphibolites yielded P-T conditions of 488–588°C and 3–5 kbar. These P-T data agree with the P-T data of ca. 450–550°C and 5–6.5 kbar by Ring & Richter (1994) and the P-T data of 520–550°C and 5.3 kbar of quartzphyllites from Brixen by Wyhlidal (2008). The metagabbros show clear magmatic textures and form together with the amphibolites the intrusive complex of Gufidaun, which represents an alkaline magmatic complex, which intruded into the Southalpine Variscan basement prior to the Variscan metamorphic event.

1. Einleitung

Das Ziel dieser Arbeit war einerseits die petrologische Untersuchung der Metamorphoseentwicklung des Amphibolit/Metagabbro Komplexes von Gufidaun mittels thermobarometrischer Methoden sowie eine

geologische Kartierung im Maßstab 1:5000. Die Bearbeitung des Amphibolit/Metagabbro Komplexes bei Gufidaun stellt eine interessante Aufgabenstellung dar, da bislang keine bekannten thermobarometrischen Daten dieser Gesteine existieren. Die vorhandene geologische Karte von Heißel & Ladurner (1936) stellt die dort anzutreffende komplexe Tektonik dar, jedoch ist eine moderne Kenntnis des Gesteinsbestandes unbedingt notwendig geworden. Obwohl der angrenzende Teil der Westlichen Dolomiten vermehrt Ziel geologischer und petrographischer Untersuchungen war (Brandner et al., 2007), fand das Gebiet um Gufidaun bisher nur in wenigen Arbeiten Erwähnung (Gisser, 1926; Heißel & Ladurner, 1936; Staindl, 1971). Unvollständig geklärt war bisher die Frage nach der genetischen Beziehung zwischen Amphibolit und Metagabbro, der Altersstellung der beiden Gesteine sowie ihre Metamorphoseentwicklung. Im Zuge der Geländearbeit wurden bereits bekannte und neue Lithologien festgestellt. Metagabbros wurden in fein- und grobkörnige Metagabbros unterschieden sowie das verschiedene Auftreten des Brixner Quarzphyllites dokumentiert. Die Gesteinseinheiten wurden anschließend mit Hilfe verschiedener Arbeitsmethoden petrographisch, petrologisch, mineralchemisch und thermobarometrisch untersucht.

2. Geographischer Überblick

Das Arbeitsgebiet befindet sich bei Gufidaun/Gudon in Südtirol (Italien) und umfasst eine Fläche von etwa 12 km². Die Ortschaft Gufidaun liegt nordöstlich von Klausen auf der östlichen Seite des Eisacktales am Eingang des Villnösser Tales auf einer Höhe von 730 m. Das in etwa 12 km lange Villnösser Tal zweigt nach Osten vom Eisacktal ab, und an dessen Ende ragen die Aferer und Villnösser Geisler auf.

Die Abgrenzung des Gebietes erstreckt sich im Norden oberhalb der Villnösser Haltestelle, vom Kropfsteiner Hof (unterhalb Feldthurns), bis nach Hauben oberhalb der Ortschaft Teis auf einer Höhe von 1258 m. Im Osten reicht das Gebiet bis nach Nigglun im Villnößtal, von dort aus zieht die Abgrenzung im Süden über Schülerbrunn und Spisserhof nach Schloss Anger, wo man dann auf die Brennerautobahn (A22) trifft. Die westliche Grenze der Kartierung verläuft orographisch rechts im Tal, etwa auf einer Höhe von 670 m (Weinbaugebiet). In einigen Bereichen des Kartierungsgebietes ist das Gelände aufgrund der steilen Hänge oder gefährlichen Abbruchzonen wie z.B. die

zahlreichen Hangsicherungen am Eingang und entlang des Villnösser Tales, nur sehr schlecht bzw. gar nicht zugänglich. Der tiefe Einschnitt des Villnösser Tales bietet jedoch sehr gute Aufschlussverhältnisse.

3. Geologischer Überblick

Geologisch gesehen liegt das Arbeitsgebiet im nördlichsten Südalpin. Die Gesteinseinheiten, die zum Südalpin zählen sind überwiegend als mesozoische Sedimentauflagen in den Dolomiten den Karawanken und den Karnischen Alpen aufgeschlossen. Der Bereich des Südalpins war im Mesozoikum dem Austroalpin benachbart. Gegenüber den helvetischen Decken unterscheiden sich die Südalpen deutlich durch ihren tektonischen Bau. Im Gegensatz zu den großen Überschiebungen im Helvetikum zeichnet sich das Südalpin durch eine südvergente Falten- und Schuppentektonik aus. Das Südalpin wird im Norden durch das Periadriatische Lineament begrenzt und taucht im Süden unter die känozoische Füllung des Po-Beckens ab. Dieses Störungssystem des Periadriatischen Lineamentes entstand in seiner heutigen Ausprägung nach der Kollisionsphase durch eine dextrale Transpression zwischen der adriatischen Mikroplatte und dem europäischen Vorland (Schmidt et al., 2004). Die Überschiebungen im Südalpin sind en-échelon (abgestufte, konsequent überlappende Falten) angeordnet, was sich mit der gleichzeitigen dextralen Seitenverschiebung entlang des periadriatischen Störungssystems erklären lässt. Dabei handelt es sich um fiederartig ausgebildete Spalten, die im Bereich von Scherzonen diagonal zur eigentlichen Scherrichtung verlaufen. Im Oligozän kam es am Periadriatischen Lineament zu einer vertikalen Krustenbewegung von mehreren km und zu einer horizontalen Bewegung von 300 bis 500 km. Die Basis der Südalpen bilden paläozoische Sedimente oder magmatische Gesteine, sie tauchen nach Süden hin an großen Flexuren und Brüchen unter die Molasse der Poebene (Bögel & Schmidt, 1976) ab. An der Periadriatischen Linie oder in unmittelbarer Nähe treten Intrusionen wie Granit- (z.B. Kreuzberg-, Ifflinger-, Brixener Granit) und Tonalitmassen verschiedenen Alters auf. Das Südalpin wurde an seinem Nordrand am stärksten herausgehoben da dort das kristalline Basement zutage tritt, während südlich davon durch stufenweises Absinken des Untergrundes jüngere Sedimente und Vulkanite auftreten. Ein durchgreifender Deckenbau im Südalpin ist nicht vorhanden obwohl

seismisch ein ausgeprägter Vorlandsüberschiebungsgürtel nachgewiesen wurde. Geologisch kartierbar sind alpidische Faltungen und intensive bruchhafte Störungsbildungen, insbesondere in Nähe der Periadriatischen Linie. Die permomesozoischen Abfolgen lagern im Südalpin ebenfalls diskordant auf dem Kristallin (Brixner Quarzphyllit) und dem schwach metamorphem Paläozoikum.

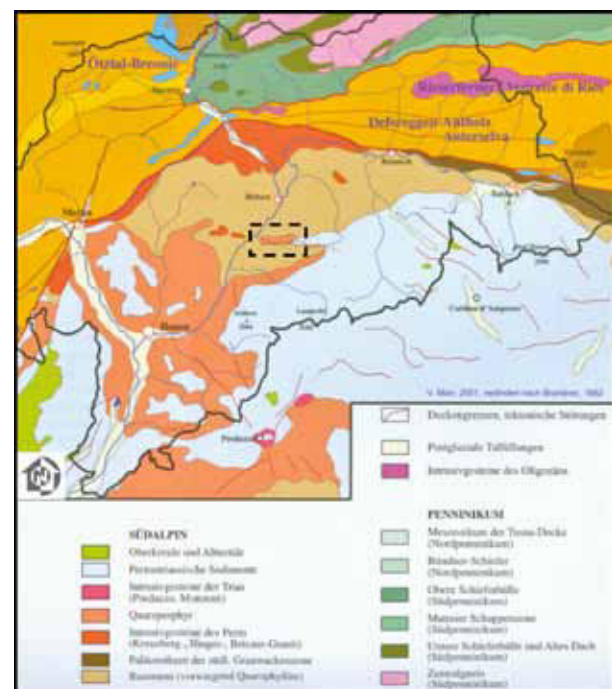


Abb. 1: Ausschnitt der geologischen Übersichtskarte von Südtirol nach Mair (2001, schriftl. Komm.) basierend auf Brandner (1982, schriftl. Mitt.). Das Rechteck kennzeichnet die Lage des Arbeitsgebietes.

Im Mittelpunkt des Arbeitsgebietes steht der Amphibolit/Metagabbro Komplex bei Gufidaun (Abb. 1). Die wichtigste Frage ist wohl jene nach der Entstehungsgeschichte des Amphibolit/Metagabbro Körpers, welcher im Brixner Quarzphyllit (kristallines Basement) eingebettet ist. Vorwiegend westlich des Eisacktales, vereinzelt jedoch auch östlich davon, sind dem Quarzphyllit auch Gneise und Glimmerschiefer zwischengeschaltet. Innerhalb des Quarzphyllits stecken an verschiedenen Stellen Intrusionskörper, die sogenannten Klausenite (Diorite).

4. Metamorphoseentwicklung und Alter

Aufgrund der vorliegenden Geologie im Arbeitsgebiet können mehrere geodynamisch aktive Phasen unterschieden werden: Die variszische Regionalmetamorphose (360–310 Ma), die permische Kontaktmetamorphose (290–250 Ma) und eine alpidische (100–30 Ma) tektonische Überprägung. Das dominante Ereignis, welches im gesamten Gebiet auftritt war jedoch die variszische Orogenese, welche die Gesteine bei niedrigen bis mittleren P-T Bedingungen überprägte (Ring & Richter, 1994; Wyhlidal, 2008). Folgende Ereignisse erfassten die Gesteine:

a) Variszische Metamorphose (360–310 Ma):

Die variszische Metamorphose erreichte ihren Höhepunkt vor 360 bis 310 Ma. In das kristalline Basement (Brixner Quarzphyllit) intrudierten jedoch schon vor-variszisch gabroide Gesteine, die heute als Amphibolite und Metagabbros in der Gegend von Klausen, bei Gufidaun vorliegen. Dieser Amphibolit/Metagabbro Körper wurde von der variszischen Metamorphose geprägt, wobei die Intrusion im Kern noch die grobkörnige primäre Textur (Metagabbro) aufweist und zum Rand hin zunehmend feinkörniges und schiefriges Aussehen erreicht (Amphibolit).

b) Permische Kontaktmetamorphose (290–250 Ma):

Durch die Extensionstektonik (Grabenbruchsystem) im Perm kam es zur Bildung von tiefreichenden Störungszonen und damit verbundener Schertektonik. Diese bildeten die Aufstiegswege für einen ausgeprägten Magmatismus, wobei hier die sogenannten „Klausenite“ in das variszische Basement intrudierten. Dadurch kam es zur Kontaktmetamorphose. Ein typisches Merkmal kontaktmetamorpher Gesteine sind die durch Mineralreaktionen hervorgerufene Knotenbildung sowie häufig das Fehlen einer Schieferung. Durch die Dioritinvasion (Klausenite) entstanden die im Arbeitsgebiet vorzufindenden Hornfelsen (kontaktmetamorphe Quarzphyllite). In dieser Phase wurde auch die Villnösser Linie angelegt (Furlani-Cornelius, 1924).

c) Alpidische tektonische Überprägung (<100 Ma) und Reaktivierung der Villnösser Linie.

Die Villnösser Linie ist wahrscheinlich eine permisch angelegte, alpidisch reaktivierte E-W verlaufende Störung. Die spröde Deformation ist besonders gut bei Schloss Summersberg, das auf Amphibolit steht, aufgeschlossen. Es entstanden zahlreiche Risse und Klüfte im Gestein sowie im Gelände erkennbare Störungszonen und Bruchgräben.

5. Lithologische Einheiten

Aufgrund der durchgeführten Detailkartierung wurden im Gebiet einige neue sowie bereits bekannte Lithologien kartiert. Von Bedeutung und Schwierigkeit war die Unterscheidung zwischen Amphibolit und Metagabbro, sowie der Grünschiefer im Gelände. Der Amphibolit bildet mit dem Metagabbro einen Intrusionskörper, der sich über die gesamte Ortschaft von Gufidaun erstreckt. Das Gestein weist eine grüne Farbe auf und besitzt eine deutlich erkennbare Schie-

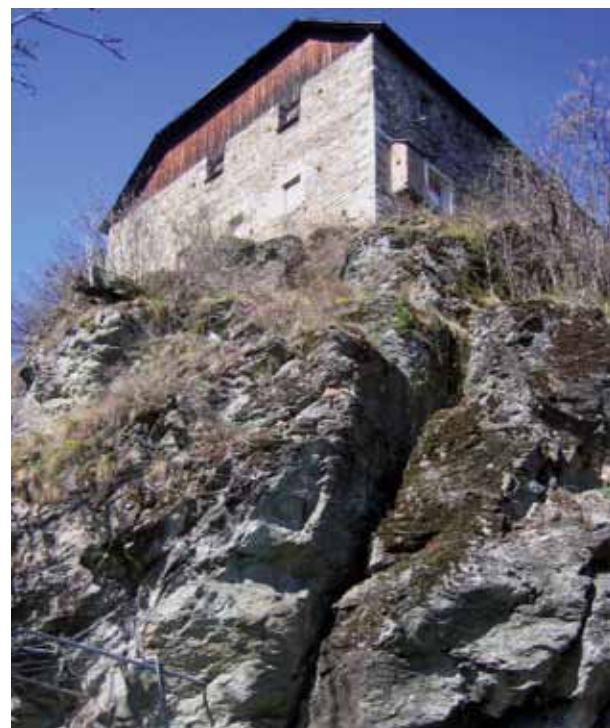


Abb. 2: Schloss Summersberg steht auf Amphibolit; das Gestein ist völlig zerklüftet und besitzt eine hellgrüne Farbe.



Abb. 3: Mittelkörniger Metagabbro (VR32).



Abb. 4: Grobkörniger Metagabbro (VR82).

ferung. Hauptsächlich aufgeschlossen findet man den Amphibolit beim Schloss Summersberg im Dorfkern (Wanderweg Richtung Villnösser Straße) sowie immer wieder als kleine Körper im Metagabbro (Abb. 2). Da diese Gesteine kaum Glimmer enthalten, sind sie sehr verwitterungsresistent und die Bildung von z.B. Rundhöcker oder Felsen wird dadurch begünstigt.

Weiters konnten mittelkörniger (Abb. 3) und grobkörniger Metagabbro (Abb. 4) beobachtet sowie der Übergang zwischen beiden Typen festgestellt und auskartiert werden. Mit dem Amphibolit bildet der Metagabbro einen Intrusionskomplex, wobei das Gestein die noch sehr gut erkennbare primäre magmatische Textur aufweist. An Handstücken der Metagabbros lässt sich makroskopisch der hohe Anteil an Amphibolen (dunkelgrüne Hornblendekristalle bis zu 1 cm Länge) deutlich erkennen.

Der im Arbeitsgebiet anzutreffende kontaktmetamorphe Quarzphyllit (Hornfels) weist starke Verwitterungsscheinungen auf. Man beobachtet Hornfelse als Kontaktgesteine zwischen den Metagabbrokörpern und den Quarzphylliten sowie im Zusammenhang mit der Intrusion der Klausenite südlich des Einganges des Villnösser Tales sowie vereinzelt im Ortskern von Gufidaun. Der Quarzphyllit tritt im gesamten Kartierungsgebiet als stark verfalteter, blättrig-schiefriger Phyllit auf. Der Amphibolit/Metagabbro Komplex steckt als Intrusionskörper im Quarzphyllit. Im Arbeitsgebiet beobachtet man nördlich der Ortschaft Gufidaun sowie südlich davon Quarzphyllit, der weit ins Villnösser Tal sowie nach

Teis reicht. Auf der anderen Talseite des Eisacktales, in Richtung Pardell und Feldthurns, findet man Klausenite im Quarzphyllit.

6. Störungen

Im Arbeitsgebiet können einige Störungszonen beobachtet werden, da das gesamte Gebiet alpidisch reaktiviert wurde. Von großer und besonderer Bedeutung ist die vorkommende „Villnösser Linie“. Es handelt sich um eine permisch angelegte, alpidisch reaktivierte E-W verlaufende Störung. Die Villnösser Linie wurde von Mutschlechner (1932) aus dem Gebiet der Peitlerkofel Gruppe, von Raniu bis etwa St. Peter im Villnöß verfolgt. Von St. Peter aus verläuft die Störungszone, sich immer an das südseitige Talgehänge haltend, bis zu den Höfen von Ganeit, wo sie dann auf die Nordseite des Tales übergreift (hier liegt Quarzphyllit auf Quarzporphyr).

Östlich der Einmündung des Flitzer Baches in den Villnösser Bach greift sie noch einmal für ein kurzes Stück auf die südliche Talflanke über. Östlich von Pardell überquert sie wieder das Villnösser Tal, um dann für längere Zeit auf der nördlichen Talseite zu verlaufen (es finden sich keinerlei Anzeichen dafür, dass sie auf der südlichen Talflanke verläuft). Beim Gasthof Stern, Nahe dem Ausgang des Villnösser Tales, zeigt der Quarzphyllit des südlichen Talhanges starke Zerrüttungen, die tektonisch entstanden sind. Der sonst flach nach SW bis SE einfallende Quarzphyllit fällt hier ziemlich steil gegen N ein. Aus den dort komplex vorherrschenden tektonischen Verhältnissen sind weiter gegen W keine genauen Anhalts-

punkte gegeben, welche eine sichere Festlegung des weiteren Verlaufs der Villnösser Linie ermöglichen (Heißel & Ladurner, 1936).

Die in E-W Richtung verlaufende Villnösser Linie schneidet das Arbeitsgebiet in zwei Schollen: nämlich in eine südliche, tiefer liegende, und in eine nördliche, die von der Störungslinie gegen Norden abfällt. In beiden Schollen finden sich Störungen, die eine Verschiebung der Schollen in horizontaler Richtung, gegen S bzw. SW, anzeigen. Das Lagerungsverhältnis lässt somit erkennen, dass die Entstehung dieser Villnösser Linie, in diesem Gebiet nicht auf Senkung der Schollen zurückgeführt werden darf, sondern auf heftige, horizontal wirkende Kräfte. Auch weiter im Osten ist die Villnösser Linie als Überschiebungslinie erkannt worden.

7. Arbeitsmethoden

Durchlichtmikroskopie

Das Polarisationsmikroskop wurde für die mikroskopische Untersuchung der Gesteinsschliffe verwendet, wobei die Mineralparagenesen als auch die Strukturen und Texturen ermittelt werden konnten. Weiters ermöglichte die Durchlichtmikroskopie eine engere Probenauswahl für die Analytik mit der Elektronenstrahlmikrosonde.

Mikrosondenanalytik

Die Mineralanalyse wurde mit der Elektronenstrahlmikrosonde des Typs JEOL JXA 8100 SUPER-PROBE am Institut für Mineralogie und Petrographie der Universität Innsbruck durchgeführt. Für die quantitativen Analysen der Minerale wurden wellenlängendiffusive Messungen durchgeführt. Die Sondenschliffe wurden mit einer Beschleunigungsspannung von 15 kV und einem Probenstrom von 10 nA gemessen. Die Messzeiten lagen bei 20 Sek. (Peak) und 10 Sek. (Background). BSE Bilder (Backscattered Electron Images) wurden als wichtiges Abbildungsverfahren verwendet. Röntgenverteilungsbilder stellen die räumliche Verteilung der einzelnen Elemente

in den Mineralen dar. Die Aufnahme erfolgte über einen definierten, flächigen Bereich. Dadurch konnten chemische Mineralzonierungen z.B. in Amphibolen, Epidoten und Granaten dargestellt und zur weiteren Interpretation herangezogen werden.

Röntgenfluoreszenzanalyse

Gemessen wurden die Haupt- und Spurenelemente von ausgewählten Gesteinsproben mittels WDXRFA Analyse (Wavelength Dispersive X-Ray fluorescence analysis, RFA: Röntgenfluoreszenzanalyse) am Institut für Mineralogie und Petrographie der Universität Innsbruck. Bei der Anlage handelt es sich um den Typ SPECTRO XEPOS. Für die Messungen wurden die ausgewählten Proben mit der Achat-Scheibenschwungmühle zu einem Pulver von etwa 5-10 g gemahlen. Die Probenmenge (mindestens 5 g) wurde anschließend im Ofen bei einer Temperatur von 1000°C über 3 Stunden geglüht und somit der Glühverlust (LOI durch H₂O bzw. CO₂ Emission) ermittelt. Zur Bestimmung der Hauptelemente wurden Schmelztabletten mit 0.6 g Probe und 4.6 g Dilithiumtetraborat Li₂B₄O₇ homogenisiert, anschließend in einem Platintiegel über einer Flamme geschmolzen und vollautomatisch in eine kreisförmige Platinform gegossen. Für die Spurenelementanalyse wurden Presstabletten von ebenfalls 0.6 g Probenpulver und 4.6 g Dilithiumtetraborat Li₂B₄O₇ in der dafür vorgesehenen Pressmaschine hergestellt.

8. Petrographie

Für die petrographischen Untersuchungen wurden an den Gesteinen Dünn- bzw. Sondenschliffauswertungen mit dem Polarisationsmikroskop (Abb. 5-8) und der Elektronenstrahlmikrosonde (BSE Bilder in Abb. 9, 11, 13, 14, 16) durchgeführt. Im Folgenden wird nur auf eine Auflistung der Mineralparagenesen in den Gesteinen eingegangen. Die verwendeten Mineralabkürzungen entsprechen der Norm nach Kretz (1983).

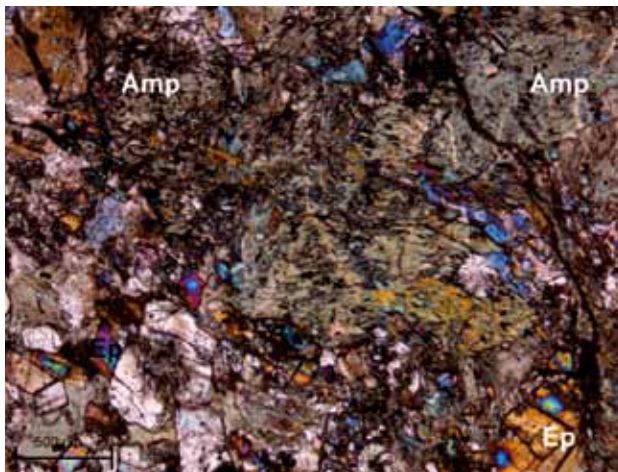


Abb. 5: Amphibole (Amp) und unregelmäßige Verteilung von zonierten Epidotkörnern (Ep) im Amphibolit (VR16). Maßstab: 500 µm. xN.

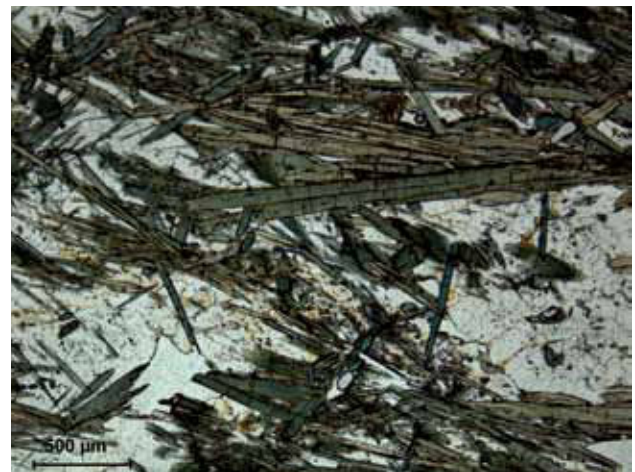


Abb. 6: Stellig-nadelige Amphibole, im Metagabbro (VR82). Maßstab: 500 µm. IIP.

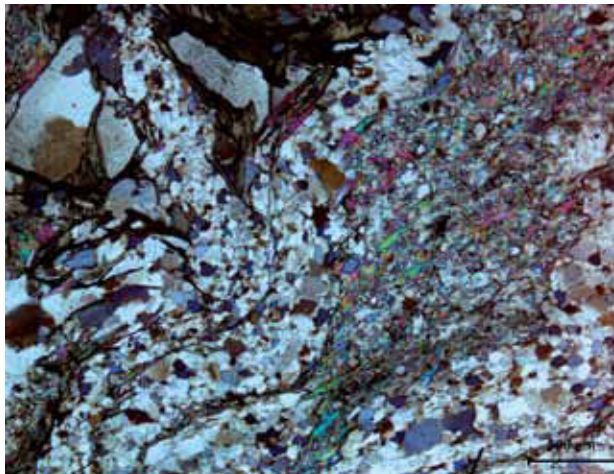


Abb. 7: Zahlreiche Granate im Hornfels sind in Lagen angereichert. Die Probe ist stark alteriert (VR14/2). Maßstab: 500 µm. IIN.

Amphibolit:

$\text{Amp} + \text{Pl} + \text{Czo}/\text{Ep} \pm \text{Chl} \pm \text{Bt} \pm \text{Ttn} \pm \text{Ilm} \pm \text{Cc} \pm \text{Qtz} \pm \text{Ap}$

Metagabbro:

$\text{Amp} + \text{Pl} + \text{Czo}/\text{Ep} + \text{Chl} + \text{Ttn} \pm \text{Qtz} \pm \text{Ilm} \pm \text{Cc} \pm \text{Ap}$

Diorit (Klausenit):

$\text{Pl} + \text{Cpx} + \text{Bt} \pm \text{Ilm} \pm \text{Mag} \pm \text{Ttn} \pm \text{Qtz} \pm \text{Py} \pm \text{Zr}$

Hornfels:

$\text{Chl} + \text{Ms} + \text{Qtz} \pm \text{Grt} \pm \text{Cc} \pm \text{Ap} \pm \text{Ilm}$

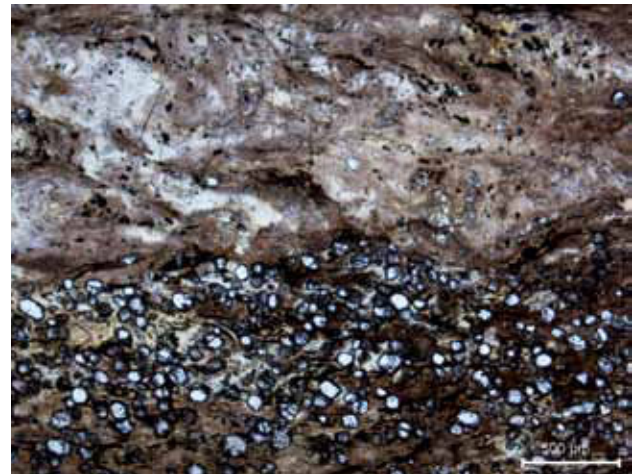


Abb. 8: Gefüge des Quarzphyllites (VR02E). Maßstab: 500 µm. xN.

Quarzphyllit:

$\text{Ms} + \text{Chl} + \text{Bt} + \text{Pl} + \text{Qtz} \pm \text{Cc}$

Orthogneis:

$\text{Pl} + \text{Kfs} + \text{Qtz} + \text{Ms} + \text{Bt}$

Grünschiefer:

$\text{Chl} + \text{Ab} + \text{Amp} \pm \text{Qtz} \pm \text{Cc} \pm \text{Ep}$

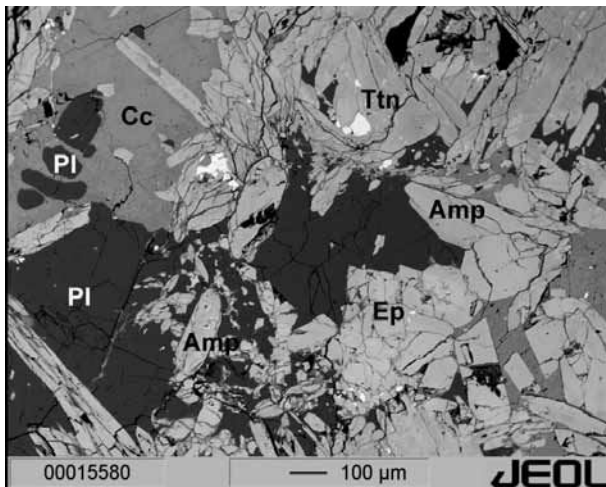


Abb. 9: Das BSE Bild zeigt einen Metagabbro mit unzonierten Amphibolen (VR03/1). Amp: Amphibol, Ep: Epidot, Pl: Plagioklas, Cc: Kalzit, Ttn: Titanit.

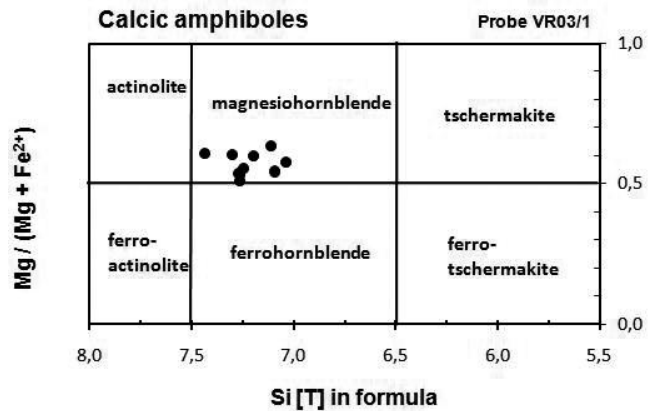


Abb. 10: Klassifizierung der Ca-Amphibole der Probe VR03/1 nach Leake et al. (1997). Diagramm Parameter: $Ca_B \geq 1.50$; $(Na + K)_A \leq 0.50$; $Ca_A < 0.50$.

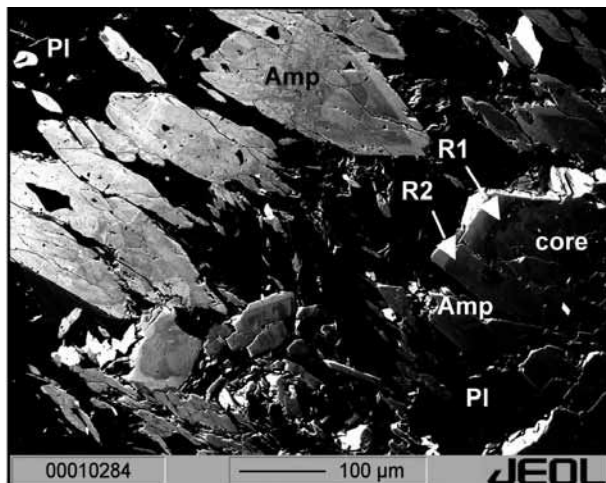


Abb. 11: Das BSE Bild zeigt die chemische Zonierung von idiomorphen Amphibolen (core, R1, R2) im Metagabbro (VR04). Amp: Amphibol, Pl: Plagioklas.

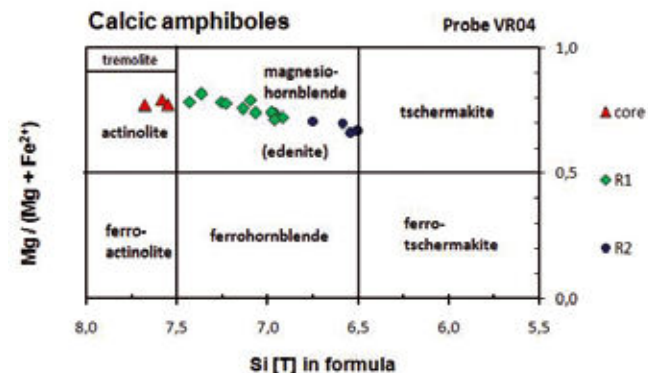


Abb. 12: Klassifizierung der Ca Amphibole der Probe VR04 nach Leake et al. (1997). Diagramm Parameter: $Ca_B \geq 1.50$; $(Na + K)_A \leq 0.50$; $Ca_A < 0.50$. Die roten Symbole kennzeichnen die Kerne (core), die Grünen die Ränder R1 und die Blauen die Ränder R2. Für das Edenit-Feld, welches sich mit dem Magnesiohornblende-feld deckt, gelten andere Parameter: $Ca_B \geq 1.50$; $(Na + K)_A \geq 0.50$; $Ti < 0.50$. Davon sind nur die Punkte R2 (blau) betroffen.

9. Mineralchemie

Die P-T Geschichte einer Probe kann durch eine Kombination verschiedener qualitativer, textureller als auch quantitativer Methoden bestimmt werden. Diese beinhalten die Untersuchung von chemischen Zonierungen und Reaktionsgefügen, von Einschlüssen und Entmischungen in den auftretenden Mineralen und die Geothermobarometrie. Markante chemische Zonierungen weisen hauptsächlich Amphibole (Abb. 11) und Epidot/Zoisite (Abb. 13) aus den Metagabbros und den

Amphiboliten auf. Plagioklas und Chlorit zeigen hingegen keine oder nur eine sehr schwache chemische Zonierung. Die Änderung der Zusammensetzung der Amphibole wurde mittels BSE Bildern und Röntgenverteilungsbildern dargestellt. Die Kationenzahlen werden in apfu (atoms per formula unit) angegeben. Für die Tabellen mit den gesamten mineralchemischen Daten wird auf die Diplomarbeit von Rofner (2010) hingewiesen.

9.1 Mineralchemie der Metagabbros

Amphibol

In den untersuchten Proben kann man zwischen nicht zonierten (Abb. 9) und zonierten Amphibolen (Abb. 10) unterscheiden. Zahlreiche Amphibole in den Metagabbros zeigen sehr starke chemische Zonierungen, wobei sich sowohl einfache als auch komplexe Zonierungen ermitteln lassen. Die untersuchten Amphibole der Metagabbros gehören nach der Nomenklatur der Amphibole von Leake et al. (1997) zu den Ca-Amphibolen. Die Abbildung 9 stellt die Zusammensetzung der nicht-zonierten Amphibole dar, Abbildung 11 zeigt die Amphibolzonierungen, welche im Kern aus Aktinolith und zum Rand hin aus Mg-Hornblende (R1) und Edenit (R2) bestehen.

Plagioklas

Die untersuchten Feldspäte der Metagabbros sind kaum, wenn überhaupt zoniert und sehr selten lassen sich Zwillingslamellen erkennen. In der Probe VR1a koexistiert Plagioklas und Kalifeldspat, wobei es sich um Plagioklase mit XAb = 99.6 und Kalifeldspäte mit XKfs = 99.7 handelt. In allen anderen Analysen ist fast reiner Albit (XAb = 0.99) zu finden. Die Plagioklase in den Metagabbros sind also sehr albitreich und variieren nicht in ihrer Zusammensetzung.

Epidot/Klinozoisit

Die Epidot/Klinozoisite zeigen deutliche chemische Zonierungen, wobei die Ränder R1, R2, R3 und der Kern (core) unterschieden werden können. Man erkennt Fe-reiche Kerne und Fe-ärmere Ränder und zudem variieren die Ti- und Al-Gehalte, wobei Ti (wie auch Fe) vom Kern zum Rand abnimmt und Al vom Kern zum Rand zunimmt. Die SiO₂-Gehalte liegen zwischen 37.40-38.66 Gew.%. Nur geringe Veränderungen zeigen die Elemente wie Mn (max. 0.28 Gew.%) und Ca (zwischen 23-24 Gew.%). Sr weist maximale Werte von 0.3 Gew.% auf. Die Analysen der Epidot/Klinozoisite weisen meistens keine REE (Rare Earth Elements) wie Ce, La und Pr auf und nur eine Analyse zeigt hohe Gehalte an Mn, Sr, Ce, La (sowie auch Pr). Bei dieser Analyse handelt es sich um den in Abbildung 13 weißen Bereich (Kern), der sich von allen anderen Analysen deutlich unterscheidet und

als Allanit innerhalb der Epidotgruppe angesprochen werden kann.

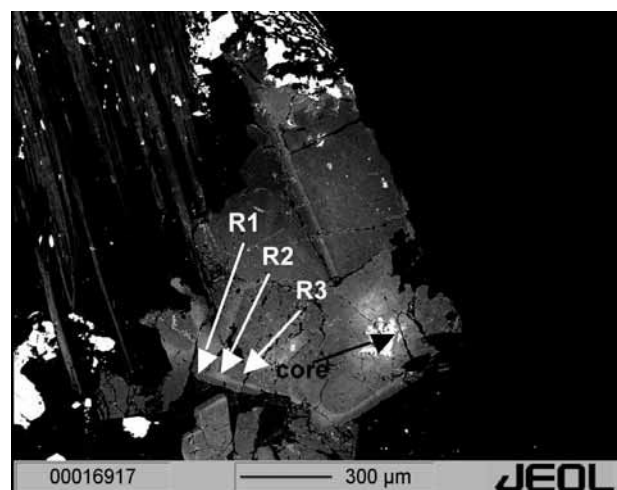


Abb. 13: BSE Bild eines chemisch zonierten Epidotes mit Allanit im Kern (core, weißer Bereich) und Rändern (R1-R3) mit unterschiedlichen REE Gehalten (VR06J).

Chlorit

Die Chlorite der untersuchten Metagabbros plotten nach Hey (1954) in das Feld der Rhipidolite und gehören somit zur Gruppe der Mg-Fe Chlorite (Dibantit-Pyknochlorit-Rhipidolit Reihe).

Kalzit

Bei den untersuchten Karbonaten handelt es sich um fast reinen Kalzit, nur untergeordnet sind Mg, Mn und Fe eingebaut. Dolomit ist nicht vorhanden. Die Kalzite der Metagabbros enthalten im Durchschnitt 98% CaCO₃, 1% MgCO₃, 0.1% FeCO₃ und <0.1% MnCO₃.

9.2 Mineralchemie der Amphibolite

Amphibol

Teilweise weisen die Amphibolite texturell zwei Generationen von Amphibolen (Amp I, Amp II) auf, die sich jedoch chemisch nicht unterscheiden. Amp I repräsentiert idiomorphe, reliktische Kristalle, während Amp II längliche, idiomorphe Nadeln bildet. Man

erkennt auch Amphibole die von Plagioklas zersetzt werden (Abb. 14). Ausgeprägte chemische Zonierungen sind in den untersuchten Amphiboliten seltener.

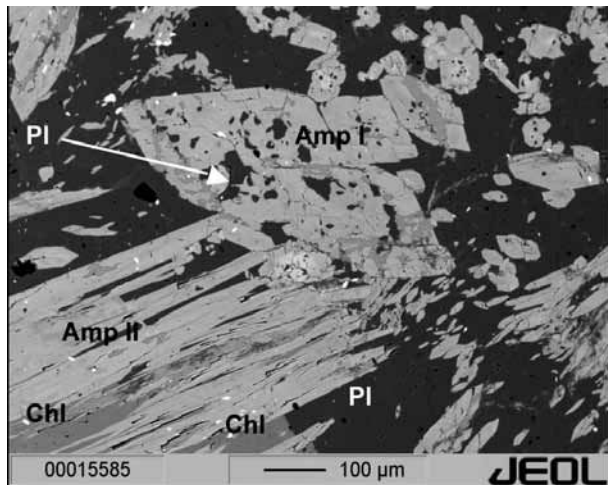


Abb. 14: Das BSE Bild zeigt zwei texturell unterschiedliche Generationen von Amphibolen, Amp I und Amp II (VR22). Amp: Amphibol, Ep: Epidot, Pl: Plagioklas, Cc: Kalzit, Chl: Chlorit.

Nach Leake et al. (1997) plotten die Amphibole beider Generationen (Amp I und Amp II) ins Feld der Mg-Hornblende (Abb. 15).

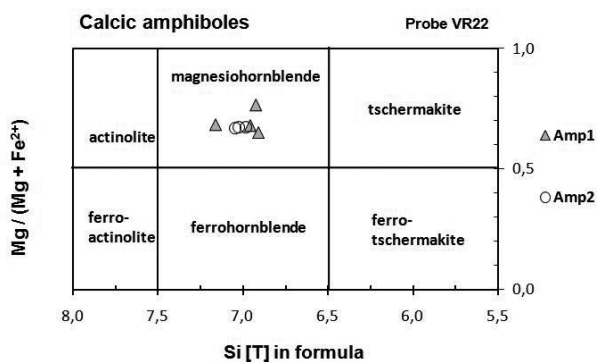


Abb. 15: Klassifizierung der Ca-Amphibole der Probe VR22 nach Leake et al. (1997). Diagramm Parameter: $\text{Ca}_B \geq 1.50$; $(\text{Na} + \text{K})_A \leq 0.50$; $\text{Ca}_A < 0.50$.

Die Amphibole, Amp I, weisen Ti-Gehalte von 0.09–0.17 Gew.% TiO₂ und Mn-Gehalte von 0.28–0.33 Gew.% MnO auf, die Amphibole, Amp II, zeigen hingegen Ti-Gehalte von 0.22 Gew.% TiO₂ und 0.26–

0.31 Gew.% MnO. Die Cr-Gehalte ändern sich bei beiden Generationen kaum (max. 0.16 Gew.% Cr₂O₃). Die Na- und K-Gehalte beider Amphibolgenerationen variieren leicht zwischen 1.28–1.91 Gew.% Na₂O und 0.31–0.40 Gew.% K₂O.

Plagioklas

Bei den untersuchten Plagioklasen handelt es sich ebenfalls um fast reinen Albit ($X_{\text{Ab}} = 0.95$) mit durchschnittlichen Anorthitgehalten <5 Mol%. Die Plagioklase zeigen keine chemischen Zonierungen und sind in ihrer Zusammensetzung sehr konstant.

Epidot/Klinozoisit

Die Epidot/Klinozoisite in den untersuchten Amphiboliten zeigen ebenfalls deutliche Zonierungen (Abb. 16), wobei die Ränder R1 und R2 und der Kern (core) unterschieden werden. Die Epidot/Klinozoisite zeigen eine Abnahme des Fe^{3+} Gehaltes vom Kern zum Rand.

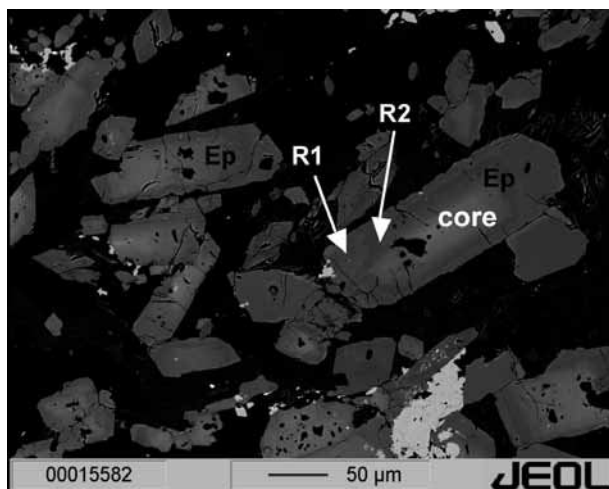


Abb. 16: BSE Bild der Zonierungen (core, R1, R2) im Epidot, ep (VR22).

Chlorit

Chlorit tritt in Amphiboliten auf, allerdings selten und wenn meist mit Hornblende und Plagioklas. Die analysierten Chlorite der Amphibolite plotten im Klassifikationsdiagramm nach Hey (1954) in das Feld der Rhipidolithe.

10. Geochemie der Amphibolite und Metagabbros

Geochemische Gesteinsklassifizierung

Die Klassifikation mittels SiO₂-Gehalt wurde mit Hilfe der RFA durchgeführt. Bei den im Arbeitsgebiet vorkommenden Metagabbros und Amphiboliten handelt es sich daher um ultrabasische bis basische Gesteine. Der höchste SiO₂-Gehalt beträgt etwa 47.5 Gew.%. Eine klassische Diskriminierung magmatischer Gesteine ist nach Cox (1979) im sogenannte TAS-Diagramm (Total Alkalies versus Silica) gegeben. In diesem Diagramm wird SiO₂ gegen Na₂O + K₂O aufgetragen wird. Die gekrümmte Linie trennt die alkalischen (oberer Teil) von den subalkalischen Gesteinen (unterer Teil).

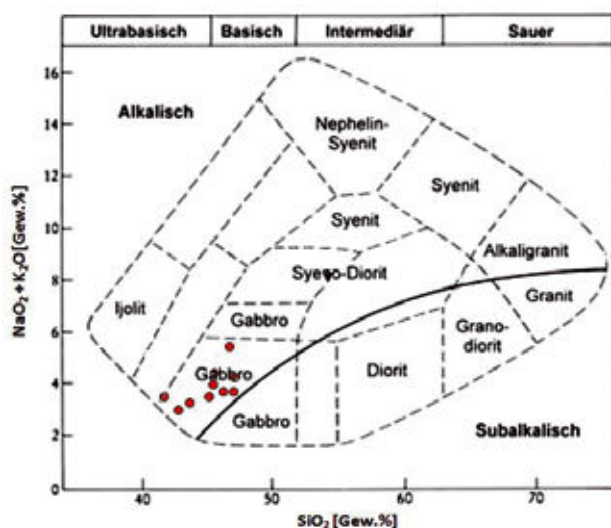


Abb. 17: Das TAS-Diagramm nach Cox (1979), abgeändert nach Wilson (1989) für plutonische Gesteine.

In Abbildung 17 ist zu erkennen, dass die Gesteinsansprache im Gelände auch mit den geochemischen Daten übereinstimmt. So fallen die Proben auch ins entsprechende Feld der alkalisch betonten Gabbros. Grobkörnige Amphibolite spiegeln daher die ehemals magmatische Textur wider und als Ausgangsgesteine kommen daher Gabbros in Frage.

Geotektonisches Setting

Nachdem die Gesteine geochemisch klassifiziert wurden, konnten diese nun geochemisch mit einem

plattentektonischen Setting korreliert werden. Von mehreren Autoren wurde mit Hilfe von unterschiedlich vielen Proben aus verschiedenen geotektonischen Positionen versucht, einzelne Felder gegeneinander abzugrenzen, die typisch für die jeweilige geotektonische Positionen sind. Die geotektonische Einordnung magmatischer Sequenzen anhand geochemischer Daten erfolgte mittels sogenannter geotektonischer Diskriminierungsdiagramme. In der Abbildung 18 ist deutlich erkennbar, dass die analysierten Proben ins Feld „within-plate basalt“ d.h. ins Feld der Intraplattenbasalte plotten. Es handelt sich daher bei den untersuchten Gesteinen um Produkte eines „Intraplattenvulkanismus“.

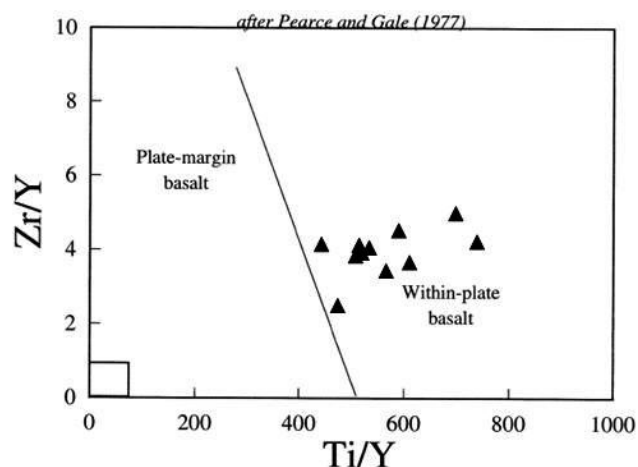


Abb. 18: Geotektonisches Diskriminierungsdiagramm Ti/Y [ppm] versus Zr/Y [ppm] nach Pearce & Gale (1977).

Nach Pearce et al. (1984) zeigen Intraplattenbasalte, ob alkalisch oder tholeiitisch, generell eine Anreicherung der Elemente Th bis Ti. Die untersuchten Gesteine entsprechen in etwa dem beschriebenen Verteilungsmuster, variieren jedoch in der Anreicherung dieser Elemente. Derartige heterogene Ergebnisse sind vor allem für kontinentale, Intraplattensteine charakteristisch, da eine starke Beeinflussung durch den subkontinentalen Mantel zu erwarten ist (Pearce et al., 1984).

11. Geothermobarometrie

11.1 Semiquantitative Thermobarometrie

Ti-in-Hornblende Geothermometer: Der Ti-Gehalt in Amphibolen kann in magmatischen und metamorphen Gesteinen als Geothermometer verwendet werden (Otten, 1984). Der Ti-Gehalt ist temperaturabhängig und nimmt bei steigender Temperatur zu (Otten, 1984; Ernst & Liu, 1998). Das Thermometer von Otten (1984) wurde für ilmenitführende Gabbros in einen Druckbereich von 6-10 kbar kalibriert. Die errechnete Durchschnittstemperatur der Metagabbros liegt bei 506°C, die Temperatur der Amphibolite bei 504°C (Otten, 1984).

Metamorphe Faziesserien nach Laird & Albee (1981): Die Amphibole der untersuchten Metagabbros und Amphibolite plotten in den Diagrammen nach Laird & Albee (1981) in Abbildung 19 in den Bereich der Niederdruck-Fazies (Abukuma Typ) und in die Mitteldruck-Fazies (Dalradian Typ).

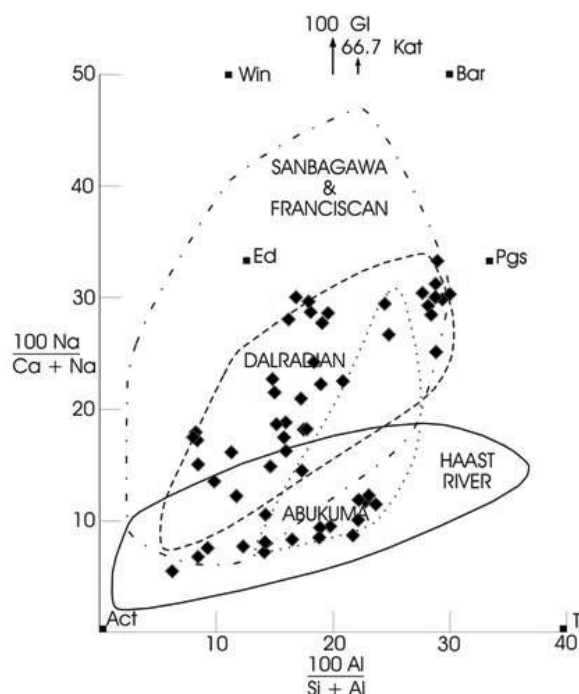


Abb. 19: Faziesserien der Amphibole nach Laird & Albee (1981), welche Amphibolanalysen verschiedener mafischer Serien aus HP-, MP- und LP-Gesteinseinheiten darstellen. Die Felder ermöglichen die Abgrenzung von Amphibolen, die unter unterschiedlichen Metamorphosebedingungen gebildet wurden. Die Symbole stellen die Analysen aus den Metagabbros dar.

11.2 Geothermobarometrie

Zur Berechnung der P-T Daten wurden hauptsächlich die Programme THERMOCALC v.3.21 von Holland & Powell (1998), und PET 5.01 von Dachs (1997) verwendet. Mit dem Programm THERMOCALC werden alle möglichen Mineralreaktionen zwischen einem definierten Set an Phasenkomponenten berechnet. Aus diesen ergeben sich einzelne Gruppen an Reaktionen, welche einen Schnittpunkt ergeben. Es ergaben sich folgende P-T Daten:

THERMOCALC v.3.21

Probe

	wobei $aH_2O = 1$	Metagabbro	Amphibolit
$T[\text{°C}]$	452 - 483	550 - 583	536 - 565
$P[\text{kbar}]$	4-5	4-5	4-5

PET steht für „Petrological Elementary Tools“ (Dachs, 1997). Dabei können zahlreiche Anwendungen wie Mineralformeln und Aktivitäten berechnet sowie Geothermometer verwendet werden. Die Ermittlung von Mineralgleichgewichten basiert auf dem intern konsistenten Datensatz von Holland & Powell (1998). Zusätzlich können die errechneten Ergebnisse in Diagrammen dargestellt werden. Es wurden das Geothermometer Amphibol-Plagioklas und das Geobarometer Amphibol-Chlorit verwendet.

Geothermometer Amphibol – Plagioklas: Die Temperaturen wurden nach der Kalibration von Holland & Blundy (1994) ermittelt (Abb. 20, 21).

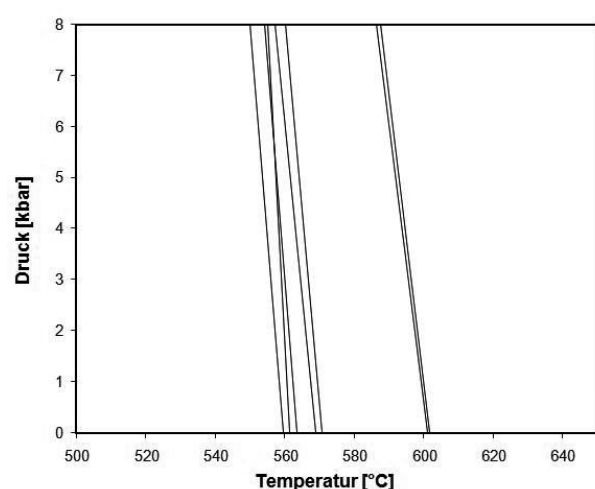


Abb. 20: Amphibol-Plagioklas Thermometrie nach Holland & Blundy (1994) nach der Kalibration 0 (Edenit – Tremolit) mittels der Reaktion Albit + Tremolit = Edenit + Quarz (Probe VR03/1, Metagabbro).

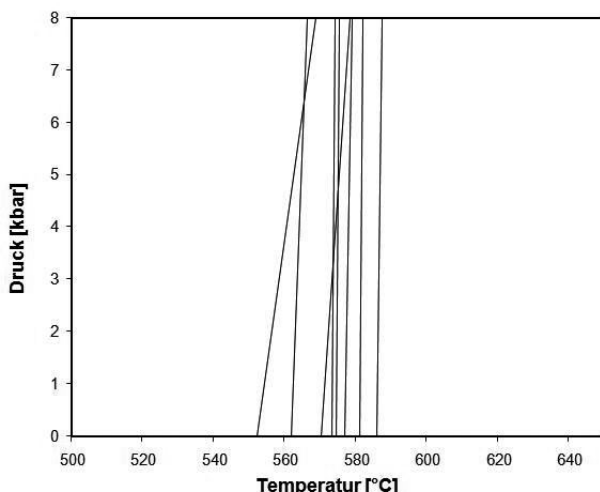


Abb. 21: Amphibol-Plagioklas Thermometrie nach Holland & Blundy (1994) mittels der Kalibration 0 der Probe VR22 (Amphibolit).

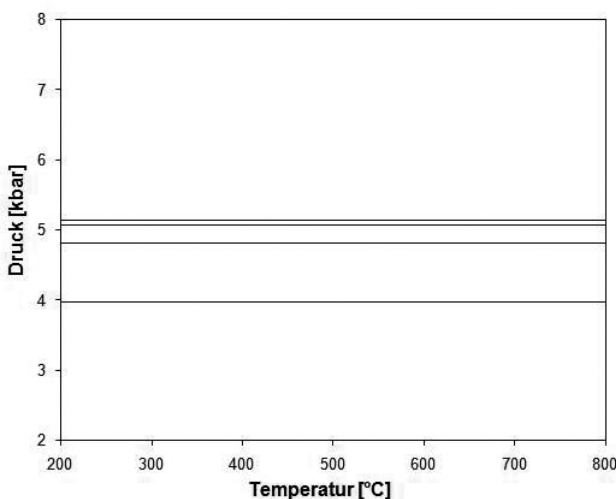


Abb. 22: Amphibol-Chlorit Barometrie nach Cho (1988, schriftl. Mitt., in Laird, 1988) der Probe VR04J (Metagabbro).

Geobarometer Amphibol – Chlorit: Die Drucke beruhen auf dem Fe-Mg Austausch zwischen Amphibol und Chlorit nach Cho (1988, schriftl. Mitt., in Laird, 1988). Eine detaillierte Studie über die Druckabhängigkeit des FeMg-1 Austausches zwischen Aktinolith und Chlorit zeigt, dass der Kd-Wert zwischen Amphibol und Chlorit druckabhängig ist und somit als Geobarometer in niedriggradigen Metabasiten angewandt werden kann (Abb. 22):

$$P \text{ [kbar]} = 10.5 \ln K_d + 0.5$$

$$\text{wobei } K_d = (\text{Mg}/\text{Fe})_{\text{Act}} / (\text{Mg}/\text{Fe})_{\text{Chl}}$$

Zusammenfassend ergaben sich folgende P-T Daten:

MATHEMATICA – PET 5.01
Amphibol-Plagioklas Thermometrie

Probe	Metagabbro	Amphibolit
VR03/1	VR15b	VR22

T [°C]

P = 5 kbar

550 – 588	Kalibration 0:
405 – 447	Kalibration 1:
488 – 568	Kalibration 0:
567 – 587	Kalibration 0:

Amphibol-Chlorit Barometrie

Metagabbro	
VR04J	VR19
P [kbar]	3.97 – 5.13 3.00 – 4.50

12. Diskussion

Den Schwerpunkt der Arbeit bildete der Amphibolit/Metagabbro Komplex bei Gufidaun und dessen geochemische und thermobarometrische Untersuchungen. Mineralchemisch wurden in beiden Gesteinsarten ähnliche Beobachtungen gemacht. Die Amphibole der Metagabbros und Amphibolite zeigen teilweise starke Zonierungen. In den Amphiboliten konnten texturell zwei Amphibolgenerations (Amp I, Amp II) unterschieden werden. Chemisch sind sie aber sehr ähnlich in ihrer Zusammensetzung. Amp I könnte möglicherweise einen reliktischen, spätmagmatischen Amphibol darstellen. Amp II weist eine prograde Zonierung, wie in den Metagabbros, auf. Die Amphibole der Metagabbros weisen eine prograde Zonierung mit einem variszisch metamorphen, aktinolithischen Kern, und Mg-Hornblende und Paragonit bzw. Edenit in den Rändern, auf. Bei den nicht zonierten Amphibolen handelt es sich um Mg-Hornblende. Es kann daher ein Temperaturanstieg in den Amphibolen (vom Kern zum Rand hin) angenommen werden. Gegen Ende oder möglicherweise auch nach der Abkühlung der Intrusion setzte eine Dekompression ein. Die Granate der Hornfelse (kontaktmetamorpher Quarzphyllit) besitzen einen variszischen Kern und einen jüngeren Anwachssaum, wobei dieser die Folge der Permischen Kontaktmetamorphose darstellt. Granat wurde nur im Hornfels gefunden, in allen anderen Gesteinen fehlt er völlig.

Thermobarometrische Berechnungen mit den Programmen THERMOCALC V.3.21 und PET 5.01 sowie semiquantitative Methoden ergaben für die Metagabbros und Amphibolite variszische Metamorphosebedingungen von 488–588°C und 3–5 kbar (Abb. 23). Die Ergebnisse aus den untersuchten Metagabbros und Amphiboliten stimmen mit den P-T Daten von ca. 450–550°C und 5–6.5 kbar von Ring & Richter (1994) gut überein. Die P-T Bedingungen von 520–550°C und 5.3 kbar aus den Quarzphylliten bei Brixen (Wylhidal, 2008), stimmen ebenfalls mit den errechneten Daten des Amphibolit/ Metagabbro Komplexes überein.

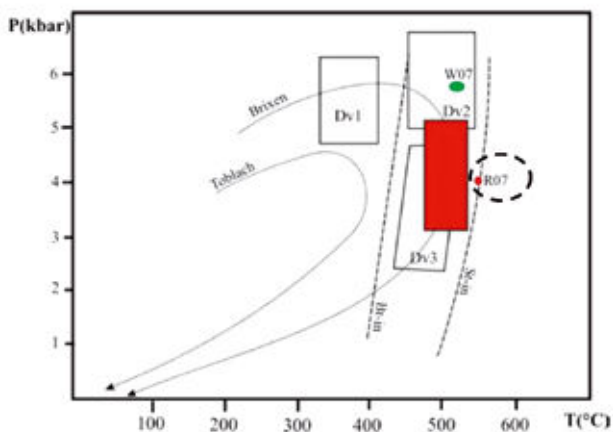


Abb. 23: P-T Diagramm mit den thermobarometrischen Daten dieser Arbeit (rotes Rechteck und strichlierter Kreis). Die Bereiche Dv1, Dv2 und Dv3 repräsentieren die P-T Abschätzungen von Deformationsevents der Gesteine von der Gegend bei Brixen und Toblach (von Ring & Richter, 1994). Die Stabilitätskurven Biotit (Bt-in) und Staurolith (St-in) stammen von Yardley (1989). Eingezeichnet sind thermobarometrische Daten von Wyhlidal (2008) (Probe W07) und Rofner (2010) (Probe R07).

Danksagung

Dank gilt Dr. Richard Tessadri für die Hilfe bei der Vorbereitung und Messung am Röntgenfluoreszenzspektrometer. Mag. Martina Tribus und Bernhard Sartory wird für die Hilfe an der Elektronenstrahlmikrosonde gedankt. Dr. Werner Thöny wird für die Durchsicht des Manuskriptes gedankt.

Literatur

- Bögel, H. & Schmidt, K. (1976): Kleine Geologie der Ostalpen. – Thun (Ott), 231 S.
- Brandner, R., Gruber, A. & Keim, L. (2007): Geologie der Westlichen Dolomiten: Von der Geburt der Neothys im Perm zu Karbonatplattformen, Becken und Vulkaniten der Trias. – GeoAlp 4: 95–121.
- Cox, K.G. (1979): The interpretation of igneous rocks. – George Allen & Hyman, London.
- Dachs, E. (1997): PET: petrological elementary tools for mathematica. – Comp. Geosci. 24: 219–235.
- Ernst, W.G. & Liu, J. (1998): Experimental phase-equilibrium study of Al- and Ti-contents of calcic amphibole in MORB – a semiquantitative thermo-barometer. – Am. Mineral. 83: 952–969.
- Furlani-Cornerlius, M. (1924): Zur Kenntnis der Villnösser Linie. – Verh. Geol. B.-A., 7: 125–131.
- Gisser, A. (1926): Zur Petrographie der Klausenite. – Der Schlern 11, 64 S.
- Heißel, W. & Ladurner, J. (1936): Geologie des Gebietes von Villnöß-Gröden-Schlern-Rosengarten. – Jb. Geol. B.-A. 86, Wien, 63 S.
- Hey, M.H. (1954): A new review of the chlorites. – Mineral. Mag. 30: 277–292.
- Holland, T.J.B. & Blundy, J. (1994): Non-ideal interactions in calcic amphiboles and their bearing on amphibole-plagioclase thermometry. – Contrib. Mineral. Petrol. 116: 433–447.
- Holland, T.J.B. & Powell, R. (1998): An internally consistent thermodynamic dataset for phases of petrological interest. – J. Metam. Geol. 16: 309–343.
- Kretz, R. (1983): Symbols for rock-forming minerals. – Am. Mineral. 68: 277 – 279.
- Laird, J. (1988): Chlorites: metamorphic petrology. – Rev. Mineral. 19: 405–442.
- Laird, J. & Albee, A.L. (1981): High pressure metamorphism in mafic schist from Northern Vermont. – Am. J. Sci. 281: 97–126.
- Leake, B.E. et al. (1997): Nomenclature of amphiboles: Report of the Subcommittee on amphiboles of the International Mineralogical Association, Commission on New Minerals and Mineral Names. – Can. Mineral. 35: 219–246.
- Mutschlechner, G. (1932): Geologie der St. Vigilier Dolomiten. – Jb. Geol. B.-A. 82: 163–273.
- Otten, M.T. (1984): The origin of brown hornblende in the Artjället gabbro and dolerites. – Contrib. Mineral. Petrol. 86: 189–199.

- Pearce, J.A., Harris, N.B.W. & Tindle A.G. (1984): Trace Element Discrimination Diagrams for the Tectonic Interpretation of Granitic Rocks. – *J. Petrol.* 25: 956–983.
- Ring, U. & Richter, C. (1994): The Variscan structural and metamorphic evolution of the eastern Southalpine basement. – *J. Geol. Soc., London*, 151: 755–766.
- Rofner, V. (2010): Petrologie und Geologie des Amphibol/Metagabbro Komplexes von Gufidaun (Südtirol, Italien). – Unveröffentl. Diplomarb., Univ. Innsbruck, 139 S.
- Schmidt, S.M., Fügenschuh, B., Kissling, E. & Schuster, R. (2004): Tectonic map and overall architecture of the Alpine orogen. – *Ecl. Geol. Helv.* 97: 93–117.
- Staindl, A. (1971): Klausen geologisch gesehen. – *Der Schlern* 45: 372–379.
- Stingl, V. & Mair, V. (2005): Einführung in die Geologie Südtirols. – Autonome Provinz Bozen, Amt für Geologie und Baustoffprüfung, Kardaun (BZ), 80 S.
- Wilson, M. (1989): Igneous petrogenesis. – London, Unwin Hyman, 456 S.
- Wylidal, S. (2008): Petrological and experimental investigations on the Permian contact metamorphic event in the Southalpine domain (South Tyrol, Italy). – Unveröffentl. Diss., Univ. Innsbruck, 262 S.
- Yardley, B.W.D. (1989): An Introduction to Metamorphic Petrology. – Longman Earth Science Series, 248 S.

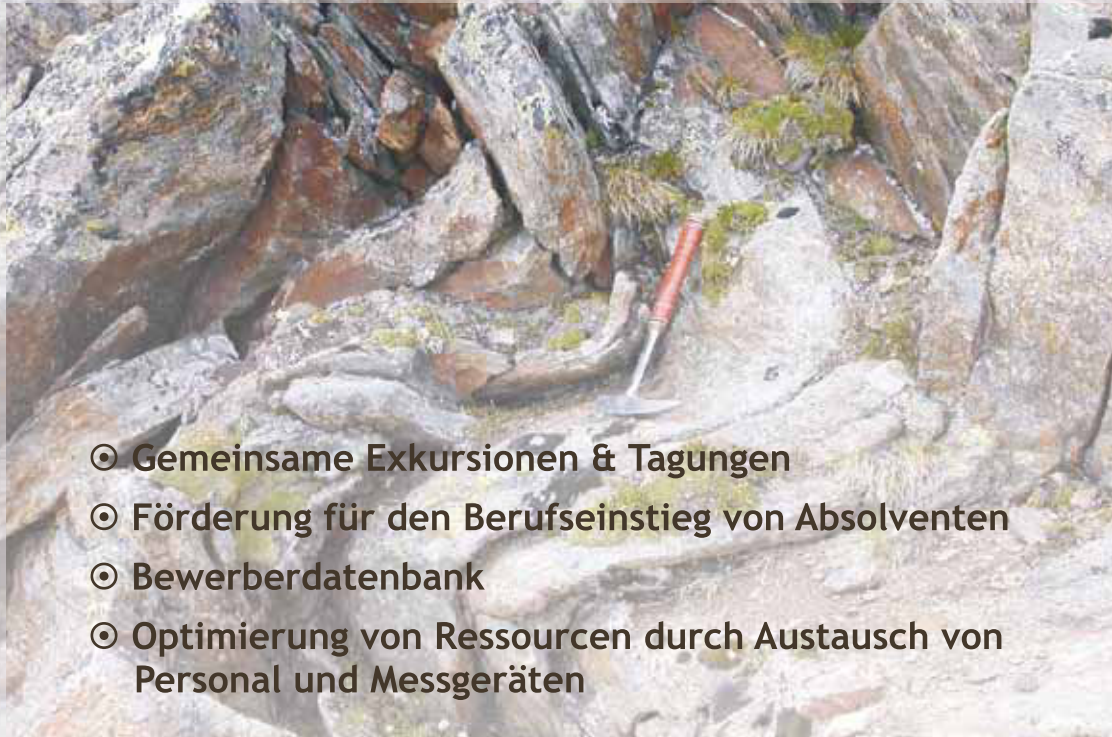
Manuskript eingereicht: 21.6.2010

Überarbeitetes Manuskript angenommen: 24.8.2010



Verband der selbständigen Geologen Österreichs

VSGÖ Verband der selbständigen Geologen Österreichs
Hölzlstraße 5 · A-5071 Wals bei Salzburg · Österreich
Tel. +43-(0)662-65 9 65-334 · Fax +43-(0)662-65 9 65-10
E-Mail geologie@geoconsult.at



- ◎ Gemeinsame Exkursionen & Tagungen
- ◎ Förderung für den Berufseinstieg von Absolventen
- ◎ Bewerberdatenbank
- ◎ Optimierung von Ressourcen durch Austausch von Personal und Messgeräten

THE COPPER-WOLFRAM DEPOSIT OF BEDOVINA (TRENTO, ITALY)

Pietro Frizzo¹, Luca Peruzzo² and Elio Dellantonio³

With 29 figures

¹ Dipartimento di Geoscienze, Università di Padova

² CNR – Istituto di Geoscienze e Georisorse, Sede di Padova

³ Museo Geologico delle Dolomiti, Predazzo (Trento)

Abstract

The W (Mo, Sn, Bi) and Cu (Pb, Zn, Ag, Te, Co, Ni, etc.) deposits of Bedovina mark the closure of the Middle-Triassic magmatic cycle of the Predazzo-Monzoni Eruptive Complex, composed of latiandesitic and latibasic lavas, monzonitic stocks with shoshonitic affinity, K-alkaline monzosyenitic bodies, and some granitic masses. The mineralization is hosted in a stockwork of veins which intersects the volcanics and, occasionally, granitoid masses, and rarely acidic and mafic veins. Two different metalliferous phases can be recognized, the first mainly wolfram-bearing, the second copper-polymetallic. The wolfram phase is represented by quartz+K-feldspar+tourmaline veins, with scheelite, minor apatite and rutile, rare cassiterite, and hematite. Sporadic synchysite-(Ce) and molybdenite occur in granite breccias.

The copper-polymetallic phase was superimposed to the wolfram one after a brittle tectonic event; it comprises quartz, chalcopyrite, minor pyrite, sphalerite, galena and traces of other sulfides and sulfosalts such as cobaltite, argentite/acantite, members of the tetraedrite-tennantite series, bismutiferous sulfosalts (arcubisite/silver-copper-cosalite), Ag (hessite) and Bi tellurides (pilsenite) with native Bi and other bismutiferous phases finely intergrown with chalcopyrite.

The mineralization of Bedovina is related to hydrothermal metal fluids derived from the crystallization of two distinct granitoid magmas: the first is of "S type" character, and probably would have generated the parageneses typical of the "wolfram phase" (W with minor Sn, REE, Th); the second is of "I type" character, is assumed to be responsible for the polymetallic associations (Cu, with Zn, Pb, Ag, Bi, etc.).

1. Introduction

The copper-wolfram Bedovina deposit outcrops of Mt. Mulàt, embedded in the Ladinian eruptive complex of Predazzo, Southern Alps (Fig. 1). It has been mined since prehistoric times for copper (Šebesta, 1992) and since 1909 also for tungsten. The mining was concentrated between 1600 and 1750 m on the north-western slope of M. Mulàt (Bedovina mine) and between 1900 and 2000 m on the south-eastern slope of that mountain (Mine of Cima del Mulàt or "Vecchia Bedovina"). The Bedovina Mine was active mainly in the twentieth century: the Consor-

tium Montanistico Oss Mazurana, which obtained the mining claim in 1895, reorganized the mine on eight levels (Fig. 2) connected by shafts and rises (Oss Mazurana, 1905-1906; Oss Mazurana and Hesser, 1909). The extracted ore was transported by cable-way to the plant of Mezzavalle, just north of Predazzo, producing copper sulfate. At the beginning of World War I the Austrian government confiscated the mine and operated with military personnel extracting about 6,000 tons of ore with an average 1.6% of Cu and 0.48% of WO_3 ; the plants of Mezzavalle were

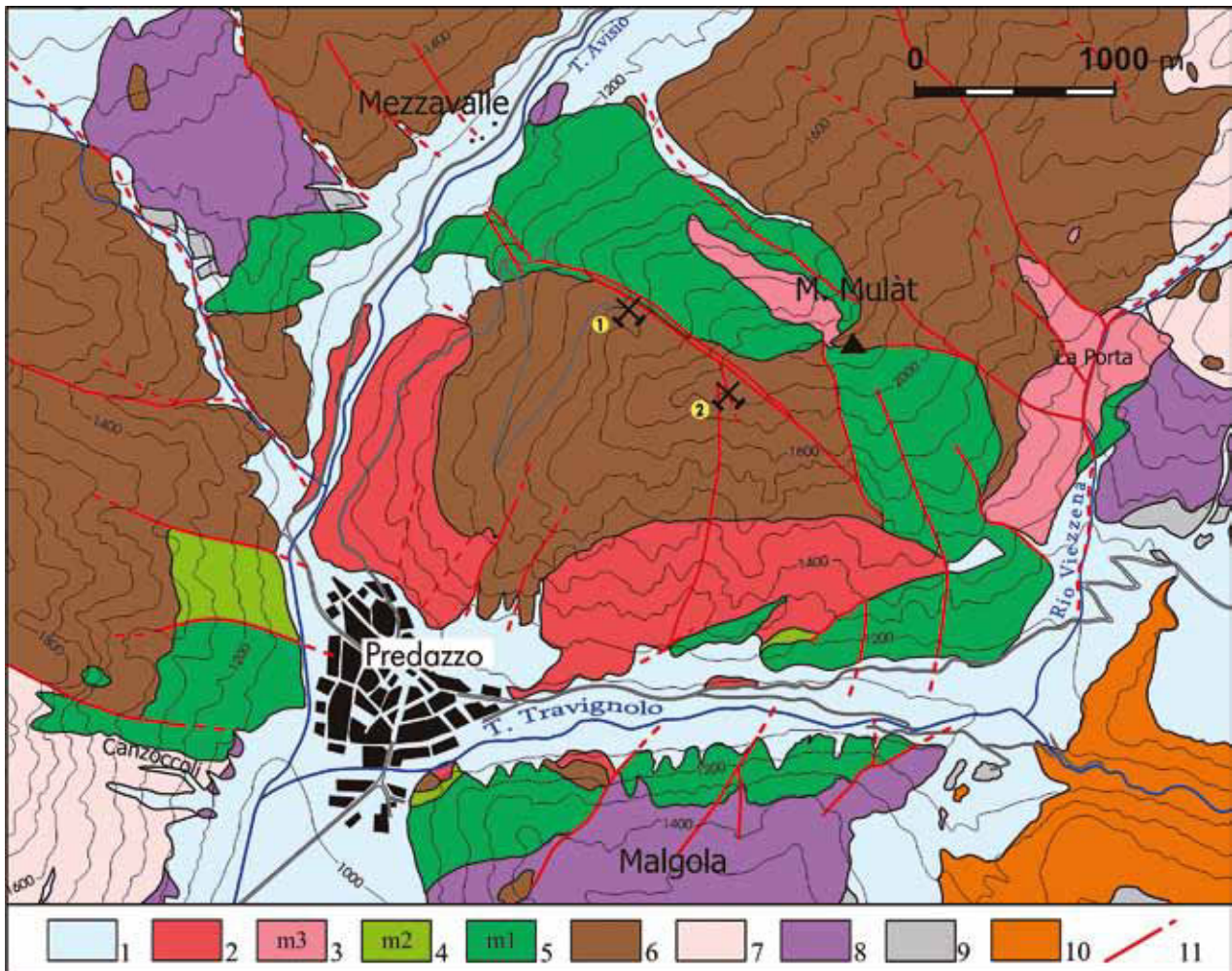


Fig. 1. Geological sketch of the Predazzo area (compiled on the basis of Vardabasso 1930, ENI-Aquater 1997, Visonà 1997 and data of the Authors). Legend: 1 - Undifferentiated Quaternary deposits. PREDAZZO ERUPTIVE COMPLEX: 2 – Biotitic amphibolic granites and muscovite-biotite tourmaliniferous leucogranites; 3 – Quartz monzo-syenites and nepheline sodalite syenites (m3); 4 – Grey-pinkish monzo-syenites and quartz-monzonites (m2); 5 – Monzonites, olivine monzo-gabbros and pyroxenite bodies (m1); 6 – Latiandesitic and andesite-basaltic lava flows, volcanoclastics and subvolcanic bodies. PERMO-TRIASSIC SERIES: 7 – Undifferentiated Sciliar Fm. (Upper Anisian – Ladinian), Contrin Fm. (Upper Anisian), Morbiac Fm. (Upper Anisian), Richthofen Conglomerate (Upper Anisian); 8 – Werfen Fm. (Lower Triassic); 9 – Undifferentiated Val Gardena sandstone and Bellerophon Fm. (Upper Permian). 10 – Dacitic-rhyolitic lavas and ignimbrites of the Volcanic Permian Complex (Lower Permian); 11 – Main faults. 1. Bedovina mine; 2. Vecchia Bedovina – M. Mulàt mine.

used to produce concentrates of chalcopyrite and scheelite. After the war the mine was returned to the Consortium Oss Mazzurana but, for lack of funding, remained inactive and was progressively abandoned. In 1939 the Cogne National Society restructured the mine and the plant of Mezzavalle, resuming the mining activity that continued until 1948. After several years of stagnation in the mid "50s, the claim was taken by the M. Mulàt Company which undertook research works also on the south-eastern slope of the M. Mulàt ("Vecchia Bedovina"); during this period a few thousand tons of raw ore were retrieved, with low concentrations (0.5% Cu and 0.06% in W), taken

from the ore already stored at landfills and storage rooms (Dellantonio, 2000). It is estimated that between 1910 and 1955 about 20,000 tonnes of raw ore with average concentrations of 1.2% Cu and 0.35% WO_3 , have been mined. At the final closure of the mine it was estimated that 50 - 70,000 t of ore were still available, with contents comparable to those mentioned above. The Cima del Mulàt Mine ("Vecchia Bedovina") includes traces of opencast mining, manholes, trenches and tunnels. Mineralization, outcropping from the ridge of M. Mulàt (2030 m) to 1910 m was followed by two galleries (Fig. 3), with portals at an altitude of 1975 and 1925 m respectively. The

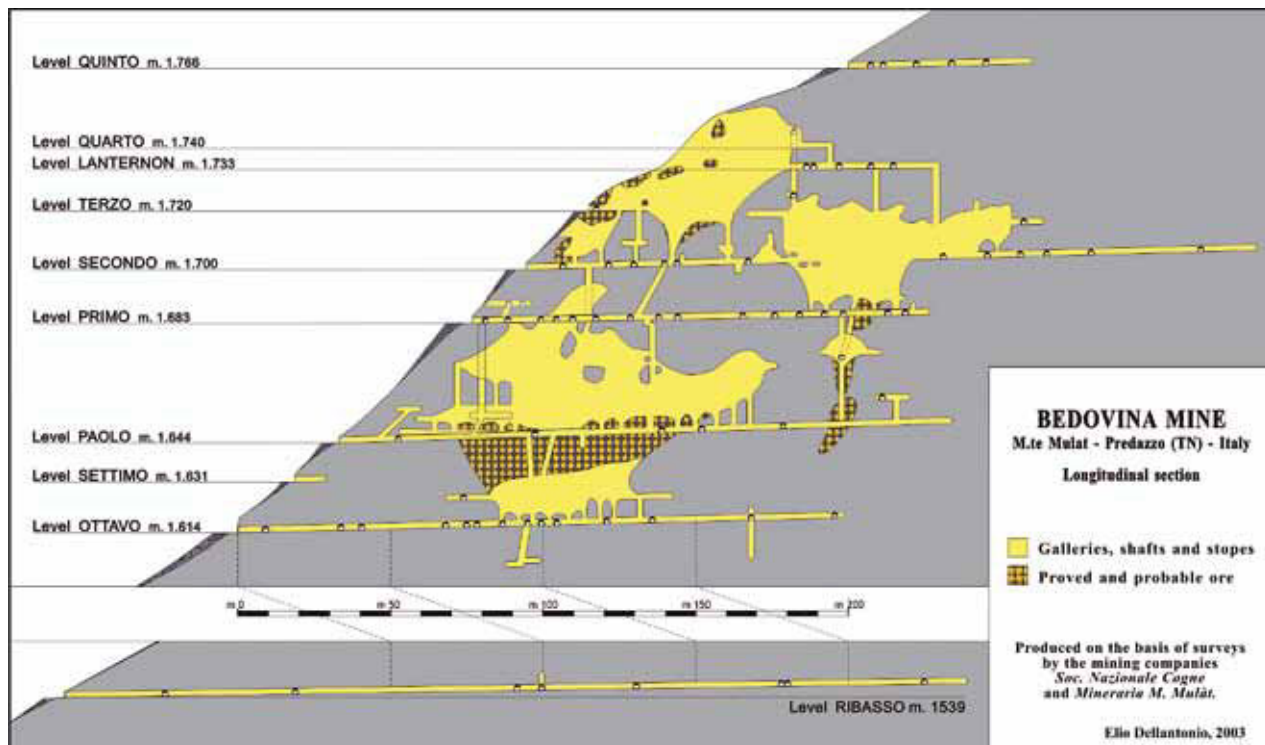


Fig. 2. Cross section of the Bedovina mine.

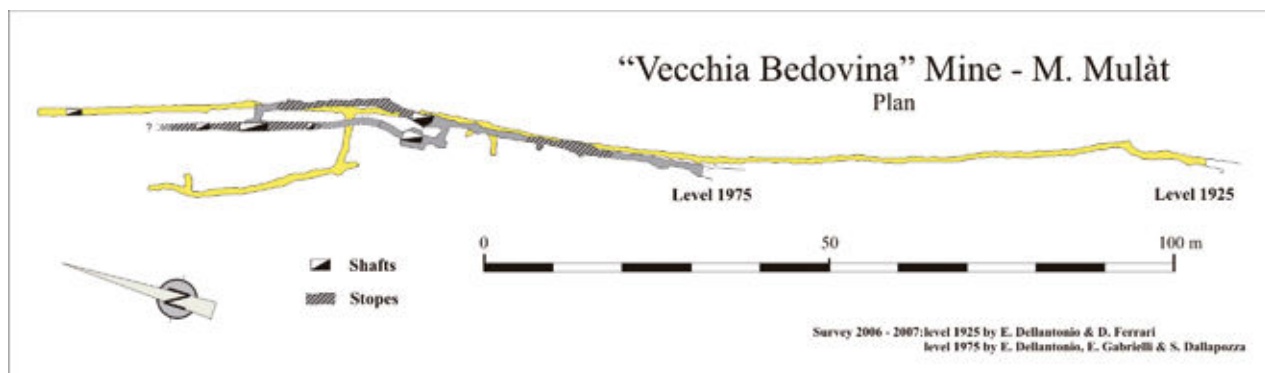


Fig. 3. Cross section of the Vecchia Bedovina-M. Mulàt mine.

lower extends for about 170 m towards the deposit, the upper one, a bit shorter, connects some digging rooms. The explorations undertaken during the '50s of the last century for estimation of ore reserves indicated 40,000 t of ore containing about 0.7% of Cu and 0.1% of W. According to some authors (e.g. Pelloux, 1919; Degiampietro, 1975, etc.) the mine was particularly flourishing in the first half of the XVI century. An examination of the traces of the underground works revealed that at least these are more recent, since they have been entirely made with the use of explosive (black powder) technique back to the XVI century (Vergani, 2002). Archival documents

demonstrate that in Predazzo, around 1730, German-speaking workers mined and smelted copper on behalf of the family Hilleprandt (Stella, 1953, 1957). On the plateau just west of the portal at an elevation of 1975 m upgrading of the raw ore took place before it was transported by mule to the furnaces of Forno and Mezzavalle. The mining was active during some years in the first half of the XIX century (Pelloux, 1919), but was abandoned due to the high cost of transporting the ore to the furnaces of Chiusa (BZ). Towards the middle of the last century when, in an effort to streamline and expand the mining activity, stockworks of the south-eastern slope (M. Mulàt Mine/"Vecchia



Fig. 4. Volcanic clasts, cemented by quartz veins with K-feldspar and chalcopyrite. Bedovina mine. The maximum length of the sample is 11cm.

Bedovina") were also explored; reserves for the two ore deposits were estimated to be 100,000 tons containing about 1% Cu and 0.1% of W. More recent estimates (Eni-Aquater, 1997), based on the assumption of the continuity of the mineralization also in the uncharted stretch of about 400 m between the two deposits, suggest possible additional reserves of 200,000 tons.

2. Geological framework

2.1 The Predazzo Eruptive Complex

The geological context of Bedovina is basically represented by the Ladinian Eruptive Complex of Predazzo (Fig. 1) produced by a single magmatic cycle developed roughly between 237 and 228 Ma. The Eruptive Complex includes effusive, intrusive and dike products, crossing the lithostratigraphic



Fig. 5. Banded mineralization of chalcopyrite and pyrite in tourmaline (black) and quartz. Vecchia Bedovina-M. Mulàt mine. The maximum length of the sample is 8cm.

sequence that ranges from Vulcaniti Atesine (Lower Permian) to the terrigenous and carbonate formations of the Lower and Middle Triassic. Magmatism started with the emission of subaerial pyroclastics of volcano-phreatic origin which was followed by emission of pyroclastics and lavas with latitic, lati-andesitic and lati-basaltic chemistry (Coltorti et al., 1996) to form a large volcanic complex with central pipe, many hundreds meters thick, lying on the Sciliar Fm. (Upper Anisian – Lower Ladinian). The large initial outflow of volcanic products was followed by the collapse of the volcanic caldera with major slumps in the M. Mulàt area (Castellarin et al., 1982). The fractures of the collapse favoured the rising of plutonic bodies (Laurenzi and Visonà, 1996). These bodies form an outer ring of monzonites (Fig. 1) with fewer masses of quartz monzo-syenites and nepheline-sodalite syenites, and an innermost semi-ring of granites (Vardabasso, 1930; Visonà, 1997).

Mineral chemistry and isotope data suggest that the Predazzo Plutonic Complex (Marrocchino et al., 2002) was generated by fractional crystallisation of different magmas injected during a multiple sequence of events related to subduction processes: Menegazzo et al. (1995) and Visonà (1997) recognize (Fig. 1) *three monzonitic units (m1, m2 and m3)* and *one granitic unit (g)*. These products derived from two different magma sources of mantle origin: the first is of shoshonitic composition and located at a depth of 10–12 km, and formed the monzonitic units m1 (monzonites and quartz-monzonites) and m2 (monzonites, olivine monzogabbros with pyroxenite masses). The second is of alkaline-sodic character, 15–17 km deep, and produced the monzonitic unit m3 (monzosyenites with masses of quartz syenite, and nepheline and sodalite syenites) and the granite unit (g) comprising biotite granites and two micas and tourmaline leucogranites. The petrological links with the previous units are not fully clarified (Visonà, 1997). The products of the two magmatic sources intruded and differentiated in subvolcanic environment without direct connection between them. Some petrological characters denote a significant level of crustal contamination at least for granites (Coltorti et al. 1996).

The swarm of dykes that intersects the eruptive complex and underlying Permian-Triassic formations is constituted of rocks equivalent to those of the volcanic succession and of the shoshonitic intrusion, but also K-basanitic, monzo-syenitic and nepheline-syenitic dykes (tinguaite), essexites, aplitic and pegmatitic dykes, and lamprophyric dykes (camptonites) are included. Terrigenous or carbonate rocks in contact with the intrusive masses show a thermo-metamorphic aureole characterized by marble locally with brucite (predazzites and "pencatites" Auct.) composed of complex Ca-silicate parageneses with diopside, vesuviane, grossular, andradite, forsterite, wollastonite, clintonite, tremolite, epidote, serpentine, and locally skarn with magnetite, hematite, pyrite and other sulfides.

2.2 The ore deposits

The copper-wolfram mineralization of Bedovina is represented by stockworks of millimetre to decimetre size veins, controlled by a series of faults and cracks crossing Mt. Mulàt in NW-SE direction (Figs. 4, 5). Along the main fault, known as "Fessuraccia",

the monzonites (north-eastern part) are in contact with the volcanics (south-western part); within these last ones the copper-wolfram mineralization is embedded. In the belt, closest to the Fessuraccia, volcanics are crossed by numerous minor fractures oriented NW, NNW and N-S; some of these, especially the most continuous, enclose tinguaite and lamprophyric dykes partly coupled (Eni-Aquater, 1997). A system of more discontinuous and polyphase fractures, successive to those followed by dykes, hosts the mineralized stockworks: these appear one after the other from the north-western (Bedovina mine) to the south-eastern side of Mt. Mulàt (M. Mulàt – Vecchia Bedovina mine), passing through the top. The most important mineralized bodies extend over distances of 100–200 m in both direction and dip, and are 1 to 4 m thick. The Bedovina deposit is composed of two subparallel stockworks 2–4 m thick, which extend over nearly 200 m with direction N40W, at a distance of almost 10 m, even with frequent convergences and divergences. The M. Mulàt mine is on a stockwork some meters thick that extends over about 200 m within the volcanics, along a tinguaite dike directed N15W.

3. Materials and methods

The study was conducted on several representative samples, selected from a rich collection located at the Geological Museum of the Dolomites of Predazzo. Some of them are part of historical collections and were taken during the mining activity in the level Primo, Paolo and Ottavo in the Bedovina Mine. Because of the difficult access to the ancient galleries of the Bedovina and Mulàt mines, only some of the studied samples were taken directly from the ore body and most of them come from the dumps. The samples were mainly studied under the optical microscope on polished and thin sections integrated with SEM-EDS analysis.

4. Mineralization

4.1 The copper-wolfram ore bodies

The copper-wolfram stockworks of Bedovina are composed of a network of prevailing quartz veins that cement a breccia of pyroclastic rocks and lavas with latitic, lati-andesitic and lati-basaltic chemi-

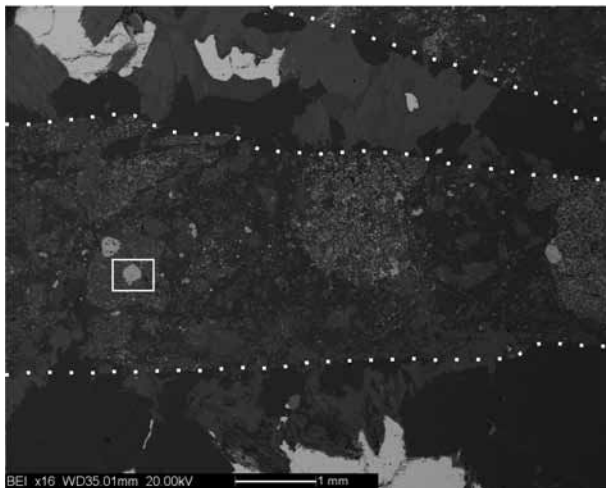


Fig. 6. Volcanic clasts, intensely altered, crossed by pneumatolytic-hydrothermal veins with quartz, tourmaline, scheelite and sulphides. The dashed lines mark the salbands. Box see Fig. 7.

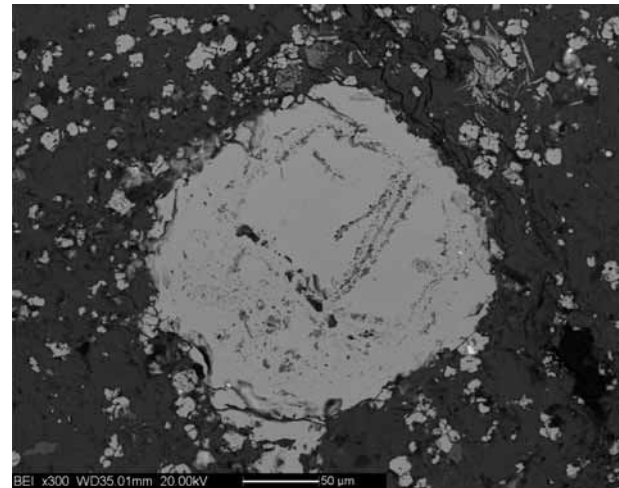


Fig. 7. Detail of Fig. 4 (box). Groundmass of the altered volcanic rock containing a phenocryst of magnetite1 with exsolutions of ilmenite, numerous tiny grains of non titaniferous magnetite2, and rare needles of rutile.

stry (in some cases with fragments of metamorphic rocks composed of quartz, plagioclase and muscovite, pulled away by magma rising through the crystalline basement); occasionally, some breccia fragments derived from acidic and basic dikes. Clasts cemented by mineralized veins show the effect of the pervasive action of pneumatolytic and hydrothermal fluids that generated the mineralization.

Clasts of lavas are characterized by a large felt-like mass with scattered phenocrysts of feldspar (K-feldspar1) locally several millimeters in size and without inclusions and, to a lesser extent, of altered femic silicates and magnetite (magnetite1). Magnetite1 phenocrysts (70–200 µm) include tiny individuals of apatite (apatite1) and plagioclase. The original groundmass hosts swarms of small grains of magnetite (magnetite2) 5–30 µm in size (skeletal the smaller, cubic the larger) and more rare rutile, partly acicular. Magnetite1 phenocrysts are titaniferous and frequently present at the nucleus oriented exsolutions of ilmenite, indicating the nature of primitive crystals from magma solidification; microgranular magnetite (magnetite2) is instead characterized by minimum content of Ti and probably represents a co-product of chloritization of femic silicates (Fig. 6 and Fig. 7). Some hematite developed around the magnetite grains of both generations.

More rarely clasts cemented by the mineralization derived from the fracturing of porphyritic dikes or masses of granitoids. In the first case it regards porphyritic breccias with feldspars and pyroxenes with

scattered quartz plagues and small crystals of apatite epigenetic on chloritized pyroxene; locally thermometamorphic effects induced by porphyritic dike on hosting lava lithotypes are recognized. The action of pneumatolytic-hydrothermal fluids on clasts of granitoid rock are evidenced by sericitization and epidotization on plagioclase and/or K-feldspar (K-feldspar2). In some cases these are alkali-feldspar granite breccias with K-feldspar occurring as large crystals, both white and dark micas, quartz, chlorite and apatite, the latter represented by two generations of crystals: the first is magmatic and linked to the solidification of granite, and the second is epigenetic and formed by the early pneumatolytic-hydrothermal alteration. The K-feldspar2, frequently sericitized, is locally replaced by chlorite and/or zeolite aggregates; biotite is transformed into chlorite.

4.2 Mineralogy

The main component of the mineralized veins is quartz. Coarse quartz is normally typical of the pneumatolytic veins in which it is frequently associated with K-feldspar (K-feldspar 3), tourmaline, mainly schorl (in granular and prismatic crystals sometimes in sheaves), and minor calcite: some tourmaline crystals show a zoned core and an irregular "fibrous" periphery. Associated to the fine grained quartz are most commonly plagues of carbonate and rare chlorite, and small magnetite crystals, locally with pyrite

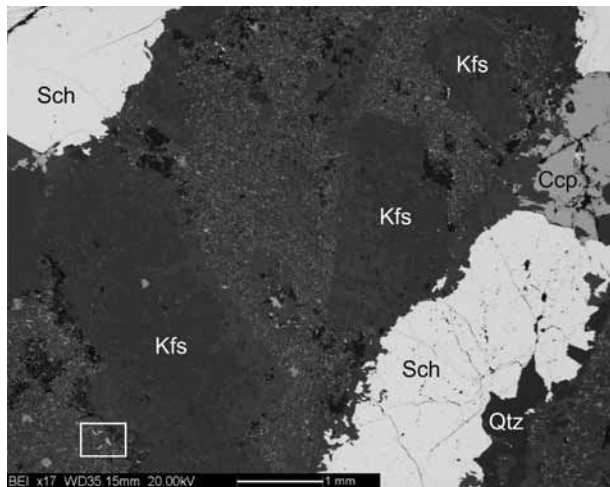


Fig. 8. Veins with scheelite (Sch), chalcopyrite (Ccp) and quartz (Qtz) cement granite clasts containing K-feldspar phenocrysts (Kfs) and tiny plates of molybdenite (in the box see Fig. 9).

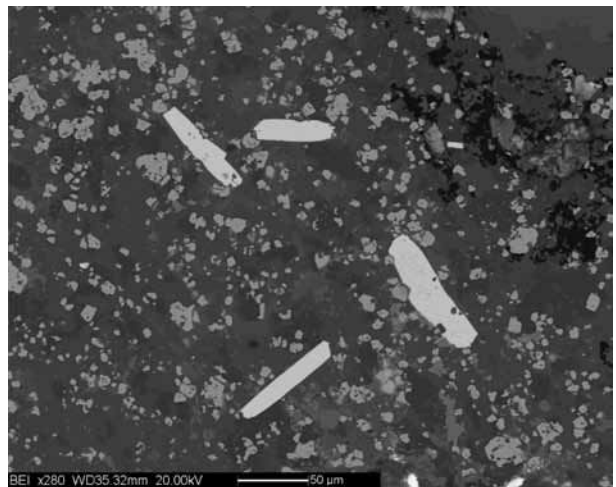


Fig. 9. Detail of Fig. 8 (box). Tiny plates of molybdenite in granite matrix.

inclusions. The metalliferous paragenesis indicates formation in two distinct phases: the first, wolfram-bearing phase, contains scheelite hosted in veins composed of quartz, K-feldspar, tourmaline, locally carbonate, chlorite, apatite and, according to Eni - Aquater (1997), allanite; the copper prevailing phase generated quartz veins with plagues and nodules of chalcopyrite accompanied by pyrite and polymetallic sulfides, less abundant, but present with a large variety of mineralogical species. The transition between lithic clasts and mineralization is usually marked by a thin band of quartz, which may occur in small "combs" of crystals oriented normally to the salband, accompanied by minor, slightly ferriferous calcite, biotite with tiny exsolutions of ilmenite, rare apatite, scattered skeletal individuals of rutile and ilmenite, magnetite grains (without titanium) and sporadic interstitial small plagues of chalcopyrite. At places chalcopyrite and quartz tend to pervade the margin of lava clasts. In the context of the Bedovina Nuova mine, sporadic occurrences of molybdenite should be reported also, independent both from the copper and the wolfram parageneses. They consist of tiny plates of molybdenite (Fig. 8 and Fig. 9), intergrown with quartz, K-feldspar and micas in a fine-grained alkali-ne granite. These are minor mineralizations genetically correlated to those of Aivola (Ricerca Predazzo), still attributable to the granitic magmatic event, but to a pulse of metalliferous fluids slightly preceding the wolfram-bearing phase. Traces of molybdenite are also reported from the debris of the dump of the

Galleria Ventosa and other sites of the magmatic complex of Predazzo and Monzoni.

4.2.1. *The wolframiferous phase*

Wolfram occurs as scheelite grains and up to several mm large crystals disseminated in quartz-feldspar-tourmaline gangue. There is no evidence of wolframite. SEM microchemical analysis identified low, but locally significant, contents of Mo in some scheelite grains. The paragenetic sequence characteristic of wolfram veins starts with the formation of quartz (which continues throughout the whole phase) and scheelite, followed and accompanied by tourmaline (which may include scheelite), K-feldspar, chlorite, occasional crystals of apatite (apatite₂, zoned for fluorine content increasing towards the edge), and finally carbonate. The quartz gangue accompanying the scheelite contains locally tiny crystals of magnetite.

The structural and textural characteristics of the mineralization of Bedovina indicate that the wolfram phase anticipates the copper phase: chalcopyrite in fact appears as late as tourmaline, which at places incorporated some relics after the selective replacement of feldspar. In other places (Fig. 10) scheelite is fractured and cemented by calcite and quartz veinlets containing chalcopyrite plagues and some small crystal of apatite. We also observed locally scheelite grains surrounded by a thin edge of sericite likely to

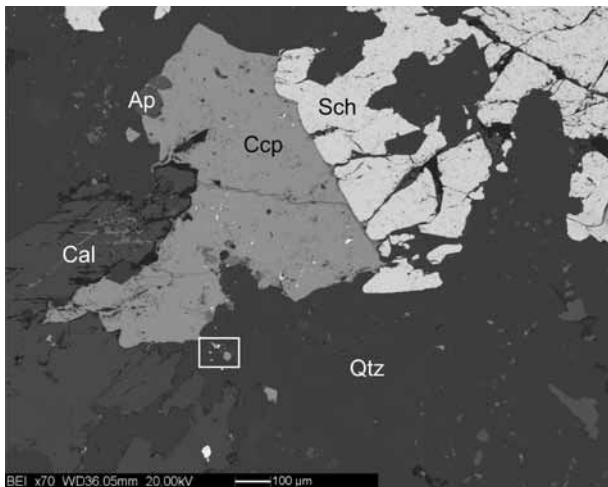


Fig. 10. Scheelite (Sch) fractured and cemented by quartz (Qtz) and calcite (Cal) gangue with chalcopyrite (Ccp) and apatite (Ap). Chalcopyrite contains small grains of galena and rare tiny tellurides. In the box, small grains of galena and sulfosalts (see Fig. 25).

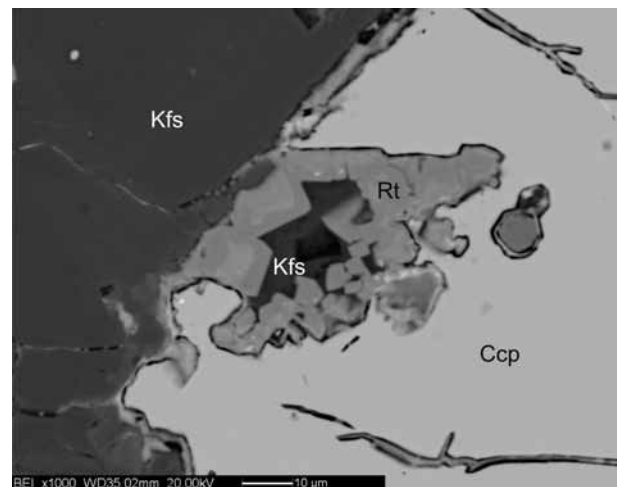


Fig. 11. Chalcopyrite (Ccp) in quartz-feldspar gangue (Kfs), containing a small "crevasse" encrusted by tiny crystals of rutile (Rt) and K-feldspar.

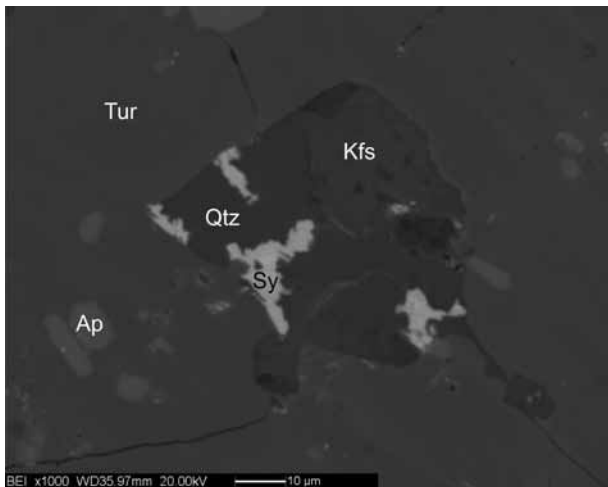


Fig. 12. Quartz (Qtz), K-feldspar (Kfs), tourmaline (Tur), apatite (Ap) and small grains of synchysite (Sy).

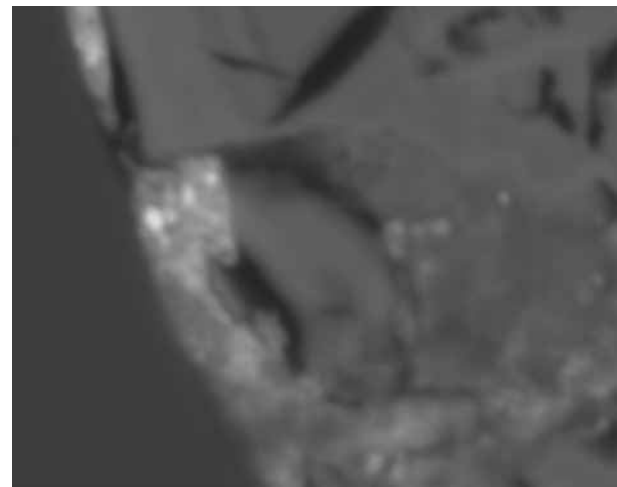


Fig. 13. Cassiterite (Cst) in quartz (Qtz) near a relic of chalcopyrite (Ccp) rimmed by an oxidation rim.

witness the action of corrosion/dissolution induced by hydrothermal polymetallic fluids.

Locally the scheelite occurs in narrow veins of quartz which cemented a granite breccia: in this context the salbands are marked by thin packages of chlorite/biotite and rutile grains. At places the quartz veinlets also contain small crystals of pyrite, scattered or in swarms with interstitial chalcopyrite.

In the quartz, K-feldspar and tourmaline gangue, which normally characterize the wolfram phase, grains of rutile and ilmenite locally are also relatively common; in some cases the K-feldspar and quartz groundmass replaced by chalcopyrite show minuscule "crevasses" covered with tiny crystals of rutile (Fig.

11). Associated with granitic breccias, locally thorian synchysite-(Ce) (Fig. 12), a REE containing fluorcarbonate occurs, according to a SEM analysis, (Ce_2O_3 ca. 24%), La (La_2O_3 ca. 14%), Nd (Nd_2O_3 ca. 9%) Pr_2O_3 (ca. 2.5%), Sm (Sm_2O_3 ca. 1%), minor amounts of various other REE and about 2.7% of ThO_2 .

Tiny grains of cassiterite (1-10 μm), with minor contents of Ti (2-3%) and Fe (1-2%), are scattered across quartz gangues (Fig. 13). The closure of the wolfram phase is marked by the crystallization of hematite as marginal accretions on grains of magnetite and in flakes disseminated in quartz.

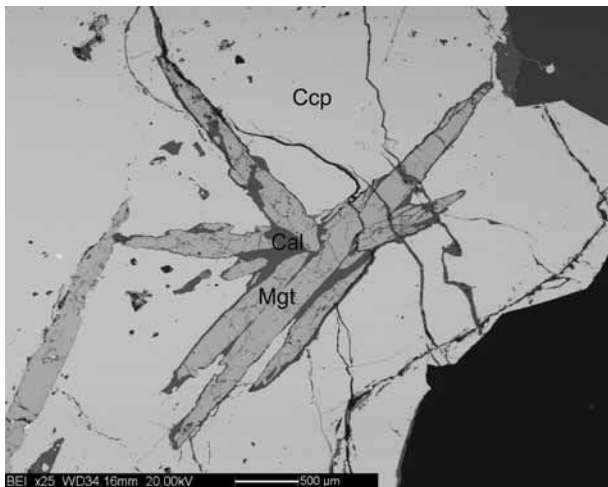


Fig. 14. Pseudomorphic magnetite (Mgt) after radiated plates of hematite (mushketowite) accompanied by some calcite gangue (Cal), inherited by penetrating chalcopyrite (Ccp). A network of thin later fractures is cemented by calcite.

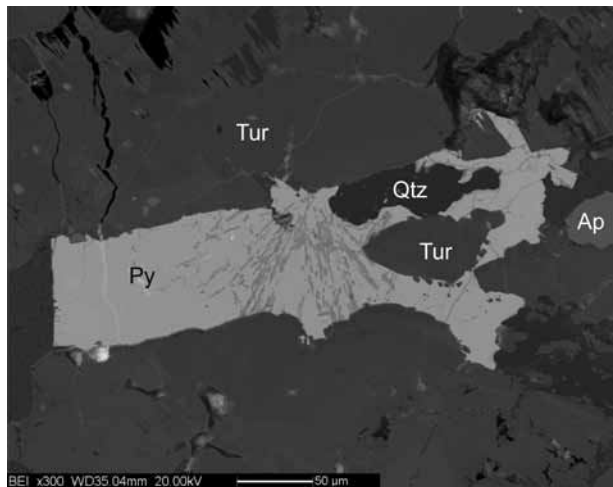


Fig. 15. Quartz (Qtz) and tourmaline (Tur), with occasional crystals of apatite (Ap) and pyrite (Py), the latter including intergrowths of ilmenite and rutile.

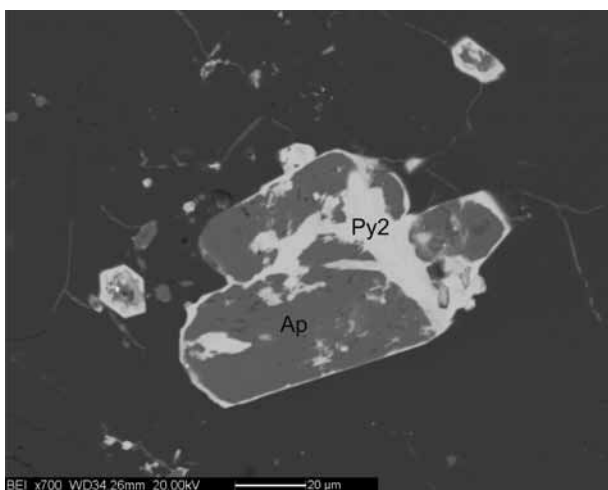


Fig. 16. Apatite (Ap) in quartz, replaced and penetrated by pyrite2 (Py2).

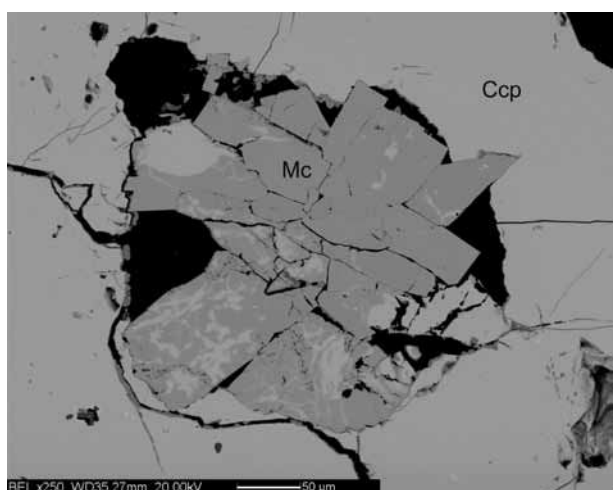


Fig. 17. Marcasite (Mc) in chalcopyrite (Ccp).

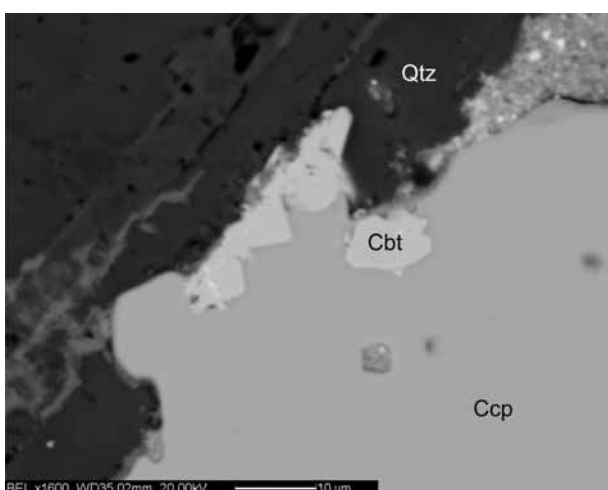


Fig. 18. Co, Fe, Ni sulfo-arsenides(Cbt) at the edge of chalcopyrite (Ccp).

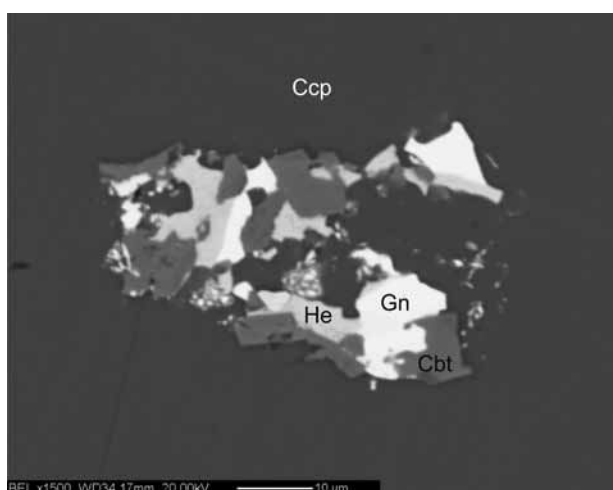


Fig. 19. Chalcopyrite (Ccp) containing a cluster of polymetallic sulfides including galena (Gn), Co, Fe, Ni sulfo-arsenides (Cbt), hessite (He) and very tiny intergrowths of sulfides, selenides and sulfosalts.

4.2.2. The sulfidic polymetallic phase

The sulfides phase mainly generated chalcopyrite accompanied by minor amounts of pyrite, sphalerite, galena and other sulphides and various sulfosalts. Chalcopyrite occurs as micrometer to millimetre large plagues interstitially developed with quartz, calcite and radially grown chlorite. Nodules, up to centimeters of chalcopyrite are common in the widening of some veins. Locally, granules of scheelite and small plagues of chalcopyrite coexist in the same vein, but usually occupy distinct sites in the gangue; in some cases, scheelite and chalcopyrite may be contiguous, but the structural, textural and paragenetic context indicates that the two mineralogical phases belong to different depositional steps, separated by an episode of brittle deformation.

Included in chalcopyrite, crystals of pyrite are common, up to a millimetre large, cubic, at places fractured and cemented by the same chalcopyrite. The main enrichments of chalcopyrite are subsequent to the formation of tourmaline; in fact, they cement its fractures and, in places, chalcopyrite appears to have selectively replaced feldspar, quartz and carbonate, which still remain as relic plagues, saving the tourmaline. Chalcopyrite also includes relics of magnetite and hematite (Fig. 14) accompanied by rests of the original quartz-carbonate gangue; in some instances, the paragenetic and textural character indicate original lamellar aggregates of hematite partially transformed into magnetite (muschketowite). The start of the sulfide formation seems still marked by pyrite1, which overlaps, even with phenomena of selective substitution, both on the metallic and gangue paragenesis of the wolframiferous event. This paragenesis is locally preserved as relics of mineral species relatively stable also under the new hydrothermal conditions, such as certain aggregates of ilmeno-rutile enclosed in pyrite1 (Fig. 15). Pyrite, locally with interstitial chalcopyrite, occurs generally as cubic crystals (few tens of microns up to 500–600 µm) scattered or aggregated in plagues. Some of these plagues are bordered and partially replaced by a rim of arsenopyrite which may in turn be surrounded by second-generation pyrite. Occasionally pyrite2 replaces, along boundaries and fractures, apatite crystals scattered in quartz (Fig. 16). Occasionally chalcopyrite hosts aggregates of marcasite (Fig. 17).

The metalliferous paragenesis accompanying chalcopyrite and pyrite is quantitatively incidental, but extraordinarily rich in mineral phases.

Pyrite may include tiny plagues of galena, chalcopyrite and sphalerite and, less frequently, Co, Fe, Ni sulfur-arsenide of the cobalt-glaucodoto family, at places grown on bravoite (Fig. 18 and Fig. 19). The SEM analysis of some cobaltite granules showed significant contents of Fe (about 6–8 wt%) and Ni (about 2–3 wt%).

Inclusions of sphalerite and galena are common in chalcopyrite. The small plagues of sphalerite locally show chalcopyrite exsolutions: in some cases "stars" of sphalerite are scattered in swarms in chalcopyrite. The sphalerite grown outside the plagues of chalcopyrite shows low Fe contents (1–2 wt%). Galena is generally poorly argentiferous: frequently, however, some of its plagues included in chalcopyrite contain or are accompanied by argentite/acantite occurring as both tiny grains (Fig. 20 and Fig. 21) and small plagues of discrete size (Fig. 22). Chalcopyrite also hosts few grains of hessite (Fig. 23 and Fig. 24), rare minuscule plagues of sulfosalts of the tetrahedrite-tennantite series slightly argentiferous and Zn-rich (7–8 wt% approx.) (Fig. 25). SEM analysis has also revealed the presence of tetrahedrite containing approx. 6 wt% of As and ca. 9 wt% of Bi and furthermore tiny plagues of a highly argentiferous sulfosalt of bismuth (approx. Bi 56 wt%, Cu 11–12 wt%, 17–18 wt% Ag, approx. S 14 wt%) for the identification of which more accurate microchemical and diffractometrical analyses are needed; it possibly represents an intergrowth of a phase like arcubisite/argento-cupro-cosalite/pavonite with other bismuth sulfosalts (Fig. 26).

In the quartz gangue accompanying the sulfides a variegated polymetallic microparagenesis is also disseminated: small grains of cobaltite (Fig. 27); tiny crystals of apatite and magnetite; grains of Ag-telluride, such as hessite, and Bi-telluride, probably pilsenite Bi_4Te_3 (Fig. 28); sporadic plagues consisting of fine intergrowths of chalcopyrite and various bismutiferous species (currently not defined), among which native Bi is recognizable. Eni – Aquater (1997) recorded also traces of electrum.

The closure of the hydrothermal sulphide-bearing event is preceded by a mild fracturing involving both the lithic clasts and the mineralized veins. A network of thin narrow veins of calcite with minor micro-quartz (flint-opal) cements the late fractures (Fig. 29). These veinlets contain rare tiny plagues of chalcopyrite and galena (galena2), and sporadic micrograins of rutile.

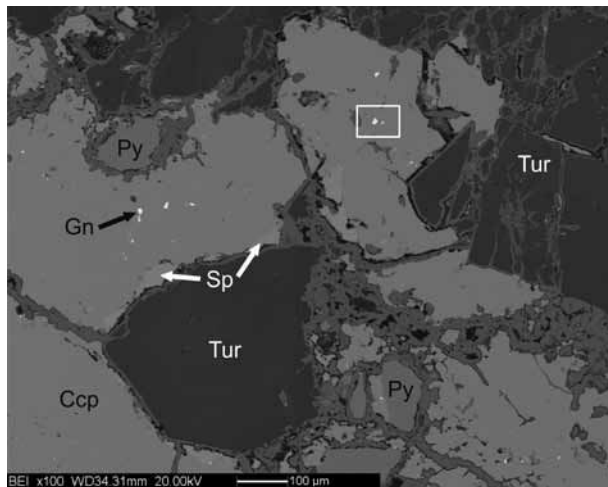


Fig. 20. Pyrite (Py) and chalcopyrite (Ccp) with small grains of sphalerite (Sp) and galena (Gn, white) associated with argentite/acantite (box, Fig. 21). Gangue of quartz and tourmaline (Tur). Alteration veinlets (mainly goethite and cuprite) cross the chalcopyrite.

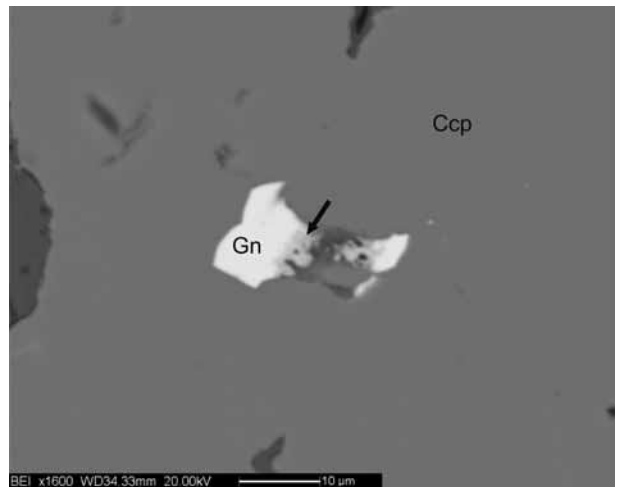


Fig. 21. Detail of Fig. 20. Chalcopyrite (Ccp) including small grains of galena (Gn) with argentite/acantite (arrow).

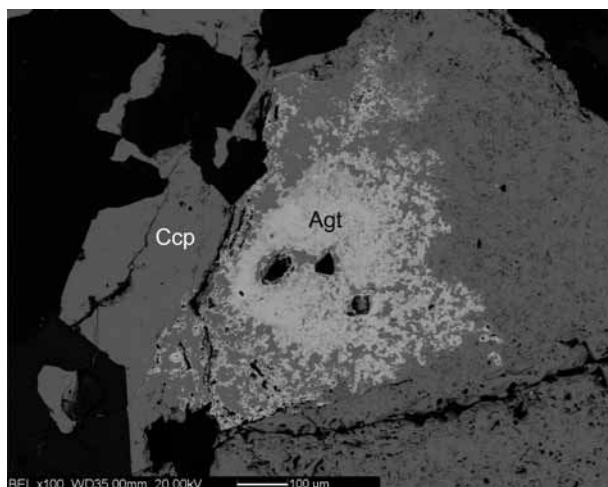


Fig. 22. Chalcopyrite (Ccp) enclosing a intergrowth with prevailing argentite (Agt), small grains of argentiferous galena and sporadic hessite.

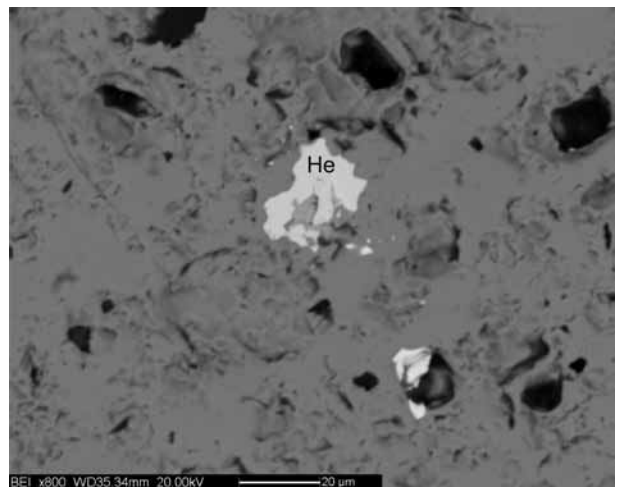


Fig. 23. Hessite (He) in argentite.

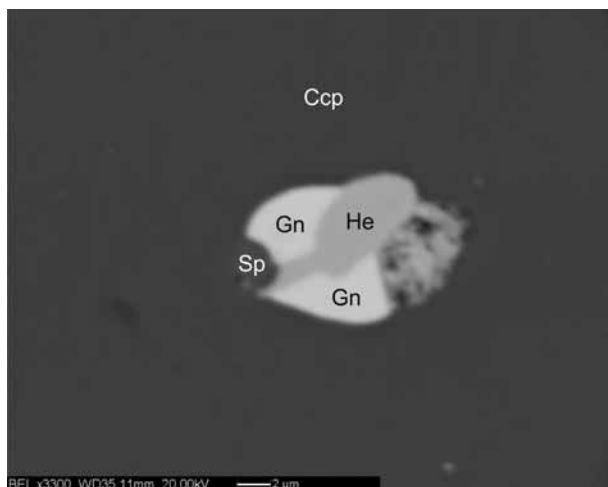


Fig. 24. Chalcopyrite (Ccp) including a polymimetic aggregate of galena (Gn), hessite (He) and sphalerite (Sp).

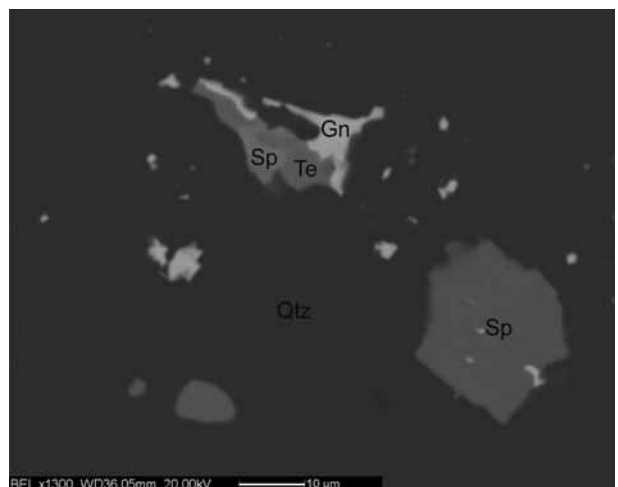


Fig. 25. Tennantite (Te), galena (Gn) and sphalerite (Sp) disseminated in gangue of quartz (Qtz). See also Fig. 10.

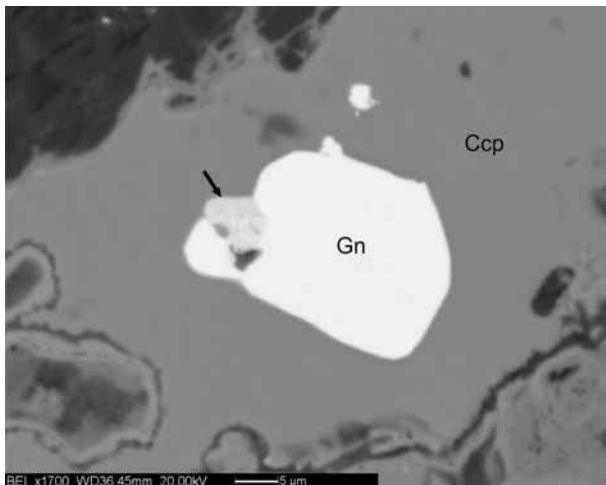


Fig. 26. Chalcopyrite (Ccp) enclosing galena (Gn) with strongly argentiferous Bi sulfosalt (arrow).

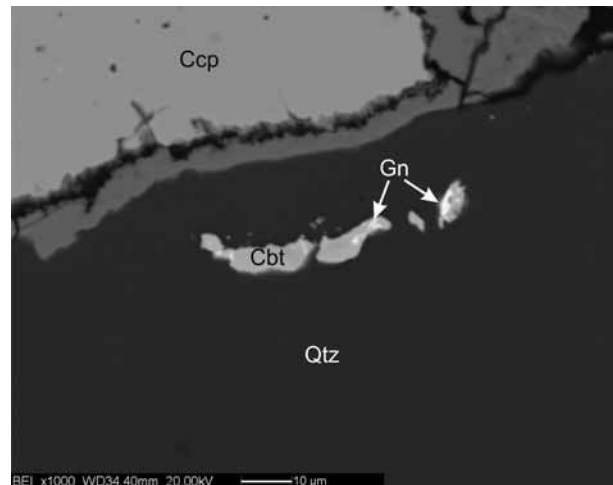


Fig. 27. Tiny grains of cobaltite (Cbt) and galena (Gn) in quartz (Qtz) close to chalcopyrite (Ccp) with an alteration vein at the quartz-chalcopyrite boundary.

Widespread supergenic alteration affects sulphides, mostly in the samples collected in the dump or outer squares of the galleries of Vecchia Bedovina. Particularly sensitive to oxidation phenomena are pyrite and chalcopyrite. Many of the minor chalcopyrite plagues isolated in the gangue are completely transformed into aggregates of covellite, malachite, azurite, cuprite, goethite etc.; nodules and the larger plagues are frequently bordered and locally crossed by characteristic composite bands of "colloform" aspect (Fig. 29) in which films of alternating goethite and cuprite are at places combined with malachite and azurite. Quite common is the alteration of pyrite to goethite which often spreads along a myriad of cryptic small uncemented fractures, presumably induced by alpine tectonics.

5 Summary and metallogenic considerations

The emplacement of the deposits of W (Mo, Sn, Bi, REE) and of Cu (with Pb, Zn, Ag, Te, Co, Ni ...) of Bedovina marks the end of the Mid-Triassic magmatic cycle of the Predazzo-Monzoni Complex. The mineralization forms a network of veins, from pneumatolytic to hydrothermal. The veins crosscut all the magmatic rocks, including the most recent terms as some minor granitic bodies and some acidic and basic dykes.

A genetic link between Bedovina mineralization and granitic intrusions has been suggested by several authors (e.g. Becke, 1895; Hoffmann, 1903; Granigg

& Koritschoner, 1913; Lazarevic & Kittle, 1913; Di Colbertaldo, 1955; Bianchi & Di Colbertaldo, 1956); some of the cited authors point out the presence of small radial growths of tourmaline crystals and traces of other minerals characteristic of the mineralization of Bedovina in the "pink granite" outcropping between Predazzo and Mezzavalle, strongly altered by pneumatolytic-hydrothermal processes. Brigo (1989) instead links scheelite mineralization and polymetallic sulfides of Bedovina with fluids derived from the monzonitic-syenitic and monzodioritic masses; some minor events bearing Mo and W would be related to the granites.

Data from our study indicate that, in the area of Bedovina, the main metalliferous event is anticipated by sporadic leaves of molybdenite genetically correlated with the mineralization of Aivola, in which molybdenite was formed during the final stages of crystallization of the host granite characterized by large K-feldspar crystals. Shortly later tectonic movements originated the bands of clastesis who guided the rise of pneumatolytic-hydrothermal metalliferous fluids, late products of granite crystallization. In a regime of decreasing temperature these fluids generate stockworks of copper-wolframiferous veins forming firstly the pneumatolytic paragenesis, carriers of wolfram (and minor Sn and REE) and later the hydrothermal mainly cupriferous mineralization, but with distinct polymetallic connotations (Fe, Zn, Pb, Ag, Co, Ni, Sb, As, Bi, etc.) evidenced by sulphides, sulfosalts, telluride, etc..

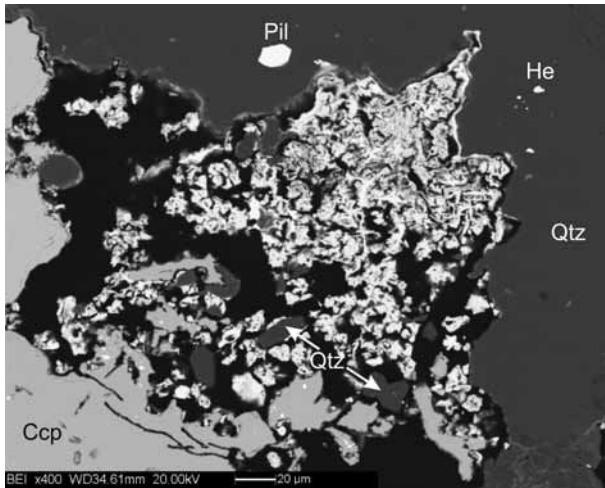


Fig. 28. Quartz (Qtz) and chalcopyrite (Ccp) surrounding a complex intergrowth of chalcopyrite, native Bi and some very tiny of not specified Bi-bearing minerals. Quartz encloses Bi-tellurides (likely pilsenite, Pil) and hessite (He)).

The paragenesis of the wolfram phase is characterized by scheelite with quartz, tourmaline, K-feldspar, some carbonate, minor biotite and chlorite, and accessory amounts of magnetite, ilmenite, apatite (with enrichment of fluorine at the edge of crystals), rutile (locally with significant contents of Fe and Sn, especially in the core), rare cassiterite (with discrete contents of Ti and Fe), synchysite-(Ce) and finally hematite. According to Champion and Blevin (2005), Sn^{4+} is related to strongly fractionated and reduced granites in which the ratio $\text{Fe}_2\text{O}_3/\text{FeO} < 1$ and $\text{Rb/Sr} \gg 1$, and it tends to disperse in titanium minerals; Cu and Mo probably correlate to slightly fractionated magmas, island-arc or Andean type, in which $\text{Fe}_2\text{O}_3/\text{FeO} > 1$ and $\text{Rb/Sr} \gg 1$.

The moderate and at places high contents of Mo checked in some grains of scheelite, the persistence of apatite2 and of REE, U and Th minerals (e.g. monazite in MoS_2 occurrences, synchysite in the wolfram paragenesis) seem to emphasize a geochemical relationship between the wolfram mineralization and the molybdenite occurrences and the relationship of both with granites, which seem to have been affected by crustal contamination processes, as suggested by Coltorti et al. (1996).

The sulfide paragenesis follows, overlapping and partly replacing, the wolfram mineralization. The essentially cupriferous characters are accompanied by evident polymetallic connotations, defined by the minor but widespread presence of Zn, Pb, Ag, Te, Co, Ni, Bi, As, Sb, etc. Sulfides were deposited by hydrothermal fluids that followed the same pathways of

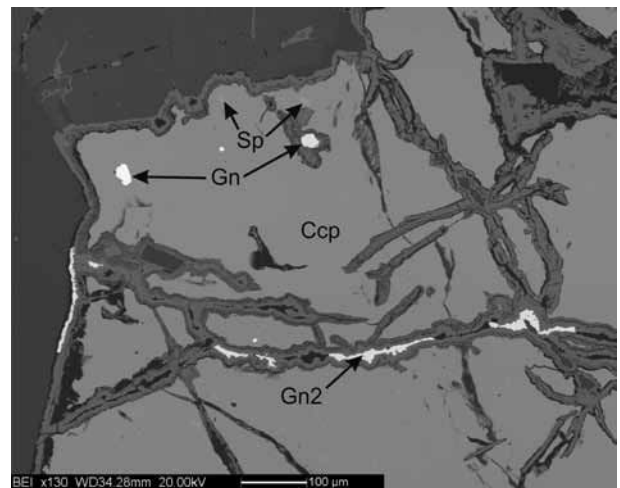


Fig. 29. Chalcopyrite (Ccp) in gangue of quartz, includes small grains of sphalerite (Sp) and galena (Gn). Alteration veinlets (mainly oxides and hydroxides of Fe and Cu) cross the chalcopyrite: some of them are arranged on late fractures cemented by carbonates and galena2 (Gn2).

wolfram reactivated by a new clastic event and in a substantially changed redox context. The transition between the wolfram phase and the copper-polymetallic sulfides phase is indeed marked by a "momentary" onset of oxidizing conditions evidenced by the crystallization of hematite present both as disseminated plates in the quartz gangue and as overgrowths on existing grains of magnetite; immediately after that, the local transformation of hematite into magnetite (mushketowite), as observed at Vecchia Bedovina, marks the establishing of the reducing conditions that accompanied the sulfides stage.

The sulfides paragenesis, which comprises tiny crystals of cobaltite, chalcopyrite with spread stars of sphalerite, but also sphalerite (with low contents of Fe), poorly argentiferous galena and several Ag-bearing minerals (sulfides such as argentite/acantite, tellurides like hessite, bismutides and sulfosalts), shows meso-epithermal characters.

Of a particular metallogenic significance is thorian synchysite-(Ce). It has been reported at M. Mulà by Ravagnani (1974) and in the Vicentine Alps by Pegoraro (1998) in the context of the Val Riolo iron mineralization, genetically related to the Middle Triassic magmatism (Frizzo, 1997; 2003). According to Förster (2000) the synchysite present in the granites with "A type" affinity of Markersbach (Erzgebirge) is derived from the leaching effect of late-magmatic fluid rich in F, CO_2 , Ca, on REE minerals such as monazite and xenotime present as accessories in the granite; fluids would have released REE and Th reprecipitating them nearby as fluocarbonates. Similar

processes may have acted in the context of Bedovina (and more generally on the granitoid masses of Predazzo and Monzoni Complexes), from where monazite in granites and thorian synchysite-(Ce) in the wolframiferous veins are reported.

Finally, it is important to stress that:

i) the metal paragenesis of the "wolfram phase" of Bedovina, is characterized by the association W, (Sn, Nb, Ta, REE, Th). In terms of metallogenesis (e.g. Beckinsale, 1979; Pitcher, 1983; Sawkins, 1990), it indicates a kinship with magmas of the leucogranitic series, and in particular with peraluminiferous "*S type*" granitoids, with $A/CNK > 1.1$. These are granites poor in magnetite and with abundant ilmenite, commonly characterized by low contents of Sr with respect to Rb, with high Rb/Sr, low K/Rb ratios and $^{87}Sr/^{86}Sr > 0.706$. Similar geochemical characters, thus favourable to W and Sn mineralogenesis, are shown by "*granites*" of Predazzo (sienogranites - sensu Eni-Aquater, 1997); in the granites, SiO_2 varies from 62 wt% to 86 wt% in positive correlation with Rb, K_2O , Be, Nb and negative with Fe_2O_3 , CaO, TiO_2 , MgO, MnO, Co, V, Zn; the concentrations of Ba and Sr are low (about 60 ppm). The contents of B (on average present with 100 ppm), F (up to 1200 ppm) and Li (60–250 ppm) are significantly high. The high concentrations of Rb and the low values of Ba and Sr, which determine high Rb/Ba (up to 40) and Rb/Sr ratios (up to 100) and low K/Rb ratios (decreasing from 200 to 100 in the more strongly sericitized rocks), indicate granitoids and magmatic-postmagmatic residual fluids rich in incompatible elements and potentially productive for W and Sn mineralization;

ii) the metal paragenesis with Cu, Zn, Pb, Ag, Te, Co, Ni, Bi, As, Sb, (and Mo?) that characterizes the sulfide "copper phase" refers to, from the metallogenetic point of view (e.g. Evans, 1993; Hutchinson, 1983 and references therein), a relationship with "*I type*" granitoids of the calcalkaline series with $A/CNK < 1.1$, Mg-rich biotite, disseminated magnetite, absent or very scarce ilmenite and monazite, Sr/Rb ratios inverted compared to "*S type*" granitoids. Other character would be a higher fO_2 .

The mineralization of Bedovina therefore seems to derive from residual metalliferous fluids produced from the crystallization of two distinct granitoid magmas: the first, marked by "*S type*" characters, would have generated the parageneses typical of the "wolfram phase" with W (Sn, REE, Th); the second, with "*I type*" characters, would be responsible for po-

lymetallic associations that characterize the "copper phase". The sporadic molybdenite occurrences could be related to this last type of magma.

Alternatively, the hypothesis of a single hybrid granitic magma could justify the complexity of the copper and wolfram parageneses and the significant contents of Mo sometimes present in the scheelite.

Acknowledgments

The authors are grateful to D. Visonà for helpful suggestions and kind discussions on the evolution of magmatism which originated the Predazzo Eruptive Complex and the several mineralization related to it. The authors appreciate A. Guastoni and A. Marzoli for the critical review of the text.

The authors express gratitude to A. Braito and G. Cincelli for collaboration during field works and to D. Ferrari for graphic elaboration of the mine sections.

This work was financially supported by Comune di Predazzo.

References

- Becke, F. (1895): Scheelit im Granit vom Predazzo. - *Tscherm. Min. Petr. Mitt.*, 14: 21-22.
- Beckinsale, R. D. (1979): Granite magmatism in the tin belt in the South-East Asia. - In: Atherton M. P., Tarney J. (eds.): *Origin of Granite Batholiths*, 34-44, Shiva, Orpington.
- Bianchi, A., Di Colbertaldo, D. (1956): Osservazioni paragenetiche sul giacimento a rame e tungsteno della Bedovina presso Predazzo. - *Rend. Soc. Miner. Ital.*, 12: 55-68.
- Brigo, L. (1989): Tungsten as a geodynamic marker in the Italian continental crust. - In: Boriani A., Bonafede M., Piccardo G.B., Vai G.B. (eds.): *The Lithosphere in Italy*, Atti dei Convegni Lincei, 80: 407-425.
- Champion, D., Blevin, P. (2005): New insights into intrusion-related gold-copper systems in the Tasmanides. - *Mining 2005*, Brisbane, 26 October, 30p.
- Castellarin, A., Lucchini, F., Rossi, P.M., Sartori, R., Simboli, G., Sommavilla, E. (1982): Note geologiche sulle intrusioni di Predazzo e Monzoni. - In: Castellarin A., Vai G.B. (eds.): *Guida alla Geologia del Sudalpino centro-orientale*. Guide Geol. Reg. Soc. Geol. It.: 211- 219.
- Coltorti, M., Siena F., Visonà D. (1996): Aspetti petrologici del magmatismo triassico dell'area di Predazzo. - Libro dei Riassunti, 78° Riunione estiva Soc. Geol. Ital.
- Di Colbertaldo, D. (1955): I minerali metallici e le gange del giacimento della Bedovina all'esame microscopico. - Rapporto inedito, 6 luglio 1955, 5pp.
- Degiampietro, C. (1975): Cronache fiemmesi attraverso nove secoli. - 308pp, Arti Grafiche Manfrini, Calliano.
- Dellantonio, E. (2000): Le miniere del territorio eruttivo di Predazzo e Monzoni. - *Natura Alpina*, 4: 65 - 77.
- Eni - Aquater (1997): Mineralizzazioni a Cu, W, Sn e associati dell'area di Predazzo-Monzoni. - Ricerca mineraria di base (Legge 6.10.1982, n. 752, art. 4), Relazione conclusiva, Ministero dell'Industria, del Commercio e dell'Artigianato, Direzione Generale delle Miniere, 54pp.
- Evans, A. M. (1993): *Ore Geology and Industrial Minerals. An Introduction*. - Blackwell Scientific Publications, 396pp, Chapman Hall, London.
- Förster, H. J. (2000): Cerite-(Ce) and thorian synchysite-(Ce) from the Niederbobritzsch granite, Erzgebirge, Germany: implications for the differential mobility of the LREE and Th during alteration. - *Can. Mineral.*, 38: 67-79.
- Frizzo, P. (1997): Le mineralizzazioni argentifere delle Alpi Vicentine. - In Brigo L, Tizzoni M. (eds): *Il Monte Calisio e l'argento nelle Alpi dall'antichità al XVIII secolo*, 43-59, Temi, Trento.
- Frizzo, P. (2003): I giacimenti e le miniere della Val Leogra e del Tretto. - In: Frizzo P. (ed): *L'argento e le "terre bianche" del Tretto e della Val Leogra*, 39-76, Menin, Schio.
- Granigg, B., Koritshoner, J. H. (1913): Die turmalinführende Kupferkies-Scheelitlagerstätte am M. Mulatto bei Predazzo (Südtirol). - *Z. Prak. Geol.*, 11: 481-497.
- Hoffmann, A. (1903): Vorläufiger Mitteilungen über turmalinführende Kupferkiese von Monte Mulatto. - Sitzb. d. Königl. Böhm. Akad. d. Wiss. II Classe (Separatabdruck), 16: 1-8.
- Hutchinson, C. S. (1983): *Economic Deposits and their Tectonic Setting*. - 487 pp, Macmillan, London.
- Laurenzi, A., Visonà, D. (1996): 40Ar/39Ar chronology of Predazzo magmatic complex (Southern Alps, Italy). - Libro dei Riassunti, 78° Riunione estiva S.G.I.
- Lazarevic, M., Kittl, E. (1913): Einige untersuchungen der kupferkiesführenden Mineralgänge am M. Mulatto bei Predazzo. - Österreichischen Zeitschrift für Berg- und Hüttenweisen (Separatabdruck), 15 pp.
- Marrocchino, E., Coltorti, M., Visonà, D., Thirwall, M.F. (2002): Petrology of Predazzo magmatic complex (Trento, Italy). - *Geochim. Cosmochim. Acta*, 66(15A, Suppl. 1): A486-A486.
- Menegazzo Vitturi, L., Visonà, D., Zantedeschi, C. (1995): Amphibole composition of Predazzo volcano-plutonic complex (Southern Alps, Italy). - *Mem. Sci. Geol.* 47: 87-94.
- Oss Mazurana, F., (1905, 1906): Miniere del Monte Mulatto. - *Bollettino dell'Alpinista*, 1(5): 94-95, 1(6): 106-108, 2(4): 164-171.
- Oss Mazurana, F., Hesser, R. (1909): Die Betriebe der Kupfererzbergbau-Gewerkschaft „Oss-Mazzurana“ in Predazzo. - *Metallurgie*, VI(18-19): 569-596.
- Pelloux, A. (1919): I minerali italiani di tungsteno. - La miniera italiana, 33(3): 91-95.
- Pitcher, W. S. (1983): Granite: typology, geochemical environments and melting relationships. - In: Atherton M. P., Gribble C. D. (eds): *Migmatites, Melting and Metamorphism*, 277-285, Shiva, Nantwich.
- Pegoraro, S. (1998): Minerali rari del Vicentino: la synchysite (Ce) della Galleria Veneziana, Val Riolo, Torrebelvicino (Vicenza). - In: Dondi, M., Puggioli, G. (eds): *Minerali d'Italia*, 16-17, Centro Documentazione Mineralogica, Bologna.

- Ravagnani, M. (1974): I giacimenti uraniferi italiani ed i loro minerali. - 188pp, Gruppo Mineralogico Lombardo, Museo Civico di Storia Naturale di Milano, Milano.
- Sawkins, F.J. (1990): Metal Deposits in Relation to Plate Tectonics. - Springer Verlag, Berlin.
- Šebesta G. (1992): La via del rame. - 221pp, Supplemento a "Economia Trentina" n. 3, Camera di Commercio, Industria, Artigianato, Agricoltura di Trento, Trento.
- Stella, A. (1953): L'industria mineraria del Principato Vescovile di Trento nei secoli XVI e XVII. Com. Econom. Sc. Triveneto Studi, Applic. e Ric. Univ. Padova, 49-93.
- Stella, A. (1957): L'industria mineraria del Trentino nel secolo XVIII. Com. Econom. Sc. Triveneto Studi, Applic. e Ric. Univ. Padova, 2:183-206.
- Vardabasso, S. (1930): Carta geologica del territorio eruttivo di Predazzo e Monzoni nelle Dolomiti di Fiemme e di Fassa, Scala 1:25.000. Regia Scuola di Ingegneria, Padova.
- Vergani, R. (2002): Gli usi civili della polvere da sparo (secoli XV-XVIII), in Economia e energia. Secc. XIII-XVIII. - In: Cavaciocchi S. (ed): Atti della XXXIV Settimana di studi dell'Istituto internazionale di Storia economica "F. Datini" (Prato, 15-19 aprile 2002), Le Monnier, Firenze.
- Visonà, D. (1997): The Predazzo multipulse intrusive body (Western Dolomites, Italy). Field and mineralogical studies. - Mem. Sci. Geol., 49: 117-125.

Manuscript submitted 2.7.2010

Revised Manuscript accepted 20.10.2010

TECTONOMETAMORPHIC EVOLUTION OF THE AUSTROALPINE NAPPES IN THE NORTHERN ZILLERTAL AREA (TYROL, EASTERN ALPS)

Andreas Piber and Peter Tropper

With 10 Figures and 3 Tables

Institute of Mineralogy and Petrography, Faculty of Geo- and Atmospheric Sciences, University of Innsbruck, Innrain 52f,
A-6020 Innsbruck, Austria

Zusammenfassung

Diese Untersuchung behandelt die tektonische Entwicklung der Austroalpinen Decken im Norden des Tauernfensters im nördlichen Zillertal (Tirol). Die bearbeiteten Einheiten sind der Kellerjochgneis (Schwaz Augengneiss), der Innsbrucker Quarzphyllit und der Wildschönauer Schiefer. Sechs unterschiedliche Deformationsabfolgen konnten gefunden werden. Die erste Deformationsphase (D_1) ist nur als reliktische Schieferung im Dünnschliff erkennbar. Im Innsbrucker Quarzphyllit manifestiert sich die erste Deformationsphase in Form von isokinalen Falten. Die dominante Foliation wurde während der zweiten Phase (D_2), welche das Resultat einer NW-SE Einengung ist, gebildet. Diese duktile Hauptdeformationsphase drückt sich ebenso in Form isokinaler Falten aus. Diese Struktur begleiten Scherbänder, welche einen W-NW-gerichteten Deckentransport anzeigen und somit D_2 daher mit der kretazischen Deckenstapelung korreliert werden kann. Die dritte duktile Deformationsphase (D_3) führte zur Ausbildung offener Falten, welche auf eine NE-SW-gerichtete Kompression hinweisen. Die vierte Deformationsphase (D_4), welche eine NNW-SSE Kompression anzeigt, ist ebenso durch offene Falten und einer Achsenoberflächenschieferung charakterisiert. Die letzte duktile Phase (D_5) führte zur Ausbildung semiduktiler Knickbänder, welche die älteren Deformationselemente diskordant durchschneiden. Die darauf folgende Sprödverformung (D_6) kann in vier Unterphasen gegliedert werden (D_{6a-d}). Die strukturelle Entwicklung dieses Gebietes kann mit Hilfe der geochronologischen Daten aus dieser Region als tektonometamorphe Entwicklung interpretiert werden. Zusammenfassend kann behauptet werden, dass die Platznahme des Innsbrucker Quarzphyllits, des Kellerjochgneises und der Wildschönauer Schiefer während der Oberkreide nach der Schließung des Hallstatt-Meliata Ozeans unter Bedingungen der oberen bis mittleren Grünschieferfazies stattgefunden hat.

Abstract

This investigation addresses the tectonic evolution of the Austroalpine nappes north of the Tauern Window in the northern Zillertal (Tyrol). The investigated units are the Kellerjochgneiss (Schwaz Augengneiss), the Innsbruck Quartzphyllites and the Wildschönau Schists. Six stages of deformation are distinguished. The first stage (D_1) is present as a relic foliation, observed only in thin sections. In the Innsbruck Quartzphyllite the first deformation stage is represented by isoclinal folds. The dominant foliation is represented in the second stage (D_2), which is the result of a NW-SE-oriented compression. This main ductile deformation event also is expressed by the formation of isoclinal folds. Associated shear bands indicate W-NW-directed transport and thus D_2 is related to the Cretaceous nappe stacking. The third ductile deformation stage (D_3) leads to the formation of open folds most likely associated with the NE-SW contraction. The fourth stage (D_4) is also characterized by open folds and an axial plane foliation, reflecting subsequent NNW-SSE compression. The last ductile stage (D_5) produced semi-ductile kink bands, which crosscut the earlier deformation structures. The subsequent brittle deformation (D_6) can be divided into four stages (D_{6a-d}). This structural succession can be interpreted in terms of the existing geochronological framework for this area, suggesting that nappe stacking of the Innsbruck Quartzphyllites, the Kellerjochgneiss and the Wildschönau Schists took place during the Late Cretaceous under middle- to upper greenschist-facies conditions, related to the closure of the Hallstatt-Meliata Ocean.

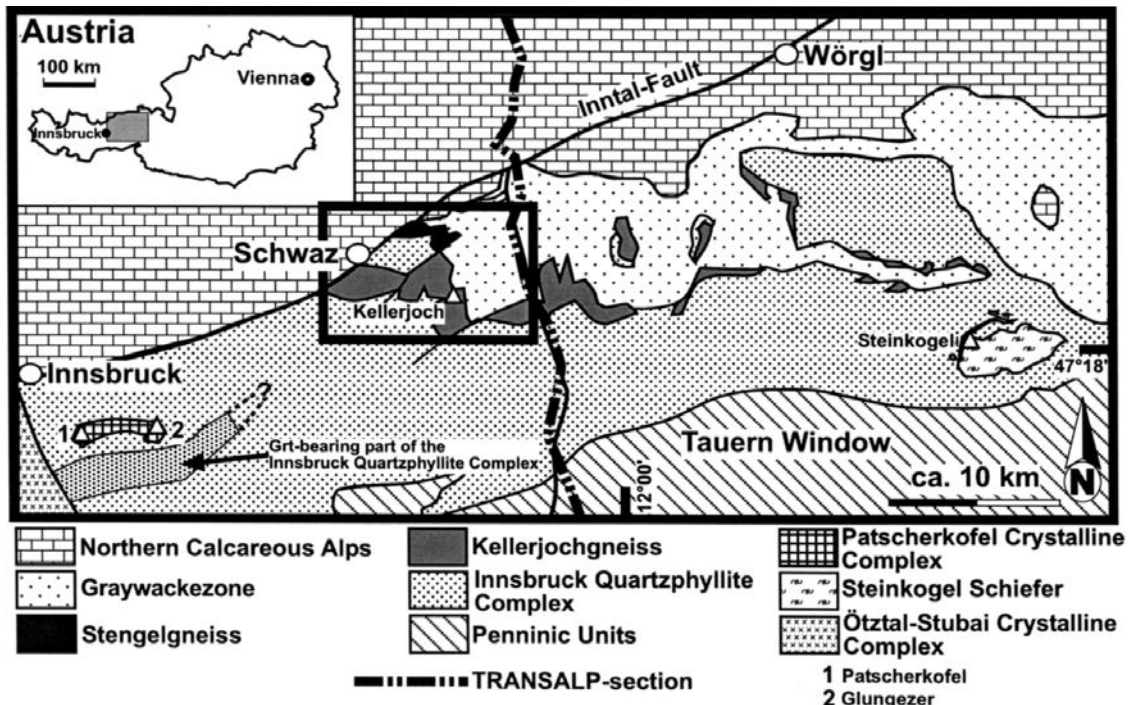


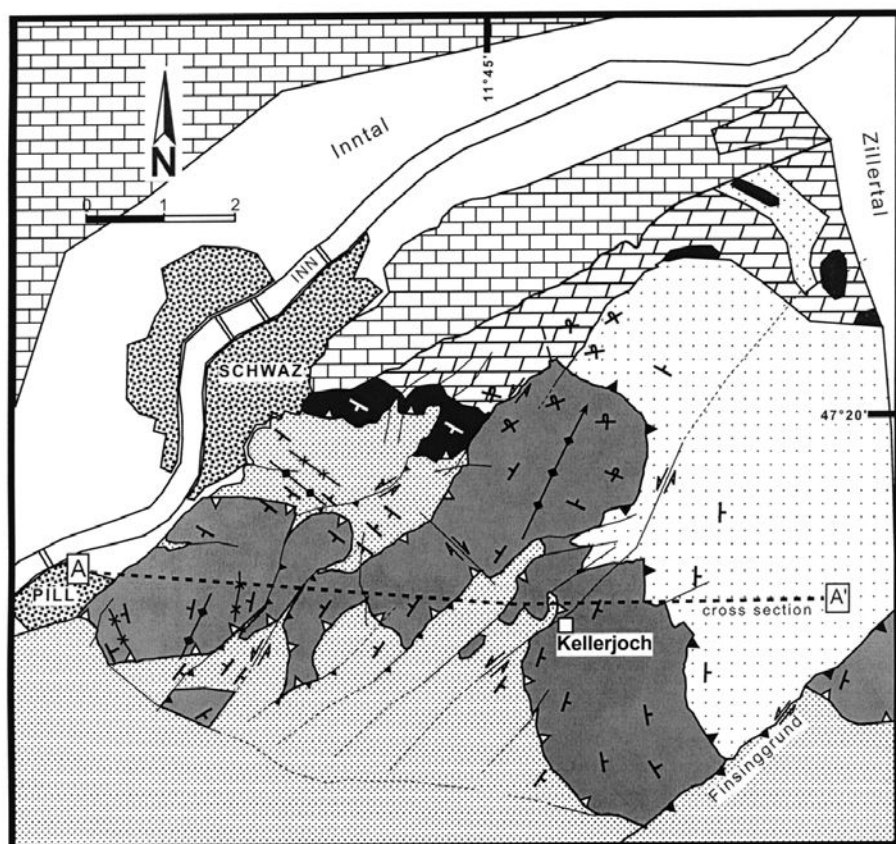
Figure 1: Tectonic overview of the Austroalpine units north of the Tauern Window. The framed area depicts the area of investigation.

1. Introduction

These investigations are closely related to the international geophysical TRANSALP-project, which intends to provide a seismic reflection-profile through the Eastern Alps along a transect between Bad Tölz in the north, located to the south of Munich, and Venice in the south (Transalp Working Group, 2002). The area of the structural investigation covers ca. 60 km² in the northern part of the Zillertal near the city of Schwaz (Fig. 1). Lithologically the investigated area consists of polymetamorphic basement units (Kellerjochgneiss or Schwaz Augengneiss), Paleozoic carbonates and quartzphyllites (Schwaz Dolomite, Innsbruck Quartzphyllite and Wildschönau Schists) (Fig. 2A). The Wildschönau Schists mainly consist of meta-greywackes. The units are strongly deformed, with abundant synformal and antiformal structures as shown in a cross-section in Figure 2B. In the northern part of the working area, a strong tectonic imbrication of the above mentioned units occurs. The contact between the three units in the area of investigation is always of tectonic nature, with the Innsbruck Quartzphyllite representing the lowermost unit and the Wildschönau schist representing the uppermost unit. Figure 2B shows a profile through a large

antiformal structure in the Kellerjochgneiss, with the Innsbruck Quartzphyllite occurring as the core.

This investigation aims to provide structural data to better constrain the tectonic evolution of the three units, i.e. the Innsbruck Quartzphyllite, the Kellerjochgneiss and the Wildschönau Schists. Our results contribute to the ongoing discussion concerning the paleogeographic setting of these units, as well as providing data for the interpretation of the seismic data along this section of the TRANSALP transect (Transalp Working Group, 2002). Based on its tectonic position in the Austroalpine nappe stack of the western part of the Eastern Alps, the Innsbruck Quartzphyllite has always been unambiguously attributed to the lower Austroalpine units (Tollmann, 1963). The Wildschönau Schists represent the Paleozoic basement of the Upper Austroalpine Tirolic nappe, which is itself a part of the Northern Calcareous Alps and hence it was always attributed to be of upper Austroalpine origin. However, the paleogeographic provenance of the intermediate basement rock units on top of the Innsbruck Quartzphyllite, namely the Patscherkofel Crystalline Complex, the Kellerjochgneiss and other similar bodies located further east (e.g. Steinkogelschiefer) is still a matter of discussion. Tollmann (1963) considered the Kellerjochgneiss to be a middle Austroalpine nappe, together



[Brick Pattern]	Trias	[Dotted Pattern]	Wildschönau-Schist	[Solid Black]	Kellerjoch-gneiss	[Stippled Pattern]	Residential area
[Diagonal Hatching]	Schwaz Dolomite		[Solid Black]	Stengelgneiss	[Cross-hatching]	Innsbruck Quartzphyllite	
					cross section		
dominant foliation		thrust	nappe boundary	antiform	synform	fault	fault presumed
							sense of movement

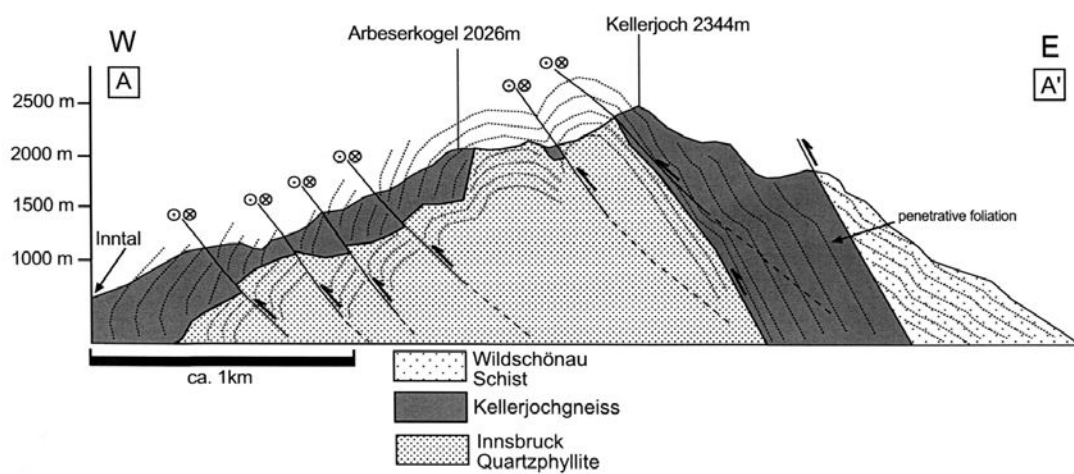


Figure 2: (A) Tectonic map of the area of investigation. (B): E – W cross section. The position of the profile is shown as a stippled line in Figure 2A. The Figure shows a large NW trending fold located in the W of the Kellerjoch. The units are intersected by several sinistral reverse strike-slip faults. These faults are thought to belong to the Inntal Fault system.

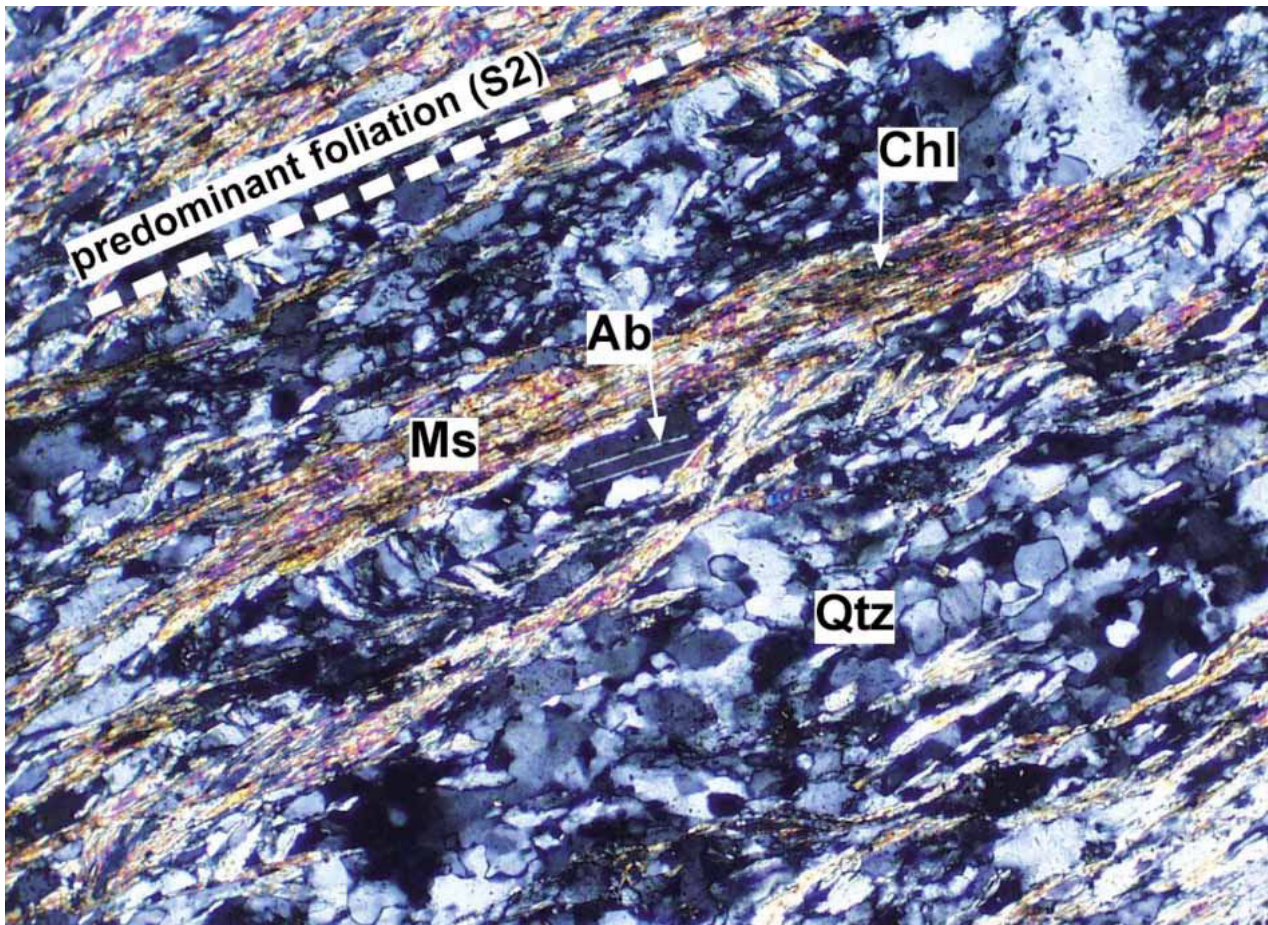


Figure 3: Photomicrograph of the mineral assemblage of the Innsbruck Quartzphyllite. Quartz (Qtz), chlorite Chl), muscovite (Ms) and albite (Ab) can be observed (sample A-133; X Nicols). The predominant foliation (S2) is also shown in the upper left corner.

with the Steinkogelschiefer and the Patscherkofel-Glungezer Crystalline Complex. On the other hand, Schmidegg (1964) interpreted these basement units as representing the base of an inverted lying Innsbruck Quartzphyllite. While the tectonic nature of the contact between the Innsbruck Quartzphyllite and the Kellerjochgneiss has been established, there is still disagreement concerning the timing of movements along this contact (e.g. Steyrer et al., 1996). Satir and Morteani (1978a) interpreted this contact to be of Variscan age, leading to the conclusion that all units, with respect to the Eo-Alpine orogeny, have to be classified as Lower Austroalpine. Tollmann (1977), on the other hand, interpreted the contact as having formed during the Alpine orogeny and thus defined it to be the boundary between the lower- and middle Austroalpine units. Fügenschuh (1995) and Steyrer et al. (1996) described a zone of ultramylonites separating the two units and suggested that the Kellerjochgneiss is a thinned relic of middle Aus-

troalpine units. According to Schmid et al. (2004) The Kellerjochgneiss and the Greywacke Zone are part of the Upper Austroalpine cover and the Innsbruck Quartzphyllite belongs to the Silvretta-Seckau nappe system, which forms the basal nappes of the Upper Austroalpine basement nappe system.

The aim of this study is therefore two-fold: 1) The primary goal is a detailed structural investigation of the area, to determine the structural successions in the Innsbruck Quartzphyllite, the Kellerjochgneiss and the Wildschönau Schists. These results will be compared with previous studies and tectonic models obtained from the three units as well as of neighboring units such as the Northern Calcareous Alps by Schmidegg, (1964), Roth (1983), Eisbacher and Brandner (1995), Ortner and Sachsenhofer (1996), Steyrer et al. (1996), Kolenprat et al. (1999), Ortner et al. (1999), Reiter (2000) and Grasbon (2001) and 2) the other aim is to relate the observed sequence of deformational events to the regional tectonic

evolution of this part of the Eastern Alps. The deformational sequence will therefore also be discussed in the context of the available geochronological and thermobarometric framework from the Austroalpine nappes north of the Tauern Window.

2. Geological overview

The Innsbruck Quartzphyllite outcrops between Mittersill in the east and Innsbruck in the west. It is typically a rather monotonous, fine-grained, greenish to grayish phyllitic schist, with the mineral assemblage muscovite + chlorite + albite + quartz ± calcite (Fig. 3). Locally, garnet-bearing schists occur south of the Patscherkofel. It has been divided into three stratigraphical units consisting of Devonian carbonatic black shales, Silurian carbonatic-sericitic phyllites and Ordovician quartzphyllites and greenschists, however numerous transitions may be found (Haditsch and Mostler 1982). Although most of the Innsbruck Quartzphyllites were affected by lower greenschist-facies metamorphism (Hoschek et al. 1980; Sassi and Spiess, 1992; Piber, 2005; Piber and Tropper, 2005), some central parts of the Innsbruck Quartzphyllite have been affected by middle greenschist-facies metamorphism (Kolenprat et al. 1999; Piber, 2005; Piber and Tropper, 2005). Geochronological investigations revealed a complex metamorphic history indicating a possible Permian- and Eo-Alpine overprint (Dingeldey et al., 1997; Rockenschaub et al., 1999; Handler et al., 2000). Recently, a number of new results have been obtained concerning the internal structure of the Innsbruck Quartzphyllite (Kolenprat et al., 1999). Large parts of the Innsbruck Quartzphyllite must therefore be considered as highly deformed, retrograde old (Variscan?) basement. These studies revealed a metamorphic zonation with garnet-free phyllites at the northern and southern rims and garnet bearing phyllites in the central part (Fig. 1), thus reflecting a slightly higher grade of metamorphism in the center. This observation was interpreted in terms of a km-scale isoclinal fold of the Innsbruck Quartzphyllite (Schmidegg 1964, Rockenschaub 1998; Kolenprat 1998). Kolenprat et al. (1999) show, that the Innsbruck Quartzphyllite has a complex deformation history, with structures ranging from pre-Alpine (Variscan) to late Alpine (Neogene) in age. The pre-Alpine foliation is preserved only locally. During the Eo-Alpine orogeny, intensive mylonitization associated with W- to NW-directed nappe stacking, occurred.

The Meso (Early Tertiary)- and Neo (Miocene)-Alpine deformation is characterized by the imbrication of the Lower Austroalpine units as a consequence of N-directed thrusting of the Austroalpine nappes over the Penninic Units and subsequent exhumation of the Tauern-Window during N-S-shortening and E-W-extension (Kolenprat et al., 1999).

The Kellerjochgneiss was first mapped on a large scale by Ampferer and Ohnesorge (1918, 1924) and is a mylonitic augengneiss. The mineral assemblage of the Kellerjochgneiss includes biotite + muscovite + plagioclase + K-feldspar + quartz ± stilpnomelane ± clinzozoisite (Fig. 4A). Accessories are titanite, rutile, zircon, epidote, apatite, hematite and ore minerals. The protolith of the Kellerjochgneiss was probably an S-type alkaline-feldspar-granite according to Steyrer and Finger (1996) and Gangl et al. (2002, 2005). Only few petrological and structural studies have been carried out so far on these rocks (Satir and Morteani, 1978a, b; Satir et al. 1980; Wezel, 1981; Roth, 1983, 1984; Piber, 2002). Metamorphic P-T conditions of an earlier overprint (Variscan) of 5.3 kbar at 400°C were determined by Satir and Morteani (1978b). A qualitative estimate of the later metamorphic overprint (Eo-Alpine) indicates temperatures <350°C at 2-3 kbar (Satir and Morteani, 1978b). In contrast, the latest P-T estimates yield temperatures between 286° – 345°C at pressures ranging from 4.3 – 6.5 kbar and are thought to represent the Eo-Alpine metamorphic overprint (Piber and Tropper, 2005; Gangl et al., 2005). Single zircon U/Pb analyses point to an intrusion age of 468 ± 1 and 469 ± 2 Ma and thus provide further evidence for pre-Variscan age data in addition to the two dominant metamorphic overprints, the Variscan and the Eo-Alpine event (Satir and Morteani, 1978a, b; Steyrer and Finger, 1996; Handler et al., 2000, Gangl et al., 2005). In his structural investigations, Roth (1983) identified deformation structures that he related to the Variscan and Alpine orogeny respectively. According to these observations early (Variscan) mylonites, related to nappe emplacement were re-activated during the N-directed nappe stacking associated with the Eo-Alpine orogeny. Afterwards, NE-SW striking and NW-verging folds formed which he related to the subsequent continental collision following the nappe transport (Roth, 1983).

The Stengelgneiss occurs only in the NE part of the area of investigation and is a mylonite that is most likely still part of the Kellerjochgneiss as indicated by geochemical investigations (Gangl et al., 2002). Additionally, a single zircon U/Pb age of 479 ± 2 Ma

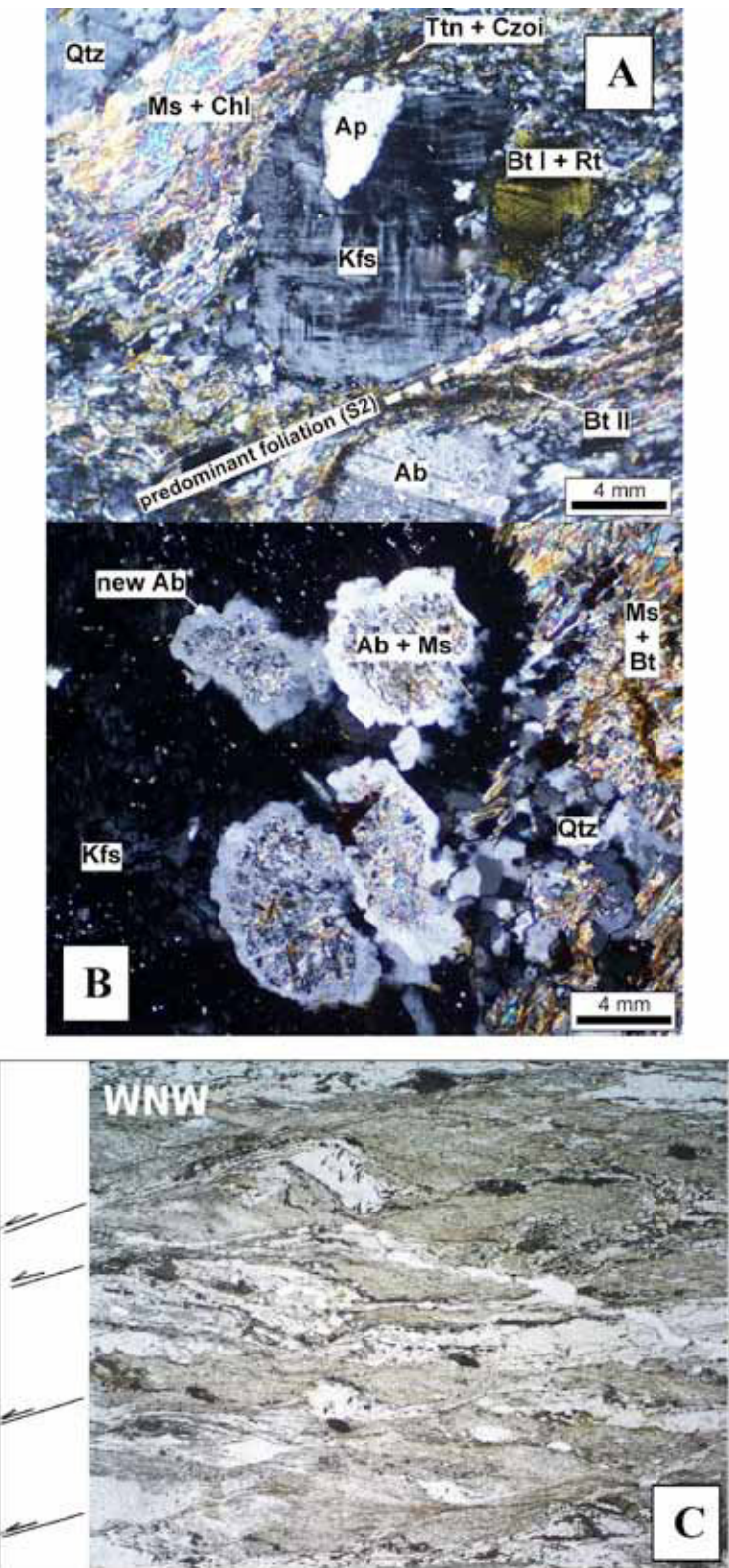


Figure 4: (A): This photomicrograph depicts the characteristic mineral assemblage of the Kellerjochgneiss (sample A-56) with relict K-feldspar (Kfs), albite porphyroblasts and relict biotite (Bt I) containing abundant rutile (Rt) needles, and chlorite (Chl) and muscovite (Ms). On the top of the picture at the rim of the K-feldspar titanite (Ttn) and clinozoisite (Czo) occur (X Nicols). (B): This photomicrograph shows albite porphyroblasts containing sericite within a relict K-feldspar crystal. Newly grown albite predominately occurs at the rim or along fractures within the old feldspar crystals (sample A-98, X Nicols). (C): This photomicrograph shows shearbands in the Kellerjochgneiss indicating top to WNW movements.

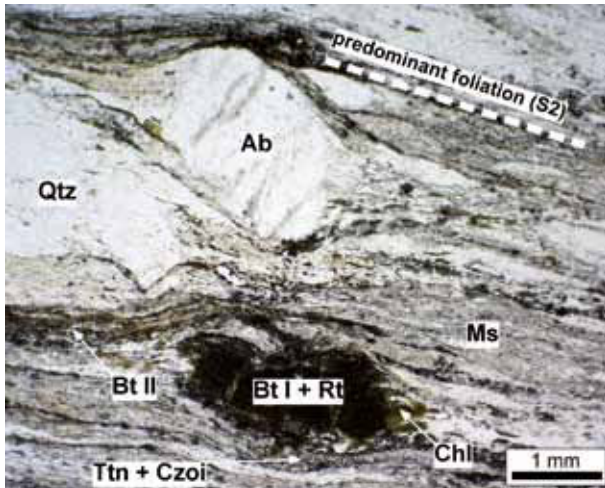


Figure 5: Photomicrograph of the comparison of pre - and synkinematically grown biotite in the Stengelgneiss. The synkinematically grown minerals, such as muscovite (Ms), biotite (Bt II), albite (Ab), chlorite (Chli) and quartz (Qtz) are strongly flattened, while the older biotite (Bt I) was rotated during deformation and titanite (Ttn) and clinozoisite (Czo) grew along its rims. Chlorite occurs in the pressure shadow of Bt I (sample A-106, II Nicols).

indicates an affiliation to the Kellerjochgneiss (Gangl et al., 2005). Similar to the Kellerjochgneiss, the Stengelgneiss displays also a mylonitic fabric but the minerals are stronger elongated along the NE-SW striking stretching lineation. The mineral assemblage of the Stengelgneiss consists of biotite + muscovite + plagioclase + K-feldspar + quartz. As accessories, titanite, rutile, zircon, epidote, apatite, hematite and ore minerals occur (Fig. 5). Strongly deformed quartz grains are stretched parallel to the lineation and quartz aggregates form rods which gave the Stengelgneiss its name.

The Wildschönau Schists and the Schwaz Dolomite are part of the Greywacke Zone (Ortner and Reiter, 1999) and according to Mostler (1973) the Western Greywacke Zone is a stratigraphic sequence of meta-sediments with volcanic intercalations, ranging from the Ordovician to the Late Devonian. The Wildschönau Schists are composed of light gray phyllites similar to the Innsbruck Quartzphyllite. Roth (1983) characterized two different varieties of the Wildschönau Schists, the sandy type and the phyllitic type. Grasbon (2001) established that these two varieties of Wildschönau Schists are intercalated even on outcrop scale and therefore these two variations will be treated together in this investigation. The mineral assemblage of the Wildschönau Schists is very similar to the Innsbruck Quartzphyllites containing the mineral assemblage muscovite + chlorite + albite + quartz ± calcite (Fig. 6). Muscovite ^{40}Ar - ^{39}Ar ages

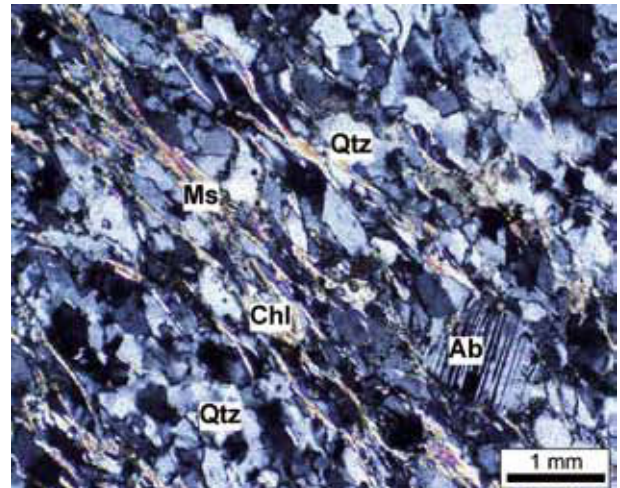


Figure 6: Photomicrograph of the mineral assemblage of the Wildschönau Schists containing muscovite (Ms), quartz (Qtz), albite (Ab) and chlorite (Chli) (sample A-101, X Nicols).

(Handler et al., 2000) from the Wildschönau Schists indicated a Variscan or Permian metamorphic overprint at 267 ± 6 Ma. In addition Angelmaier et al. (2000) obtained ^{40}Ar - ^{39}Ar ages of 264 ± 11 Ma on muscovite, which correlates very well with the age of Handler et al. (2000). Although few ^{40}Ar - ^{39}Ar data from the Wildschönau Schists yield late Variscan ages (Handler et al., 2000), ^{40}Ar - ^{39}Ar ages from the central Greywacke Zone yield 102 – 98 Ma (Schmidlechner et al., 2006) and ^{87}Rb - ^{87}Sr ages of 137 to 127 Ma and ^{40}K - ^{39}Ar ages of 113 to 92 and 113 to 106 Ma from the Greywacke Zone close to Zell am See give reasonable evidence for an Eo-Alpine metamorphic overprint around ca. 300°C (Kralik et al., 1987).

In the Western Greywacke Zone, modern thermo-barometric data were lacking until recently. Based on index minerals, Hoschek et al. (1980) estimated lower greenschist facies conditions for the Wildschönau Schiefer. Piber (2005) obtained P - T conditions of 4.5 kbar and 330°C, based on multi-equilibrium thermobarometry on one sample of the Wildschönau Schists. Geochronological investigations by Handler et al. (2000) and Anglmeier et al. (2000) in this area indicate only a Permian metamorphic overprint so far. However, investigations from the central Greywacke Zone yield clear evidence for a Cretaceous metamorphic overprint around ca. 300°C (Kralik et al., 1987; Schmidlechner et al., 2006).

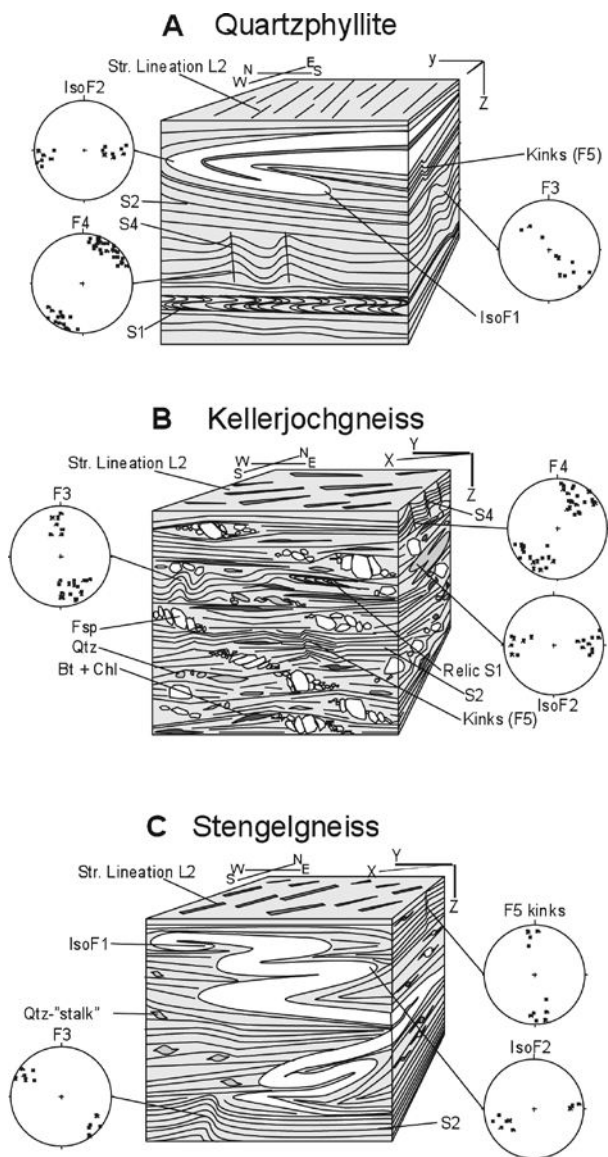


Figure 7: Block diagrams showing the tectonic structures of the Innsbruck Quartzphyllite (A) the Kellerjochgneiss (B) and the Stengelgneiss (C). In addition, stereo plots showing the orientation of the different fold axes and stretching lineations, are added to the tectonic block images.

3. Structural data

Ductile deformation

Based on structural data obtained in the field and petrographic and textural observations in oriented thin sections, four stages of ductile ($D_1 - D_4$) and one stage of semiductile (D_5) deformation could be distinguished. The spatial relationship of the structural elements is illustrated in Figures 7 A – C, showing idealized block diagrams of a sample of each of the

units discussed. The structural successions of the investigated units are also shown in Table 1, which give a comprehensive overview of the observed structures.

Deformation D_1

Relict D_1 structures, such as a foliation and isoclinal folds, are preserved in all investigated units. In the Innsbruck Quartzphyllite and in the Kellerjochgneiss, a relict of an earlier foliation (S_1) is visible in very few thin sections. Due to the intensive overprint of the earlier foliation S_1 by S_2 , the orientation of S_1 could not be determined in these units. Remnants of a stretching lineation (L_1), which seems to accompany S_1 , rarely occur and exhibit no clear orientation. In the Wildschönau Schists, remnants of a relict S_1 foliation show a strike ranging from NNE-SSW to NW-SE. In addition, this deformational event also causes isoclinal folding (iso- F_1) of intercalated quartz segregations in the Innsbruck Quartzphyllite and the Stengelgneiss with wavelengths up to a few centimeters as shown in Figure 7A, B and 8A, B. These folds are absent in the Kellerjochgneiss and the Wildschönau Schists.

Deformation D_2

A younger foliation (S_2), which is the dominant foliation in the area of investigation, overprints S_1 in the Innsbruck Quartzphyllite (Fig. 7A). Occasionally a stretching lineation occurs in the Innsbruck Quartzphyllite in quartz-rich aggregates, quartz- and calcite-rich ribbons and/or carbonate-rich aggregates. This lineation (L_2) strikes ENE-WSW (Fig. 7A). During this stage of deformation, the relict isoclinal folds (iso- F_1) in the Innsbruck Quartzphyllite were also refolded and formed a second generation of isoclinal folds (iso- F_2) with hinge lines striking ENE-WSW (Fig. 7A, Fig. 8A). The S_2 foliation is also the dominant mylonitic foliation in the Kellerjochgneiss and the Stengelgneiss (Fig. 7B, C, Fig. 8B, C). Stretching lineations (L_2) in the Kellerjochgneiss and the Stengelgneiss trend NE-SW (Fig. 7B, C). Isoclinal folds (iso- F_2) with WSW-ENE striking hinges, similar to the Innsbruck Quartzphyllite, were also found in the Kellerjochgneiss and Stengelgneiss (Fig. 7B, C, Fig. 8B, C). Accompanying the ENE-WSW striking isoclinal folds (iso- F_2), a stretching lineation (L_2), which strikes NE-SW, also occurs. Locally small top-NW

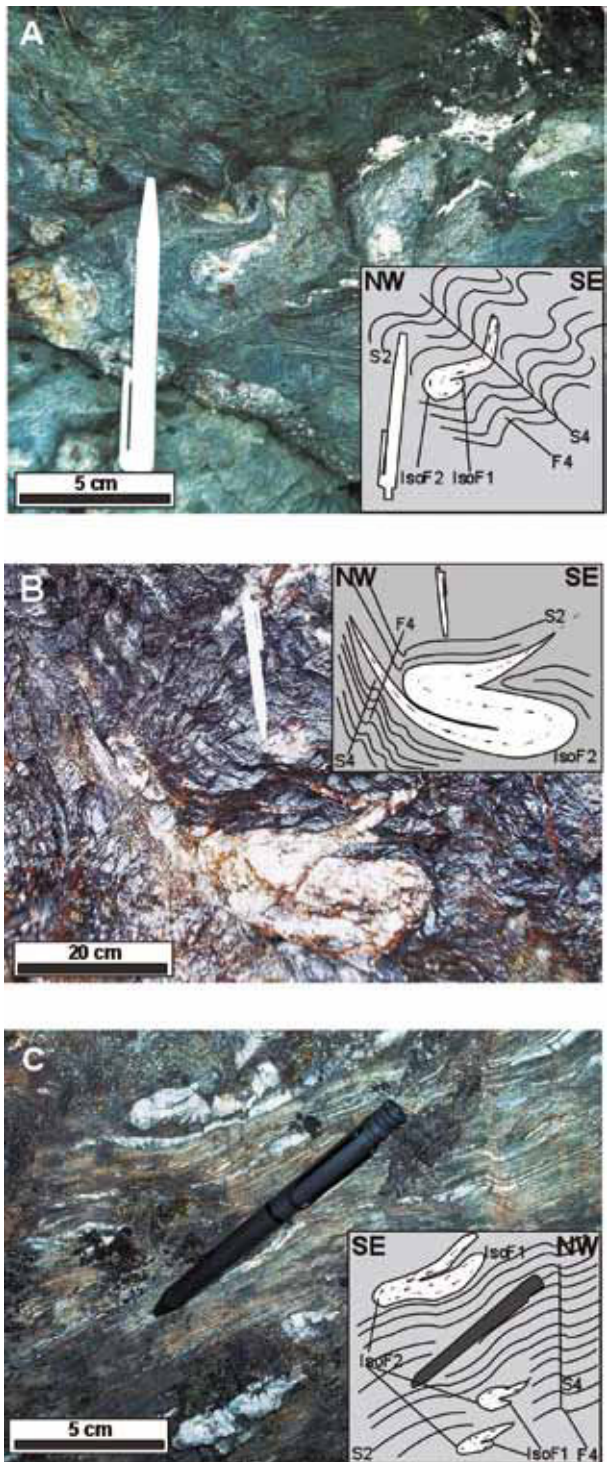


Figure 8: This image shows a sequence of fold structures in the Innsbruck Quartzphyllite (A), the Kellerjochgneiss (B) and the Stengelgneiss (C). Referring to (A) and (B) the folds (F_3) with NW-SE striking hinge lines can not be seen because of the NW-SE orientation of the outcrop. The same applies to the kink bands in the Stengelgneiss (C).

to WNW shear bands (Fig. 4B), crosscutting S_2 , also occur in the Kellerjochgneiss. These shear bands indicate ongoing deformation under cooler conditions. The Stengelgneiss shows the same structural features as the Kellerjochgneiss and therefore ENE-WSW striking isoclinal folds (iso- F_2) accompany the stretching lineation (L_2), which strikes NE-SW, (Fig. 7C). In the Wildschönau Schists, S_2 shows a wide range in orientations with strikes ranging from WNW-ESE to NE-SW whereas NW-SE to N-S striking directions are dominant (Fig. 9). During this deformation stage, tight folds (F_2), striking ENE-WSW were also formed (Fig. 9). Similar to the two units discussed above, the stretching lineation in the Wildschönau Schists shows preferred orientation varying from NNE-SSW to ENE-WSW (Fig. 9). Preferred orientation may also be indicated by stretched mineral fibers trending NNE-SSW (L_2) which coincides with the stretching lineation in the Kellerjochgneiss.

Deformation D_3

During this stage, folding of S_2 led to the generation of open folds (F_3) with NW-SE striking hinge lines (Fig. 7A). These folds were observed in the northern part of the studied area, especially in the vicinity of tectonic contacts between the Kellerjochgneiss and the Innsbruck Quartzphyllite. These folds vary in size and occur as small scale folds with wavelengths ranging from several centimeters up to a few meters. Their interlimb angle can be open to tight (down to ca. 35°). A probably younger, second lineation (crenulation lineation), striking NW-SE (L_3), was observed in the Innsbruck Quartzphyllite. This crenulation lineation is formed by chlorite. In the Kellerjochgneiss, tight folds (F_3), overprinting the S_2 foliation, with NW-SE striking hinge lines similar to the Innsbruck Quartzphyllite, also occur (Fig. 7B). These folds show a vergence towards the NE (Fig. 7C) and only occur sporadically in the NW and W of the area of investigation, in proximity to the tectonic boundary between the Kellerjochgneiss and the Innsbruck Quartzphyllite. In the Kellerjochgneiss, a second lineation (crenulation lineation - L_3), striking NW to SE was occasionally found, which is also formed by chlorite. The Stengelgneiss shows similar structural features as the Kellerjochgneiss, but younger NW-SE (F_3) striking open folds, overprinting F_1 and F_2 isoclinal folds are rare (Fig. 7C, Fig. 8C). A NW-SE striking lineation has not been found in the Stengelgneiss. NW-SE striking

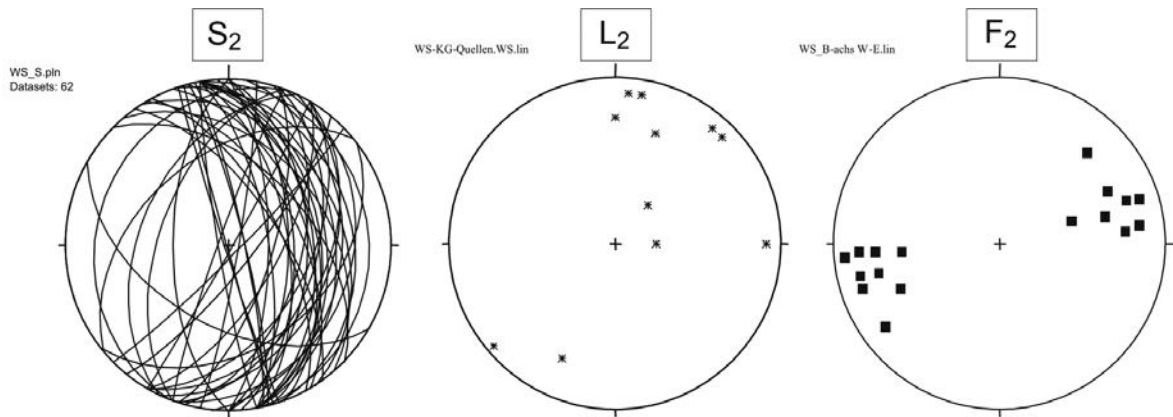


Figure 9: These stereo plots show the orientation of the predominant foliation (S_2), lineation (L_2) and folds (F_2) of the Wildschönau Schist.

folds (F_3) also occur rarely in the Wildschönau Schist. Similar to the stretching lineation L_2 which formed during D_2 , a possible second generation of lineations (crenulation lineation - L_3) striking in NW-SE direction occurs locally, which is also formed by chlorite. Due to the broad spread in the measured directions, these data have to be considered with caution.

Deformation D_4

In the Innsbruck Quartzphyllite the subsequent deformation stage led to the formation of a younger generation of folds, (F_4), which show NE-SW striking hinge lines (Fig. 7A, Fig. 8A). The interlimb angles of these folds are gentle to tight (ca. 25°) (Fig. 8A). Locally another foliation (S_4) developed as an axial plane foliation to F_4 , which ordinarily strikes E-W. A large fold structure with a hinge line striking SW to NE and a wave length of more than one kilometer occurs in the central section of the area of investigation (Fig. 2B). Its hinge line dips towards the NE. In the Wildschönau Schists, numerous open chevron folds (F_4) occur, which strike NNE-SSW, and represent the youngest fold generation observable in this unit.

Deformation D_5

The latest semi-ductile structures occur as kink bands and can be found in all units. Due to different lithological characteristics their orientation varies strongly and thus no characteristic strike direction could be discerned.

Brittle deformation

An analysis of the brittle faults was done using the program TECTONIC FP v. 1.6.01 by Ortner et al. (2002). Since the brittle structures are part of the youngest tectonic activity (D_6) in the area, they crosscut all lithologies. The data from all units showed that brittle deformation took place in four stages ($D_{6a} - D_{6d}$).

(1) The oldest brittle faults are NW-SE to WNW-ESE striking strike-slip faults (D_{6a}) with a dextral sense of motion and conjugate sinistral strike-slip faults, which strike NNW-SSE (Fig. 10A). (2) The next generation of brittle faults, overprinting D_{6a} , is expressed through thrust faults (D_{6b}) which strike E-W to NW-SE (Fig. 10B). (3) The younger Zillertal-parallel faults, which crosscut (D_{6b}) in the working area, strike NNW-SSE (D_{6c}) (Fig. 10C). They commonly dip steeply to the NE and are normal faults with oblique dextral motions. (4) The youngest faults are the Inntal-parallel faults which are the dominant faults occurring in the whole area. These faults strike NE-SW and are mostly strike slip faults (D_{6d}) with an oblique normal or reverse sense of motion (Fig. 10D, Fig. 2B). These NE-SW striking faults are more common toward the tectonic contact between Innsbruck Quartzphyllite and Kellerjochgneiss. These faults and their subsystems cause an intensive imbrication of the units, especially in the northern part of the area of investigation, where Innsbruck Quartzphyllite, Stengelgneiss and Schwaz Dolomite are strongly imbricated. The NE-SW striking faults cause lateral displacements which can range up to several kilometers. The largest sinistral lineament, crosscutting the

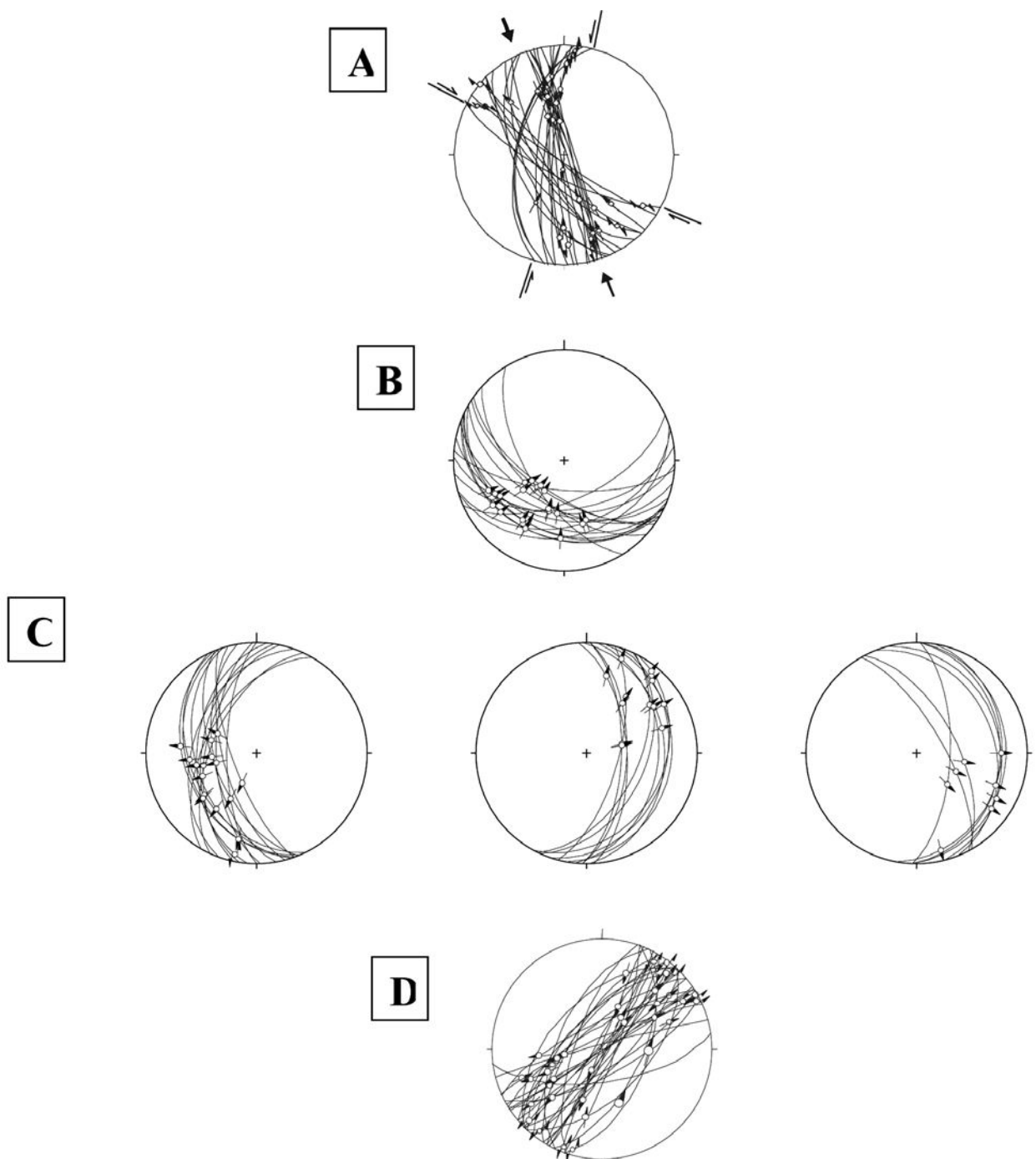


Figure 10: (A): This stereo plot shows the orientation of the oldest brittle faults, representing D_{6a} , occurring in the area of investigation. Conjugated sinistral strike-slip faults are also illustrated in this plot. (B): Examples of thrust faults (D_{6b}), which lead to strong imbrication of the lithologies to the vicinity of the Inn Valley, indicating a NE-SW contraction. (C): Examples showing normal faults from the area of investigation caused by E-W extension (D): Examples of faults reflecting the ongoing Miocene deformation. The plot shows Inn-Valley parallel sinistral strike-slip faults. They are accompanied by synthetic Riedel shear faults.

1A Deformation Sequence of the Innsbruck Quartzphyllite			
lithological unit	deformation stage	tectonic structures	character of deformation
Innsbruck Quartzphyllite	D1	relic S ₁ axial plane foliation of iso F ₁	ductile
	D2	penetrative S ₂ foliation; WSW-ENE striking iso F ₂ folds E-W striking stretching lineation L ₂	ductile
	D3	NW-SE striking mineral lin. L ₃ NW-SE striking F ₃ folds	ductile
	D4	NE-SW striking open to tight F ₄ folds S ₄ foliation	ductile
	D5	kink bands	semi ductile
	D6a	NW to SE striking dextral strike-slip faults	brittle
	D6b	NW-SE to W-E striking thrust faults	brittle
	D6c	N to S striking normal faults	brittle
	D6d	NE-SW to NNE-SSW striking sinistral strike-slip faults	brittle

1B Deformation Sequence of the Kellerjochgneiss & Stengelgneiss			
lithological unit	deformation stage	tectonic structures	character of deformation
Kellerjochgneiss	D1	relic S ₁ foliation N-S striking relic stretching lineation	ductile
	D2	penetr. S ₂ foliation; NE-SW to E-W striking stretching lineation ENE-WSW striking iso F ₂ folds shear bands top to the WNW - NW	ductile ductile
	D3	NW to SE striking mineral lin. L ₃ NW to SE striking F ₃ folds	ductile
	D4	NE to SW striking open to tight small scale F ₄ folds	ductile
	D5	kink bands	semi ductile
	D6a	NW to SE striking dextral strike-slip faults	brittle
	D6b	NW-SE to W-E striking thrust faults	brittle
	D6c	N to S striking normal faults	brittle
	D6d	NE-SW to NNE-SSW striking sinistral strike-slip faults	brittle

1C Deformation Sequence of the Wildschönau Schist			
lithological unit	deformation stage	tectonic structures	character of deformation
Wildschönau Schist	D1	S ₁ foliation	ductile
	D2	S ₂ foliation; NE to SW striking stretching lineation L ₂ ENE to WSW striking F ₂ folds	ductile
	D3	NW to SE striking mineral lin. L ₃ NW to SE striking F ₃ folds	ductile
	D4	NNE to SSW striking F ₃ folds	ductile
	D5	kink bands	semi ductile
	D6a	NW to SE striking dextral strike-slip faults	brittle
	D6b	NW-SE to W-E striking thrust faults	brittle
	D6c	N to S striking normal faults	brittle
	D6d	NE-SW to NNE-SSW striking sinistral strike-slip faults	brittle

Table 1: Compilation of the deformation sequence of the Innsbruck Quartzphyllite, the Kellerjochgneiss the Stengelgneiss and the Wildschönauer Schists from this investigation.

Wildschönau Schists and the Kellerjochgneiss, is represented by the Finsinggrund Fault (Fig. 2A), which strikes NE-SW with an oblique motion trending to NE. This fault offsets the Wildschönau Schists from the Kellerjochgneiss by about 3 kilometers, which was also established from previously published geological maps by Roth (1983).

4. Discussion

Comparison of the structural successions with previous investigations

The structural data from this work (Table 1) may be compared to structural data from other authors, such as Roth (1983), Ortner and Sachsenhofer (1996), Steyrer et al. (1996), Kolenprat et al. (1999), Ortner et al. (1999) and Grasbon (2001) as shown in Tables 2, 3A-C. Recently Kolenprat et al. (1999) developed a structural model for the Innsbruck Quartzphyllite to the south of Innsbruck (Table 2). In their model, the authors correlate the observed deformation stages with the deformation sequence in the Eastern Alps from further west near the Swiss border, obtained by Froitzheim et al. (1994). Kolenprat et al. (1999) describe a relic Pre-Alpine foliation (S_2), which is the axial plane foliation of relict isoclinal folds (iso- F_1). An indicator for the Pre-Alpine age of the foliation (S_2) is the post- S_2 /pre- S_3 garnet growth of Permian garnets in mica schists. The Cretaceous evolution of the Innsbruck Quartzphyllite has been associated with the Trupchun Phase by these authors. These structures are expressed as a penetrative mylonitic foliation (S_3) with E-W stretching lineations and W-E striking isoclinal folds (iso- F_3). Shearbands within layers of chlorite-bearing schists indicate top-to-NW motions that post-date the Trupchun Phase. These movements were interpreted as being associated with post-Trupchun NW directed nappe stacking. Kolenprat et al. (1999) found no structural features that could be correlated with the Dukan Ela Phase, which is associated with the extensional collapse and formation of Gosau basins during the Uppermost Cretaceous (80 – 67 Ma, Froitzheim et al. 1994). Deformation structures, associated with the Alpine Tertiary evolution during the Blaisun Phase (50–35 Ma) are open chevron folds with NE to SW trending hinge lines (F_{4a}) and an axial plane foliation (S_4). Subsequent semi-ductile structures are expressed as kink bands, which were correlated with the Turba Phase

(35 – 30 Ma.). The following brittle deformation is polyphase (D_{6a} - D_{6d}).

Concerning the Innsbruck Quartzphyllite, our relic S_1 axial plane foliation and the F_1 isoclinal folds (Tab. 3A) are in a good correlation with the relic S_2 foliation from the structural succession scheme of Kolenprat et al. (1999) in Table 2. Furthermore, the dominant D_2 and D_3 deformation structures agree with their observations, except that the NW-SE striking folds and NW-SE striking stretching lineations were not observed by Kolenprat et al. (1999) and we did not observe top to the NW shear bands (Tab. 3A). The data from the structural succession scheme of Grasbon (2001) are also similar to the structural data from this work, except that she did not observe any relic D_1 structures.

Concerning the Kellerjochgneiss the structural succession of Grasbon (2001) as seen in Table 3B, is again very similar to the structural data from this investigation, except for the absence of relic D_1 deformation structures and the NE-SW striking small scale folds (F_4). Steyrer et al. (1996) also proposed a similar succession of structures. Our D_2 shearbands are in accordance with their shear bands indicating motions top to the W to NW during D_2 . Their NE-SW striking folds can also be correlated with the ENE-WSW striking folds (F_2). Furthermore, they observed chevron folds which are similar to our NE-SW striking open F_4 folds (Tab. 3B). The NE striking folds described by Roth (1983) may be compared to the ENE-WSW striking folds assigned in our scheme to D_2 . His W-NW striking folds may also be correlated to the F_3 folds, which strike NW-SE. However, the remainder of our deformation scheme does not correlate with the deformation sequence of Roth (1983).

Concerning the Wildschönau Schists, the structural data from this work are compared in Table 3C with the structural succession of Grasbon (2001). Similar to the Innsbruck Quartzphyllite and the Kellerjochgneiss, Grasbon (2001) did not identify any relic D_1 deformation structures within the Wildschönau Schists. Her N(E)-S(W) striking folds with the accompanying (N)NE-(S)SW striking stretching lineation can be correlated to the ENE-WSW striking F_2 folds and the NE-SW striking stretching lineation (L_2). The NE-SW striking chevron folds may be compared with the NNE-SSW striking open folds (F_4) from this investigation (Tab. 3C).

Tectonic Scheme of the Innsbruck Quartzphyllite		
Kolenprat et al. (1999 & oral com.)		
presumed age	Deformation stage	structures
Permian or Variscan	Dv1 Dv2	relic iso F ₁ S ₂ foliation Garnet post S ₂ pre S ₃
Cretaceous Trupchun Phase 100-80 ma.	D3a	mylonitic S ₃ str. lineation top to the W W-E striking iso F ₃ folds
post Trupchun Phase	D3b	shear bands top to the NW
Blaisun Phase/50-34 ma.	D4	NE-SW striking open F _{4a} folds S ₄ foliation
Blaisun Phase/50-34 ma.	D5	kink bands

Table 2: Tectonic scheme of the westernmost part of the Innsbruck Quartzphyllite by Kolenprat et al. (1999).

3 A Comparison of the Deformation Sequence of the Innsbruck Quartzphyllite			
Kolenprat (1999 & oral com.)		this study	
Deformation stage	structures	structures	Deformation stage
Dv1 Dv2	relic iso F ₁ S ₂ foliation Garnet post S ₂ pre S ₃	relic S ₁ axial plane foliation of iso F ₁	D1
D3a	mylonitic S ₃ str. lineation top to the W W-E striking iso F ₃ folds	penetrative S ₂ foliation WSW-ENE striking iso F ₂ folds E - W striking str. lineation L ₂	D2
D3b	shear bands top to the NW	NW-SE striking mineral lin. L ₃ NW-SE striking F ₃ folds	D3
D4	NE-SW striking open F _{4a} folds penetrative S ₄ foliation	NE-SW striking open to tight F ₄ folds S ₄ foliation	D4
D5	kink bands	kink bands	D5
Grasbon (2001)		this study	
Deformation stage	structures	structures	Deformation stage
		relic S ₁ axial plane foliation of iso F ₁	D1
D1	NE-SW striking folds NE-SW striking stretching lineation	penetrative S ₂ foliation WSW-ENE striking iso F ₂ folds E - W striking str. lineation L ₂	D2
D1	shear bands top to the NW	NW-SE striking mineral lin. L ₃ NW-SE striking F ₃ folds	D3
D2	NW-SE striking folds NW-SE striking stretching lineation	NE-SW striking open to tight F ₄ folds S ₄ foliation	D4
D3	E-W striking folds shear bands top to the N/S NE-SW striking chevron folds	kink bands	D5

Table 3A: Correlation between the deformation sequence of the Innsbruck Quartzphyllite from this investigation with the deformation sequences deduced by Kolenprat et al. (1999) and Grasbon (2001).

Geochronological constraints on the evolution of the Austroalpine nappes north of the Tauern Window

Recently there have been several geochronological investigations in the western part of the Innsbruck Quartzphyllite in the vicinity of the Brenner Fault and the overlying Patscherkofel Crystalline Complex. Dingeldey et al. (1997) conducted one Ar-Ar stepwise heating experiment on a sample from the western part of the Innsbruck Quartzphyllite. They found a rejuvenation of the phengite age from 250 Ma to 35 Ma, indicating that the temperature of the Alpine metamorphic overprint probably exceeded 350°C in this area. Recently, Ar-Ar and Rb-Sr dating has been performed on samples from the Brenner area by Rockenschaub et al. (1999). The Ar-Ar plateau ages (206 – 268 Ma) and Rb-Sr ages (229 – 255 Ma) of phengites from porphyritic orthogneisses within the Innsbruck Quartzphyllite, as well as one monazite microprobe age (280 ± 25 Ma), gave indications for a Permian event (Rockenschaub et al., 1999). They also obtained Eo-Alpine Ar-Ar ages of 135 Ma for synkinematically grown phengites from the dominant foliation S_2 in the northern and central parts of the Innsbruck Quartzphyllite. This result might indicate the onset of the Eo-Alpine metamorphic event and hence put an age constraint on the earliest stage of the Alpine deformation. While these ages show considerable spread due to incomplete resetting and partial mineral growth during the Eo-Alpine orogeny, these results represent the only current absolute age constraint on Alpine deformation in the sequence. In addition to these metamorphic mineral ages, there are also a few data available on the low temperature cooling history (<300°C), based on fission track measurements, available. Fügenschuh et al. (1997) obtained two fission track ages on zircon from the western part of the Innsbruck Quartzphyllite which yielded ages of 42 and 67 Ma. A fission track age on apatite yielded 13 ± 2 Ma. This age is similar to the apatite fission track age of 14.3 ± 2.8 Ma, obtained by Grundmann and Morteani (1985).

Satir and Morteani (1978a) conducted the first geochronological investigations in the Kellerjochgneiss. They obtained a protolith intrusive age of the orthogneisses of 425 Ma based on a Rb-Sr isotope study. Latest protolith intrusive age data based on U/Pb single zircon dating yield 468 ± 1 and 469 ± 2 Ma (Gangl et al., 2005). Satir and Morteani (1978a) also applied the Rb-Sr whole rock isochrone method

to the Kellerjochgneiss to infer the age of the metamorphic overprint, which yielded 322 ± 24 Ma, which is clearly Variscan. Additional Rb-Sr data on phengites from the Kellerjochgneiss yielded cooling ages of 260 and 273 Ma. Furthermore, their data also constrain the Variscan age of the metamorphic overprint. Based on Th-U-Pb model ages of monazite and thorite, Steyrer and Finger (1996) obtained ages of 323 ± 9 and 353 ± 26 Ma. In addition, there are a few data constraining the low-temperature evolution of the Kellerjochgneiss. There are only two fission track ages of apatites from the study of Grundmann and Morteani (1985) available, which yielded 14.5 ± 2.2 and 17.6 ± 1.5 Ma. Zircon and apatite ages from Angelmaier et al. (2000) yielded ages of 57 – 63 Ma and 13 ± 1 Ma.

Muscovite Ar-Ar ages (Handler et al., 2000) from the Wildschönau Schiefer indicate a Variscan or Permian metamorphic overprint at 267 ± 6 Ma. In addition Angelmaier et al. (2000) obtained Ar-Ar ages of 264 ± 11 Ma, which correlates very well with the age of Handler et al. (2000). ^{40}Ar - ^{39}Ar ages from the central Greywacke Zone yielded 102 – 98 Ma (Schmidlechner et al., 2006), ^{87}Rb - ^{87}Sr ages and ^{40}K - ^{39}Ar close to Zell am See yielded 137 to 127 Ma and 113 to 106 Ma. One zircon and one apatite fission track age available from Wildschönau Schists yielded 116 ± 4 Ma and 38 ± 5 Ma (Angelmaier et al., 2000), respectively.

Compiling the published muscovite Ar-Ar data (Handler et al., 2000; Schmidlechner et al. 2006), biotite Rb-Sr data (Satir and Morteani, 1978a,b), zircon fission track ages (Angelmaier et al., 2000) and apatite fission track data (Grundmann and Morteani, 1985; Angelmaier et al., 2000; Fügenschuh, 1995) from this area, allows time constraints to be placed on the deformation sequence in the three units. While D_1 is clearly related to a pre-Alpine event of probably Variscan age, D_2 can unambiguously be attributed to the early stages of the Eo-Alpine event. Since the closure temperature of the zircon fission track system is ca. 260–220°C (Fügenschuh, 2005, pers. comm.), this puts time constraints on the last stages of ductile (D_4) and/or semiductile (D_5) deformation. These data establish that all three units experienced temperatures of 300 – 400°C at pressures ranging from 4 to 6.5 kbar at around 90 – 135 Ma, based on available Ar-Ar and Rb-Sr age data (Rockenschaub et al., 1999). Although some Ar-Ar data from the Wildschönau Schists yielded late Variscan ages (Handler et al., 2000), Ar-Ar ages from the cen-

Comparison of the Deformation Sequence of the Kellerjochgneiss			
Grasbon (2001)		this study	
Deformation stage	structures	structures	Deformation stage
		relic S ₁ foliation N-S striking str. lin. L ₁	D1
D1	NE-SW striking folds NE-SW striking stretching lineation	penetr. S ₂ foliation WSW-ENE striking iso F ₂ folds NE-SW to E-W str. lin. L ₂	D2
D1	shear bands top to the NW-W	shear bands top to the NW-W	D2
D2	NW-SE striking folds NW-SE striking stretching lineation	NW-SE striking F ₃ folds NW-SE striking mineral lin. L ₃	D3
D3	E-W striking folds shear bands top to the SSW (N)E-(S)W striking chevron folds	NE-SW striking open F ₄ small scale folds	D4
		kink bands	D5
Steyrer et al. (1996)		this study	
Deformation stage	structures	structures	Deformation stage
Dv1/Dv2	penetrative mylonitic foliation top N sF ₁ ; muscovite1 stretch. lin. N-S/NNE-SSW	relic S ₁ foliation N-S striking str. lin. L ₁	D1
D1	semiductile shearbands deform. of musc. 1/2nd mica gener. lineation N-S, S-vergent transport	penetr. S ₂ foliation WSW-ENE striking iso F ₂ folds NE-SW to E-W str. lin. L ₂	D2
		shear bands top to the NW-W	
D2	(S)E-(N)W contraction N-S to NE-SW striking folds	NW-SE striking F ₃ folds NW-SE striking mineral lin. L ₃	D3
D3	chevron folds	NE-SW striking open F ₄ small scale folds	D4
D4	brittle deformation	kink bands	D5
Roth (1983)		this study	
Deformation stage	structures	structures	Deformation stage
Dv1/Dv2	1. N-S contraction S-vergent nappe stacking/ 2. E-W contraction early zenith of T, following variscan double mylonitization stretch. lin. N-S/folds strike NE-N	relic S ₁ foliation N-S striking str. lin. L ₁	D1
D1	nappe stacking top (N)NE folds strike W-NW	penetr. S ₂ foliation WSW-ENE striking iso F ₂ folds NE-SW to E-W str. lin. L ₂	D2
		shear bands top to the NW-W	
D2	motions top to (S)E folds E-SE vergent folds strike N-NE	NW-SE striking F ₃ folds NW-SE striking mineral lin. L ₃	D3
D3	N-S contraction conjugated faults strike NE-SW and NW-SE	NE-SW striking open F ₄ small scale folds	D4
D4	brittle deformation	kink bands	D5

Table 3B: Correlation between the deformation sequence of the Kellerjoch Gneiss from this investigation with the deformation sequences deduced by Grasbon (2001), Steyrer et al. (1996) and Roth (1983).

tral Greywacke Zone yielded 102 – 98 Ma (Schmidlechner et al., 2006) and Rb-Sr ages of 137 to 127 Ma and K-Ar ages of 113 to 92 and 113 to 106 Ma from the Greywacke Zone close to Zell am See give reasonable evidence for an Eo-Alpine metamorphic overprint around ca. 300°C (Kralik et al., 1987). Zircon fission track ages from the Wildschönau Schists indicate temperatures of ca. 260–220°C already at 116 Ma, which is in disagreement with the Ar-Ar data from Schmidlechner et al. (2006). Clearly more zircon fission track data are needed for this unit. Concerning the correlation to the structural sequence of Kolenprat et al. (1999) and the ages of synkinematically grown phengites, ductile deformation in the area of investigation (D_2 – D_4) probably took place during the Eo-Alpine metamorphic event. These conditions prevailed until approximately 40 – 60 Ma when then the zircon fission track ages indicate temperatures <220–260°C. Probably around this time, semi-ductile deformation (D_5) took place which is in agreement with the proposed tectonic model of Kolenprat et al. (1999)

Tectonic implications for the evolution of the Austroalpine nappes in the northern Zillertal area

Tectonic data indicate that the Kellerjochgneiss as a recumbent fold structure "embedded" between the Innsbruck Quartzphyllite below, and the Wildschönau Schist above. The first deformation stage, which is responsible for the folding of the Kellerjochgneiss, probably is D_2 . This event caused tight folding of the Kellerjochgneiss and the Innsbruck Quartzphyllite, resulting in a large scale fold structure. Compression from NW to SE during D_3 led to an open refolding of these lithologies. Afterwards, this structure was intersected and imbricated due to subsequent brittle deformation (D_{6a-d}). Especially SE-NW striking sinistral strike slip faults with oblique thrust motions are responsible for strong imbrication of the different lithologies in the vicinity of the Inn Valley. The data from the TRANSALP seismic profile from the area north of the Tauern Window show S-dipping reflectors, especially in the Northern Calcareous Alps, indicating strong imbrication. The area between the NCA and the Tauern Window shows rather weak reflections, indicating thrusting of the crystalline units on top of the NCA in the North (Transalp Working Group, 2002). These thrusting movements along SE-dipping faults, as shown in Figure 2B, were also found in the

Kellerjochgneiss (D_{6b}). No other structural features could be discerned in this area from the seismic data, due to insufficient resolution of the data and the lack of lithological contrast.

The data presented above display the similarity of deformation structures occurring within the Innsbruck Quartzphyllite, the Kellerjochgneiss and the Wildschönau Schist. Each lithological unit also exhibits a similar succession of deformation processes. S_2 forms the penetrative foliation in all three units. The D_2 stretching lineations of the Innsbruck Quartzphyllite, the Kellerjochgneiss and the Wildschönau Schists indicate a E-W movement during D_2 . In accordance with the structural succession scheme of the Innsbruck Quartzphyllite given by Kolenprat et al. (1999), the W-E to SW-NE striking stretching lineations (L_2), the isoclinal F_2 folds ($\text{iso-}F_2$) of the Innsbruck Quartzphyllite and the isoclinal F_2 folds ($\text{iso-}F_2$) of the Kellerjochgneiss are thought to have formed during a W-directed nappe transport. Subsequent deformation continuing during D_2 caused the formation of shear bands, which can be seen in the Innsbruck Quartzphyllite and the Kellerjochgneiss, which also indicate a top to W-NW motion. These structures are interpreted to be the result of ongoing nappe stacking towards W-NW under somewhat cooler conditions. During D_3 , the NW-SE striking folds (F_3), occurring subordinated in all three lithological units, are interpreted as extensional collapse folding as a result of E-W extension. Similar folds with comparable axial trend also have been reported by Froitzheim et al (1994) from the Austroalpine tectonic units in Graubünden (Switzerland). In addition, similar folds were described by Brandner and Eisbacher (1996) in the adjacent Northern Calcareous Alps and by Reiter (2000) in the Triassic sediments near Schwaz. In contrast to extensional collapse folding, the folds described by Brandner and Eisbacher (1996) and Reiter (2000) are attributed to NNE-SSW-directed contraction, which is thought to have taken place in the latest Cretaceous or even the Paleocene. In analogy to the observations and interpretations made by Froitzheim et al. (1994) and Fügenschuh (1995) D_4 and the formation of F_4 folds can be attributed to northwards thrusting of the Alpine basement nappes onto the Penninic units. Since this part of Austroalpine nappe pile cooled to temperatures below 200°C (Fügenschuh, 1995), the open NE-SW striking chevron folds are most probably related to this event. Kink bands reflect the youngest structures in the ductile-semiductile regime.

Comparison of the Deformation Sequence of the Wildschönau Schist			
Grasbon (2001)		this study	
Deformation stage	structures	structures	Deformation stage
		S_1 foliation	D1
D1	N(E)-S(W) striking folds (N)NE-(S)SW striking stretching lineation	S_2 foliation WSW-ENE striking F_2 folds NE-SW striking str. lin. L_2	D2
D1	shear bands top to the N(W)		
D2	NW-SE striking folds shear bands top to the NE	NW-SE striking F_3 folds NW-SE striking mineral lin. L_3	D3
D3	shear bands top to the S NE-SW striking chevron folds	NNE-SSW striking F_4 chevron folds	D4
		kink bands	D5

Table 3C: Correlation between the deformation sequence of the Wildschönauer Schiefer from this investigation with the deformation sequence deduced by Grasbon (2001).

In accordance with the geodynamic model of Froitzheim et al (1994) and the two-stage model of Neubauer et al. (2000), the ductile structural data can be viewed in a larger geodynamic context. Both models suggest the Alpine geodynamic evolution can be considered in terms of two orogenic cycles with five stages of tectonic evolution: (1) Late Cretaceous nappe imbrication with sinistral transpression (Trupchun phase), (2) Late Cretaceous extension (Ducan-Ela phase), (3) Early Tertiary collisional deformation (Blaisun phase), (4) Early to Mid – Oligocene extension (Turba phase), (5) Late Oligocene post-collisional shortening (Domleschg phase).

The ENE-WSW striking folds (F_2) and the accompanying stretching lineations (L_2), which strike E-W to NE-SW, are all in agreement with the W directed Eo-Alpine nappe stacking of the Austroalpine units during the Late Cretaceous, related to the closure of the Hallstatt-Meliata Ocean. Thermobarometric investigations of the Kellerjochgneiss and the Stengelgneiss by Piber (2002) were based on synkinematically grown minerals, which constitute the predominant foliation (S_2). Therefore the $P-T$ results from these lithologies can be directly related to the D₂ deformation, which therefore took place under Eo-Alpine greenschist-facies metamorphic conditions. The data suggest that the Kellerjochgneiss has been metamorphosed under similar pressures (4.3 – 6.5 kbar) as the Innsbruck Quartzphyllite and the Wildschönau Schists (4.4 – 5.9 kbar) at a similar temperatures ranging from 286 to 345°C (Piber, 2005; Piber and

Tropp, 2005). The NW-directed shearbands, which Kolenprat et al. (1999) attributed to D₂, reflect displacement under greenschist conditions and may also be related to this event. According to Froitzheim et al. (1994) the NW-SE striking folds (F_3 of the Innsbruck Quartzphyllite, the Kellerjochgneiss and the Wildschönauer Schists) can be related to the initial extensional collapse during the Late Cretaceous and Paleocene. This rarely observed "collapse folding" displays folds which show no axial-plane cleavage. These folds also could be an expression of changing in contraction regime of clockwise rotation of 60° during the early Oligocene caused by collision processes and blocking of the Alpine wedge (Thöny et. al, 2004). Zircon fission track data from the Innsbruck Quartzphyllite Complex (Fügenschuh, 1995) and the Kellerjochgneiss (Angelmaier et al., 2000) show evidence for cooling of the Alpine basement nappes during latest most Cretaceous and Paleocene, hence extensional collapse folding would be more reasonable for the formation of F_3 folds in contrast to NNE-SSW directed contraction as described by Brandner and Eisbacher (1996) and Reiter (2000) for the same time.

The open NE-SW striking folds (F_4 of the Innsbruck Quartzphyllite and the Kellerjochgneiss) and the NNE-SSW striking chevron folds of the Wildschönau Schists (F_4) are comparable with the NW-N directed ductile to semiductile shear within the Austroalpine nappe pile during the Early Eocene, which was postulated by Froitzheim et al. (1994) and Fügenschuh (1995). The kink bands (D₅) may be correlated to the

ongoing contraction and the initial exhumation of the Tauern Window.

The temporal sequence of the brittle deformation can be interpreted in terms of the established geological framework developed by authors working in surrounding areas (Ortner et al., 1999; Reiter, 2000). The oldest brittle faults (D_{6a}) in the area of investigation are NW-SE striking faults with a dextral shear sense, which are conjugate to NNW-SSE striking sinistral strike-slip faults. These faults are correlated with similar faults in the Angerberg area, which are described by Ortner et al. (1999). The faults in the Angerberg area considered to be part of a pre-Oligocene deformation with a NW-SE/NNW-SSE contraction (Ortner et al., 1999). The subsequent deformation (D_{6b}) in the Early Oligocene (NE-SW/NNE-SSW contraction) caused thrust faults showing motions towards the NE, crosscutting the faults of D_{6a} . These faults can be correlated to faults occurring in calcareous marls and turbiditic sandstones in the Angerberg area described by Ortner et al. (1999). Normal faults indicating E-W extension (D_{6c}) are assumed to be generated during the Miocene by E-W (WSW-ENE) extension and may be associated with the uplift of the Tauern Window. Ortner et al. (1999) found similar faults in Miocene deposits. The youngest faults (D_{6d}) that can be determined in the area of investigation are sinistral strike-slip faults, which are mostly parallel to the Inntal-Fault. These faults are probably the result of the ongoing Miocene deformation characterized by N-S contraction, which were described by Reiter (2000) and Ortner et al. (1999). Overall, the brittle deformation (D_{6a-d}) sequence may be the consequence of continuing contraction of the Austroalpine realm and coeval uplift of the Tauern Window.

5. Conclusions

Based on geochronological and structural evidence from the three lithological units, it is possible to distinguish between pre-Alpine (D_1) and Alpine ($D_2 - D_6$) deformation structures. The earliest stage

of deformation (D_1) can be linked with a pre-Alpine event (Permian and/or Variscan). The first stage of Eo-Alpine deformation (D_2) can be correlated with the W-directed nappe stacking during the Middle to Late Cretaceous. Thermobarometric data indicate that the onset of this event during Early to Mid Cretaceous took place under greenschist-facies conditions. The ongoing W-directed nappe transport led to intensive folding of all units and mylonitization of the Kellerjochgneiss. The subsequent nappe transport and stacking under progressive cooling accompanied by detachment of upper crustal parts during the Mid-to Late Cretaceous led to the formation of shear-bands within the basement nappes. This event was then followed by the extensional collapse during the Uppermost Cretaceous (D_3), which was succeeded by Early Tertiary collisional deformation events and the overriding of the Austroalpine nappe pile onto the Penninic units (D_4). The early to middle Oligocene extension related to the onset of exhumation of the Tauern Window resulted in the last ductile deformation stage (D_5). The last brittle stages (D_{6a-d}) of the deformation sequence are probably associated with movements along the major fault lines in the area due to late Oligocene post-collisional shortening.

Thermobarometric estimates indicate that the Kellerjochgneiss, the Innsbruck Quartzphyllites and parts of the Wildschönau Schists seem to have been in similar crustal positions during low-grade metamorphic overprint. The $P-T$ conditions of 286 – 345°C and 4.3 – 6.5 kbar also indicate that the Eo-Alpine metamorphic overprint possibly took place in a geodynamic setting with a moderate to low geotherm. U/Pb zircon age constraints of the Kellerjochgneiss and the bordering Stengelgneiss, which are in good accordance to zircon ages of metaporphyric rocks of the Greywacke zone (Gangl et al., 2005), and the similarity of the temperature – time data of the Innsbruck Quartzphyllite, the Kellerjoch Gneiss and the Wildschönau Schists from the Eo-Alpine metamorphic event therefore indicate that all units are part of the Upper Austroalpine unit, which agrees with the paleogeographic model by Schmid et al. (2004).

Acknowledgements

The authors thank Bernhard Sartory for his help with the electron microprobe and Manfred Rockenschaub for his comments.

6. References

- Ampferer, O. and Ohnesorge, Th. (1918): Geologische Spezialkarte der Österreichisch – Ungarischen Monarchie, 1:75 000, Blatt Rattenberg (5048). – Wien, Geologische Reichsanstalt.
- Ampferer, O. and Ohnesorge, Th. (1924): Erläuterungen zur geologischen Spezialkarte der Republik Österreich, 1:75 000, Blatt Innsbruck-Achensee (5047). – Geologische Bundesanstalt, Wien.
- Angelmaier, P., Frisch, W. and Dunkl, I. (2000): Thermo-chronological constraints for the TRANSALP section of the Tauern Window. 2nd international TRANSALP-Colloquium, Munich, 17.
- Brandner, R. and Eibacher, G. (1996): Role of high – angle faults during heteroaxial contraction, Inntal thrust sheet, Northern Calcareous Alps, Western Austria. – Geologische Paläontologische Mitteilungen Universität Innsbruck, 20: 389 – 406.
- Dingeldey, C., Dallmeyer, D. R., Koller, F. and Massonne H. J. (1997): P-T-t history of the Lower Austroalpine Nappe Complex in the „Tarentaler Berge“ NW of the Tauern Window: implications for the geotectonic evolution of the central Eastern Alps. – Contributions to Mineralogy and Petrology, 129: 1-19.
- Eibacher, G. and Brandner, R. (1995): Role of high-angle faults during heteroaxial contraction, Inntal thrust sheet, Northern Calcareous Alps, Western Austria. – Geologische Paläontologische Mitteilungen Universität Innsbruck, 20: 389-406.
- Froitzheim, N., Schmid, S. M. and Conti, P. (1994): Repeated change from crustal shortening to orogenparallel extension in the Austroalpine units of Graubünden. – Eclogae Geologicae Helvetiae, 87: 559-612.
- Fügenschuh, B. (1995): Thermal and kinematic history of the Brenner area (Eastern Alps, Tyrol). – Unpublished PhD Thesis, ETH Zürich, 155 pp.
- Fügenschuh, B., Seward, D. and Mancktelow, N. (1997): Exhumation in a convergent orogen: the western Tauern Window. – Terra Nova, 9: 213-217.
- Gangl, S., Piber, A. and Tropper, P. (2002): Geochemical investigations of the orthogneisses from the Kellerjoch (Northern Zillertal, Tyrol, Eastern Alps). – PAN-GEO I, Programm und Kurzfassungen, 53.
- Gangl, S., Piber, A., Tropper, P., Klötzli, U., Finger, F. and Mirwald, P. W. (2005): Geochemical evidence for Lower Ordovician magmatism in the crystalline nappes north of the Tauern Window. – Geophysical Abstracts, 7: 03975.
- Grasbon, B. (2001): Großmassenbewegungen im Grenzbereich Innsbrucker Quarzphyllit, Kellerjochgneis, Wildschönauer Schiefer Finsinggrund (vorderes Zillertal). – Unpublished Master Thesis, University of Innsbruck, 141 pp.
- Grundmann, G. and Morteani, G. (1985): The young uplift and thermal history of the central eastern Alps (Austria, Italy), evidence from apatite fission track ages. – Jahrbuch der Geologischen Bundesanstalt Wien, 128: 197-216.
- Haditsch, G. and Mostler, H. (1982): Zeitliche und stoffliche Gliederung der Erzvor-kommen im Innsbrucker Quarzphyllit. – Geologische Paläontologische Mitteilungen Universität Innsbruck, 12: 1-40.
- Handler, R., Genser, J., Freidl, G., Heidorn, R., Neubauer, F., Fritz, H. and Tenczer, V. (2000): Ar-Ar ages of white mica from Austroalpine basement units along the TRANSALP section: Tectonic implications. – 2nd international TRANSALP Colloquium, Munich, 17.
- Hoschek, G., Kirchner, E. C., Mostler, H., and Schramm, J. M. (1980): Metamorphism in the Austroalpine units between Innsbruck and Salzburg (Austria) – a synopsis. – Mitteilungen der Österreichischen Geologischen Gesellschaft, 71/72: 335-341.
- Kolenprat, B. (1998): Bericht 1997 über geologische Aufnahmen im Altkristallin und Unterostalpin im Raum Glungezer auf Blatt 148 Brenner. – Jahrbuch der Geologischen Bundesanstalt Wien, 141: 292.
- Kolenprat, B., Rockenschaub, M. and Frank, W. (1999): The tectonometamorphic evolution of Austroalpine units in the Brenner Area (Tirol, Austria)-structural and tectonic implications. – Tübinger Geowissenschaftliche Arbeiten, Serie A, 52: 116-117.
- Kralik, M., Krumm, H. and Schramm, J. M. (1987): Low Grade and Very Low Grade Metamorphism in the Northern Calcareous Alps and in the Greywacke Zone: Illite Crystallinity Data and Isotopic Ages. In: Flügel, H. W. and Faupl, P. (eds.): Geodynamics of the Eastern Alps. Deuticke, 164 – 178, Vienna.

- Mostler, H. (1973): Alter und Genese ostalpiner Spatmagnesite unter besonderer Berücksichtigung der Magnesitlagerstätten im Westabschnitt der Nördlichen Grauwackenzone (Tirol, Salzburg). - Verhandlungen der Universität Innsbruck, 86: 237-266.
- Neubauer, F., Genser, J. and Handler, R. (2000): The Eastern Alps: Result of a two-stage collision process. - Mitteilungen der Österreichischen Geologischen Gesellschaft, 92: 117-134.
- Ortner, H., Reiter, F. and Acs, P. (2002): Easy handling of tectonic data: the programs TectonicVB for Mac and TectonicsFP for Windows. - Computers in Geosciences, 28: 1193-1200.
- Ortner, H., Brandner, R. and Gruber, A. (1999): Kinematic evolution of the Inn Valley Shear Zone from Oligocene to Miocene. - Tübinger Geowissenschaftliche Arbeiten Serie A, 52: 192-193.
- Ortner, H. and Reiter, F. (1999): Kinematic history of the Triassic South of the Inn Valley (Northern Calcareous Alps, Austria) Evidence for Jurassic and Late Cretaceous large scale faulting. - 3rd Workshop on Alpine Geological Studies, Biella Oropa.
- Ortner, H. and Sachsenhofer, R.F. (1996): Evolution of the Lower Inn Valley Tertiary and constraints on the development of the source area. In: Oil and Gas in Thrust belts and Basins/ Alpidic Regions. Central and Eastern Europe. - In: Liebl, W. and Wessely, G. (eds.), EAPG Special Publication 5.
- Piber, A. (2002): Tectonometamorphic evolution of the Austro-Alpine nappes in the northern Zillertal-Area, Eastern Alps. - Unpublished Master Thesis, University of Innsbruck, 268 pp.
- Piber, A. (2005): The metamorphic evolution of the Austroalpine nappes north of the Tauern Window (Innsbruck Quartzphyllite Complex - Patscherkofel Crystalline Complex - Kellerjochgneiss and Wildschönau Schists). - Unpublished Ph.D. Thesis, University of Innsbruck, 261 pp.
- Piber, A. and Tropper, P. (2005): The polymetamorphic evolution of the Austroalpine Innsbruck Quartzphyllite Complex. - Mitteilungen der Österreichischen Mineralogischen Gesellschaft, 151: 103.
- Reiter, F. (2000): Strukturell-stratigraphische Neubearbeitung der Schwazer Trias westlich des Zillertales. - Unpublished Master Thesis, University of Innsbruck, 176 pp.
- Rockenschaub, M. (1998): Bericht 1997 über geologische Aufnahmen in der Quarzphyllitzone und im Tauernfenster auf Blatt 148 Brenner. - Jahrbuch der Geologischen Bundesanstalt Wien, 141: 295.
- Rockenschaub, M., Kolenprat, B. and Frank, W. (1999): The tectonometamorphic evolution of Austroalpine units in the Brenner area (Tirol, Austria) - new geochronological implications. - Tübinger Geowissenschaftliche Arbeiten Serie A, 52: 118-119.
- Roth, R. (1983): Petrographie und Tektonik der mittelostalpinen Kellerjochgneis-Decke und angrenzender Gebiete zwischen Schwaz und Märzengrund (Tirol). - Unpublished PhD Thesis, University of Münster, 196 pp.
- Roth, R. (1984): Variszische und alpidische Deformationsgeschichte im Grenzbereich zwischen Unter-, Mittel- und Oberosalpinen Decken südöstlich von Schwaz (Tirol). - Mitteilungen der Österreichischen Geologischen Gesellschaft, 77: 73-91.
- Sassi, F. P. and Spiess, R. (1992): Further Data on pre-Alpine metamorphic pressure conditions of the Austridic phyllitic complexes in the Eastern Alps. - In: Carmignani, L. and Sassi, F. P. (eds.), Contributions to Geology of Italy with special regard to the Paleozoic basements. IGCP Mo. 276, Newsletter 5: 297-307.
- Satir, M. and Morteani, G. (1978a): Kaledonische, herzynische und alpidische Ereignisse im Mittelostalpin nördlich der westlichen Hohen Tauern, abgeleitet aus petrographischen und geochronologischen Untersuchungen. - Geologische Rundschau, 68: 1-40.
- Satir, M. and Morteani, G. (1978b): P-T conditions of the high-pressure Hercynian event in the Alps as deduced from petrological, Rb-Sr and 180/160 data on phengites from the Schwazer Augengneise (Eastern Alps, Austria). - Schweizerische Mineralogische und Petrographische Mitteilungen, 58: 289-301.
- Satir, M., Friedrichsen, H. and Morteani, G. (1980): 180/160 and D/H study of the minerals from the Steinkogelschiefer and the Schwazer Augengneis (Salzburg/Tirol, Austria). - Schweizerische Mineralogische und Petrographische Mitteilungen, 60: 99-109.
- Schmid, S. M., Fügenschuh, B., Kissling, E. and Schuster, R. (2004): Tectonic map and overall architecture of the Alpine orogen. - Eclogae Geologicae Helvetiae 97/1: 93-117.
- Schmidegger, O. (1964): Die Ötztaler Schubmasse und ihre Umgebung. - Verhandlungen der Geologischen Bundesanstalt, 1957/1: 76-77.
- Schmidlechner, M., Neubauer, F. and Handler, R. (2006): Extent and age of metamorphism of the central Grauwacken Zone, Eastern Alps: a Ar-Ar study. - Pangeo 2006, Innsbruck University Press, 314-315.

- Steyrer, H. P. and Finger, F. (1996): Der Schwazer Augengneis: ein östlicher Ausläufer des Ötztal Kristallins? - Mitteilungen der Österreichischen Mineralogischen Gesellschaft, 141: 226-227.
- Steyrer, H. P., Genser, J., Handler, R. and Neubauer, F. R. (1996): Zur Struktur und Kinematik des Ostalpins nordwestlich des Tauernfensters: das Profil vom Innsbrucker Quarzphyllit zur Grauwackenzone. In: Amman, R., Kurz, W. and Steyrer, H.P. (Eds.), TSK 6: 407-408.
- Thöny, W., Ortner, H. and Scholger, R. (2004): Geodynamic reconstruction of the Miocene paleogeography from paleomagnetic and geological data. - Berichte des Institutes für Erdwissenschaften der Karl-Franzens Universität Graz, 9: 406.
- Tollmann, A. (1963): Ostalpensynthese. - Franz Deuticke, Vienna, 256 pp.
- Tollmann, A. (1977): Geologie von Österreich, Bd.1, Die Zentralalpen. - Franz Deuticke, Vienna, 766 pp.
- Transalp Working Group (2002): First deep seismic reflection images of the Eastern Alps reveal giant crustal wedges and transcrustal ramps. *Geophysical Research Letters*, Vol. 29, No.10, 10.1029/2002GL014911, 2002.
- Wezel, F. (1981): Geologische-petrologische Kartierung des Kellerjochgebietes (Zillertal, Tirol, Österreich) unter besonderer Berücksichtigung des tektonischen Makro und Mikrogefüges. - Unpublished Master Thesis, TU Berlin, 196 pp.

Manuscript submitted: 1.6.2010

Revised manuscript accepted: 12.11.2010

PERMAFROST WORKSHOP OBERGURGL

14. – 15. Oktober 2010
Universitätszentrum Obergurgl, Tirol

VORWORT

Alpiner Permafrost (Blockgletscher, Permafrost in Lockersedimenten, Spaltenfrost) ist auch in den Ost- und Südalpen weit verbreitet. Die Bedeutung des Permafrostes in den Alpen wurde lange unterschätzt, erst der Klimawandel mit seiner seit etwa 1990 spürbaren Erwärmung hat auch in der Öffentlichkeit das Interesse für den Permafrost in den Alpen geweckt.

Inzwischen gibt es auch in Österreich mehrere Arbeitsgruppen die sich mit dem Thema „Alpiner Permafrost“ befassen. Ziel dieser Veranstaltung ist, alle, alle, die sich in Österreich und Südtirol mit Alpinem Permafrost befassen oder an diesem Thema interessiert sind, zu einem Workshop einzuladen. Dieser Workshop soll dazu dienen, neue Daten und Ergebnisse über Alpinen Permafrost in den Ostalpen und Südalpen zu präsentieren und diskutieren sowie Ideen und Gedanken zum Thema Alpiner Permafrost auszutauschen.

Der Permafrost Workshop verlief sehr erfolgreich, wurde letztlich von mehr als 40 Teilnehmern besucht. An der Diskussion über die Zukunft der Permafrostforschung in Österreich am 14. Oktober haben Vertreter aller Arbeitsgruppen in Österreich und Südtirol teilgenommen und alle Diskussionsteilnehmer begrüßen die Bildung einer „Arbeitsgruppe Permafrost Österreich“ mit dem Ziel, in Zukunft nach Außen als geschlossene Gruppe aufzutreten, die Permafrostforschung in Österreich und Südtirol besser zu koordinieren und für ein langfristiges Permafrost-Monitoring geeignete „key sites“ auszuwählen und entsprechend zu bearbeiten und betreuen.

Karl Krainer

ORGANISATION

Karl Krainer

Institut für Geologie und Paläontologie, Universität Innsbruck, Innrain 52, A-6020 Innsbruck.

Tel.: +43 512 507 5585, email: Karl.Krainer@uibk.ac.at

Helmut Hausmann, Ewald Brückl

Institut für Geodäsie und Geophysik, Technische Universität Wien, Gusshausstraße 27-29, A-1040 Wien.

Tel.: +43 1 58801 12823 oder 12820, email: hausmann@mail.tuwien.ac.at, ebrueckl@mail.tuwien.ac.at

WORKSHOP PROGRAMM

13. Oktober Anreise, gemütliches Treffen am Abend

14. Oktober Vorträge und Posterpräsentationen, Diskussion über die Zukunft der Permafrostforschung in Österreich

15. Oktober Exkursion zum Blockgletscher Äußerer Hochebenkar

16. Oktober Abreise

Kurzfassungen der Beiträge (Vorträge und Poster)

C4AUSTRIA CLIMATE CHANGE CONSEQUENCES FOR THE CRYOSPHERE

Bollmann, E.¹, Briese, C.², Fischer, A.³, Krainer, K.⁴, Pfeifer, N.², Rieg, L.¹, Sailer, R.^{1,5}, Stötter, J.¹

¹ Institut für Geographie, Universität Innsbruck

² Institut für Fernerkundung und Photogrammetrie, TU Wien

³ Institut für Meteorologie und Geophysik, Universität Innsbruck

⁴ Institut für Geologie und Paläontologie, Universität Innsbruck

⁵ alpS, Centre for Climate Change Adaption and Technology, Innsbruck

In Folge des globalen Klimawandels und dessen regionalen Folgen erfahren die Europäischen Alpen seit den 1980er Jahren einen überdurchschnittlich hohen Temperaturanstieg. Für die nahe Zukunft ist für die Alpenregionen ein weiterer Temperaturanstieg prognostiziert, welcher weitreichende Folgen für die Kryosphäre haben wird. Besonders augenscheinlich sind die veränderten Klimabedingungen an den stark schmelzenden Alpengletschern zu erkennen. Aufgrund dessen finden intensive Forschungsbemühungen zu Klima-Gletscher-Beziehungen seit mehreren Jahrzehnten statt. Im Gegensatz dazu, werden den raumzeitlichen Veränderungen des alpinen Permafrosts und damit einhergehende Folgeerscheinungen erst in jüngerer Zeit verstärkte Aufmerksamkeit zugewendet.

Das vom Österreichischen Klima- und Energiefonds geförderte Projekt C4AUSTRIA zielt ab, neue Methoden für ein flächenhaftes Monitoring ausgewählter Komponenten der Kryosphäre, wie beispielsweise Gletscher, Toteis, Permafrostflächen (in Schuttmaterial und Felswänden) sowie Blockgletschern zu entwickeln und zu testen. Ein Schwerpunkt des Projekts liegt auf der Anwendung von Laserscanningverfahren – sowohl flugzeuggestützt (ALS) in full-wave und gepulster Form als auch terrestrisch (TLS) – um Veränderungen der Kryosphäre räumlich zu erfassen und darüber hinaus Veränderungsraten zu quantifizieren. Dazu wurden verschiedene Untersuchungsregionen und Ziele festgelegt: 1) Weiterführung des weltweit einzigartigen ALS-Datensatzes am Hintereisferner (17 Befliegungskampagnen seit 2001) um die Auswirkungen des Klimawandels auf Flächen- und Volumenänderungen des Gletschers und Toteis zu erfassen. Neben den Untersuchungen am Gletscher selbst, wird im Hintereisfernergebiet zudem das Potential von multi-temporalen ALS-Daten für die Erfassung

von flächenhaft ausschmelzenden Permafrostgebieten (Rofenberg) evaluiert. 2) ALS-Befliegungen an Blockgletschern im Äußeren Hochebenkar, Inneren Reichenkar, Innerer Ölgrube und im Schrankar mit dem Ziel sowohl Veränderungen der Blockgletscheroberfläche, welche durch Ausschmelzen des Eisanteils und Deformation bedingt, sind zu erfassen, sowie Fließbewegungen (Richtung und Geschwindigkeit) abzuleiten. 3) Um die Auswirkungen des Klimawandels auf ausschmelzendes Eis in Felswänden und damit einhergehende Steinschläge zu erfassen, werden multitemporale TLS-Messungen im Krummgampental (Kaunertal) durchgeführt.

Die angewandten Fernerkundungsmethoden werden durch verschiedene in-situ Messungen in den Testgebieten unterstützt und evaluiert.

Präsentiert werden erste Ergebnisse des Projekts wie beispielsweise Oberflächenhöhenänderungen und Deformation der Blockgletscher sowie Volumenänderungen des Hintereisferners.

WIE BEEINFLUSST PERMAFROST DEN ABFLUSS? – ANSATZ UND ERSTE DATEN VOM EINZUGSGEBIET KRUMGAMPENTAL, ÖTZTALER ALPEN

Hausmann, H.¹, Krainer, K.², Brückl, E.¹, Chirico, G. B.³, Blöschl, G.⁴, Eipeldauer, S.¹, Illnar, R.¹, Komma, J.⁴

¹ Institut für Geodäsie und Geophysik, Technische Universität Wien, Gusshausstrasse 27-29, A-1040 Wien

² Institut für Geologie und Paläontologie, Universität Innsbruck, Innrain 52, A-6020 Innsbruck

³ Dipartimento di Ingegneria Agraria e Agronomia del Territorio, Università di Napoli Federico II, Napoli

⁴ Institut für Wasserbau und Ingenieurhydrologie, Technische Universität Wien, Karlsplatz 13, A-1040 Wien

Wie beeinflusst Permafrost im Lockergestein das hydrologische Regime? Diese Arbeit zeigt wie im Rahmen des Projekts „Permafrost in Austria“ diese Fragestellung untersucht wird und präsentiert erste Ergebnisse des Einzugsgebietes Krumgampental (Ötztaler Alpen, Tirol). Für die Erfassung der Permafrostverbreitung wurde zunächst eine seismische Methode verwendet. Mit einem empirisch-statistischen Modell (Höhe, Strahlung) wurden diese Daten flächenhaft extrapoliert. Als Nachweis für die Existenz von Permafrost wurden kontinuierliche Aufzeichnungen von BTS-Loggern verwendet. Zur Quantifizierung der Sedimentspeicher wurden geophysikalische Methoden (Georadar, Seismik) in Kombination mit geomorphometrischen Analysen verwendet. Für

die hydrologische Untersuchung stehen Feldbeobachtungen, Wasserproben, Sedimentproben, und Abflußmessungen an vier Pegel zur Verfügung. Zur Trennung des Grundwasseranteils von Oberflächen- und Zwischenabfluss wurde eine Rezessionsanalyse des Basisabflusses angewandt.

Das Krumgampental (2400–3300 m) hat eine Fläche von 5.5 km², einen mittleren Jahresniederschlag von 1500 mm, die mittlere Jahrestemperatur an der in der Nähe liegenden meteorologischen Station (2500 m) beträgt -0.7°C. Die vorherrschenden Untergründe bestehen aus Moränenablagerungen (27% LIA, 18% prä-LIA), Schutthalde (17%), Blockgletscher (5%), und Fels (33%). Permafrost mit aktiven Schichtdicken von ~5 m wurden in Höhenlagen von 2500 (nordseitig) bis 2850 m detektiert. Die Mittelwerte für die Sedimentspeicher betragen 8 m (Schutthalde), 6 m (prä-LIA Moränenablagerung), 5 m (LIA Moränenablagerung), und 20 m (Blockgletscher). Die aufgezeichneten Abflussdaten sind durch die Prozesse der Schneeschmelze, Grundwasserabfluss sowie Oberflächen- und Zwischenabfluss mit Spitzenwerten von 2000 l/s charakterisiert. Die Abflussdaten vom Jahr 2009 zeigen eine Anreicherung von Grundwasser von Ende April bis Anfang August. Die Rezessionsanalyse ergab eine Reaktionszeit von über 30 Tagen für das Grundwassersystem. Der Vergleich zwischen Grundwasserspeicher aus der Rezessionsanalyse und dem Sedimentspeicher aus den geophysikalischen Untersuchungen zeigen ähnliche Werte.

PERMAFROST IM FELS – ERSTE ERGEBNISSE DER SEISMISCHEN TOMOGRAPHIE AM SONNBLICKGIPFEL (3106 m, HOHE TAUERN)

Hausmann, H.¹, Staudinger, M.², Brückl, E.¹, Riedl, C.²

¹ Institut für Geodäsie und Geophysik, Technische Universität Wien, Gusshausstrasse 27-29/128-2, 1040 Wien.

² Zentralanstalt für Meteorologie und Geodynamik, ZAMG Kundenservice Salzburg und Oberösterreich, Freisaalweg 16, 5020 Salzburg.

Die vorliegende Studie wurde im Rahmen des ÖAW-Projektes ‚Permafrost in Austria‘ durchgeführt, um durch Messung von Felstemperatur, meteorologischen und geophysikalischen Parametern rund um den Sonnblickgipfelaufbau (3106 m, Hohe Tauern, Salzburg) den Einfluss des Klimawandels auf den Permafrost zu dokumentieren. Der verwendete Datensatz umfasst vier seismische Tomographien während

der Sommer 2008 und 2009 sowie Felstemperaturen dreier 20 m tiefer Bohrlöcher. Die Anordnung der seismischen Tomographie besteht aus einem 120 m langen Profil. Die seismischen Signale wurden an der Oberfläche angeregt und an Bohrlochgeophonen registriert. Die Darstellung des seismischen Wellenfelds zeigt die zeitliche Variation von P- und vertikal polarisierten S-Wellen. Im Vergleich zu der Messung bei noch teilweise gefrorener aktiven Schicht (Anfang des Sommers) zeigt das ankommende Wellenfeld nach vollständigem Auftauen (Ende des Sommers) eine deutliche Verzögerung mit geringerer lateraler Streuung. Die Laufzeitdifferenzen der P-Wellen zeigen ebenfalls diese Verzögerung und können den Auftau-Prozessen in der aktiven Schicht (< 1 m) zugeordnet werden. Die beobachteten Felstemperaturen zeigen während eines Sommers Temperaturschwankungen bis in ca. 8 m Tiefe. Die aus der Inversion von Laufzeiten resultierende Geschwindigkeitsverteilung des Untergrundes am Sonnblickgipfel indiziert geklüfteten Fels bis in diese Tiefe. Eine 1D-Modellierung der Wärmeleitung ergibt in dieser Tiefe eine Änderung der thermischen Eigenschaften des Permafrosts. Ab einer Tiefe von 8 m zeigen die Laufzeitdifferenzen keine starken Änderungen des sich in Permafrost befindlichen Fels/Kluftsystems. Die Ergebnisse der Temperaturdaten sowie jene der seismischen Tomographie deuten auf die Existenz tief reichender Prozesse im Untergrund hin, welche die zukünftige Stabilität des Gipfelaufbaus beeinflussen könnten.

INTERNE STRUKTUR UND DYNAMIK ZWEIER BLOCKGLETSCHER: ÖLGRUBE UND KAISERBERGTAL (ÖTZTALER ALPEN)

Hausmann, H.¹, Ullrich, C.², Krainer, K.³, Brückl, E.¹

¹ Institut für Geodäsie und Geophysik, Technische Universität Wien, Gusshausstrasse 27-29, A-1040 Wien.

² Bundesamt für Eich- und Vermessungswesen, Gruppe Vermessungswesen, Schiffamtsgasse 1-3, 1020 Wien.

³ Institut für Geologie und Paläontologie, Universität Innsbruck, Inrain 52, A-6020 Innsbruck.

Die Dynamik aktiver Blockgletscher hängt maßgebend von deren interner Struktur und Eisgehalt ab. Beobachtete Verschiebungsraten stehen daher im Zusammenhang mit der Struktur der Blockgletscher. In dieser Studie werden die Ergebnisse der mit geophysikalischen Methoden erfassten Struktur der Blockgletscher Ölgrube und Kaiserbergtal präsentiert.

Basierend auf dieser Struktur wird ein Kriechmodell angewendet um die dynamischen Prozesse und das geophysikalische Modell selbst zu diskutieren.

Die Ölgrube ist ein zusammengesetzter, zungenförmiger, Blockgletscher mit zwei Stirnflächen, ist 880 m lang, 250 m breit und reicht von 2800 bis 2380 m. Charakteristisch sind die zur Stirn zunehmenden Verschiebungsraten (von 0.4 bis 2 m/a) und der steile Frontwall von 40–45°. Die Auswertung der Georadar und Seismik Daten ergaben die folgende Struktur; 5 m Blockschutt, 25–30 m Permafrost, und 13 m ungefrorene Sedimente. Ein Eisgehalt von 45–60 % wurde aus Schweremessungen in Kombination mit der Struktur ermittelt. Das Kriechmodell wurde für zwei Bereiche berechnet und ergab je nach angenommenen Luftgehalt (0 oder 10 %) Werte von 1 bzw. 2.2 m/a (Wurzelbereich) sowie 1.6 bzw. 5.9 (Stirnbereich) m/a. Das auf den geophysikalischen Daten basierende Kriechmodell ermöglicht die Beschreibung der folgenden dynamischer Prozesse; (i) die zur Stirn ihn zunehmenden Verschiebungsraten können durch zunehmende Dichten erklärt werden, (ii) eine Zone mit steiler Geländeneigung entspricht steilem Untergrund und ergibt eine Ausdünnung des Permafrosts sowie einen lokalen Anstieg der Dichte, (iii) Die Richtungsänderung der Verschiebungen kann mit der ermittelten Neigung des Untergrunds erklärt werden.

Der Kaiserberg Blockgletscher zeigt ein spatenförmiges Erscheinungsbild mit den Ausmaßen von 550 m Breite und 350 m Länge und reicht von 2710 m bis 2585 m. Die Verschiebungsraten betragen im Teil der geophysikalischen Messungen 1 – 2 m/a und nehmen entlang der Fließrichtung (von W nach O) zum Rand hin zu (3 – 4 m/a). Die interne Struktur ergab einen 5.5 m dicken Blockmantel, 23 m Permafrost und 8 m ungefrorene Sedimente. Der Eisgehalt wurde mit Werten von 25–40 % ermittelt. Das Kriechmodell ergab je nach angenommenen Luftgehalt (0 oder 10 %) Werte von 0.3 bzw. 0.8 m/a. Die festgestellte Struktur des Blockgletschers gibt einen Hinweis auf die Entstehung der spatenförmigen Erscheinungsform. Die im Kriechmodell verwendete Struktur produziert Verschiebungsraten ähnlich jenen aus der direkten Beobachtung und gibt einen Hinweis auf die Plausibilität der geophysikalischen Interpretation.

PHOTOGRAMMETRISCHE BEWEGUNGSMESSUNGEN AN DEN HOCHEBENKAR-BLOCKGLETSCHERN

Kaufmann, V.

Institut für Fernerkundung und Photogrammetrie; Technische Universität Graz; Steyergasse 30; A-8010 Graz, Austria

Oberflächliche Bewegungsmessungen an Blockgletschern können mit unterschiedlichen Methoden durchgeführt werden. Eine besonders leistungsfähige ist jene der Photogrammetrie, welche auf eine bereits viele Jahrzehnte lange Tradition in der Hochgebirgsforschung zurückblicken kann. Die bildgestützte Bewegungsmessung fand ihre erste Umsetzung in der terrestrischen Photogrammetrie. Nach einer anfänglichen Blütezeit wurde diese Vermessungsmethode jedoch durch die Luftbildauswertung abgelöst. Billige digitale Spiegelreflexkameras und auch automatische Auswerteprogramme lassen wiederum eine Wiedergeburt der terrestrischen Photogrammetrie im Gletscher-Monitoring erahnen.

In diesem Beitrag werden am Beispiel der beiden Blockgletscher im Äußeren und Inneren Hochebenkar, Ötztal, moderne digital-photogrammetrische Auswertemethoden zur Quantifizierung der Morphodynamik von Blockgletschern vorgestellt. Im Zuge von Studienarbeiten wurden sowohl Luftbild- als auch terrestrische Zeitreihenaufnahmen ausgewertet. Die zugrunde liegenden photogrammetrischen Prozessierungsketten werden für beide photogrammetrischen Aufnahmedispositionen im Detail diskutiert.

Das raum-zeitliche Bewegungsverhalten der beiden genannten Blockgletscher wird sowohl in numerischer als auch in graphischer Form dargestellt. Zur eindrücklichen Visualisierung der relativ langsamen und daher direkt visuell nicht wahrnehmbaren Blockgletscherbewegung wurden Zeitraffersequenzen in Form von Computeranimationen erstellt.

Neue, erstmals vorzustellende Auswerteergebnisse beziehen sich auf die vergleichende Analyse von hochauflösenden Orthophotos der Geo-Browser Google Maps und Microsoft Bing Maps mit älteren Datensätzen.

BLOCKGLETSCHERBEWEGUNG UND KLIMAWANDEL IN ZENTRALÖSTERREICH IN DEN LETZTEN 15 JAHREN

Kellerer-Pirkbauer, A.^{1, 2}, Viktor Kaufmann, V.², Lieb, G.K.¹ und Avian, M.²

¹ Institut für Geographie und Raumforschung, Universität Graz

² Institut für Fernerkundung und Photogrammetrie, Technische Universität Graz

Aktive Blockgletscher sind Kriechphänomene des kontinuierlichen und diskontinuierlichen Permafrosts und werden in ihrer Bewegung unter anderem von klimatischen Bedingungen und in der Folge von Bodentemperaturverhältnissen beeinflusst. Eine Zunahme der Bodentemperatur in aktiven Blockgletschern führt zur Erwärmung und folgend zum partiellen Abtauen des Permafrosts. Dies bewirkt eine höhere Verfügbarkeit von flüssigem Wasser was wiederum eine Bewegungszunahme des Blockgletscherkörpers bewirken kann. Bei weiterer Erwärmung und Abtauen des Permafrostes kommt es jedoch zur reibungsbedingten Geschwindigkeitsabnahme sowie letztendlich nach kompletter Permafrostdegradation zu einer völligen Inaktivität des nunmehr eisfreien Blockgletscherkörpers. Neben diesen klimatischen Faktoren sind es jedoch auch andere Faktoren wie beispielsweise Hangneigung, Topographie des Blockgletscheruntergrundes, seitliche Reibung, Wassergehalt sowie Dicke, Dichte, Schuttanteil, Schuttverteilung und interne Struktur des Blockgletscherkörpers, welche die Blockgletscherbewegung beeinflussen können. In diesem Vortrag wird von den diesbezüglichen Forschungsarbeiten im Bereich der Blockgletscher Dösen (Ankogel Gruppe), Weißenkar sowie Hinteres Langtalkar (beide Schobergruppe) berichtet. Für die gegenständliche Fragestellung liefern jährlich durchgeführte geodätische Bewegungsmessungen, Klimastationen in den Untersuchungsgebieten sowie Bodentemperatursensoren an und nahe der Oberfläche der untersuchten Blockgletscher die Datenbasis. Am Dösener Blockgletscher werden seit 1995 jährlich geodätische Messungen durchgeführt sowie seit 2006 ein intensives Bodentemperatur- und Klimamonitoring betrieben. Am Weißenkar Blockgletscher wurde im Jahr 1997 ein ähnliches geodätische Messprogramm sowie ein Bodentemperaturmonitoring initiiert. Am Hinteren Langtalkar Blockgletscher erfolgte die Einrichtung eines geodätischen Messnetzes im Jahr 1998. Ähnlich der Situation am Dösener Blockgletscher wurde auch hier im Jahr 2006 ein intensives Bodentemperatur- und Klimamonitoring

eingerichtet und seither erfolgreich betrieben. Ergebnisse der einzelnen Messprogramme sowie die Erkenntnisse der Korrelationsanalysen werden im Vortrag vorgestellt und diskutiert.

MODELLIERUNG GRAVITATIVER MASSENBEWEGUNGEN ZUR ABSCHÄTZUNG DES GEFAHRENPOENTIALS FÜR ALPINTOURISTINNEN UND -TOURISTEN SOWIE INFRASTURKTUR IM GEBIET GROSSGLOCKNER-PASTERZE

Kern, K.¹, Lieb, G.K.¹, Seier, G.¹ und Riedl, C.²

¹ Institut für Geographie und Raumforschung, Universität Graz

² Zentralanstalt für Meteorologie und Geodynamik (ZAMG)

Felssturz, Steinschlag und andere gravitative Massenbewegungen kommen in Hochgebirgen besonders häufig vor und sind daher von großem Interesse für die Gefahrenbeurteilung. Kommt es zu einer räumlichen Überlagerung des Prozessraumes von Massenbewegungen mit Personen oder Infrastruktur, können diese Prozesse schnell zu Naturgefahren werden. Das Untersuchungsgebiet Großglockner-Pasterze ist eine der beliebtesten Bergtourismusdestinationen Österreichs und verfügt somit über sehr hohes Risikopotential. Ziel dieser Studie ist die Erstellung einer Gefahrenhinweiskarte für Sturz- und flächige Abtragungsprozesse zur Abschätzung des derzeitigen und zukünftigen Gefahrenpotentials für Alpintouristinnen und -touristen sowie Infrastruktur.

In einem ersten Schritt werden mit Hilfe eines Dispositionsmodells potentielle Ursprungsgebiete für Massenbewegungen erfasst und mobilisierbare Fels- und Schuttmassen abgeschätzt. Gemeinsam mit einem Digitalen Höhenmodell (DHM) fließen die Informationen aus dem Dispositionsmodell dann in ein Prozessmodell zur Ermittlung der Reichweite und Ausbreitung des sich hangabwärts bewegenden Materials ein. Neben der Modellierung des derzeitigen Gefahrenpotentials erfolgt auch die Auseinandersetzung mit einem möglichen zukünftigen Szenario für 2030. Die Erstellung des Dispositionsmodells und die Abschätzung der mobilisierbaren Massen erfolgen unter besonderer Berücksichtigung von Gletscherschwund und Permafrost-Degradation, wobei sowohl das Ansteigen der Permafrost-Untergrenze als auch die Vergrößerung der sommerlichen Auftautiefe Berücksichtigung finden.

Das Ergebnis der Arbeit umfasst zwei Gefahrenhinweiskarten (gegenwärtige und zukünftig mögliche Gefährdungssituation) in einem mittleren Maßstab, die eine Klassifizierung der Gefährdungswahrscheinlichkeit bzw. -intensität beinhalten. Die Überlagerung dieser Information mit den markierten Wegen und Routen macht jene Abschnitte dieser Infrastrukturen erkennbar, an denen Maßnahmen zur Erhöhung der Sicherheit von Alpintouristinnen und -touristen sinnvoll sein können. Eine Validierung der Ergebnisse erfolgt durch Lokalisierung von Unfallstellen und Wegabschnitten, an denen bereits zusätzliche Sicherungsmaßnahmen oder Neutrassierungen vorgenommen werden mussten.

ENTWICKLUNG EINES EXPERTENSYSTEMS ZUR ÜBERWACHUNG GEFÄHRLICHER FELSWÄNDE – KONZEPT UND ERSTE ERGEBNISSE (KITZSTEINHORN, HOHE TAUERN)

Keuschnig, M., Hartmeyer, I., Otto, J-C. & Schrott, L.

Department of Geography and Geology, University of Salzburg,
Hellbrunnerstraße 34A, A-6020 Salzburg

Die Stabilität von Felswänden im Hochgebirge ist im Kontext der Klimaveränderungen ein wichtiger Risikofaktor für die lokale Bevölkerung, den Tourismus und für die Infrastruktur. Zahlreiche Felsstürze und Steinschläge in den Hitzesommern 2003 und 2005 im Alpenraum weisen auf eine mögliche Zunahme von gravitativen Massenbewegungen als Reaktion auf veränderte Klimabedingungen hin. Um auf solche Gefahren und Risiken vorbereitet zu sein, ist innerhalb des nächsten Jahrzehnts die Entwicklung von Klima-Anpassungsstrategien notwendig. Dafür ist das Verständnis der kurz- und mittelfristigen Reaktionen von Felswänden auf klimatische Veränderungen wie Temperatur und Niederschlag von entscheidender Bedeutung.

Das Projekt MOREXPERT erfasst und analysiert relevante Faktoren (Felstemperaturen, Permafrostverbreitung, Gesteinseigenschaften, Klüftigkeit, Felsbewegungen, Kluftwasser, Lufttemperatur, Strahlung, Niederschlag, u.a.) und identifiziert kritische Schwellenwerte und deren Sensitivität gegenüber Veränderungen. Das Hauptziel ist die Entwicklung eines innovativen Expertensystems, basierend auf einer kombinierten Überwachung (Monitoring) der Oberflächen- und Untergrundbedingungen. Verwendet wer-

den state-of-the-art Technologien wie terrestrisches Laserscanning und geophysikalische, geothermische, geotechnische und klimatologische Methoden. Eine große Herausforderung ist die Integration und das Management der im Untersuchungsgebiet erhobenen Datensätze und deren Transformation in praktische, zielgruppengerichtete Information (Decision Support System). Durchgeführt wird das Projekt am Kitzsteinhorn (3204 m, Gemeinde Kaprun, Bundesland Salzburg – Österreich). Das Untersuchungsgebiet bietet alle Voraussetzungen für die Entwicklung und der Anwendung kosteneffektiver Adoptionsstrategien in Hochgebirgsräumen. Hauptziel des Projekts ist die Entwicklung einer kombinierten Methodenstrategie für die Überwachung der Oberfläche und des oberflächennahen Untergrundes von Felswänden. Dies umfasst die folgenden Schritte und Teilziele:

- Erfassung von hochauflösten Daten der externen und internen Einflussfaktoren;
- Quantifizierung der Oberflächendynamik auf verschiedenen Skalenniveaus;
- Erweiterung bzw. Spezifizierung des systemtheoretischen Verständnis von Felswänden und deren Sensitivität (Schwellenwerte) in Bezug auf Klimaveränderungen im Hochgebirge;
- Entwicklung eines Überwachungssystems (Expertensystem) für Felswände mit automatisierten und semiautomatisierten Datenanalysen;
- Entwicklung eines Systems zur Entscheidungsfindung (Decision Support System) für unterschiedliche Zielgruppen.

Präsentiert werden die Projektstruktur, das Untersuchungsgebiet und erste Ergebnisse aus den geologischen, geomorphologischen und geophysikalischen Voruntersuchungen.

DER EINFLUSS SCHMELZENDEN PERMAFROSTES AUF DIE WASSERQUALITÄT UND DIE AQUATISCHEN ORGANISMEN ALPINER SEEN – UNTERSUCHUNGEN AN SEDIMENTEN

Koinig, K.A.¹, Ilyashuk, E.¹, Tessadri, R.², Lackner, R.¹, Köck, G.³, Psenner, R.¹

¹ Institut für Ökologie, Universität Innsbruck, Technikerstraße, A-6020 Innsbruck

² Institut für Mineralogie und Petrographie, Universität Innsbruck, Innrain 52, A-6020 Innsbruck

³ Österreichische Akademie der Wissenschaften und Institut für Zoologie, Universität Innsbruck, Technikerstraße, A-6020 Innsbruck

Das Schmelzen der Permafrostböden in den hochalpinen Regionen wird nachhaltig von der rezenten Erwärmung beeinflusst. Das Schmelzwasser, das aus dem Permafrost und den Blockgletschern abrinnt, hat auf aquatische Ökosysteme unerwartete Auswirkungen: diese reichen von einer Erhöhung der Leitfähigkeit bis hin zu einem Anstieg der Metallkonzentrationen auf ein Niveau, das nicht nur toxisch ist, sondern auch einer vielfachen Überschreitung der Grenzwerte für Trinkwasser entspricht. Dabei ist der Prozess, der die Zusammensetzung und v.a. die Metallkonzentration im Schmelzwasser steuert, noch nicht bekannt. Gut belegt ist, dass hohe Metallkonzentrationen aquatische Lebewesen beeinflussen: so kommt es u.a. zu Deformationen und zur Änderung der Artenzusammensetzung. Diesen Sommer wurden aquatische Organismen auf verschiedenen Trophieebenen - von Algen (Diatomeen), über Würmer (Oligochaeten) und Insekten (Chironomiden), bis hin zu Fischen (Saibling) - in zwei Hochgebirgsseen mit Permafrost im Einzugsgebiet untersucht. Um die zeitliche Entwicklung des Metallanstiegs, die daraus resultierenden Änderungen in der Artenzusammensetzung oder toxische Auswirkungen zu erfassen, haben wir kurze Sedimentkerne entnommen. Die Ergebnisse der Untersuchung an den Sedimenten werden mit den Temperaturmessdaten der letzten 220 Jahre, den gemessenen Änderungen atmo-sphärischer Depositionen und mit Daten aus Eiskernen und Moorprofilen verglichen werden. Hier präsentieren wir die ersten Ergebnisse der Sedimentuntersuchung.

BLOCKGLETSCHER UND NATURGEFAHREN: DER AKTIVE BLOCKGLETSCHER „MURFREIT“ IN DER NÖRDLICHEN SELLAGRUPPE, DOLOMITEN

Krainer, K. und Mussner, L.

Institut für Geologie und Paläontologie, Universität Innsbruck, Innrain 52, 6020 Innsbruck

Der Blockgletscher „Murfreit“ befindet sich in der nördlichen Sellagruppe auf der „Mittelterrasse“, südlich des Grödner Joches bzw. westlich der Pisciadú-Hütte auf einer Seehöhe von 2670 m. Der Blockgletscher ist 420 m lang und 1100 m breit und bedeckt eine Fläche von 33.6 ha. Die Stirn endet auf einer Seehöhe von 2590 m, die Wurzelzone liegt auf 2770 m. Er zeigt eine lobate Form und für aktive Blockgletscher typische morphologische Erscheinungsformen wie steile und meist unbewachsene Stirn, steile Flanken und im westlichen Teil ausgeprägte transversale Rücken und Vertiefungen sowie eine Depression im Wurzelbereich. Außerdem sind im Sommer an der Oberfläche ein, zeitweise auch zwei Thermokarstseen entwickelt, an deren Rändern unter einer dünnen Schuttdecke massives Eis aufgeschlossen ist. Das Eis ist ziemlich rein, grobkristallin und deutlich gebändert. Der Blockgletscher wird aus den steilen Felswänden oberhalb der Wurzelzone mit Hauptdolomitschutt beliefert. In der oberflächlichen Schuttlage überwiegen Gerölle mit Korndurchmessern von 1 – 10 und 11 – 20 cm, Gerölle mit Durchmessern von > 60 cm sind selten.

Die Wassertemperaturen der Blockgletscherquellen (< 1°C), BTS-Messungen und Bewegungsmessungen bestätigen, dass der Blockgletscher Eis enthält.

Im Gegensatz zu den beiden Blockgletschern im Bereich der Hohen Gaisl fließt beim Blockgletscher Murfreit ein Großteil der Schmelzwässer oberflächlich ab, der Abfluss zeigt starke saisonale und tägliche Schwankungen.

Georadar-Messungen zeigen, dass der Blockgletscher bis zu ungefähr 30 m mächtig ist, wobei im oberen Abschnitt ähnliche Strukturen wie am Blockgletscher im Gletscherkar (Hohe Gaisl) auftreten, die auf einen massiven Eiskern mit Scherbahnen im Eis hinweisen.

Bewegungsmessungen zeigen, dass derzeit der westliche Abschnitt des Blockgletschers noch aktiv ist mit jährlichen Bewegungsraten von meist 5 – 10 cm, stellenweise bis zu 40 cm. Die Stirn des Blockgletschers ist meist um die 20 m, im westlichen, aktiven Teil bis zu 40 m mächtig. Die steile Stirn reicht lokal bis an die Abbruchkante der Terrasse. Dadurch konnten im Jahr 2003 Starkniederschläge auch Teile der steilen Stirn mobilisieren und damit Murgänge auslösen, die die Straße von Wolkenstein zum Grödner Joch vermut haben. Vor allem die immer noch aktive und entsprechend steile westliche Stirn des Blockgletschers stellt nach wie vor ein Gefahrenpotential dar, Starkniederschläge können hier jederzeit weitere Murgänge auslösen.

BLOCKGLETSCHERINVENTAR ÖTZTALER – STUBAIER ALPEN

Krainer, K.¹ und Ribis, M.²

¹ Institut für Geologie und Paläontologie, Universität Innsbruck, Innrain 52, 6020 Innsbruck

² Michael Pfurtscheller Weg 4, 6166 Fulpmes

Im Rahmen des Projektes PermaNET wurde zunächst ein Datenerhebungsblatt für ein Blockgletscherinventar Tirol erstellt. Dieses Datenblatt enthält unter anderem folgende Daten: Nummer (nach Einzugsgebiet), geographische Bezeichnung, Koordinaten, Höhe der Stirn, Wurzelzone und mittlere Höhe, maximale Länge und Breite, Fläche, Exposition, Oberflächenmorphologie, Form, Entstehung, Zustand (aktiv, inaktiv, fossil), Gewässer-Einzugsgebiet, Gebirgsgruppe, Festgesteine im Einzugsgebiet, Quellaustritte im Stirnbereich, Angaben über vorhandene Wasseranalysen, Pegeldaten, Literatur. Diese Daten sind aus den Luftbildern oder Laserscannaufnahmen oft nur beschränkt oder gar nicht zu erfassen. Auch die Unterscheidung in aktiv, inaktiv und fossil ist aus den Luftbildern nur schwer zu treffen, da es zwischen diesen Typen fließende Übergänge gibt und der gegenwärtige Zustand eines Blockgletschers meist erst durch Bewegungsmessungen und andere Untersuchungen erfasst werden kann.

In den Ötztaler und Stubaier Alpen konnten auf österreichischem Gebiet insgesamt 1200 Blockgletscher festgestellt werden. Davon wurden ungefähr 350 als aktiv, 350 als inaktiv und 500 als fossil eingestuft.

Allein im Einzugsgebiet der Ötztaler Ache konnten 421 Blockgletscher lokalisiert werden, die eine Fläche von ca. 30.5 km² bedecken. Davon wurden 135 als aktiv (14.1 km²), 142 als inaktiv (8.1 km²) und 174 als fossil (8.3 km²) klassifiziert.

Im Einzugsgebiet der Pitze (Pitztal) wurden 133 Blockgletscher aufgenommen mit einer Gesamtfläche von ca. 7.7 km². Davon sind 43 aktiv (3.3 km²), 46 inaktiv (1.9 km²) und 44 fossil (2 km²). Im Kaunertal (Einzugsgebiet der Fagge) wurden 123 Blockgletscher identifiziert mit einer Fläche von 7.3 km². Davon sind ungefähr 39 aktiv (3.4 km²), 42 inaktiv (2 km²) und 42 fossil (1.9 km²). Eine große Anzahl von 205 Blockgletschern befindet sich in den Nauderer Bergen, diese bedecken immerhin eine Fläche von ca. 12.9 km². Ein beträchtlicher Teil (95) wurde als aktiv eingestuft (7.2 km²), 35 als inaktiv (1.4 km²) und 75 als fossil (4.3 km²). Die größten aktiven Blockgletscher sind bis zu ca. 1650 m lang (z.B. Reichenkar) und bedecken eine Fläche von knapp 0.6 km².

Die meisten aktiven Blockgletscher sind nach Norden (NNW –NNE) exponiert. Nach Süden exponierte Blockgletscher sind relativ selten und liegen um ca. 400 m höher als nach Norden exponierte Blockgletscher. Die meisten aktiven Blockgletscher (mittlere Höhe) in den Ötztaler Alpen liegen zwischen 2600 und 2850 m Seehöhe.

PERMAFROSTMONITORING SONNBLICK – ERSTE ERGEBNISSE UND ERKENNTNISSE

Kroisleitner, C., Schöner, W., Reisenhofer, S. und Weyss, G.

Abteilung Klimaforschung/Department Climate Research, Bereich Daten, Methoden, Modelle/Division Data, Methods, Modeling, Zentralanstalt für Meteorologie und Geodynamik, Hohe Warte 38, 1190 Wien

Seit dem Jahr 2006 finden am Sonnblick im Zuge des Projektes PERSON (PERmafrostmonitoring SONnblick) Messungen der Bodenoberflächentemperatur (BOT) statt, welche durch Messungen der Basistemperatur der Schneedecke (BTS) ergänzt werden.

Es konnten aufgrund der BOT-Messungen erste Ergebnisse, wie zum Beispiel die Untergrenze der Permafrostverbreitung in zwei unterschiedlich exponierten Untersuchungsgebieten, festgestellt werden. Im süd- bis südostexponierten Gebiet Goldbergspitze ergab die Regression aus BOT und Seehöhe eine Untergrenze von ca. 2700m ü. NN. In der nord- bis

nordwestexponierten Wintergasse lag diese Grenze bei etwa 2500m ü. NN. Generell zeigt sich in den jeweils etwa 1km² großen Untersuchungsgebieten allerdings eine sehr heterogene Verteilung der Oberflächentemperatur die sehr stark durch kleinräumige, topographische Unterschiede bestimmt wird.

Da BOT-Sensoren nach dem Abschmelzen der winterlichen Schneedecke stark dem atmosphärischen Einfluss unterworfen sind, wurden Anfang September 2010 im Untersuchungsgebiet Wintergasse 5 Bohrlöcher mit unterschiedlichen Tiefen zwischen 30cm und 130cm gebohrt. Die Bohrlöcher wurden in mehreren Tiefen und an der Bodenoberfläche mit Temperatursensoren ausgestattet. Dies ermöglicht die Messung des Wärmegradienten zwischen Fels und Oberfläche und der bodennahen Temperatur ohne atmosphärischen Einfluss. Durch diese Messungen an der Schnittstelle Erde/Atmosphäre, sollen in Zukunft grundlegende Informationen über die Verbreitung und das Verhalten von Permafrost gewonnen werden.

PERMAFROST IM FELS – ERSTE DATEN DER HORIZONTALBOHRUNG AN DER GRAWAND IM SCHNALSTAL (ALPENHAUPTKAMM, SÜDTIROL, 3.200 m)

Lang, K.¹, Mair, V.¹, Tonidandel, D.¹, Leiter, J.²

¹ Amt für Geologie und Baustoffprüfung, Autonome Provinz Bozen – Südtirol, Eggentaler Str. 48, I-39053 Kardaun

² Institut für Geographie, Universität Innsbruck, Innrain 52, A-6020 Innsbruck.

Der Grat der Grawand (3.251 m) im hintersten Schnalstal (Südtirol) verläuft ziemlich genau in Ost-West-Richtung und ist Teil des Alpenhauptkammes. Anstoß zur Durchführung der Bohrungen und Messungen waren die teilweise schlechten Stabilitätsverhältnisse am Bergkamm. Der Felskamm der Grawand war bis vor einigen Jahrzehnten noch vom Eis des Hochjochfengers bedeckt. Wegen des Abschmelzens des Eises liegen heute die nackten Felsflanken frei. Der zum Teil stark zerlegte Hangabschnitt stellte eine zunehmende Gefährdung des darunter liegenden Skiwegs durch Stein- und Blockschlagereignisse bis hin zu möglichen Felsstürzen dar. Die Schnalstaler Gletscherbahn AG wollte zudem Informationen über die allgemeine Standfestigkeit des Felskammes gewinnen, um bereits bestehende Infrastrukturen eventuell zu schützen und zukünftige Investitionen besser zu planen. Bei dem an der Grawand aufgeschlossenen

Gestein handelt es sich um Metasedimente des ostalpinen Ötztalkristallin. Die Metasedimente an der Grawand bestehen aus einer Wechsellagerung von Paragneisen und Glimmerschiefern, die einen unterschiedlichen Mineralbestand und somit verschiedene Farbgebung aufweisen. Aus diesem Grund sind die Lagerungsverhältnisse der Gesteine besonders deutlich zu erkennen und zu verfolgen. Die Gesteine sind stark isokinal verfaltet, wobei die Schieferung im Bereich der Schenkel mehr oder weniger konstant gegen NNE einfällt. Weitere bedeutende Strukturelemente, die den E-W streichenden Bergkamm kennzeichnen, sind 3 Kluftsysteme (K1, K2 und K3). Der Verschnitt dieser Kluftsysteme mit der Schieferungsfläche bewirkt das Entstehen von Pultflächen, welche ideale Abgleitflächen für Blöcke und ganze Felspartien bilden. Der Bergkamm zeigt einen starken Zerlegungsgrad, der mit der oberen Aufschicht des Permafrosts, der aktiven Schicht, in Verbindung steht.

Die in den Bohrlöchern installierten hochempfindlichen Messgeräte für Bewegung (Stangenextensometer) und Temperatur (Thermistorenketten) dienen somit zum Einen als Beobachtung der möglichen Hangbewegungen und zum Anderen als Forschungsstation zur Untersuchung der klimatisch bedingten Veränderungen des Permafrosts.

Das erste Bohrloch (B1) verläuft ziemlich genau senkrecht zur Schieferung der Gesteine und hat eine Länge von 162 m. In diesem Bohrloch wurden fünf Stangenextensometer installiert, welche die inneren Bewegungen (thermische Dilatation) des Festgestein messen und registrieren.

Das zweite Bohrloch (B2) verläuft ziemlich genau in Nord-Süd-Richtung, hat eine Länge von 133 m und erreicht sowohl an der Nord- als auch an der Südseite die Oberfläche. Es wurde mit Thermistorenketten ausgestattet, welche automatisch ein Temperaturprofil im gesamten Bohrloch aufzeichnen.

Weiters wurden beide Bohrlöcher mit optischen Bohrlochaufnahmen befahren, die einen Aufschluss der inneren Struktur des Festgestein geben. Bereits bei den Bohrarbeiten wurden in verschiedenen Tiefen immer wieder große, offene Klüfte angefahren, was den Bohrfortschritt wesentlich verlangsamt. Diese Klüfte waren nicht mit Eis verfüllt.

Die Temperatur- und Bewegungsdaten beider Bohrlöcher können seit Dezember 2009 über eine GSM Leitung (vom Datenlogger zur Bergstation der Seilbahn) und Internetverbindung vom PC aus eingesehen werden. Eine erste Analyse der Temperaturdaten hat ergeben, dass an der Nordseite der Gra-

wand bis in einer Bohrlochlänge von 5 m extreme Temperaturschwankungen herrschen. Weiters wurde festgestellt, dass im Bohrloch von Anfang Dezember 2009 bis Anfang Juni 2010 durchgehend Minusgrade herrschen. Im Sommer herrschen im Bohrloch an der Nordseite der Grawand zwar während des Tages bis in eine Länge von 4 m Plusgrade, an wenigen Tagen im Sommer wurden bis in eine Länge von maximal 2 m permanent Plusgrade gemessen. Ab einer Länge von 4 m herrschen im Bohrloch durchgehend Minusgrade.

An der Südseite der Grawand sind die Tage häufiger, an denen die Temperatur im Bohrloch Plusgrade erreicht. Der dauerhaft gefrorene Bereich liegt wesentlich tiefer, und zwar über 25 m Bohrlochlänge.

HUBSCHRAUBER-GESTÜTZTE VERMESSUNG VON STEILEN UND UNZUGÄNGLICHEN GEBIETEN

Legat, K., Trimmel, W., Mendes-Cerveira, P. J.

Vermessung AVT ZT GmbH, Eichenweg 42, A-6460 Imst

Eine wesentliche Grundlage für die Dokumentation und das Verständnis von klimatisch bedingten Umweltveränderungen sind hochauflösende räumliche Daten. Für die flächenhafte Aufnahme mit hoher Qualität bietet sich die luftgestützte Vermessung mit Photogrammetrie und Laserscanning an. Die Vermessung AVT hat gemeinsam mit ihrem Partner Bewag Geoservice ein hubschraubergestütztes Messsystem entwickelt, das für die Aufnahme in topographisch schwierigen Umgebungen ideal geeignet ist. Für die Vermessung von steilen Oberflächen kann die Sensorik zur Seite geneigt werden, um eine bestmögliche Aufnahmegeometrie zu erzielen.

Mit diesem Messsystem wurden im September 2009 das Gebiet der Bliggspitze / Kaunertal und im August 2010 der Gross Kärpf im Kanton Glarus / Schweiz aufgenommen. Anhand von Daten dieser Befliegungen wird die Leistungsfähigkeit dieses Messsystems demonstriert. Darüber hinaus werden Vergleiche mit Daten aus früheren Befliegungen in diesen Gebieten gezogen. Dadurch erhält man ein Bild über die geometrischen Veränderungen in dem Gebiet.

PERMAFROST UND BLOCKGLETSCHER – EIN THEMA FÜR DIE SCHULISCHE UND INFORMELLE UMWELTBILDUNG?

Lieb, G.K.¹, Nutz, M.² und Krobath, M.³

¹ Institut für Geographie und Raumforschung, Universität Graz

² KommunikationsDesign, Graz

³ Umweltbildungszentrum Steiermark, Graz

Die Begriffe Permafrost und Blockgletscher finden sich in den Lehrplänen der österreichischen Schulen nicht. Es wäre jedoch falsch, daraus den Schluss zu ziehen, dass man diese Themen somit nicht in den Fächern Geographie und Wirtschaftskunde sowie Biologie und Umweltkunde behandeln könne/dürfe. Ganz im Gegenteil: Lehrerinnen und Lehrer sind nicht nur in der Wahl der Unterrichtsmethoden, sondern vielfach auch der Inhalte frei, um die in den Lehrplänen definierten Lehrziele zu erreichen. Dies ist in vielen Fällen durch die Behandlung einer komplexen Querschnittsmaterie wie dem Permafrost sehr effizient möglich und kann bei entsprechender methodischer Umsetzung zum Aufbau von persönlichen Qualifikationen in den Bereichen Umwelt- und Synthesekompetenz bei Schülerinnen und Schülern beitragen.

Im Bereich der informellen Umweltbildung hat der Permafrost hingegen längst Eingang in die Inhalte etwa von Informationstafeln und Lehrwegbroschüren gefunden, wenn auch die schwerpunktmaßige Behandlung des Themas bislang noch selten ist. Eine solche bietet sich jedoch im übergeordneten Kontext des globalen Klimawandels an, weil für erlebnisorientiertes Umwelt-Lernen die (intakte) Hochgebirgs-Landschaft ein ideales Erlebnis-Setting darstellt, das mittels relativ einfacher Inszenierungstechniken ein vertieftes Freizeiterlebnis fördert. Dieses wiederum kann die Möglichkeit eröffnen, bei den Konsumentinnen und Konsumenten solcher Angebote Bewusstseinsänderungen hervorzurufen und in weiterer Folge die Bereitschaft zu nachhaltigem Handeln zu steigern.

Der Vortrag diskutiert die Rahmenbedingungen, die die Vermittlung des Themas Permafrost und Blockgletscher im schulischen und informellen Bereich vorfindet. Dies wird mit Hilfe zweier konkreter Umsetzungsbeispiele veranschaulicht:

- Ein im Rahmen des Projekts PermaNET (Teil der Europäischen Territorialen Kooperation, kofinanziert vom Europäischen Regionalentwicklungs-fonds ERDF im Rahmen des Alpine Space Programms: www.alpine-space.eu) entwickeltes Lernmodul mit Schülerinnen und Schülern der Sekundarstufe als wichtigster Zielgruppe.
- Der erste speziell dem gegenständlichen Thema gewidmete Erlebnisweg in den österreichischen Alpen, der „Blockgletscherweg Dösental“ (Hohe Tauern), der seit 2002 existiert und seit 2009 auch über eine nach umweltdidaktischen Prinzipien gestaltete Begleitbroschüre verfügt.

BLOCKGLETSCHERKATASTER IN SÜDTIROL – PILOTSTUDIE MIT VORBILDCHARAKTER FÜR DEN GESAMTEN ALPENRAUM?

Mair V.

Amt für Geologie und Baustoffprüfung, Autonome Provinz Bozen – Südtirol, Eggentaler Str. 48, 39053 Kardaun

Im Rahmen des Projektes PROALP (Kartierung und Überwachung von Permafrost-Phänomenen in den Alpen) wurde ein Inventar der Blockgletscher in Südtirol erstellt. Als Basis für die Kartierung der Blockgletscher wurde in einem ersten Schritt die Struktur der Datenbank (GIS) entwickelt. Das Datenmodell für die Kartierung der Blockgletscher lehnt sich an das Klassifikationsschema von Burger et al. (1999) und an verschiedene Inventare des Alpenraums an (Carton et al. 1988, 1993; Frauenfelder 1997; Guglielmin & Smiraglia 1997; Imhof 1994, Juen 1999). Der Datensatz wird in Form von Polygonen dargestellt. Größere Blockgletscher, die eine Unterteilung in einen inaktiven und einen aktiven Teil zulassen, werden als Teilflächen dargestellt. Bestehende Kartierungen wie aus dem CARG- Projekt wurden in den Blockgletscherkataster eingearbeitet. In diesem Fall ist die Quelle im Datensatz zitiert.

Die Zuweisung der Information über die Aktivität der einzelnen Blockgletscher erfolgte neben der visuellen Interpretation der Morphologie mit Hilfe des digitalen Geländemodells (Auflösung 2,5 x 2,5 m aus dem Jahr 2006), der Orthofotos verschiedener Generationen (2000, 2003, 2006, 2008) sowie mit Hilfe der Radarinterferometrie. Aufgrund der Lage der Blockgletscher oberhalb des dichten Vegetationsgürtels eignet sich diese Technik sehr gut für die Analyse von Hangbereichen, die sich verändern. Das Grund-

prinzip der differenziellen Radarinterferometrie beruht auf der Kombination von zwei Radarszenen des gleichen Gebiets, die jedoch zu zwei verschiedenen Zeitpunkten und somit von zwei leicht unterschiedlichen Positionen des Radarsensors aufgenommen wurden (Zilger et al. 2006, Mair et al. 2008). Im Rahmen dieses Projektes kamen Radarszenen der Erdbeobachtungssatelliten ERS-1/-2 und ENVISAT (Europa) sowie JERS und ALOS-PALSAR (Japan) zum Einsatz.

Die Struktur des Blockgletscherkatasters konnte ohne großen Aufwand an die Erfordernisse der Datenbank des Interreg IVB Projektes PermaNET – Permafrost long-term monitoring network angepasst werden und diente dieser sogar als Vorbild.

Derzeit enthält der Kataster 1779 Blockgletscher, davon wurden etwa 20% als intakte (aktiv und inaktiv) und 70% als fossile Blockgletscher bewertet. Bei etwa 10% konnte nicht mit Sicherheit Auskunft über den Status der Aktivität gegeben werden.

Die Datenbank wird vom Amt für Geologie und Baustoffprüfung gewartet und wird bei weiteren Detailuntersuchungen und neuen Erkenntnissen ergänzt. Die Daten sind im GeoBrowserPro über die website der Abteilung Informationstechnik für alle Bürger zugänglich.

STOFFKONZENTRATIONEN IM ABFLUSS VON BLOCKGLETSCHERN

Nickus, U.¹, Thies, H.², Krainer, K.³ und Tessadri, R.⁴

¹ Institut für Meteorologie und Geophysik, Universität Innsbruck, Innrain 52, A-6020 Innsbruck

² Institut für Ökologie Universität Innsbruck, Technikerstraße, A-6020 Innsbruck

³ Institut für Geologie und Paläontologie Universität Innsbruck, Innrain 52, A-6020 Innsbruck

⁴ Institut für Mineralogie und Petrographie Universität Innsbruck, Innrain 52, A-6020 Innsbruck

Der Abfluss von aktiven Blockgletschern weist in der Regel ausgeprägte saisonale und tägliche Schwankungen auf. Messungen der elektrischen Leitfähigkeit und 180 Werte im Abfluss von aktiven Blockgletschern in den österreichischen Alpen weisen auf die wechselnden Beiträge von Schmelzwasser aus der winterlichen Schneedecke, der Eisschmelze und von Grundwasser hin (e.g. Krainer & Mostler 2002, Krainer et al. 2007). Über die in Blockgletscherabflüssen vorliegenden Stoffkonzentrationen und deren saisonale Variabilität ist in der Literatur bisher nur wenig bekannt. Messungen im Schnalstal

(Südtirol), Ötztal und im Kaunertal (Nordtirol) zeigen eine meist ausgeprägte Zunahme der Konzentration von Ionen und Metallen zwischen Frühsommer und Herbst und bestätigen Ergebnisse von Williams et al. (2006) aus den Rocky Mountains. Kalzium, Magnesium und Sulfat bestimmen mit einem relativen Anteil von bis zu 98% die Gesamtionensumme. Maximale Werte der elektrischen Leitfähigkeit liegen über 500 $\mu\text{S}/\text{cm}$. Auch der Gehalt an Metallen kann in Blockgletscherabflüssen stark erhöht sein. So übersteigen z.B. im Kaunertal (Krumgampen) die Konzentrationen an Nickel und Aluminium die für Trinkwasser geltenden Grenzwerte um den Faktor 10 bis 30. Die Herkunft der im Abfluss von aktiven Blockgletschern gemessenen hohen Konzentrationen an Ionen und Metallen ist noch nicht geklärt. Vergleiche mit Bächen, die nicht mit Schmelzwasser aus Blockgletschern gespeist werden, legen den Schluss nahe, dass als Folge des Anstiegs der Lufttemperatur vermehrt Stoffe aus dem Eis aktiver Blockgletscher freigesetzt werden. Dies kann die chemische Zusammensetzung von Hochgebirgsbächen und -seen, in deren Einzugsgebiet aktive Blockgletscher liegen, längerfristig verändern, wie am Beispiel von Rasass See und Schwarzsee ob Sölden gezeigt werden konnte (Thies et al. 2007).

PERMAFROSTVERBREITUNG IN DEN HOHEN TAUERN – EIN ZWISCHENBERICHT AUS DEM PROJEKT PERMALP.AT

Otto, J-C.¹, Rupprechter, M.¹, Ebohon, B.¹, Keller, F.², Schrott, L.¹

¹ Fachbereich Geographie und Geologie, Universität Salzburg

² Academia Engiadina & Pädagogische Hochschule Graubünden, Samedan, Schweiz

Im Projekt „permalp.at“, das von mehreren Partnern unterstützt wird, wird die räumliche Verbreitung des Permafrostes im Bereich der Hohen Tauern untersucht (www.permalp.at). Hauptziel des Projektes ist die Modellierung der Permafrostverbreitung durch die Anpassung der bestehenden, bewährten Ansätze des topoklimatischen Schlüssels (vergl. PERMAKART) auf die lokalen Bedingungen des Untersuchungsgebietes unter Einbeziehung vorliegender und neu erhobener Daten aus Österreich. Der topoklimatische Schlüssel enthält empirische Werte in welchen Geländepositionen (Höhe, Hangneigung, Exposition) Permafrostbedingungen vorherrschen. Die einfließenden Daten stammen aus lokalen Test-

gebieten innerhalb der Hohen Tauern, die unterschiedliche Geländeeigenschaften bezüglich der Gletscher-, Vegetations-, Schutt- und Felsanteile aufweisen. Die Berechnungen werden auf Basis eines digitalen Geländemodells mit einer Auflösung von 10 m umgesetzt, um das stark strukturierte Gelände des Hochgebirges möglichst genau abzubilden. Zur Verbesserung der Modellierung werden zusätzliche Einflüsse auf die Verbreitung des Permafrostes, z.B. die Oberflächenbedeckung oder die Solarstrahlung miteinbezogen. Als Modelloutput ersetzt eine indexbasierte Darstellung des Permafrostvorkommens die bisher verwendeten „scharfen“ Untergrenzen von möglichem und wahrscheinlichem Permafrost. Durch den fließenden Übergang und die Angabe von einem Indexwert der Auftretenswahrscheinlichkeit von Permafrost zwischen 0 und 100 wird die Qualität der Karte deutlich verbessert.

Zudem werden Temperatur-, Gelände- und Untergrunddaten mit geomorphologisch-geophysikalischen Methoden erhoben, um die gegenwärtige Permafrostverbreitung mit hoher räumlicher Auflösung und Genauigkeit zu erfassen. Seit 2008 sind ca. 600 Messungen der Basistemperatur der winterlichen Schneedecke (BTS) in den Hohen Tauern durchgeführt und 25 Temperatur-Datalogger zur Gewinnung von Zeitreihen der Bodentemperatur installiert worden. Im Testgebiet Kreuzkogel wurden die BTS-Werte bereits gut durch das Modell reproduziert. Die BTS-Werte zeigen eine hohe Variabilität in Zusammenhang mit dem Oberflächenmaterial der Messstandorte (Vegetation, Blockschutt, Feinschutt). Die Auswertungen bestätigen, dass Blockschutt die Auftretenswahrscheinlichkeit von Permafrost erhöht, während Vegetation diese stark senkt. An weiteren 19 Standorten in den Testgebieten wurden bislang Geoelektrikmessungen (2D elektrische Widerstandsmetrie) durchgeführt, die es ermöglichen, lokale Eisvorkommen indirekt über hohe Widerstandswerte zu detektieren.

Eine erste Abschätzung der Permafrostverbreitung in den Hohen Tauern ist bereits mit dem abgeänderten Modellierungsansatz erfolgt und lässt auf eine Fläche von ungefähr 760 km² (ca. 18 % des Untersuchungsgebietes) schließen, wobei auf ca. 260 km² mit einer Auftretenswahrscheinlichkeit von über 50 % zu rechnen ist.

FELSTEMPERATUREN UND PERMAFROSTVERBREI-TUNG AM HOHEN SONNBLICK, 3106 m, HOHE TAU-ERN, SALZBURG

Riedl, C.¹, Klee, A.¹, Böckli, L², Staudinger, M.¹

¹ Zentralanstalt für Meteorologie und Geodynamik (ZAMG), Salzburg, Österreich

² Geographiedepartment, Universität Zürich, Schweiz

Im Rahmen des ÖAW Projekts „Permafrost in Austria“ wird seit Sommer 2006 in drei 20 m Bohrlöchern die Felstemperatur gemessen, um die Auswirkungen des aktuellen Klimawandels auf den Permafrost zu dokumentieren. Die Lage der Bohrlöcher erstreckt sich in einem Abstand von etwa 30 m vom Sonnblickgipfel in Richtung Süden. Der Gipfelaufbau ist nicht vergletschert jedoch beginnt direkt unterhalb des am tiefsten gelegenen Bohrlochs ein Dauerschneefeld und das obere Goldbergkees.

Die Felstemperaturen zeigen, dass die Erwärmung im Sommer (Juni bis September) bis in eine Tiefe von 15 Metern wirkt und das mit einer Verzögerung von etwa einem halben Jahr. Die maximale Auftauschicht beträgt 100 cm.

Für die Modellierung der Permafrostverteilung des Sonnblickgipfelaufbaus im Rahmen des Alpine Space Projekts PermaNET stehen neben den Felstemperaturen aus den Bohrlöchern die über 120 jährige Klimazetitreihe des Sonnblickobservatoriums, aktuelle meteorologische Daten, zahlreiche oberflächennahe Temperatursensoren sowie geophysikalische Parameter (z.B. seismische Tomographie) zur Verfügung.

LASERSCANNING MONITORING VON PERIGLAZIALEN PROZESSFORMEN – POTENTIALE UND LIMITATIONEN

Sailer, R.^{1,2}, Erik Bollmann, E.¹, Briese, C.³, Fischer, A.⁴, Krainer, K.⁵, Rieg, L¹, Stötter, J.¹

¹ Institut für Geographie, Universität Innsbruck

² alpS, Centre for Climate Change Adaption and Technology, Innsbruck

³ Institut für Fernerkundung und Photogrammetrie, TU Wien

⁴ Institut für Meteorologie und Geophysik, Universität Innsbruck

⁵ Institut für Geologie und Paläontologie, Universität Innsbruck

Die Kryosphäre mit ihren Komponenten Gletscher, Permafrost und dessen Leitform Blockgletscher reagieren sensibel auf klimatische Veränderungen. Unterschiedlichste Verfahren zum Nachweis und Monitoring von Gletschern und Permafrost wurden bisher entwickelt

und angewandt (Längenmessungen, Seismik, Geoelektrik, Bodenradar). In jüngster Vergangenheit gewinnen Fernerkundungsverfahren zunehmend an Bedeutung. Ein vielversprechendes Instrument zur flächenhaften Erfassung und Analyse von Oberflächenveränderungen bieten dabei terrestrische (TLS) und flugzeuggestützte (ALS, Airborne Laserscanning) Laserscanningverfahren.

In den vergangenen Jahren wurden in den Ötztaler und Stubaieralpen immer wieder Laserscanningbefliegungen durchgeführt. Die längste durchgehende und damit weltweit einzigartige ALS Datenreihe existiert in der Region Hintereisferner/Rofental. Die ersten Befliegungen haben im Jahr 2001 stattgefunden und bis 2010 wurde mindestens eine Laserscanningkampagne pro Jahr durchgeführt. Hauptziel dieser Messungen war die Erstellung von Gletscher-Massenbilanzen. Darüber hinaus hat sich gezeigt, dass die hohe ALS Präzision und Genauigkeit Analysen von periglazialen Prozessformen zulassen, die bisher flächen- und volumenmäßig nicht quantifizierbar waren. Demzufolge ist bei einem konsistenten (sowohl die Datenaufnahme als auch die Nachprozessierung betreffenden) ALS Monitoring in Neigungsbereichen unter 35° der Messfehler kleiner als ± 0.04 m. Mit zunehmender Steilheit des Geländes nimmt der Fehler zu, liegt bei Neigungen unter 60° immer noch unter ± 0.15 m und steigt bis 80° auf ± 1.0 m an. Aufbauend auf den Ergebnissen einer fundierten Fehleranalyse werden die Ergebnisse diverser periglazialer Prozessaktivitäten quantifiziert (Fläche-, Volumen-, Höhenänderungen) und präsentiert. Besonderes Augenmerk wird dabei auf Oberflächenveränderungen am Rofenberg, die durch Permafrostdegradation hervorgerufen werden, gelegt. Es zeigt sich, dass insbesondere durch jährliche ALS Messungen ein Nachweis dieser permafrostinduzierten Oberflächenveränderungen erfolgen kann.

Laserscanningverfahren werden auch vermehrt zur Erfassung und Quantifizierung der Veränderungen von Blockgletschern herangezogen. Das Projekt C4AUSTRIA setzt sich zum Ziel, auf Basis von ALS sowohl Fließgeschwindigkeiten als auch Volumenänderungen von Blockgletschern zu quantifizieren. Erste ALS Auswertungen liefern darüber hinaus ein sehr differenziertes Bild von Veränderungen der Oberfläche, die mit herkömmlichen Verfahren nicht oder nur punktuell nachweisbar waren.

GEOMON4D – A NEW HIGH SPEED TOOL FOR GEOELECTRICAL MONITORING IN PERMAFROST REGIONS

Supper, R., Ita, A., Römer, A., Jochum, B., Ottowitz, D.

Geological Survey of Austria, Department of Geophysics, Neulinggasse 38, 1030 Vienna

Changes of climate parameters due to global warming generate increased permafrost "warming" in Alpine regions, thus involving severe environmental and engineering problems.

The applicability of the geoelectric method for permafrost investigations (repeated measurements at larger time intervals) was recently demonstrated by several authors. Results suggest that the interpretation of resistivity changes should allow observing seasonal freezing and thawing processes thus leading to a better understanding of related processes. However for detailed analysis of these processes permanent geoelectrical monitoring has to be applied, which so far has never been performed due to the technological challenge of operating such a system in remote areas.

Within recent years the Department of Geophysics of the Geological Survey of Austria has developed a new geoelectrical instrument, called the GEOMON4D. The GEOMON4D is a tool for high speed (approx. 3000 measurements per hour in single channel mode) ground resistivity and self-potential measurement. Recording of the full signal enable effective noise analysis and filtering. Moreover, a completely open architecture allows installation of any number of current or potential electrodes by adding parallel or serial cards. Due to GPRS data transfer maintenance is performed fully remote-controlled. Data, such as measurement results, test sequences and log files, containing information about system and GPRS connection status are sent automatically via email to the data processing center. Consequently, immediate availability of information can be guaranteed.

For the special case of permafrost monitoring the GEOMON4D had to be further adapted. The key limitation of the standard Geomon4D as well as other commercial instruments is that the measuring range is limited and therefore most of the time the measured potential differences are in the range of saturation. Therefore a constant current source was developed. Consequently the injected current can be kept very small and constant so that the measured poten-

tial differences stay under the saturation range of the instrument and polarization effects are adjusted.

Additionally a specific lightning protection device had to be developed for all input and output channels to protect the system from lightning strokes.

Within this talk the requirements for a permanent geoelectrical monitoring system will be discussed and first results presented.

ERSTE ERGEBNISSE DER KERNBOHRUNGEN AUF DEM AKTIVEN BLOCKGLETSCHER IN LAZAUN, SCHNALSTAL(SÜDTIROL)

Tonidandel, D.¹, Leiter, J.², Mair, V.¹, Lang, K.¹

¹ Amt für Geologie und Baustoffprüfung, Autonome Provinz Bozen – Südtirol, Eggentaler Str. 48, I-39053 Kardaun

² Institut für Geographie, Universität Innsbruck, Innrain 52, A-6020 Innsbruck.

Im Rahmen des Interreg IVB Projektes PermaNET wurden auf dem aktiven Blockgletscher in Lazaun im hintersten Schnalstal (Südtirol) zwei Kernbohrungen abgeteuft. Ziel der Bohrungen ist es, Aufschlüsse der inneren Struktur von Blockgletschern zu erhalten, die Eiskerne auf ihre chemische Zusammensetzung zu analysieren und Messdaten über die Bewegungsdynamik und das Temperaturverhalten zu gewinnen. Dazu wurden in den Bohrlöchern Inklinometerrohre, Koaxialkabel und Thermistorenketten eingebaut.

Die erste Bohrung wurde auf einer Lobe im mittleren Bereich des Blockgletschers auf einer Seehöhe von 2.580 m abgeteuft. Die Endbohrtiefe beträgt 40 m. Das erhaltene Bohrprofil kann in sechs Bereiche unterteilt werden:

(1) 0 bis 3 m: Dezimeter bis Meter große Glimmerschieferblöcke (active layer); (2) 3 bis 14 m: Wechselfolge von Dezimeter bis Meter großen Glimmerschieferblöcken und einer Eis-Kies-Sand Mischung; (3) 14 bis 16 m: Glimmerschieferblöcke mit zwischengelagertem Kies; (4) 16 bis 24 m: Wechselfolge von Dezimeter bis Meter großen Glimmerschieferblöcken und einer Eis-Kies-Sand Mischung; (5) 24 bis 28 m: Dezimeter bis Meter große Glimmerschieferblöcke und (6) 28 bis 40 m: Dezimeter bis Meter große Glimmerschieferblöcke mit Zwischenlagerungen von schluffigem Sand und Kies. Dieser Bereich bildet wahrscheinlich die untere Grenze des Blockgletschers. Es könnte sich hierbei um eine Grundmoräne handeln.

Die erste Inklinometermessung hat gezeigt, dass sich der Blockgletscher bis in einer Tiefe von 24 m

(Basis der zweiten Eisschicht), im Laufe eines Monats (Mitte August bis Mitte September 2010) etwa 1,2 cm bewegt hat. Die höchste Bewegungsrate (1,8 cm) wurde an der Basis der ersten Eisschicht in einer Tiefe von 14 m gemessen. Ab einer Tiefe von 24 m befinden sich die Bewegungen im Submillimeter Bereich.

Die zweite Kernbohrung wurde im Stirnbereich des Blockgletschers auf einer Seehöhe von 2.538 m abgeteuft und erreichte eine Bohrtiefe von 32 m. Auch in diesem Fall kann das Bohrprofil, ähnlich wie das oben genannte, in sechs Bereiche unterteilt werden. Der Unterschied besteht vor allem in der geringeren Mächtigkeit der Eisschichten. Der erste durch das Vorhandensein von Eis charakterisierte Abschnitt be-

findet sich zwischen 4 und 10 m Bohrtiefe, der zweite zwischen 16 und 18 m. Die schluffigen Sand- und Kiesschichten befinden sich ab einer Tiefe von 25 m. Diese Schichten werden mit der Grundmoräne der ersten Bohrung korreliert.

Vom zweiten Bohrloch sind noch keine Inklinometerdaten vorhanden.

Der Einbau des Koaxialkabels und der Thermistorenkette in beiden Bohrlöchern hat erst kürzlich stattgefunden. Erste Daten werden ab Mitte Oktober 2010 erwartet. Die chemischen Analysen der Eisbohrkerne werden am Institut für Geologie der Universität Innsbruck durchgeführt.

Gredleriana

9

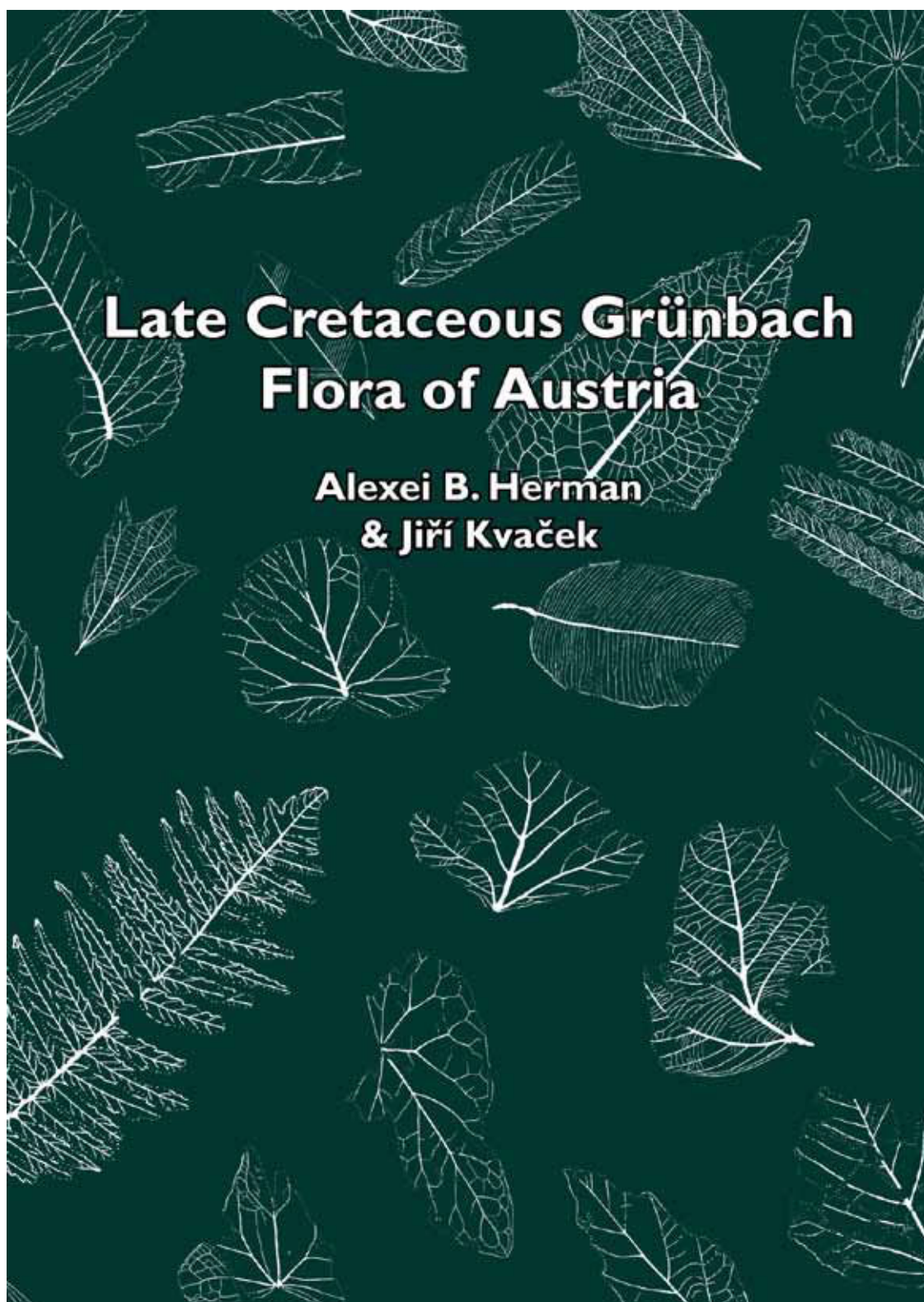


2009

NATURMUSEUM SÜDTIROL
MUSEO SCIENZE NATURALI ALTO ADIGE
MUSEUM NATÖRA SÜDTIROL

Die Veröffentlichungsreihe „Gredleriana“ des Naturmuseums Südtirol (Bozen) ist ein Forum für naturwissenschaftliche Forschung in und über Südtirol. Sie stellt eine Kommunikationsplattform dar für alle jene, die in Südtirol forschen oder in der Ferne Südtirol und den alpinen Raum als Ziel ihrer naturwissenschaftlichen Forschung haben.

Band 9/2009: 25 Euro (Abonnement: 20 Euro), 340 Seiten, ISSN 1593-5205



BOOK REVIEW
LATE CRETACEOUS GRÜNBACH FLORA OF AUSTRIA

Evelyn Kustatscher

Naturmuseum Südtirol, Bindergasse 1, 39100 Bolzano, Italy; e-mail: Evelyn.Kustatscher@naturmuseum.it

The Grünbach Flora is one of the most important Upper Cretaceous floras of Europe and one of the few antracophilous (mire) floras in the Northern Hemisphere for this time period. The plant fossils (over 1000 specimens) are derived from the lower Campanian Grünbach Formation in the Neue Welt Basin (near Vienna, Austria) and is nowadays stored in several collections in Austria (e.g., Natural History Museum und Austrian Geological Survey in Vienna) and Czech Republic (e.g., Narodni Muzeum, Prag). The plant remains are represented by leaf impressions, compression, fructifications and fossil wood belonging to 53 species mostly of angiosperms and ferns. Although collected since the 19th century, the flora has been poorly studied and described and it is almost unknown within the palaeobotanical community.

This monograph gives, for the first time, an extensive and detailed description of the flora. The historical overview provides a good insight on the previous studies, done e.g. by Unger, Ettingshausen and Krasser. The geological setting is briefly explained; the attribution of the flora to the lower Campanian is based on foraminifers and palynomorphs. The sporomorphs are enlisted and briefly discussed. The microflora is characterized by the "Normapollen" group, typical of the ancient angiosperms, although even several reworked Triassic genera have been found.

The description of the flora is extensive and detailed. Almost for each of the species also drawings are provided in order to show the venation pattern and other details of the leaves that are hard to see in the macrofossils. Additionally several pictures, arranged in 36 plates, complete the detailed description and discussion for each taxon. Within the flora four new genera (*Gosauopteris*, *Gruenbachia*, *Theiaiphyllum* and *Compositiphyllum*) are introduced as well as 27 new species.

The flora is used also for palaeofloristic and phytogeographic considerations. The Grünbach flora is a typical flora of the Euro-Sinian palaeophytogeographic region. The authors suggest that during the formation of the Grünbach flora the area was a large island, temporarily connected to the continent. The flora reflects a highly diversified ecology, from shallow fresh water tables, to swampy lowland, juglandaceous forests and mesophytic coniferous forests. According to the palaeoclimatic analysis using nearest living relative (NRL), leaf margin analysis (LMA) and Climate Leaf Analysis Multivariate Program (CLAMP) the flora grew in a humid subtropical frost-free climate, with hot summers and short dry seasons.

Palaeoecological interpretations of the flora reveal that the plants were thriving in different biotopes ranging from aquatic and mire communities to wetland and mesophytic forests.

In short, this monograph contains a comprehensive description of an important Late Cretaceous flora that was poorly discussed and studied so far. It is, however, not restricted only to the description of the plant fossils themselves but gives also important contributions on the palaeoclimate and palaeophytogeography during the Upper Cretaceous in Central Europe. Written by two experts in Cretaceous fossil floras and covering every possible angle of interpretation (ecology, geography, climate, geology, biostratigraphy) this book will be very valuable not only to palaeobotanists but also to specialists working on palaeoclimate. This volume is especially important since it gives a detailed overview of one of the most important floras of the Upper Cretaceous of Europe, a time that is very important for the evolution of the angiosperms.

Late Cretaceous Grünbach Flora of Austria. Herman, A.B., Kvaček, J., 2010. Verlag Naturhistorisches Museum Wien, 224 pp. ISBN: 978-3-902421-43-2.

Gredleriana

9



2009

NATURMUSEUM SÜDTIROL
MUSEO SCIENZE NATURALI ALTO ADIGE
MUSEUM NATÖRA SÜDTIROL

Die Veröffentlichungsreihe „Gredleriana“ des Naturmuseums Südtirol (Bozen) ist ein Forum für naturwissenschaftliche Forschung in und über Südtirol. Sie stellt eine Kommunikationsplattform dar für alle jene, die in Südtirol forschen oder in der Ferne Südtirol und den alpinen Raum als Ziel ihrer naturwissenschaftlichen Forschung haben.

Band 9/2009: 25 Euro (Abonnement: 20 Euro), 340 Seiten, ISSN 1593-5205

Geo.Alp

Veröffentlichung des Instituts für Geologie und Paläontologie der Universität Innsbruck
und des
Naturmuseums Südtirol/Museo Scienze Naturali Alto Adige, Bozen/Bolzano

ISSN 1824-774

Inhalt

Natalia Zavialova, Evelyn Kustatscher & Johanna H.A. van Konijnenburg-van Cittert: Spore ultrastructure of Selaginellites leonardii and diversity of Selaginellalean spores.....	1-17
Christian Pott & Michael Krings: Gymnosperm foliage from the Upper Triassic of Lunz, Lower Austria: an annotated checklist and identification key	19-38
Verena Rofner, Peter Tropper & Volkmar Mair: Petrologie, Geochemie und Geologie des Amphibolit/Metagabbro Komplexes von Gufidaun (Südtirol, Italien).....	39-53
Pietro Frizzo, Luca Peruzzo, & Elio Dellantonio: The copper-wolfram deposit of Bedovina (Trento, Italy).....	55-70
Andreas Piber und Peter Tropper: Tectonometamorphic evolution of the Austroalpine nappes in the northern Zillertal area (Tyrol, Eastern Alps)	71-92
Permafrost Workshop Obergurgl, Kurzfassungen der Beiträge (Vorträge und Poster)	93-108
Buchbesprechung.....	109-110